Dissertation

Accumulation model of antibody binding in staining experiments

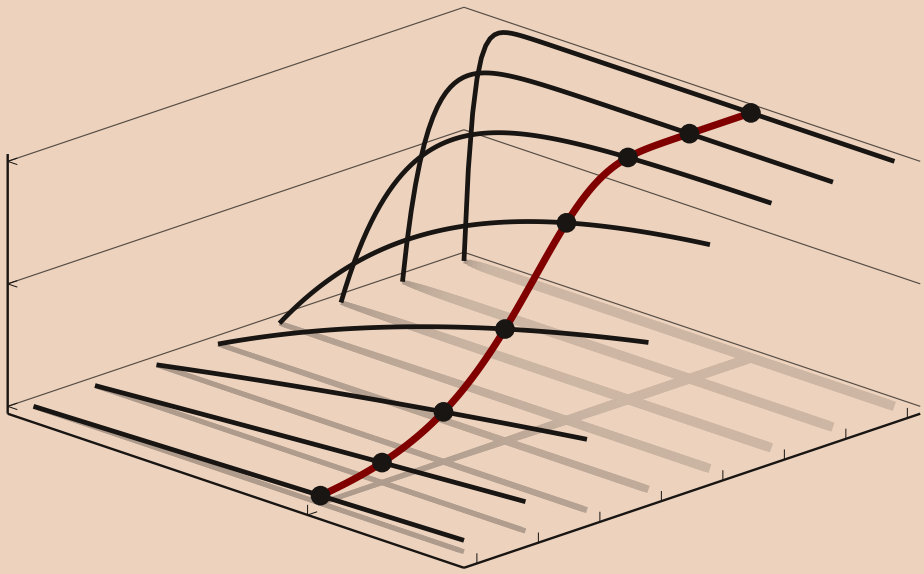

UNIVERSITY OF COLOGNE

Dominik B. Tschimmel

This page intentionally left blank.

Accumulation model of antibody binding in staining experiments

Inaugural-Dissertation

zur

Erlangung des Doktorgrades

der Mathematisch-Naturwissenschaftlichen Fakultät

der Universität zu Köln

vorgelegt von

Dominik Bruno Tschimmel

aus Dormagen

angenommen im Jahr 2026

This page intentionally left blank.

Abstract

The selective binding of antibodies to antigens has been used for decades in biological research and has become a useful tool for medical diagnostics and therapy. Perhaps one of the earliest applications are staining experiments that indicate the presence of antigens in cells or tissue. Despite the development of highly specialized applications, this simple staining still belongs to the standard repertoire of immunostaining.

In this dissertation, we model the macroscopically observable binding behavior of antibodies in staining experiments. The guiding principles are two aspects that apply to most staining experiments: the finite antibody incubation time, and washing steps that remove unbound antibodies prior to the evaluation of the staining result. Thus, the staining result can only comprise antibodies that have withstood washing, leading us to describe the binding of measurable antibodies as an accumulation process with finite stopping time.

We construct the equations for the accumulation model from Langmuir kinetics and corresponding adaptations to multiple binding-site types so that we can consider heterogeneous cellular structures. After describing the immediate consequences of the accumulation process, we prove that the accumulation model satisfies all the properties that are expected from the experimental setting of staining experiments. Next, we shift the focus to the estimation of the model parameters and develop the accessibility analysis, which is a characterization method for experimental systems. Using experimental data, we validate the underlying principles of the accumulation model and test the accessibility analysis that is implemented and published in the form of Julia packages. Finally, we take the opportunity to propose and illustrate two applications of the accessibility analysis: the selection of initial antibody concentrations for staining experiments and a multi-staining multiplexing method that separates staining signals based on antibody binding properties.

This page intentionally left blank.

Published results and contributions

Many of the ideas and results of my doctoral research are already publicly available in the following papers/preprints:

[Methods-Paper] Dominik Tschimmel, Momina Saeed, Maria Milani, Steffen Waldherr, and Tim Hucho. "Computational epitope heterogeneity analysis in immunostainings from antibody-dilution series". In: *Communications Biology* 9, 238, (Feb. 2026). ISSN: 2399-3642. DOI: https://doi.org/10.1038/s42003-026-09517-x.

[Theory-Preprint] Dominik Tschimmel, Steffen Waldherr, and Tim Hucho. "Modelling the effect of antibody depletion on dose-response behavior for common immunostaining protocols". In: *arXiv (Preprint)* (2024). Preprint. DOI: 10.48550/arXiv.2409.06895. arXiv: 2409.06895 [q-bio.QM].

Except for the abstract and the introduction of [Methods-Paper], I wrote the papers/preprints. Furthermore, I developed the mathematical model, analyzed the data, and created the figures. Hence, their content will be included in this dissertation.

For the analysis methods presented in this dissertation and in [Methods-Paper], I developed the following Julia packages (newest versions, developed and used for this dissertation):

[ADA.jl] Dominik Tschimmel. *AdaptiveDensityApproximation.jl*. Version v0.4.0. 2025. DOI: 10.5281/zenodo.17741453.

[ADAR.jl] Dominik Tschimmel. *AdaptiveDensityApproximationRecipes.jl*. Version v0.3.1. 2025. DOI: 10.5281/zenodo.17741445.

[ADMR.jl] Dominik Tschimmel. *AntibodyMethodsDoseResponse.jl*. Version v0.3.4. 2025. DOI: 10.5281/zenodo.17741435.

[AMDRC.jl] Dominik Tschimmel. *AntibodyMethodsDoseResponseConvenience.jl*. Version v0.4.2. 2025. DOI: 10.5281/zenodo.17741413.

[AMDRR.jl] Dominik Tschimmel. *AntibodyMethodsDoseResponseRecipes.jl*. Version v0.1.3. 2025. DOI: 10.5281/zenodo.17741349.

[FOF.jl] Dominik Tschimmel. *FittingObjectiveFunctions.jl*. Version v0.2.3. 2025. DOI: 10.5281/zenodo.17741331.

I did not conduct meaningful experiments for [Methods-Paper]. However, I designed the experiments and I was responsible for the intermediate and final evaluation of the experiments conducted by

---

[Maike Siobal] Maike Siobal. Laboratory Assistant; Performed the incubation-time experiments.

[Momina Saeed] Momina Saeed. MSc student; Performed the antibody-mix experiments and the multi-staining experiments.

Because of my involvement and since the experiments are specifically designed for my dissertation, the data from these experiments will also be included in this dissertation. However, the data will be treated as external data. The respective experimenter and the source

[Raw-Data] *Data Repository for the raw data.* DOI: 10.5281/zenodo.17689412. URL: https://github.com/Translational-Pain-Research/Accessibility_Analysis_Data.

for the raw data will always be cited.

Furthermore, it should be noted that the master's theses of Maria Milani and [Momina Saeed] were closely tied to my doctoral research and thus contain results and figures that are similar to those in [Methods-Paper]. Among others, because I supervised their theses and provided the data analysis.

Although this dissertation is written independently of the papers/preprints in order to restructure the results, there will be considerable overlap in content. When substantial parts are identical (e.g., in mathematical definitions, theorems or figures), references to the corresponding papers/preprints will be provided. Furthermore, the use of content from the papers/preprints will be declared at the beginning of each chapter (if applicable).

This page intentionally left blank.

Contents

This page intentionally left blank.

List of Figures

1
Introduction

Antibodies have become an invaluable tool for biological research and medical therapy, mainly because of their ability to bind selectively to specific target molecules. With the emergence of proper quantification, antibody-based applications have become compatible with mathematical modeling and computational analysis. Although highly controlled setups with precise measurements are the natural choice for modeling approaches, even elementary antibody-based techniques can benefit. In fact, elementary antibody-based techniques are usually broadly available, such that a corresponding modeling approach could be used by many a researcher, which motivates this dissertation.

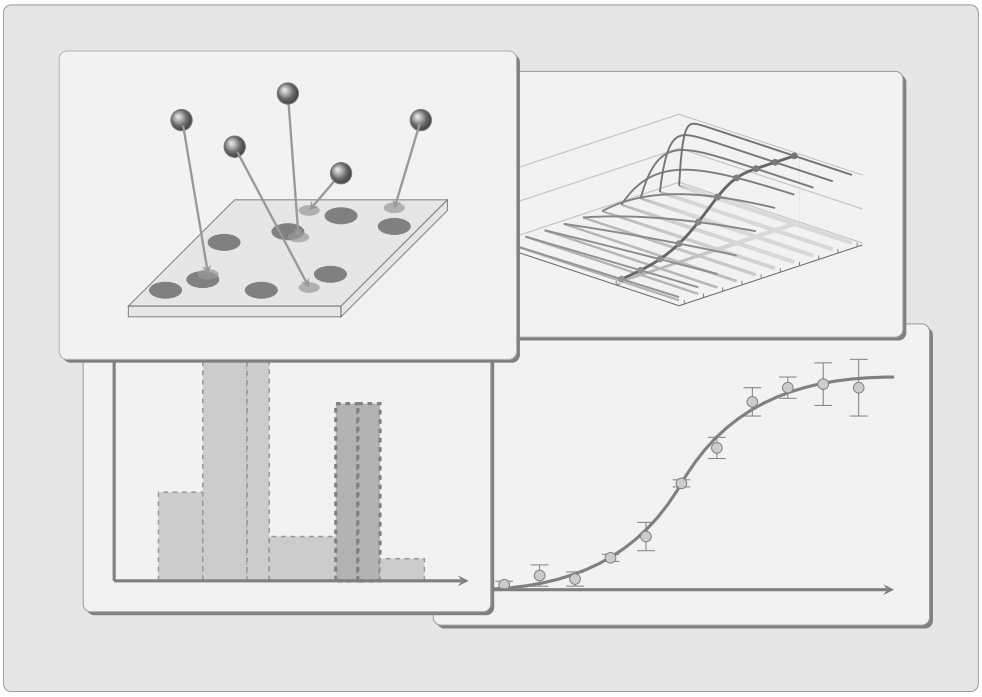

1.1 Antibodies and antibody-staining

Antibodies are an integral part of our immune response, with their ability to recognize and selectively bind to a wide range of biological structures. This binding selectivity is achieved by special binding regions, the **paratopes**, that perfectly match the binding region on the target structure, called **epitope** [Cam+15, section 44.2].

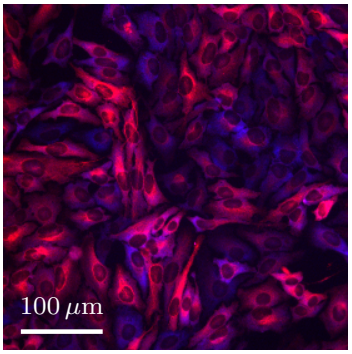

Figure 1.1: {Adapted from [Methods-Paper], raw data from [Momina Saeed; Raw-Data]} Example of antibody-staining (see Figure 5.5).

For decades, the binding properties of antibodies have been used in biological research to detect and localize proteins of interest in tissue samples or cell lines [Mye89]. By now, antibodies have become a ubiquitous research tool in certain areas of biology [Bor+10; Uhl+16]. This widespread use has even extended into clinical practice, be it for diagnostic purposes [De +10] or the treatment of diseases (e.g., cancer treatment [Axe+24; Gua+24], etc.).

From the perspective of a non-biologist, staining experiments might be the most iconic application, as they produce easily recognizable images like Figure 1.1. There are many staining methods and experimental protocols to achieve such images. For example, one can distinguish between the label that is used to detect the antibodies (fluorescent, radioactive, enzymatic), the attachment method of the detection label (direct vs indirect), the isotypes (IgA, IgG, etc.) or structure (monomer, dimer, etc.) of the antibodies, and the biological sample that is stained (cells, tissue, etc.) [Piñ+22; Par+25]. Most of the differences between the staining methods and protocols will not matter to us in this dissertation, assuming that data is of sufficient quality. But there is a commonly performed experimental step in staining experiments that is of particular interest to us: the washing, which removes/reduces the background signals of unbound antibodies.

For lack of a better term, we will generally call these staining experiments **antibody-staining** in this dissertation, without distinguishing between detection labels or sample types.

1.2 Modeling approach and goals

Restricting our considerations to generic antibody-staining has the advantage that our results will apply to a large class of experiments. The disadvantage is that this restriction also limits our modeling approach to a few macroscopic observables that are part of most antibody-staining experiments. Among those observables are antibody concentration, staining intensity, and external parameters like temperature or incubation time.

There is already a well-established binding model that describes antibody binding in terms of antibody concentration, epitope concentration, and rate constants: *mass-action kinetics* [Har+14; RDW16; ET21]. However, we will see that the washing steps require a modified mass-action model. The unbound antibodies that are washed away might have affected the binding process, but they are essentially unobservable in the resulting staining. Thus, a model for antibody-staining should not depend on those antibodies, which motivates the first goal of this dissertation.

Goal 1: Develop a mathematical model for the binding of antibodies that are detectable with generic antibody-staining experiments, using only macroscopic observables (and model parameters).

A mathematical model at the macroscopic level can only provide a few insights for generic antibody-staining experiments. However, this does not need to discourage us. Aside from the intrinsically interesting properties of the mathematical model itself, the insights might provide valuable lessons or could explain some experimental observations. Nevertheless, using the model to characterize specific antibody-staining systems might provide greater utility to a larger group of researchers. This motivates the second goal of this dissertation.

Goal 2: Develop a method to characterize antibody-staining systems using the mathematical model.

1.3 Scope and outline

The main focus of this dissertation is the mathematical description of the binding model (Goal 1) and the development of a characterization method (Goal 2). In consequence, we assume the perspective of non-biologists. As such, we may also take the liberty to depart from the established terminology of biologists when descriptive or abstract naming is better suited to illustrate

biological concepts or to focus on the important aspects of the model. Hence, this dissertation has very few prerequisites in terms of biological background knowledge. However, a certain degree of mathematical education will be necessary to understand all the details.

As the two goals already suggest, this dissertation comprises two major parts. In the first part, we consider the mathematical model of antibody binding in antibody-staining experiments. For this purpose, Chapter 2 introduces the Langmuir model and useful adaptations, emphasizing the underlying principles. In Chapter 3, we define the abstract experimental setting of antibody-staining and develop the binding model for this setting. The remainder of the chapter is then spent on deriving and proving properties of the binding model, which we call *accumulation model*.

In the second part, we will shift the focus from purely theoretical aspects to the estimation of model parameters in order to provide a characterization method for antibody-staining systems. Thus, we begin Chapter 4 by discussing the relevant aspects and limitations of experimental data. Next, we modify the accumulation model to facilitate the estimation of its parameters. Finally, we conclude Chapter 4 by defining the parameter estimation process that will culminate in the characterization method for experimental antibody-staining systems, which we call *accessibility analysis*. In Chapter 5, we check the assumptions of the accumulation model with experimental data from [Methods-Paper; Momina Saeed; Maike Siobal; Raw-Data]. Furthermore, we use the data to demonstrate the feasibility of the accessibility analysis, which is implemented and published in the form of Julia packages [AMDRC.jl; AMDRR.jl; ADMR.jl; ADA.jl; ADAR.jl; FOF.jl]. Finally, we illustrate potential applications of the accessibility analysis.

2

Background: The Langmuir model

Binding phenomena have been studied for a long time. Thus, we will not need to develop our antibody-binding model from scratch. Instead, we can adapt an already existing model. The most promising model for this approach is the Langmuir model, together with its generalization to heterogeneous particles and binding sites. Since our antibody-binding model will inherently share many properties with the Langmuir model, we consider the fundamental principles of the Langmuir model in this chapter.

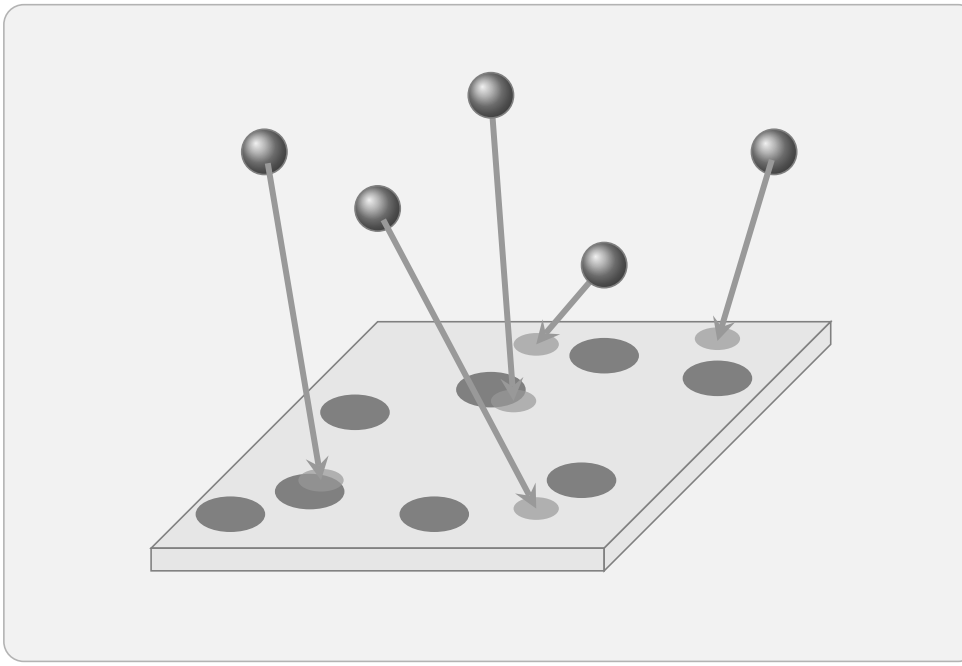

2.1 The Langmuir model

Antibody binding is commonly described in terms of *mass-action kinetics* [Lau93; Har+14; RDW16; ET21]. Interestingly, the same mathematical equations, up to the physical dimensions, also describe the monolayer binding of particles to a solid surface. However, in the monolayer context, the equations are called *Langmuir kinetics* [LS08; Mar10; Sal17; Mal+20]. Here, we prefer the monolayer context, as we will consider epitopes on a 2-dimensional hypersurface in the next chapter.

2.1.1 Langmuir rates

The Langmuir rates describe the binding/adsorption rate $r_\mathrm{a}(t)$ of unbound particles and the unbinding/desorption rate $r_\mathrm{d}(t)$ of bound particles at time t. These rates are given by (cf. [LS08; Lat15; Sal17])

$$r_\mathrm{a}(t) = k_\mathrm{a} \cdot a(t) \cdot g(t) \qquad \text{and} \qquad r_\mathrm{d}(t) = k_\mathrm{d} \cdot x(t) \ . \tag{2.1}$$

Here, we have already chosen the notation for the intended context of antibody-staining.

- The *concentration of unbound particles*, $a(t)$, will become the concentration of unbound ***a***ntibodies.
- The *amount of vacant binding sites*, $g(t)$, will become the amount of vacant epitopes/anti***g***ens.
- The *amount of bound particles*, $x(t)$, will become the amount of bound antibody-epitope comple***x***es.

Both k_a and k_d are proportionality constants, the so-called **rate constants**, that convert the dimensions/units.

Although the binding and unbinding of a finite number of particles (and binding sites) is a stochastic and discontinuous process, the binding rates describe a continuous process to keep calculations simple. Thus, bound particles $x(t)$ and vacant binding sites $g(t)$ are real-valued quantities; hence the term "*amount of ...*". We can justify the continuous model as an approximation of the stochastic, discontinuous jumps caused by the discrete binding/unbinding events, as illustrated in Figure 2.1. Especially for a high concentration of particles and a large number of binding sites, the continuous curve $x(t)$ becomes a good approximation of the actual number of bound particles $N_x(t)$.

Since we intend to adapt the Langmuir model to describe antibody binding in antibody-staining experiments, it is worthwhile to consider the Langmuir model and Langmuir rates more closely.

The general setting of the Langmuir model comprises a solid, flat surface with identical, non-overlapping, and independent binding sites randomly scattered across the surface, as illustrated in Figure 2.2. Furthermore, identical and independent particles occupy an enclosed volume adjacent to the flat surface. Whenever such a particle comes into contact with a binding site, it binds with a certain probability. For simplicity, this probability is the same, irrespective of the particle trajectory and the location of the binding site on the flat surface.

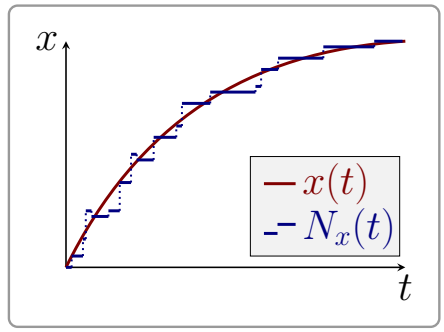

Figure 2.1: Illustration of continuous rates as an approximation of stochastic, discontinuous binding events. The amount of particles $x(t)$ describes a continuous curve that approximates the actual number of bound particles $N_x(t)$ at time t.

Assuming that all remaining external parameters are constant, we can express the binding rate as a function of the particle concentration $a(t)$ and the amount of binding sites $g(t)$:

$$r_{\mathrm{a}}(t) = f(a(t), g(t)) \ .$$

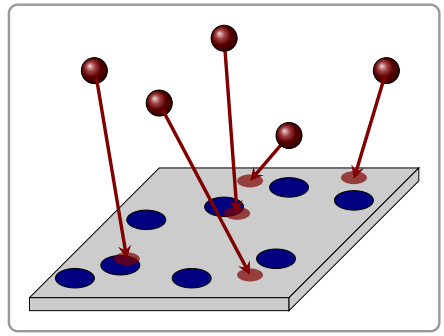

Figure 2.2: Illustration of the binding scenario that results in Langmuir kinetics. Binding sites (blue) scattered on a flat surface that is hit randomly by particles (red).

To obtain the shape of this function, we need a final assumption about the movement of the particles. Since we have begun to describe an idealized system, we continue along this route, assuming that all positions in the enclosed space are identical. Thus, without knowledge about the exact locations of all particles, each position in space is equally likely to be occupied by a particle at any given point in time. In consequence, each location on the flat surface is equally likely to be hit by a particle.

When we increase the concentration of particles, there will be a proportional increase in the number of particles that hit the flat surface, leading to a linear increases in the probability that a particle hits a binding site. In summary,

this boils down to the condition

$$f(\beta a(t), g(t)) = \beta f(a(t), g(t)) \qquad \forall\ \beta \geq 0\ .$$

which states that increasing the concentration of particles will lead to a linear increase in the binding rate $r(t)$.

With the same argument, it follows that an increase in the amount of binding sites will also lead to a linear increase in the binding rate

$$f(a(t), \gamma g(t)) = \gamma f(a(t), g(t)) \qquad \forall\ \gamma \geq 0\ .$$

Since the function f is linear in both arguments, it has the following property,

$$f(\beta x, \gamma y) = \beta\gamma f(x, y) \qquad \forall\ \beta, \gamma, x, y \geq 0\ .$$

Choosing $x = y = 1$, $\beta = a(t)$, and $\gamma = g(t)$, we obtain

$$r_\mathrm{a}(t) = f(a(t), g(t)) = f(a(t) \cdot 1, g(t) \cdot 1) = a(t)g(t)f(1, 1)\ .$$

By relabeling the constant value $f(1, 1)$ to k_a, we obtain the adsorption rate of the Langmuir model

$$r_\mathrm{a}(t) = k_\mathrm{a} a(t) g(t)\ .$$

In the Langmuir model, the binding of a particle is not permanent. Particles can unbind over time. Having assumed that the binding events are independent of each other, it is only natural to assume the same for the unbinding events. Furthermore, without describing the properties of the binding mechanism and the positions of other particles that could collide with bound particles, the binding state is essentially a black box. So, on average, it is reasonable to describe the unbinding as a decay process of the form $-\lambda x(t)$. Since the minus sign is absorbed by the interpretation of $r_\mathrm{d}(t)$ as an unbinding rate, and using the symbol k_d for the decay constant λ, we obtain the desorption rate of the Langmuir model,

$$r_\mathrm{d}(t) = k_\mathrm{d} x(t)\ .$$

2.1.2 The Langmuir rate equation

The rates $r_\mathrm{a}(t)$ and $r_\mathrm{d}(t)$ determine the change in bound particles per unit time $\frac{d}{dt}x(t)$. Since $r_\mathrm{a}(t)$ describes the binding of particles and $r_\mathrm{d}(t)$ describes the unbinding of particles, $\frac{d}{dt}x(t)$ is given by (cf. [LS08; Lat15; Sal17])

$$\frac{d}{dt}x(t) = r_\mathrm{a}(t) - r_\mathrm{d}(t) = k_\mathrm{a} a(t) g(t) - k_\mathrm{d} x(t)\ . \tag{2.2}$$

This differential equation is known as the **Langmuir rate equation**. Its solution $x(t)$ describes the amount of bound particles over time. Of course, to derive a solution, the terms $a(t)$ and $g(t)$ need to be specified further.

One of the common scenarios assumes the conservation of particles and binding sites. This means that the total/initial amount of particles and the total/initial amount of binding sites do not change over time. As a consequence, the amount of vacant binding sites $g(t)$ at time t is exactly the difference between the total/initial amount of binding sites, which we denote by g, and the amount of bound particles $x(t)$ at time t,

$$g(t) = g - x(t) \ . \tag{2.3}$$

We can find a similar term for the concentration of unbound particles. Let V denote the volume that contains the particles, then the total amount of unbound particles is given by $N_a(t) = Va(t)$. In the same way as for the binding sites, we denote the total/initial amount of particles by N_a. The conservation of particles now implies that the amount of free particles $N_a(t)$ at time t is exactly the difference between the total amount of particles N_a and the amount of bound particles $x(t)$ at time t,

$$N_a(t) = N_a - x(t) \ .$$

Because of the reduction of unbound particles, we call this scenario the **depletion case**.

When we convert the particle amounts back into the corresponding particle concentrations, we obtain

$$Va(t) = N_a(t) = N_a - x(t) = Va - x(t) \qquad \Rightarrow \qquad a(t) = a - \frac{1}{V}x(t) \ .$$

Unlike the term for the amount of vacant binding sites (2.3), the term for the concentration of unbound particles requires a conversion factor $\frac{1}{V}$.

In preparation for later chapters, we may abstractly write $\beta := \frac{1}{V}$ for the conversion factor between the amount of bound particles and the concentration of unbound particles:

$$a(t) = a - \beta x(t) \ . \tag{2.4}$$

Instead of understanding β solely as a unit conversion, we may interpret it more generally as a depletion strength, which determines how much the concentration of unbound particles decreases for a given amount of bound particles. Hence, we may call $\beta > 0$ the **depletion factor**.

Using the expressions for the concentration of unbound particles (2.4) and the amount of vacant binding sites (2.3) in the Langmuir rate equation (2.2), we obtain

$$\frac{d}{dt}x(t) = k_{\mathrm{a}}(a - \beta x(t))(g - x(t)) - k_{\mathrm{d}}x(t) \ . \tag{2.5}$$

In addition to the depletion case, there is another common scenario. The total amount of binding sites is conserved, but the concentration of unbound particles is constant $a(t) \equiv a$. This can be achieved with a particle reservoir that adds or removes particles. Hence, we may call this scenario the **reservoir case**.

Of course, when the total amount of binding sites is much smaller than the total amount of particles, the concentration of unbound particles is approximately constant. In addition, for a small depletion factor, the concentration of unbound particles is also approximately constant.

For the reservoir case, the Langmuir rate equation (2.2) becomes

$$\frac{d}{dt}x(t) = k_{\mathrm{a}}a(g - x(t)) - k_{\mathrm{d}}x(t) \ . \tag{2.6}$$

2.1.3 Concentrations versus particle amounts

We have used particle numbers to derive the rate equation, but we have expressed the rate equation in terms of particle concentrations. Furthermore, instead of surface concentrations, we used amounts of binding sites. So, what is the natural dimension: concentration or amount?

For the natural dimension of unbound particles, we can consider two containers, C_1 and C_2, as illustrated in Figure 2.3, where C_2 has twice the volume. However, both containers have identical particle concentrations and identical binding-site surfaces at time t. In this scenario, there are twice as many particles in container C_2 as in container C_1. Does this also mean that the binding rate at time t is higher for container C_2, or are the binding rates the same? If the binding rate for container C_2 is higher, then the particle amount determines the binding rate. If both containers have the same binding rate, then the particle concentration determines the binding rate.

To determine whether the binding rates differ, we only need to observe that particle binding is a local event. That is, particles need to be close to the binding-site surface; otherwise, they cannot bind. For a short time span Δt, only particles in the small volume segment ΔV close to the binding-site

surface can bind. For a sufficiently short time span Δt, the volume segment ΔV is the same for both containers. And since the binding rate at time t is obtained by the limit $\Delta t \to 0$, we can always consider sufficiently small volume segments. Thus, the binding rate at time t is the same for both containers, and particle concentration is the natural dimension.

In the depletion case, the containers will eventually show different binding rates as time progresses. The binding and unbinding of particles leads to a greater change in the concentration of unbound particles in the smaller container. This follows from (2.4), since the depletion factor is given by $\beta = \frac{1}{V}$.

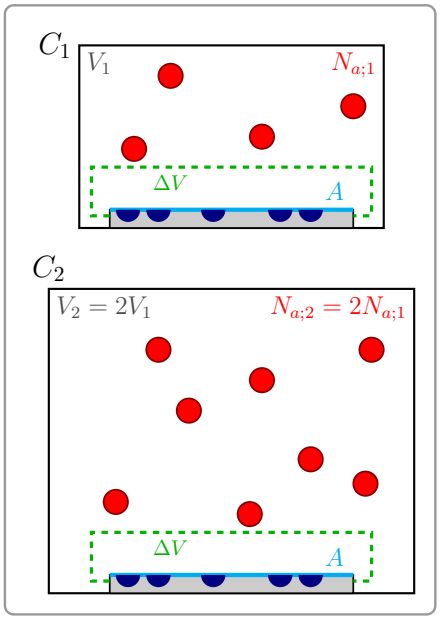

Figure 2.3: Illustration of two containers with identical binding-site surfaces and identical particle concentrations but different volumes. Here, V_i denotes the volume, $N_{a;i}$ denotes the particle number, and A denotes the binding-site surface area for container i. In both cases, only the volume segment ΔV is relevant for particle binding in a short time span Δt.

For the natural dimension of binding sites, we consider two containers, C_3 and C_4, that have the same volume and particle amount/concentration, but C_4 has two binding-site surfaces, as illustrated in Figure 2.4. We assume that the three binding-site surfaces (one in C_3 and two in C_4) have the same size and shape, as well as the same amount of binding sites. Thus, C_3 and C_4 have the same surface concentration of binding sites, where C_4 has twice as many binding sites, but on a surface that is twice as large.

As before, we consider a short time span Δt. In this time span, twice as many particles will bind in container C_4, since C_4 has twice as many binding sites. Thus, we would assume that the binding rate in C_4 is twice as large as in C_3, and we should conclude that amount is the natural dimension of binding sites. However, this conclusion is based on our definition of the binding rate as a change in the number of bound particles.

If we measure bound particles in terms of their surface concentration, we should also evaluate the binding rate as an increase in surface concentration. This means that the larger amount of particles that bind in C_4 is counteracted by the larger surface area: twice as many particles bind, but there is also twice as much surface area. Thus, C_3 and C_4 have the same binding rate in terms

of surface concentration. A similar argument can be made for the unbinding of particles.

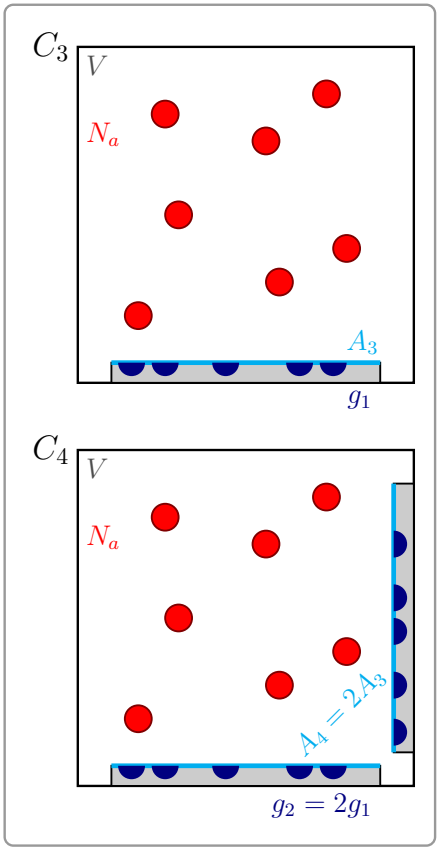

Figure 2.4: Illustration of two containers with identical volumes, identical particle amounts/concentrations and identical binding-site concentrations but different binding-site surface areas. Here, V denotes the volume, N_a denotes the particle number, A_i denotes the binding-site surface area and g_i denotes the amount of binding sites for container i.

In summary, we find that the natural dimension of binding sites depends on the dimension of bound particles. Both are the same. This is hardly surprising, as bound particles only describe a subset of binding sites: those occupied by particles. In that regard, we are free to choose the dimension, yet we chose amount over surface concentration for two reasons.

First, the depletion of unbound particles depends on the amount of bound particles, not on their surface concentration. Thus, when we compare systems with different binding-site surfaces, we intuitively understand the depletion behavior when we use binding-site amounts. Second, we will consider the binding behavior of antibodies (the particles) in complex cellular environments. Here, the surface that contains the epitopes (the binding sites) is a 2-dimensional hypersurface, so the surface area usually remains unknown. Furthermore, the experiments that we will consider in Chapter 4 and Chapter 5 compare antibody concentrations across different cell samples, leading to the aforementioned comparison of systems with different binding-site surfaces.

2.1.4 Solutions of the Langmuir rate equation

Although we will hardly rely on the explicit solutions of the Langmuir rate equations, we briefly present them here for completeness.

The solution of the rate equation for the reservoir case (2.6) is well established (see, e.g., [Lau93, section 2.2.1.a]) and can be obtained by separation of variables. When x_0 denotes the initial value $x(t_0)$, the solution is given by

$$\Rightarrow \quad x(t) = x_0 e^{-(k_\mathrm{a} a + k_\mathrm{d})(t-t_0)} + \frac{g}{1 + \frac{k_\mathrm{d}}{k_\mathrm{a} a}} \left(1 - e^{-(k_\mathrm{a} a + k_\mathrm{d})(t-t_0)}\right) . \tag{2.7}$$

The depletion case is more complicated. Following the steps of [Edw+98] (see Appendix B.1.1 for a proof), the general solution of the Langmuir rate equation for the depletion case can be expressed as

$$x(t) = \frac{z_1 - z_2 \frac{x_0 - z_1}{x_0 - z_2} e^{(z_1 - z_2)(t-t_0)}}{1 - \frac{x_0 - z_1}{x_0 - z_2} e^{(z_1 - z_2)(t-t_0)}} ,$$

where

$$z_1 = \frac{(k_\mathrm{a} a + \beta k_\mathrm{a} g + k_\mathrm{d}) - \sqrt{(k_\mathrm{a} a + \beta k_\mathrm{a} g + k_\mathrm{d})^2 - 4\beta k_\mathrm{a}^2 a g}}{2\beta k_\mathrm{a}}$$

and

$$z_2 = \frac{(k_\mathrm{a} a + \beta k_\mathrm{a} g + k_\mathrm{d}) + \sqrt{(k_\mathrm{a} a + \beta k_\mathrm{a} g + k_\mathrm{d})^2 - 4\beta k_\mathrm{a}^2 a g}}{2\beta k_\mathrm{a}} .$$

2.2 Heterogeneous particles and binding sites

The idealized assumptions of the Langmuir model might be too restrictive for antibodies in complex systems. Fortunately, the assumption of identical binding sites can easily be generalized to a finite number of different binding site types. The general idea has already been described in [Lan18].

2.2.1 Multiple binding site types

As before, we consider independent, non-overlapping binding sites on a flat surface. However, we now allow for a finite set of different binding site types. In the context of the Langmuir model, a binding site is characterized by the rate constants k_a and k_d. Thus, we can describe different binding site types as a set of tuples $\{(g_i, k_{\mathrm{a};i}, k_{\mathrm{d};i})\}_{i=1}^{N}$, where g_i denotes the amount of binding sites for the respective binding-site type.

Of course, different rate constants imply different binding behaviors, so it becomes necessary to describe the binding process for each type of binding site separately. Hence, let $\{x_i\}_{i=1}^N$ denote the amounts of bound particles for each binding site type.

Since we assume that the binding site types are independent of each other, the arguments for the Langmuir rates carry over without modification. In summary, the rate equation becomes

$$\frac{d}{dt}x_i(t) = k_{\mathrm{a};i}a(t)(g_i - x_i(t)) - k_{\mathrm{d};i}x_i(t) \qquad \forall\, i \in \{1,\dots,N\}\ . \tag{2.8}$$

Here, we consider the depletion case and the reservoir case again. The reservoir case, as before, assumes $a(t) \equiv a$, leading to independent differential equations

$$\frac{d}{dt}x_i(t) = k_{\mathrm{a};i}a(g_i - x_i(t)) - k_{\mathrm{d};i}x_i(t) \tag{2.9}$$

for all $i \in \{1,\dots,N\}$.

To obtain the depletion case, we observe that the total amount of bound particles is just the sum over the binding site types $\sum_{j=1}^N x_j(t)$. Thus, the concentration of free particles in the depletion case is given by

$$a(t) = a - \beta\sum_{j=1}^{N} x_j(t)\ ,$$

yielding a system of coupled differential equations

$$\frac{d}{dt}x_i(t) = k_{\mathrm{a};i}\left(a - \beta\sum_{j=1}^{N} x_j(t)\right)(g_i - x_i(t)) - k_{\mathrm{d};i}x_i(t)\ , \tag{2.10}$$

where $i \in \{1,\dots,N\}$.

2.2.2 Multiple particle types

In the same way in which we have incorporated multiple types of binding sites, we can also incorporate multiple types of particles. For example, [Svi+03] discusses this procedure for the reservoir case and a single binding site type. Here, we may consider the general case of multiple binding site types and multiple particle types.

To avoid confusion, let us always use Roman letters for the binding site type and Greek letters for the particle type. The Langmuir rate equation then reads

$$\frac{d}{dt}x_{i\mu}(t) = k_{\mathrm{a};i\mu}a_\mu(t)g_i(t) - k_{\mathrm{d};i\mu}x_{i\mu}(t) \ .$$

Note that we distinguish the bound particles with respect to the particle type $x_{i\mu}(t)$ but not the vacant binding sites $g_i(t)$. This expresses the assumption that the different particle types can all bind to the binding site type i, unless $k_{\mathrm{a};i\mu} = 0$. Thus, the amount of binding sites is given by

$$g_i(t) = g_i - x_i(t) = \left(g_i - \sum_{\nu=1}^{M} x_{i\nu}(t)\right) \ .$$

We can adopt the approach of [Svi+03] to express the initial/constant particle concentrations a_μ as $f_\mu a$, where the f_μ denote the fraction of particles that belong to type μ. Then we obtain

$$\frac{d}{dt}x_{i\mu}(t) = k_{\mathrm{a};i\mu}f_\mu a\left(g_i - \sum_{\nu=1}^{M} x_{i\nu}(t)\right) - k_{\mathrm{d};i\mu}x_{i\mu}(t) \tag{2.11}$$

for the reservoir case and

$$\frac{d}{dt}x_{i\mu}(t) = k_{\mathrm{a};i\mu}\left(f_\mu a - \beta\sum_{j=1}^{N} x_{j\mu}(t)\right)\left(g_i - \sum_{\nu=1}^{M} x_{i\nu}(t)\right) - k_{\mathrm{d};i\mu}x_{i\mu}(t) \tag{2.12}$$

for the depletion case.

2.2.3 Analytical solutions

The simple case of identical particles and identical binding sites has analytical solutions that are available in the literature. Unfortunately, this is not generally the case for multiple binding site types or multiple particle types. Only the reservoir case for multiple binding site types but identical particles seems to have a closed-form solution, as the equations decouple into independent differential equations

$$\frac{d}{dt}x_i(t) = k_{\mathrm{a};i}a(g_i - x_i(t)) - k_{\mathrm{d};i}x_i(t) \qquad \forall\ i \in \{1,\dots,N\}.$$

These decoupled differential equations are just the standard Langmuir rate equation for identical particles. Hence, their solutions are given by (2.7):

$$x_i(t) = x_{0,i}e^{-(k_{\mathrm{a};i}a + k_{\mathrm{d};i})(t-t_0)} + \frac{g_i}{1 + \frac{k_{\mathrm{d};i}}{k_{\mathrm{a};i}a}}\left(1 - e^{-(k_{\mathrm{a};i}a + k_{\mathrm{d};i})(t-t_0)}\right) \ , \tag{2.13}$$

for all $i \in \{1,\dots,N\}$.

This page intentionally left blank.

3
The accumulation model

Having introduced the basic ideas of the Langmuir model, we can proceed to develop our antibody binding model. Guided by the experimental procedure of antibody-staining, we will develop a model of antibody accumulation, starting from our understanding of the Langmuir model. In this chapter, we will mainly be concerned with the mathematical properties of the resulting model, deferring practical considerations to the next chapter.

This chapter uses content that I contributed to [Methods-Paper] and [Theory-Preprint]:

- Section 3.1 combines and significantly extends the motivation and interpretation of the accumulation model of [Methods-Paper] and uses the (mathematical) definitions of [Theory-Preprint].
- Section 3.2 recreates the results for multiple epitope classes of [Theory-Preprint], following the general structure but using natural units.

The respective sections, in particular, and this chapter in general, contain additional new content beyond the highlighted differences.

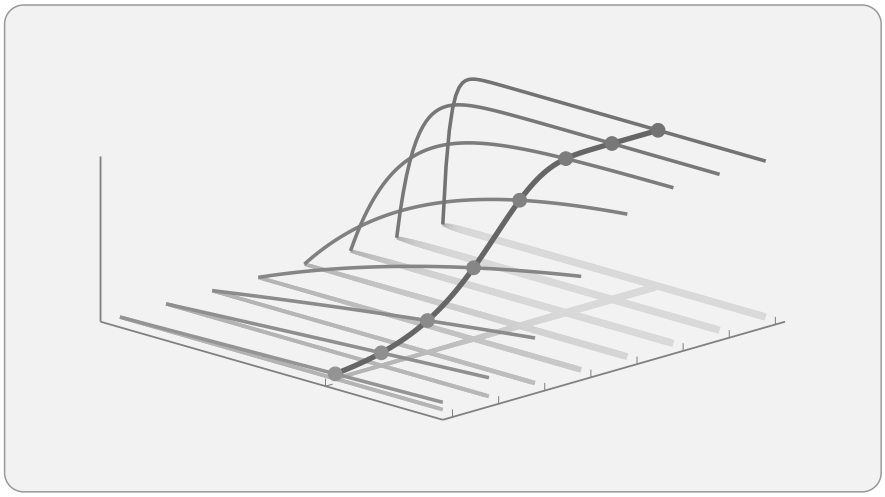

3.1 Experimental setting and antibody accumulation

Although mass-action kinetics/Langmuir kinetics are well established models for the description of antibody binding, they fail to describe the amount of antibodies that can be measured at the end of an antibody-staining experiment. Washing steps, which are usually performed in antibody-staining experiments, remove any unbound antibodies and thus constitute a perturbation of the system.

3.1.1 Abstract experimental setup

Before we can address the effect of washing steps, it is helpful to sketch the abstract experimental setting for antibody-staining experiments that we consider in this dissertation.

In general, we assume epitopes to be scattered over a 3-dimensional structure that is immobilized to the bottom of a container, e.g., a Petri dish or a well in a multi-well plate. This structure can be a biological sample, e.g., individual cells or tissue. Even non-biological structures that contain epitopes are permissible. However, to avoid naming all possibilities every time, we will generally refer to cells or (biological) samples in this dissertation, understanding that we include arbitrary 3-dimensional structures.

At time $t = 0$, an antibody solution is added to the container. The way in which the antibody solution is added to the container defines two scenarios that we have already discussed for the Langmuir model: the **depletion case** and the **reservoir case**. In the depletion case, a fixed volume of antibody solution is added to the container, such that the binding of antibodies decreases the concentration of unbound antibodies. In the reservoir case, a flow setup is used. Here, the antibody solution flows from a reservoir through the cell container, replenishing bound antibodies, as illustrated in Figure 3.1.

During the **incubation phase**, the antibody solution remains in contact with the cells for a certain time τ that we simply call **incubation time**. In the depletion case, the antibody solution simply remains untouched during the incubation phase, whereas the antibody solution continues to flow through the container in the reservoir case.

After the incubation phase, the container is **washed**. In the depletion case, this means that the antibody solution is exchanged for an antibody-free solution. This solution-exchange is then repeated several times with a fresh antibody-free solution. In the reservoir case, we may assume the same

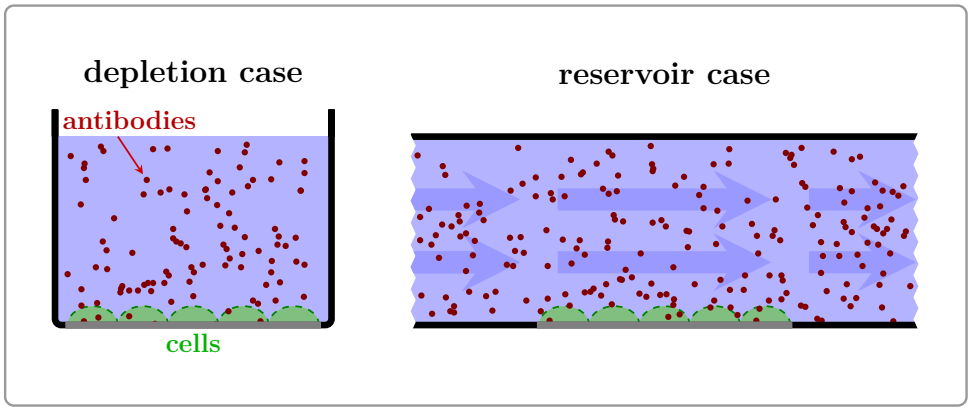

Figure 3.1: Illustration of the depletion case and the reservoir case of antibody-staining. The depletion case has a fixed number of antibodies in a finite volume, leading to a variable concentration of unbound antibodies. The reservoir case has a fixed concentration of unbound antibodies but an indefinite number of particles.

procedure to keep both systems comparable. However, in a real experiment it may be more convenient to switch reservoirs and have an antibody-free solution flowing through the container. Finally, the amount of bound antibodies is measured.

In this chapter, we consider a **homogeneous** antibody solution, where the individual antibody molecules are identical. The only exception is Section 3.3, where we explicitly focus on antibody mixtures. Furthermore, we do not consider comparisons between different antibody solutions in this chapter. We only describe a theoretical antibody solution. In that regard, it makes sense to speak about the binding properties of epitopes, although the binding behavior of antibodies is usually a combination of antibody and epitope properties.

Our main focus in this chapter is the mathematical description of antibody binding. Hence, we make the usual convenient assumptions that can be summarized as *idealized conditions* and neglect experimental limitations. For example, we assume that external parameters, such as temperature or pressure, remain constant and that neither antibodies nor epitopes denature. In addition, we assume that identical repetitions of experiments under exactly the same conditions are possible.

Remark 3.1.1 (**Antibody terminology**).
The term “antibody” can be slightly ambiguous. We will follow the

common practice of using the term “antibody” to specify the antibody type of an antibody solution, e.g., with phrases like “an antibody against ...”. On the other hand, “antibody” can refer to a single molecule. “Antibodies” could be misunderstood in a similar way (antibody types vs multiple individual antibodies).

Usually, the surrounding context will be sufficient to disambiguate the meaning. However, when an explicit disambiguation becomes necessary, we can use terms like “individual antibody” or “antibody types”, etc.

3.1.2 Antibody accumulation equations

So far, we have not assumed anything that completely invalidates the Langmuir model. There is just one assumption that cannot be maintained: binding sites on a flat surface.

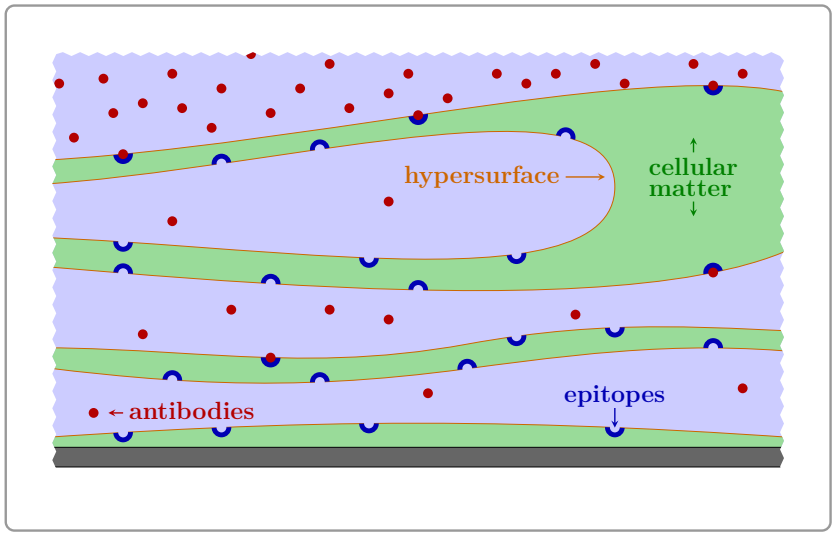

Figure 3.2: Illustration of the binding landscape in an antibody staining experiment. Epitopes are scattered on the hypersurface (orange) at the interface between cellular matter (green) and antibody solution (light blue).

Instead of a flat surface, epitopes are scattered throughout the cell. Nevertheless, the 3-dimensional cellular scaffold still defines a 2-dimensional hypersurface, given by the interface between the cellular matter and the antibody solution, as illustrated in Figure 3.2. In itself, the hypersurface is not

incompatible with the Langmuir model. However, unlike a flat surface, the location of an epitope on the hypersurface can influence its binding properties. For example, narrow cavities can limit the diffusion of antibodies, reducing the local antibody concentration. Thus, in order to use Langmuir kinetics, we must include the location of an epitope as an additional binding property. In consequence, structurally/biologically identical epitopes can have different binding properties.

Although Langmuir kinetics generally apply, there is an important detail that fundamentally distinguishes our experimental setting from the setting of the Langmuir model. The measurement is made after the incubation phase and after several washing steps that disrupt the system. This has two effects. First, the kinetics of the antibodies are not directly observable. Second, antibodies that can be measured/observed have bound semi-permanently to the epitopes. This does not exclude temporary binding of antibodies. But since temporary binding cannot be observed, we may regard all temporary events as obstructions that affect the semi-permanent binding. Hence, we set the desorption/unbinding rate constants $k_{\mathrm{d};i}$ to zero, leading to the following system of differential equations for the amount of bound antibodies:

$$\frac{d}{dt}x_i(t) = k_{\mathrm{a};i}a(t)(g_i - x_i(t)) \qquad \forall\, i \in \{1,\dots,N\}\ . \tag{3.1}$$

In the depletion case, the antibody concentration is given by

$$a(t) = a - \beta\sum_{i=1}^{N} x_i(t)\ ,$$

and in the reservoir case, it is given by $a(t) \equiv a$.

Remark 3.1.2 (**Concentration terminology**).
To avoid confusion between a and $a(t)$ when we speak about antibody concentration, let us adopt the following terminology. We call $a(t)$ **effective** antibody concentration and a **initial** antibody concentration.

Of course, there is no difference between the effective antibody concentration and the initial antibody concentration in the reservoir case.

Although (3.1) seems innocent enough, we need to be careful about the indices $i \in \{1,\dots,N\}$. Contrary to the Langmuir model, where the indices correspond to the binding-site type, the indices in (3.1) do not necessarily correspond to the epitope type in the biological sense. This is a consequence

of the hypersurface, where the location of an epitope can influence its binding properties.

Here, we can choose from one of two modeling approaches. We could consider **intrinsic rate constants**, that is, the rate constants that the isolated epitope would exhibit. Then, we would need to model the local antibody concentration (and other binding obstructions) explicitly. This would allow us to use the indices for the biological epitope type, but it would require more elaborate terms for the effective antibody concentration $a(t)$ in (3.1). Alternatively, we could consider the **apparent rate constant**, that is, the rate constant as it appears in the complex cellular environment. Then, we would distinguish epitopes solely based on their apparent rate constants, and the indices would no longer correspond to the biological type of an epitope.

The cellular landscape in an experiment is usually complex, varies from biological sample to biological sample, and depends on the specific experimental setup. Thus, it will be difficult, if not impossible, to model diffusion limitations in a general form; therefore, we prefer the apparent rate constant approach. In this way, we can also capture additional effects, such as the unobserved behavior of temporary binding or **avidity**, where multiple paratopes of the antibodies can bind independently of each other [Har+14; ET21]. Hence, we understand all rate constants to be apparent rate constants from now on and we define:

Definition 3.1.3 ({Adapted from [Theory-Preprint]}).
An **epitope class** (g, k_a) is a collection of epitopes with the same binding rate constant $k_\mathrm{a} > 0$, where $g > 0$ denotes the amount of epitopes.

The technical name "epitope class" is intended to avoid confusion with epitope type, reminding us that epitopes of the same class are identical in behavior, not in structure. The restrictions $g > 0$ and $k_\mathrm{a} > 0$ are necessary to avoid non-existent epitopes ($g = 0$) or structures where antibodies cannot bind ($k_\mathrm{a} \leq 0$).

We can summarize our description of antibody binding in antibody-staining experiments with the following initial value problems (**IVPs**).

Definition 3.1.4 ({Adapted from [Theory-Preprint]}).
Let $\{(g_i, k_{\mathrm{a};i})\}_{i=1}^{N}$ be epitope classes, let $a > 0$ be an initial antibody concentration, and let $\beta > 0$ be a depletion factor. Then we call the

initial value problem

$$\begin{cases} \dfrac{d}{dt}x_{\mathrm{R};i}(t) = k_{\mathrm{a};i}a(g_i - x_{\mathrm{R};i}(t)) \ , \\ \\ x_{\mathrm{R};i}(0) = 0 \end{cases} \qquad \forall\ i \in \{1, \dots, N\}$$

reservoir accumulation IVP and the initial value problem

$$\begin{cases} \dfrac{d}{dt}x_{\mathrm{D};i}(t) = k_{\mathrm{a};i}\left(a - \beta\sum_{j=1}^{N} x_{\mathrm{D};j}(t)\right)(g_i - x_{\mathrm{D};i}(t)) \ , \\ \\ x_{\mathrm{D};i}(0) = 0 \end{cases} \qquad \forall\ i \in \{1, \dots, N\}$$

depletion accumulation IVP.

Choosing the initial values $x_{\mathrm{R};i}(0) = 0$ and $x_{\mathrm{D};i}(0) = 0$ is motivated by the common setting of antibody-staining, where no antibodies are present in the system before the incubation phase begins. Furthermore, choosing $t_0 = 0$ for the initial value is convenient, as the incubation time τ then agrees with the endpoint of the time interval $[t_0, t_0 + \tau] = [0, \tau]$ for the incubation phase.

However, these choices do not restrict the generality of the model. First, there is no explicit time dependence in the equations. Thus, we can declare any time t_0 as zero point, even negative values. Second, detectable antibodies bind semi-permanently in antibody-staining experiments. Initially, bound antibodies just reduce the available epitopes and the initial concentration of unbound antibodies in the depletion case. Hence, positive initial values can be achieved by considering a suitably modified accumulation IVP. We simply let the system develop until the amounts of bound antibodies reach the desired initial values and choose this time point as the zero point t_0. The formal version of these arguments can be found in Appendix B.2.1.

Following the abstract description of the experimental setting, we measure the amount of bound antibodies after the incubation phase $[0, \tau]$ and the subsequent washing steps.

Definition 3.1.5 ({Adapted from [Theory-Preprint]}).
Let $\tau \geq 0$ denote an incubation time. If the reservoir accumulation IVP has a unique solution $x_{\mathrm{R}} \colon [0, \tau] \longrightarrow \mathbb{R}^N$ for all initial antibody concentrations $a \in I \subseteq \mathbb{R}_{>0}$, we call $a \mapsto x_{\mathrm{R}}(\tau; a)$ the **reservoir**

accumulation model over I. Furthermore, we call the function

$$a \longmapsto X_{\mathrm{R}}(a) \coloneqq X_{\mathrm{R}}(\tau; a) \coloneqq \sum_{i=1}^{N} x_{\mathrm{R};i}(\tau; a)$$

(reservoir accumulation) dose-response curve (over I).

The **depletion accumulation model** $a \mapsto x_{\mathrm{D}}(\tau; a)$ and the **(depletion accumulation) dose-response curve** $a \mapsto X_{\mathrm{D}}(a)$ are defined in the same way.

Following a common abuse of notation, we identify functions $x \mapsto f(x)$ with their expressions $f(x)$ and simply call $x_{\mathrm{R}}(a) \coloneqq x(\tau; a)$ the reservoir accumulation model, etc. Furthermore, note that we added the initial antibody concentration as an additional argument, separated by a semicolon. This semicolon is quite important because it reminds us that the initial antibody concentration is only a parameter of the accumulation IVPs. It merely selects an initial value problem from a family of initial value problems, whose solutions are always functions of time. Thus, we should vary the initial antibody concentration only in one of two cases. First, before considering the time development, i.e., as a selection of the concrete IVP. Second, after the incubation time τ, when the time development is completed. This matches the experimental procedure, where a condition is prepared before the antibody is incubated. Different conditions are then compared after all incubation phases have been completed.

Remark 3.1.6 (**Why dose-response curves?**).
Since the measurement principle of antibody-staining precludes a direct observation of the time development, there remain only two ways to probe a system of interest in the context of the accumulation model. We can vary the incubation time, or we can vary the initial antibody concentration (or a combination of both). In practice, initial antibody concentrations are more convenient, as different cell samples allow for parallel staining experiments with different initial antibody concentrations (see Subsection 4.1.4).

Based on the definition of dose-response curves, we might also define the total amount of epitopes, irrespective of their class.

Definition 3.1.7.
Let $\{(g_i, k_{\mathrm{a};i})\}_{i=1}^{N}$ be epitope classes, then we denote the **total amount of epitopes** by

$$G := \sum_{i=1}^{N} g_i \ .$$

Let us conclude our discussion of the definitions with an important detail that could easily be overlooked: the uniqueness of solutions. The uniqueness ensures that an initial state suffices to predict the behavior of the system. Otherwise, external selection criteria would be necessary to select one of the possible solutions. Fortunately, this will not be necessary, as the accumulation IVPs belong to a class of initial value problems that always have a unique local solution.

Proposition 3.1.8 (cf. [Wal98, chapter III, §10, XI])**.**
Let $X \subset \mathbb{R}^n$ be open and $f\colon X \longrightarrow \mathbb{R}^n$ be locally Lipschitz continuous. Then the initial value problem

$$\frac{d}{dt}x(t) = f(x(t)) \ , \qquad x(t_0) = x_0$$

has a unique solution $x\colon (a,b) \to \mathbb{R}$ on a maximal open interval (a,b) around t_0. If $x([t_0,b)) \subset K \subset X$, where K is compact, then there is a unique solution

$$y\colon (a,\infty) \longrightarrow \mathbb{R}^n$$

for the initial value problem with $x(t) = y(t)$ for $t \in (a,b)$.

Essentially, this proposition summarizes the properties of autonomous systems given in [Wal98, chapter III, §10, XI]. Unfortunately, [Wal98] does not provide detailed proofs for the multidimensional case. However, the steps of [Wal98, chapter II, §6] should mostly carry over. Alternatively, see [Hir+04, section 17.4].

To apply the last proposition, we need to show that the accumulation IVPs are locally Lipschitz continuous autonomous systems.

Lemma 3.1.9 ({Adapted from [Theory-Preprint]}).
The accumulation IVPs are autonomous systems of the from

$$\frac{d}{dt}x_{\mathrm{R}}(t) = f(x_{\mathrm{R}}(t)) \quad \textit{and} \quad \frac{d}{dt}x_{\mathrm{D}}(t) = h(x_{\mathrm{D}}(t)) \ ,$$

where $f, h\colon \mathbb{R}^N \to \mathbb{R}^N$ *are locally Lipschitz continuous on* $\mathbb{R}^N$.

Proof 3.1.10 ({Adapted from [Theory-Preprint]}).
By definition of the accumulation IVPs (Definition 3.1.4), we have

$$f(x) = \begin{pmatrix} k_{\mathrm{a};1}a(g_1 - x_1) \\ \vdots \\ k_{\mathrm{a};N}a(g_N - x_N) \end{pmatrix}$$

and

$$h(x) = \begin{pmatrix} k_{\mathrm{a};1}\left(a - \beta\sum_{j=1}^{N} x_j\right)(g_1 - x_1) \\ \vdots \\ k_{\mathrm{a};N}\left(a - \beta\sum_{j=1}^{N} x_j\right)(g_N - x_N) \end{pmatrix} .$$

Since all components f_i and h_i of f and h are polynomials, continuity of the components as well as the existence and continuity of all partial derivatives $\frac{\partial}{\partial x_j}f_i(x)$ and $\frac{\partial}{\partial x_j}h_i(x)$ are obvious. The local Lipschitz continuity of the components now follows from [Wal98, chapter III, §10, Lemma V]. □

3.1.3 Interpretations and immediate consequences

Before we attempt to derive the mathematical properties of the accumulation IVPs, e.g., the global existence of unique solutions, we may first consider some qualitative aspects.

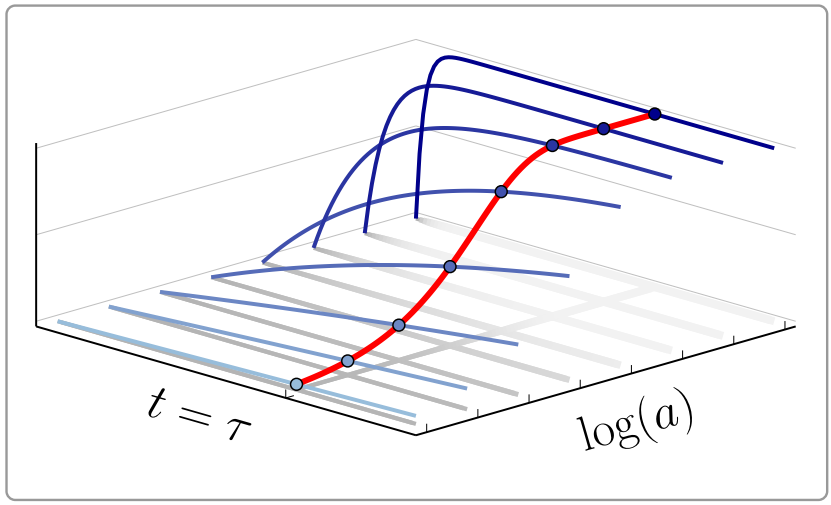

Figure 3.3: Illustration of the accumulation principle. Higher initial antibody concentrations (darker shade of blue) accumulate faster than lower initial antibody concentrations (lighter shade of blue), leading to larger amounts of bound antibodies after the incubation time τ. Considering the dependence of the amount of bound antibodies at $t = \tau$ on the initial antibody concentration a yields the dose-response behavior (red curve).

Accumulation principle

As the name suggests, the accumulation IVPs describe the accumulation of antibodies on the hypersurface of the cellular scaffold. In that regard, we may understand the antibody concentration as a binding pressure. This binding pressure (together with the binding constants) determines the rate at which antibodies accumulate on the cellular hypersurface. Thus, if everything else is identical, higher initial antibody concentrations will lead to larger amounts of antibodies that bind for a given incubation time τ. Figure 3.3 illustrates the dose-response behavior as a consequence of the antibody-concentration-dependent accumulation rate and the finite incubation time, which we call **accumulation principle** for short.

In fact, Figure 3.3 also suggests another important aspect of the accumulation principle: incomplete binding levels. For dose-response behavior that is supposed to convey information about the epitope landscape (and the antibody), the system must not reach complete epitope coverage $X(\tau) = G$ (saturation) or complete antibody depletion $X(\tau) = \beta^{-1}a$ in the depletion case. If that were to happen, the resulting **depletion/saturation curves**

would be

$$\begin{cases} Y_{\mathrm{R}}(a) = G = \sum_{i=1}^{N} g_i & \text{in the reservoir case ,} \\ Y_{\mathrm{D}}(a) = \min\{\beta^{-1}a, G\} & \text{in the depletion case .} \end{cases}$$

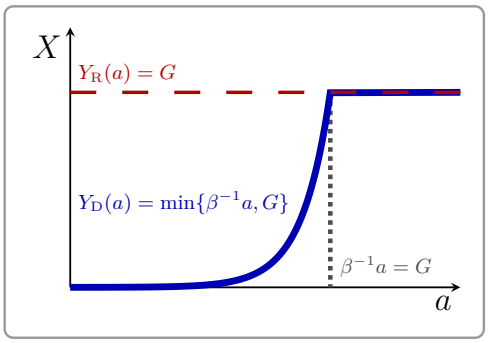

Figure 3.4: Illustration of depletion/saturation curves of the accumulation model.

Neither Y_{R} nor Y_{D} produce sensible dose-response curves, as the curves are independent of the binding properties of the epitopes (see Figure 3.4 for an illustration). Hence, depletion/saturation curves should be avoided if the goal is to learn something about the antibody-staining system.

Figure 3.3 shows another important property of the accumulation principle. When the accumulation principle applies, both the incubation time τ and the initial antibody concentration a should affect the resulting amount of bound antibodies. Increasing the initial antibody concentration and increasing the incubation time should both result in larger amounts of bound antibodies. However, initial antibody concentration and incubation time have different side effects, as we will argue below.

Random walk interpretation

The accumulation IVPs describe antibody accumulation on a macroscopic scale. Nevertheless, we may speculate about the microscopic behavior to obtain some qualitative predictions.

On the microscopic scale, movement is affected by Brownian motion [Phi+12, Section 3.4.2], adding a random component to the movement of antibodies. Thus, antibody trajectories are not deterministic from a macroscopic perspective. Nevertheless, electrostatic forces might induce directed movement. However, the presence of multiple epitopes and antibodies, not to mention the countless charges in the surrounding structures, makes long-range targeted movement of antibodies unlikely. Hence, random-walk motion is a good

approximation for the large-scale movement of antibodies. Then, when the antibodies reach proximity to epitopes, the attractive forces between epitope and paratope, which facilitate binding, can dominate the antibody movement.

Using the random-walk assumption for the movement of antibodies, we can compare the effects of incubation time and initial antibody concentration. For this purpose, let us assume that we have performed an antibody-staining experiment and that we want to increase the amount of bound antibodies in a subsequent staining experiment. Of course, we consider a scenario in which neither all antibodies bind (in the depletion case) nor all epitopes are bound, which would obviously prevent larger amounts of bound antibodies.

To increase the amount of bound antibodies in the second experiment, we have two options. First, we could use higher initial antibody concentrations. Second, we could use longer incubation times. Clearly, increasing the initial antibody concentration leads to different effects than increasing the incubation time, which is especially obvious for the depletion case. Increasing the initial antibody concentration means that more antibodies remain in the system after a given amount has bound, thus maintaining a higher antibody concentration. Increasing the incubation time, on the other hand, only prolongs the random-walk movement of a smaller concentration of unbound antibodies.

Taking into account the unobserved behavior of antibody binding, we find that increasing the antibody concentration differs from increasing the incubation time, even for the reservoir case, where the amount of unbound antibodies remains constant. Recall that we observe only the semi-permanently bound antibodies at the end, which does not rule out temporary binding during the incubation phase. This temporary binding can affect the semi-permanent binding, as acknowledged by the apparent rate constants. For example, antibodies can get trapped by weak epitopes, which we understand as epitopes that only allow temporary binding of antibodies.

Especially for low antibody concentrations, the majority of antibodies might only hop from one weak epitope to another before reaching an epitope that facilitates semi-permanent binding. In the worst case, longer incubation times would only prolong the hopping between weak epitopes, but not necessarily increase the amount of semi-permanently bound antibodies. In contrast, increasing the initial antibody concentration could saturate the weak epitopes, such that antibodies can reach the epitopes that allow for semi-permanent binding.

Interestingly, the difference between increasing the antibody concentration and increasing the incubation time also affects the proportions in which antibodies bind to the different epitope classes. To understand this difference,

let us consider an epitope E^* in a deep cavity of the cellular scaffold. Let us also assume that there are many other epitopes E_i of the same biological type along the way to E^*. Since a path to epitope E^* needs to get past many epitopes E_i, a trajectory that leads to E^* is more specific and less likely to occur due to a random walk. In other words, the epitopes E_i are more accessible than the epitope E^*. See Figure 3.5 for an illustration.

If we increase the incubation time, we increase the possible length of the random walk. However, this does not increase the chance of binding to the epitope E^* over the chance of binding to the epitopes E_i. An antibody must still follow a few specific trajectories that all stay clear of the epitopes E_i in order to bind to the epitope E^*. Increasing the antibody concentration, on the other hand, increases the number of antibodies in the system. These additional antibodies can clog the epitopes E_i, such that another antibody can reach the epitope E^* through simpler trajectories, which increases the likelihood of an antibody binding to the epitope E^*.

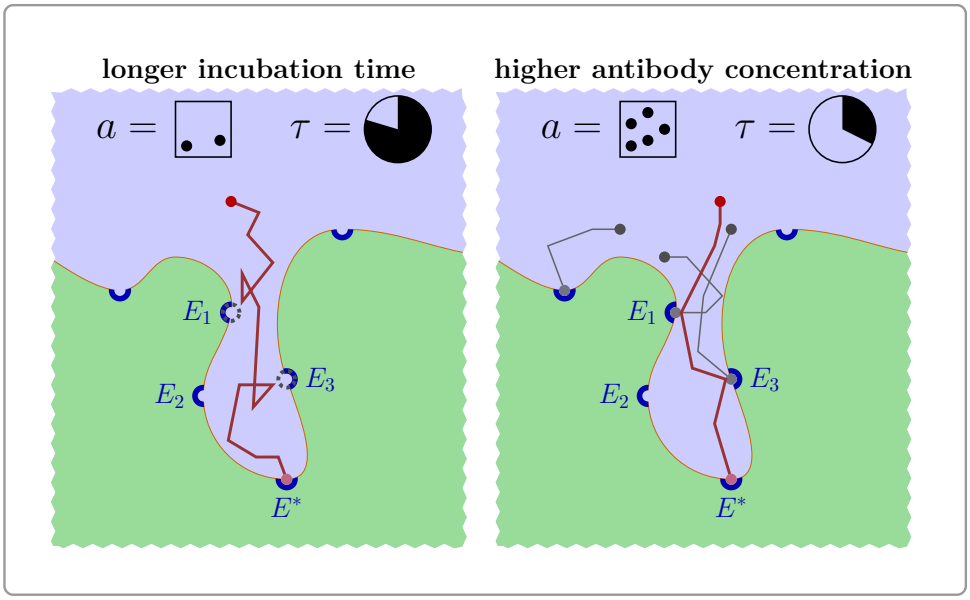

Figure 3.5: Both, increasing the incubation time and increasing the initial antibody concentration, can increase the amount of bound antibodies after the incubation phase. However, increasing the incubation time primarily increases binding to accessible epitopes, as random walks to inaccessible epitopes are highly unlikely. Increasing the initial antibody concentration will fill up accessible epitopes, such that trajectories to less accessible epitopes become simpler and thus more probable.

In summary, increasing the incubation time will primarily lead to more antibodies binding to accessible epitopes. In contrast, increasing the initial antibody concentration will also facilitate binding to less accessible epitopes. Hence, compensating for short incubation times with higher initial antibody concentrations reduces the difference between accessible and less accessible epitopes.

Remark 3.1.11 (**Epitope accessibility**).
In our random-walk example, epitope classes arose from the locations of identical epitopes. Of course, biologically different epitopes can also lead to distinct epitope classes. Unfortunately, we will not be able to detect the reasons for distinct epitope classes with dose-response curves.

Nevertheless, the term "*accessibility*" is well motivated as a name for the effects that determine the apparent rate constant k_a of an epitope. Not only does it cater to the location aspect, but it is also fitting figuratively for the description of any effect that promotes or hinders the binding of an antibody.

3.2 Properties of the accumulation equations

In the reservoir case, the epitopes do not compete for the available antibodies, so the reservoir accumulation IVP decouples into independent differential equations

$$\frac{d}{dt}x_{\mathrm{R};i}(t) = k_{\mathrm{a};i}a(g_i - x_{\mathrm{R};i}(t)) \qquad \forall\, i \in \{1,\dots,N\}\ .$$

This allows us to solve the differential equations individually for each epitope class. Using Proposition 3.1.8 and Lemma 3.1.9 we find, that

$$x_{\mathrm{R};i}(t) = g_i(1 - e^{-k_{\mathrm{a};i}at}) \qquad \forall\, i \in \{1,\dots,N\} \tag{3.2}$$

defines the unique solution of the reservoir accumulation IVP for all $t \geq 0$. Because of the closed-form expression, we can easily see that the solution has the following properties.

Remark 3.2.1 (**Reservoir accumulation properties**).
The following properties hold for all epitope class configurations $\{(g_i, k_{\mathrm{a};i})\}_{i=1}^N$, all initial antibody concentrations $a > 0$, and all in-

cubation times $\tau > 0$.

Unique global solution

The reservoir accumulation IVP has a unique solution

$$x_{\mathrm{R}} \colon [0, \infty) \to \mathbb{R}^N, \qquad t \mapsto x_{\mathrm{R}}(t; a) \ .$$

Accumulation principle

Antibodies accumulate over time:

$$\frac{d}{dt} x_{\mathrm{R};i}(t) \geq 0 \qquad \forall\ t \geq 0 \ .$$

Natural bounds

The amount of bound antibodies cannot exceed the amount of epitopes:

$$0 \leq x_{\mathrm{R};i}(\tau; a) \leq g_i \qquad \Rightarrow \qquad 0 \leq X_{\mathrm{R}}(\tau; a) \leq G \ .$$

Natural dose-response behavior

Higher initial antibody concentrations imply larger amounts of bound antibodies,

$$\frac{d}{da} x_{\mathrm{R};i}(\tau; a) \geq 0 \qquad \Rightarrow \qquad \frac{d}{da} X_{\mathrm{R}}(\tau; a) \geq 0 \ .$$

Limit behavior

Without antibodies, no binding occurs,

$$\lim_{a \to 0} x_{\mathrm{R};i}(\tau; a) = 0 \qquad \Rightarrow \qquad \lim_{a \to 0} X_{\mathrm{R}}(\tau, a) = 0 \ ,$$

and for an infinitely high initial antibody concentration, epitope saturation is reached,

$$\lim_{a \to \infty} x_{\mathrm{R};i}(\tau; a) = g_i \qquad \Rightarrow \qquad \lim_{a \to \infty} X_{\mathrm{R}}(\tau; a) = G \ .$$

3.2.1 Depletion accumulation IVP

The competition among the epitope classes for the available antibodies, i.e., the term

$$a - \beta \sum_{j=1}^{N} x_{\mathrm{D};j}(t) \ ,$$

leads to a system of coupled differential equations

$$\frac{d}{dt} x_{\mathrm{D};i}(t) = k_{\mathrm{a};i} \left(a - \beta \sum_{j=1}^{N} x_{\mathrm{D};j}(t) \right) (g_i - x_{\mathrm{D};i}(t)) \qquad \forall\ i \in \{1, \dots, N\} \ ,$$

for the depletion accumulation IVP. Hence, we cannot simply solve the differential equations for the epitope classes independently. In fact, we will not even be able to obtain a closed-form solution.

To overcome the difficulties of the coupling, let us imagine that we can control the effective antibody concentration. So, instead of just keeping the effective antibody concentration constant, we can arrange for every continuous function $a(t)$. In this scenario, the equations decouple into

$$\frac{d}{dt} x_i(t) = k_{\mathrm{a};i} a(t)(g_i - x_i(t)) \qquad \forall\ i \in \{1, \dots, N\} \ ,$$

and the solution for the initial values $x_{\mathrm{D};i}(0) = 0$ becomes

$$x_i(t) = g_i(1 - e^{-k_{\mathrm{a};i} A(t)}) \ , \qquad \text{where} \qquad A(t) = \int_0^s a(s)\ ds \ , \tag{3.3}$$

for all $i \in \{1, \dots, N\}$.

Intuitively, we may understand the term $A(t)$ as the accumulated effect of the effective antibody concentration over time. Hence, we may define:

Definition 3.2.2 ({Adapted from [Theory-Preprint]}).
Let $\alpha \colon [0, \infty) \to \mathbb{R}_{\geq 0},\ t \mapsto \alpha(t)$ with $\alpha(0) > 0$ be a continuous function that describes the effective antibody concentration for an accumulation IVP. Then we call

$$A(t) \coloneqq \int_0^t \alpha(s)\ ds$$

the **cumulative antibody concentration**.

Note that we introduce the notation $\alpha(t)$ for the effective antibody concentration, because we need to avoid notation conflicts when we use the initial

antibody concentration as an additional argument of the effective antibody concentration, i.e., $\alpha(t; a)$.

The guiding principle for this subsection will now be to use the solution shape (3.3), where the effective antibody concentration is given by the depletion accumulation term

$$\alpha(t) \coloneqq a - \beta \sum_{j=1}^{N} x_{\mathrm{D};j}(t) \ .$$

In this way, we can derive the properties of the depletion accumulation IVP without a closed-form solution.

Although our approach seems quite intuitive, we must be careful about the coupling of the equations, which can easily be overlooked in the abstract notation $\alpha(t)$ and $A(t)$. In fact, we even have to show that the solution shape (3.3) is valid for the system of coupled equations.

Because of Proposition 3.1.8 and Lemma 3.1.9, we already know that the depletion accumulation IVP has a unique solution on $[0, T)$ for a maximal $T > 0$. Let us call this maximal $T > 0$ the **maximal existence time** of the depletion accumulation IVP. Of course, the maximal existence time depends on the initial antibody concentration a, the epitope classes $\{(g_i, k_{\mathrm{a};i})\}_{i=1}^{N}$, and the depletion factor β:

$$T = T(a, \{(g_i, k_{\mathrm{a};i})\}_{i=1}^{N}, \beta) \ .$$

However, to avoid unnecessarily long terms, we suppress the dependencies in the notation and simply write T in the following. Eventually, we will even show that $T = \infty$ for all epitope classes, all depletion factors $\beta > 0$, and all initial antibody concentrations $a > 0$.

Theorem 3.2.3 ({Adapted from [Theory-Preprint]}).
Let $\{(g_i, k_{\mathrm{a};i})\}_{i=1}^{N}$ be epitope classes, $a > 0$ be an initial antibody concentration, $\beta > 0$ be a depletion factor, and let $T > 0$ be the corresponding maximal existence time. A vector-valued function $v\colon [0, T) \to \mathbb{R}^N$ with $v(0) = 0$ is the solution of the corresponding depletion accumulation IVP if and only if its components satisfy the integral equations

$$v_i(t) = g_i \left(1 - e^{-k_{\mathrm{a};i} \int_0^t \left(a - \beta \sum_{j=1}^{N} v_j(s) \right) \, ds} \right)$$

for all $i \in \{1, \ldots, N\}$.

Proof 3.2.4 ({Adapted from [Theory-Preprint]}).
Let $v\colon [0,T) \to \mathbb{R}^N$ be a vector-valued function with $v(0) = 0$ that satisfies the integral equations

$$v_i(t) = g_i \left(1 - e^{-k_{\mathrm{a};i} \int_0^t \left(a - \beta \sum_{j=1}^N v_j(s)\right)\, ds}\right)$$

for all $i \in \{1, \dots, N\}$.

For the time derivatives of the components we calculate

$$\begin{aligned}
\frac{d}{dt} v_i(t) &= k_{\mathrm{a};i} g_i e^{-k_{\mathrm{a};i} \int_0^t \left(a - \beta \sum_{j=1}^N v_j(s)\right)\, ds} \; \frac{d}{dt} \int_0^t \left(a - \beta \sum_{j=1}^N v_j(s)\right) ds \\
&= k_{\mathrm{a};i} \left(a - \beta \sum_{j=1}^N v_j(t)\right) g_i e^{-k_{\mathrm{a};i} \int_0^t \left(a - \beta \sum_{j=1}^N v_j(s)\right) ds} \\
&= k_{\mathrm{a};i} \left(a - \beta \sum_{j=1}^N v_j(t)\right) \left(g_i - g_i \left(1 - e^{-k_{\mathrm{a};i} \int_0^t \left(a - \beta \sum_{j=1}^N v_j(s)\right) ds}\right)\right) \\
&= k_{\mathrm{a};i} \left(a - \beta \sum_{j=1}^N v_j(t)\right) (g_i - v_i(t)) \quad ,
\end{aligned}$$

where we have used $v_i(t) = g_i\left(1 - e^{-k_{\mathrm{a};i} \int_0^t \left(a - \beta \sum_{j=1}^N v_j(s)\right) ds}\right)$ in the last step. Thus, v solves the depletion accumulation IVP.

Let now $y\colon [0,T) \to \mathbb{R}^N$ solve the depletion accumulation IVP. Because of the uniqueness of the solution, it follows that $y(t) = v(t)$ for all $t \in [0,T)$. But then y also satisfies the integral equations. □

Given the integral equation shape, we can prove the *Accumulation principle* of Remark 3.2.1 for the depletion accumulation IVP. However, because of the coupling between the integral equations, we need to prove a small technical property first.

Lemma 3.2.5 ({Adapted from [Theory-Preprint]}).
Let $\{(g_i, k_{\mathrm{a};i})\}_{i=1}^{N}$ be epitope classes, $a > 0$ be an initial antibody concentration, $\beta > 0$ be a depletion factor, and let $T > 0$ be the corresponding maximal existence time. Furthermore, let $x_{\mathrm{D}} \colon [0, T) \to \mathbb{R}^N$ denote the unique solution of the corresponding depletion accumulation IVP. Then the following equivalence relations hold for all times $t \in [0, T)$:

$$\begin{aligned} \exists\, i \in \{1, \dots, N\} \colon \quad & \frac{d}{dt} x_{\mathrm{D};i}(t) = 0 \\ \Leftrightarrow \quad & \frac{d}{dt} x_{\mathrm{D};i}(t) = 0 \quad \forall\, i \in \{1, \dots, N\} \end{aligned}$$

and

$$\begin{aligned} \exists\, i \in \{1, \dots, N\} \colon \quad & \frac{d}{dt} x_{\mathrm{D};i}(t) > 0 \\ \Leftrightarrow \quad & \frac{d}{dt} x_{\mathrm{D};i}(t) > 0 \quad \forall\, i \in \{1, \dots, N\}\ . \end{aligned}$$

Proof 3.2.6 ({Adapted from [Theory-Preprint]}).
We only show the first case, $\frac{d}{dt} x_{\mathrm{D};i}(t) = 0$, as all steps and arguments will be the same for the second case, $\frac{d}{dt} x_{\mathrm{D};i}(t) > 0$.

First, we observe that the direction "$\Leftarrow$" is trivial. For the opposite direction, assume that $\frac{d}{dt} x_{\mathrm{D};i}(t) = 0$ for an arbitrary $i \in \{1, \dots, N\}$. Because of Theorem 3.2.3, the function $x_{\mathrm{D};i}$ satisfies the integral equation

$$x_{\mathrm{D};i}(t) = g_i \left(1 - e^{-k_{\mathrm{a};i} \int_0^t \left(a - \beta \sum_{j=1}^{N} x_{\mathrm{D};j}(s) \right) ds} \right)\ .$$

In the proof of Theorem 3.2.3, we have already calculated that we can express the derivative as

$$\frac{d}{dt} x_{\mathrm{D};i}(t) = k_{\mathrm{a};i} \left(a - \beta \sum_{j=1}^{N} x_{\mathrm{D};j}(t) \right) g_i e^{-k_{\mathrm{a};i} \int_0^t \left(a - \beta \sum_{j=1}^{N} x_{\mathrm{D};j}(s) \right) ds}\ .$$

Since all $x_{\mathrm{D};j}(t)$ are differentiable, and thus continuous on $[0, T)$, it

follows that $s \mapsto x_{\mathrm{D};j}(s)$ is bounded on $[0,t]$ for all $j \in \{1,\dots,N\}$. So,

$$\int_0^t \left(a - \beta \sum_{j=1}^{N} x_{\mathrm{D};j}(s) \right) ds$$

is finite and

$$e^{-k_{\mathrm{a};i} \int_0^t \left(a - \beta \sum_{j=1}^{N} x_{\mathrm{D};j}(s) \right) ds}$$

is positive. By Definition 3.1.4, all g_i and $k_{\mathrm{a};i}$ are also positive. Hence, the condition $\frac{d}{dt} x_{\mathrm{D};i}(t) = 0$ leads to

$$0 = \frac{dx_{\mathrm{D};i}}{dt}(t) = k_{\mathrm{a};i} \left(a - \beta \sum_{j=1}^{N} x_{\mathrm{D};j}(t) \right) g_i e^{-k_{\mathrm{a};i} \int_0^t \left(a - \beta \sum_{j=1}^{N} x_{\mathrm{D};j}(s) \right) ds}$$

$$\Rightarrow \qquad 0 = a - \beta \sum_{j=1}^{N} x_{\mathrm{D};j}(t) \ .$$

Finally, we note that $0 = a - \beta \sum_{j=1}^{N} x_{\mathrm{D};j}(t)$ is not a condition for a specific i, but applies to all $i \in \{1,\dots,N\}$. That is, let $\ell \in \{1,\dots,N\}$ be arbitrary. Then, since $0 = a - \beta \sum_{j=1}^{N} x_{\mathrm{D};j}(t)$, it follows that

$$\frac{d}{dt} x_{\mathrm{D};\ell}(t) = k_{\mathrm{a};\ell} \left(a - \beta \sum_{j=1}^{N} x_{\mathrm{D};j}(t) \right) g_\ell e^{-k_{\mathrm{a};\ell} \int_0^t \left(a - \beta \sum_{j=1}^{N} x_{\mathrm{D};j}(s) \right) ds} = 0 \ .$$

Thus, $\frac{d}{dt} x_{\mathrm{D};i}(t) = 0$ for all $i \in \{1,\dots,N\}$, which concludes the proof. □

Before we can prove the property of interest, we need to recall a simple property from calculus: Positive derivatives imply that a positive function remains positive.

$$\left.\begin{array}{l} f(a) \geq 0 \\ \frac{d}{dt} f(t) > 0 \quad \forall\ t \in [a,T) \end{array}\right\} \quad \Rightarrow \quad \left\{\begin{array}{ll} f(t) > 0 & \forall t \in (a,T) \ , \\ f(t) \geq 0 & \forall t \in [a,T) \ . \end{array}\right. \tag{3.4}$$

A formal statement and a proof can be found in Appendix B.2.2.

Theorem 3.2.7 ({Adapted from [Theory-Preprint]}).
Let $\{(g_i, k_{\mathrm{a};i})\}_{i=1}^N$ be epitope classes, $a > 0$ be an initial antibody concentration, $\beta > 0$ be a depletion factor and let $T > 0$ be the corresponding maximal existence time. Furthermore, let $x_{\mathrm{D}} \colon [0, T) \to \mathbb{R}^N$ denote the unique solution of the corresponding depletion accumulation IVP. Then

$$\frac{d}{dt} x_{\mathrm{D};i}(t) > 0 \qquad \forall\, t \in [0, T) \ , \quad \forall\, i \in \{1, \dots, N\} \ .$$

Proof 3.2.8 ({Adapted from [Theory-Preprint]}).
From the differential equations of the depletion accumulation IVP,

$$\frac{d}{dt} x_{\mathrm{D};i}(t) = k_{\mathrm{a};i} \left(a - \beta \sum_{j=1}^{N} x_{\mathrm{D};j}(t) \right) (g_i - x_{\mathrm{D};i}(t)) \ ,$$

and the initial value $x_{\mathrm{D}}(0) = 0$, it follows that

$$\frac{dx_{\mathrm{D};i}}{dt}(0) = k_{\mathrm{a};i} a g_i > 0 \qquad \forall\, i \in \{1, \dots, N\} \ .$$

Assume now, that there is a $t_- \in (0, T)$ such that $\frac{dx_{\mathrm{D};i}}{dt}(t_-) \leq 0$ for an arbitrary $i \in \{1, \dots, N\}$. Because of the continuity of $\frac{d}{dt} x_{\mathrm{D};i}(t)$, which follows from the continuity of the right-hand side of the differential equations, our assumption implies that there is a t_0 with $0 < t_0 \leq t_-$, for which $\frac{dx_{\mathrm{D};i}}{dt}(t_0) = 0$. Lemma 3.2.5 now yields $\frac{dx_{\mathrm{D};i}}{dt}(t_0) = 0$ for all $i \in \{1, \dots, N\}$.

Since the depletion accumulation IVP is an autonomous system with a locally Lipschitz continuous map, general properties of autonomous systems [Wal98, Chapter III, §10, XI] would then imply that $x_{\mathrm{D}}(t) \equiv 0$. However, $\frac{dx_{\mathrm{D};i}}{dt}(0) > 0$ and (3.4) imply that there is an $\varepsilon > 0$ such that $x_{\mathrm{D};i}(\varepsilon) > 0$. This is a contradiction. Hence, there is no t_0 for which any $\frac{dx_{\mathrm{D};i}}{dt}(t_0) = 0$, and thus $\frac{d}{dt} x_{\mathrm{D};i}(t) > 0$ for all $t \in [0, T)$, and for all $i \in \{1, \dots, N\}$. □

The last theorem suffices to prove the *Natural bounds* of Remark 3.2.1 for the depletion accumulation IVP.

Theorem 3.2.9 ({Adapted from [Theory-Preprint]}).
Let $\{(g_i, k_{\mathrm{a};i})\}_{i=1}^N$ be epitope classes, $a > 0$ be an initial antibody concentration, $\beta > 0$ be a depletion factor, and let $T > 0$ be the corresponding maximal existence time. Furthermore, let $x_{\mathrm{D}} \colon [0, T) \to \mathbb{R}^N$ denote the unique solution of the corresponding depletion accumulation IVP and let G denote the total amount of epitopes. Then

$$0 \leq x_{\mathrm{D};i}(t) < \min\{\beta^{-1}a, g_i\} \qquad \text{and} \qquad 0 \leq \sum_{j=1}^{N} x_{\mathrm{D};j}(t) < \min\{\beta^{-1}a, G\}$$

for all times $t \in [0, T)$ and all $i \in \{1, \ldots, N\}$.

Proof 3.2.10 ({Adapted from [Theory-Preprint]}).
Since x_{D} solves the depletion accumulation IVP, we have $x_{\mathrm{D}}(0) = 0$. Furthermore, according to Theorem 3.2.7, $\frac{d}{dt} x_{\mathrm{D};i}(t) > 0$ for all $t \in [0, T)$ and all $i \in \{1, \ldots, N\}$. Thus, because of (3.4), it follows that

$$0 \leq x_{\mathrm{D};i}(t) \qquad \forall\, t \in [0, T)\ , \quad \forall\, i \in \{1, \ldots, N\}\ .$$

By Theorem 3.2.3 and the corresponding proof, we have

$$\frac{d}{dt} x_{\mathrm{D};i}(t) = k_{\mathrm{a};i} \left(a - \beta \sum_{j=1}^{N} x_{\mathrm{D};j}(t) \right) g_i e^{-k_{\mathrm{a};i} \int_0^t \left(a - \beta \sum_{j=1}^{N} x_{\mathrm{D};j}(s) \right) ds}$$

for all $t \in [0, T)$ and all $i \in \{1, \ldots, N\}$. Theorem 3.2.7 implies $\frac{d}{dt} x_{\mathrm{D};i}(t) > 0$, such that

$$0 < a - \beta \sum_{j=1}^{N} x_{\mathrm{D};j}(t) \quad \Rightarrow \quad \sum_{j=1}^{N} x_{\mathrm{D};j}(t) < \beta^{-1} a\ .$$

At the beginning of the proof, we have already proven that the sum consists only of non-negative values, i.e., $0 \leq x_{\mathrm{D};i}(t)$. Thus, it also follows that

$$x_{\mathrm{D};i}(t) < \beta^{-1} a \quad \forall\, i \in \{1, \ldots, N\}\ .$$

It remains to show that $x_{\mathrm{D};i}(t) < g_i$. Since x_{D} solves the depletion accumulation IVP,

$$\frac{d}{dt} x_{\mathrm{D};i}(t) = k_{\mathrm{a};i} \left(a - \beta \sum_{j=1}^{N} x_{\mathrm{D};j}(t) \right) (g_i - x_{\mathrm{D};i}(t))$$

holds for all $i \in \{1, \dots, N\}$. Since

$$\frac{d}{dt} x_{\mathrm{D};i}(t) > 0 \qquad \text{and} \qquad a - \beta \sum_{j=1}^{N} x_{\mathrm{D};j}(t) > 0 \ ,$$

it follows that $g_i - x_{\mathrm{D};i}(t) > 0$, which is equivalent to $x_{\mathrm{D};i}(t) < g_i$.

Finally, summing over all epitope classes, the inequality becomes

$$\sum_{i=1}^{N} x_{\mathrm{D};i}(t) \leq \sum_{i=1}^{N} g_i = G \ .$$

□

Because of Proposition 3.1.8, the global existence and uniqueness of a solution for the depletion accumulation IVP is merely a corollary of the last theorem.

Corollary 3.2.11 ({Adapted from [Theory-Preprint]}).
For all epitope class configurations $\{(g_i, k_{\mathrm{a};i})\}_{i=1}^{N}$, all initial antibody concentrations $a > 0$, and all depletion factors $\beta > 0$, there exists a unique solution $x_{\mathrm{D}} \colon [0, \infty) \to \mathbb{R}^N$ for the corresponding depletion accumulation IVP. That is, the maximal existence time is $T = \infty$.

There is a second, simple corollary that will help us prove the *Natural dose-response behavior* of Remark 3.2.1 for the depletion accumulation IVP.

Corollary 3.2.12 ({Adapted from [Theory-Preprint]}).
Let $x_{\mathrm{D}} \colon [0, \infty) \to \mathbb{R}^N$ be the unique solution of a depletion accumulation IVP. Then the components $x_{\mathrm{D};i} \colon [0, \infty) \to \mathbb{R}$ are strictly concave.

Proof 3.2.13 ({Adapted from [Theory-Preprint]}).
As a solution of the depletion accumulation IVP, the components of x_{D} satisfy

$$\frac{d}{dt} x_{\mathrm{D};i}(t) = k_{\mathrm{a};i} \left(a - \beta \sum_{j=1}^{N} x_{\mathrm{D};j}(t) \right) (g_i - x_{\mathrm{D};i}(t)) \ .$$

From Theorem 3.2.9 it follows that

$$a - \beta \sum_{j=1}^{N} x_{\mathrm{D};j}(t) \geq 0 \qquad \text{and} \qquad g_i - x_{\mathrm{D};i}(t) \geq 0 \ ,$$

such that $\frac{d}{dt} x_{\mathrm{D};i}(t)$ decreases as the $x_{\mathrm{D};j}(t)$ increase. Finally, since $\frac{d}{dt} x_{\mathrm{D};i}(t) > 0$ by Theorem 3.2.7, all $x_{\mathrm{D};i}(t)$ are strictly monotonically increasing, which means that all $\frac{d}{dt} x_{\mathrm{D};i}(t)$ are strictly monotonically decreasing. □

Now we can prove the *Natural dose-response behavior* for the cumulative antibody concentration.

Lemma 3.2.14 ({Adapted from [Theory-Preprint]}).
Let $\{(g_i, k_{\mathrm{a};i})\}_{i=1}^{N}$ be epitope classes, $0 < a < b$ be initial antibody concentrations, $\beta > 0$ be a depletion factor, and let

$$\alpha(t; a) := a - \beta \sum_{j=1}^{N} x_{\mathrm{D};j}(t; a)$$

be the effective antibody concentration of the depletion accumulation IVP. Then $\alpha(t; a) < \alpha(t; b)$ and $A(t; a) < A(t; b)$ for all times $t \geq 0$.

Proof 3.2.15 (**Proof idea** (detailed proof in Appendix B.2.3)).
The main idea is to consider the function $f(t) = \alpha(t; b) - \alpha(t; a)$, which satisfies $f(0) > 0$. To show the statement of the lemma, we can use a proof by contradiction. That is, we assume that there is a $t_- > 0$ such that $f(t_-) \leq 0$. The continuity of f then implies that there must be a smallest $t_0 > 0$ with $f(t_0) = 0$.

Since $f(t) > 0$ for $t < t_0$, it follows that $A(t; b) > A(t; a)$ for all $t \leq t_0$, which in turn yields $x_{\mathrm{D};i}(t; b) > x_{\mathrm{D};i}(t; a)$ for all $t \leq t_0$.

Hence, $x_{\mathrm{D};i}(t; b) - x_{\mathrm{D};i}(t; a)$ is strictly positive and finite. Since also $g_i - x_{\mathrm{D};i}(t; b)$ and $a - \beta X(t; a)$ are strictly positive and finite, upper and lower bounds can be defined, which show that

$$\frac{1}{k_{\mathrm{a};i}} \left(\frac{d}{dt} x_{\mathrm{D};i}(t; a) - \frac{d}{dt} x_{\mathrm{D};i}(t; b) \right) > 0 \qquad \forall\, t \in [0, t_0] \ .$$

Using (3.4) then yields $f(t_0) > 0$, which contradicts the assumption that there is a t_- with $f(t_-) \leq 0$.

Having proven the *Natural dose-response behavior* for the cumulative antibody concentration, the version for the depletion accumulation model becomes a simple application of Theorem 3.2.3.

Theorem 3.2.16 ({Adapted from [Theory-Preprint]}).
Let $\{(g_i, k_{\mathrm{a};i})\}_{i=1}^N$ be epitope classes, $\beta > 0$ be a depletion factor, and let $0 < a < b$ be initial antibody concentrations. Then

$$x_{\mathrm{D};i}(t;a) < x_{\mathrm{D};i}(t;b) \qquad \forall\ i \in \{1,\dots,N\}\ , \quad \forall t \geq 0\ .$$

Furthermore, when $k_{\mathrm{a};i} < k_{\mathrm{a};j}$ for $i, j \in \{1,\dots,N\}$ with $i \neq j$, then

$$\frac{x_{\mathrm{D};i}(t;a)}{g_i} < \frac{x_{\mathrm{D};j}(t;a)}{g_j} \qquad \forall\ t \geq 0\ .$$

Proof 3.2.17 ({Adapted from [Theory-Preprint]}).
Because of Theorem 3.2.3 and Definition 3.2.2 we have

$$x_{\mathrm{D};i}(t;a) = g_i(1 - e^{-k_{\mathrm{a};i}A(t;a)})\ .$$

According to Lemma 3.2.14, $A(t;a) < A(t;b)$ for all $a < b$. Thus,

$$x_{\mathrm{D};i}(t;a) = g_i(1 - e^{-k_{\mathrm{a};i}A(t;a)}) < g_i(1 - e^{-k_{\mathrm{a};i}A(t;b)}) = x_{\mathrm{D};i}(t;b)\ .$$

For the second part of the theorem, we observe that $k_{\mathrm{a};i} < k_{\mathrm{a};j}$ implies

$$\frac{x_{\mathrm{D};i}(t;a)}{g_i} = 1 - e^{-k_{\mathrm{a};i}A(t;a)} < 1 - e^{-k_{\mathrm{a};j}A(t;a)} = \frac{x_{\mathrm{D};j}(t;a)}{g_j}\ .$$

□

Let us conclude this subsection with the construction of lower and upper bounds that will help us prove the *Limit behavior* of Remark 3.2.1 for the depletion accumulation model. With Theorem 3.2.3 and Definition 3.2.2 in mind, we can easily construct such bounds by considering the cumulative antibody concentration. The basic idea is to find two constant antibody

concentrations $a_\downarrow$ and $a_\uparrow$, such that $a_\downarrow t \leq A(t;a) \leq a_\uparrow t$.

For the upper bound, we can just use the initial antibody concentration $a_\uparrow = a$. The lower bound requires a little more inventiveness.

Definition 3.2.18.
The **reservoir depleted concentration** is defined by

$$a_*(t;a) = \max\{0, a - \beta X_\mathrm{R}(t;a)\} \ .$$

The special case $t = \tau$ is denoted by $a_*(a) \coloneqq a_*(\tau;a)$.

With the reservoir depleted concentration and the initial antibody concentration, we obtain the desired bounds.

Lemma 3.2.19 ({Adapted from [Theory-Preprint]}).
Let $a_*(t;a)$ be the reservoir depleted concentration, then the inequalities

$$a_*(t;a)t \leq A(t;a) \leq at$$

hold for all times $t \geq 0$, all initial antibody concentrations $a > 0$, and all depletion factors $\beta > 0$.

Proof 3.2.20 ({Adapted from [Theory-Preprint]}).
Because of Theorem 3.2.9, we have

$$0 \leq \sum_{j=1}^{N} x_{\mathrm{D};j}(t;a) \quad \Rightarrow \quad \alpha(t;a) \coloneqq a - \beta \sum_{j=1}^{N} x_{\mathrm{D};j}(t;a) \leq a$$

for all $t \geq 0$, all $a > 0$, and all $\beta > 0$. By Definition 3.2.2 this implies $A(t;a) \leq at$ for all $t \geq 0$, all $a > 0$, and all $\beta > 0$.

Using Theorem 3.2.3 and Definition 3.2.2, we obtain

$$x_{\mathrm{D};i}(t;a) = g_i(1 - e^{-k_{\mathrm{a};i}A(t;a)}) \leq g_i(1 - e^{-k_{\mathrm{a};i}at}) = x_{\mathrm{R};i}(t;a)$$

for all $i \in \{1, \ldots, N\}$, all $t \geq 0$, all $a > 0$, and all $\beta > 0$. Using the definition of the dose-response curve (Definition 3.1.5), it follows that

$$a - \beta X_\mathrm{R}(t;a) = a - \beta \sum_{j=1}^{N} x_{\mathrm{R};j}(t;a) \leq a - \beta \sum_{j=1}^{N} x_{\mathrm{D};j}(t;a) = \alpha(t;a) \ .$$

By Theorem 3.2.7, all $x_{\mathrm{D};j}(t;a)$ are monotonically increasing as functions of t, such that $\alpha(t;a)$ is monotonically decreasing. Hence,

$$a - \beta X_{\mathrm{R}}(t;a) \leq \alpha(s;a) \qquad \forall s \in [0,t],\ \forall\ t \geq 0\ .$$

Together with Definition 3.2.2, this implies

$$(a - \beta X_{\mathrm{R}}(t;a))t \leq A(t;a)\ .$$

Finally, since

$$0 \leq a - \beta \sum_{j=1}^{N} x_{\mathrm{D};j}(t;a) = \alpha(t;a)\ ,$$

it follows that $0 \leq A(t;a)$. So, in summary, we have

$$a_*(t;a)t = \max\{0, a - \beta X_{\mathrm{R}}(t;a)\}t \leq A(t;a)$$

for all $t \geq 0$, all $a > 0$, and all $\beta > 0$. □

Corollary 3.2.21 ({Adapted from [Theory-Preprint]}).
Let $\{(g_i, k_{\mathrm{a};i})\}_{i=1}^{N}$ be epitope classes and let $a_*(t;a)$ be the reservoir depleted concentration, then the inequalities

$$x_{\mathrm{R};i}(t; a_*(t;a)) \leq x_{\mathrm{D};i}(t;a) \leq x_{\mathrm{R};i}(t;a)$$

and

$$X_{\mathrm{R}}(a_*(t;a)) \leq X_{\mathrm{D}}(a) \leq X_{\mathrm{R}}(a)$$

hold for all $i \in \{1, \ldots, N\}$, all times $t \geq 0$, all initial antibody concentrations $a > 0$, and all depletion factors $\beta > 0$.

Proof 3.2.22.
By Lemma 3.2.19, we have

$$a_*(t;a)t \leq A(t;a) \leq at\ .$$

Using Theorem 3.2.3 and Definition 3.2.2, it follows that

$$\underbrace{g_i(1 - e^{-k_{\mathrm{a};i}a_*(t;a)t})}_{x_{\mathrm{R};i}(t;a_*(t;a))} \leq \underbrace{g_i(1 - e^{-k_{\mathrm{a};i}A(t;a)})}_{x_{\mathrm{D};i}(t;a)} \leq \underbrace{g_i(1 - e^{-k_{\mathrm{a};i}at})}_{x_{\mathrm{R};i}(t;a)}\ .$$

Since the inequalities hold for all times $t \geq 0$ and for every component $i \in \{1, \ldots, N\}$, they also hold for the dose-response curves, which are just the sum over all components at the time $t = \tau$ (see Definition 3.1.5). □

3.2.2 Depletion accumulation model/dose-response curve

The depletion accumulation model is obtained from the solution of the depletion accumulation IVP by fixing an incubation time and then considering the dependence on the initial antibody concentration (see Definition 3.1.5). However, without a closed-form expression for the solution of the IVP, there is no closed-form expression for the depletion accumulation model.

Fortunately, the properties of the last subsection carry over without modification. After all, we only restrict our considerations to a single time point, the incubation time τ, and emphasize the dependence on the initial antibody concentration. This allows us to prove the *Limit behavior* of Remark 3.2.1 for the depletion accumulation model.

Theorem 3.2.23.
Let a denote the initial antibody concentration. Then the limits

$$\lim_{a \to 0} x_{\mathrm{D};i}(\tau; a) = 0 \qquad \textit{and} \qquad \lim_{a \to \infty} x_{\mathrm{D};i}(\tau; a) = g_i$$

hold for all incubation times $\tau > 0$, all depletion factors $\beta > 0$, and all $i \in \{1, \ldots, N\}$.

Proof 3.2.24.
We can prove the limits with the sandwich theorem from basic calculus. That is, we need to show that

(I) $\lim_{a \to 0} x_{\mathrm{R};i}(\tau; a) = 0$ and $\lim_{a \to \infty} x_{\mathrm{R};i}(\tau; a) = g_i$

(II) $\lim_{a \to 0} x_{\mathrm{R};i}(\tau; a_*(a)) = 0$ and $\lim_{a \to \infty} x_{\mathrm{R};i}(\tau; a_*(a)) = g_i$.

Because of the inequalities

$$x_{\mathrm{R};i}(\tau; a_*(a)) \leq x_{\mathrm{D};i}(\tau; a) \leq x_{\mathrm{R};i}(\tau; a)$$

of Corollary 3.2.21 and the sandwich theorem, it will follow that

$$\lim_{a\to 0} x_{\mathrm{D};i}(\tau;a) = 0 \qquad \text{and} \qquad \lim_{a\to\infty} x_{\mathrm{D};i}(\tau;a) = g_i \ .$$

For the reservoir accumulation model, we already know that the limits (I) hold. To prove the limits (II), we observe that they are almost the same as the limits (I), except for the dependence $a_*(a)$. So, we only need to show that $\lim_{a\to 0} a_*(a) = 0$ and $\lim_{a\to\infty} a_*(a) = \infty$ to conclude the proof.

Since $\lim_{a\to 0} x_{\mathrm{R};i}(\tau;a) = 0$, it follows that $\lim_{a\to 0} X_{\mathrm{R}}(\tau;a) = 0$ and thus

$$\lim_{a\to 0} a_*(a) = \lim_{a\to 0} \max\{0, a - \beta X_{\mathrm{R}}(\tau;a)\} = 0 \ .$$

And because of the natural bounds for the reservoir accumulation model, i.e., $X_{\mathrm{R}}(\tau;a) \leq G$, we have

$$a - \beta X_{\mathrm{R}}(\tau;a) \geq a - \beta G \ .$$

Thus,

$$\begin{aligned} \lim_{a\to\infty} a_*(a) &= \lim_{a\to\infty} \max\{0, a - \beta X_{\mathrm{R}}(\tau;a)\} \\ &\geq \lim_{a\to\infty} a - \beta G = \infty \ . \end{aligned}$$

□

Since the limit behavior holds for each component of the depletion accumulation model, it also holds for the depletion accumulation dose-response curve, which is just the sum of all components.

Corollary 3.2.25.
Let a denote the initial antibody concentration. Then the limits

$$\lim_{a\to 0} X_{\mathrm{D}}(\tau;a) = 0 \qquad \textit{and} \qquad \lim_{a\to\infty} X_{\mathrm{D}}(\tau;a) = G$$

hold for all incubation times $\tau > 0$ and all depletion factors $\beta > 0$.

With this corollary, we have proven the last property of Remark 3.2.1 for the depletion accumulation IVP. To simplify the comparison with Remark 3.2.1, we should summarize our results in a similar form.

Remark 3.2.26 (**Depletion accumulation properties**).
The following properties hold for all epitope class configurations $\{(g_i, k_{\mathrm{a};i})\}_{i=1}^{N}$, all initial antibody concentrations $a > 0$, all depletion factors $\beta > 0$, and all incubation times $\tau > 0$.

Unique global solution (Corollary 3.2.11)
The depletion accumulation IVP for multiple epitope classes has a unique solution

$$x_{\mathrm{D}} \colon [0, \infty) \to \mathbb{R}^N, \qquad t \mapsto x_{\mathrm{D}}(t; a) \ .$$

Accumulation principle (Theorem 3.2.7)
Antibodies accumulate over time:

$$\frac{d}{dt} x_{\mathrm{D};i}(t) \geq 0 \qquad \forall\, t \geq 0 \ .$$

Natural bounds (Theorem 3.2.9)
The amount of bound antibodies cannot exceed the amount of epitopes or the initial amount of antibodies:

$$0 \leq x_{\mathrm{D};i}(\tau; a) \leq \min\{\beta^{-1} a, g_i\} \quad \text{and} \quad 0 \leq X_{\mathrm{D}}(\tau; a) \leq \min\{\beta^{-1} a, G\} \ .$$

Natural dose-response behavior (Theorem 3.2.16)
Higher initial antibody concentrations imply larger amounts of bound antibodies. That is, let $a < b$, then

$$x_{\mathrm{D};i}(\tau; a) < x_{\mathrm{D};i}(\tau; b) \qquad \Rightarrow \qquad X_{\mathrm{D}}(\tau; a) < X_{\mathrm{D}}(\tau; b) \ .$$

Limit behavior (Theorem 3.2.23 and Corollary 3.2.25)
Without antibodies, no binding occurs,

$$\lim_{a \to 0} x_{\mathrm{D};i}(\tau; a) = 0 \qquad \Rightarrow \qquad \lim_{a \to 0} X_{\mathrm{D}}(\tau, a) = 0 \ ,$$

and for an infinitely high initial antibody concentration, epitope saturation is reached,

$$\lim_{a \to \infty} x_{\mathrm{D};i}(\tau; a) = g_i \qquad \Rightarrow \qquad \lim_{a \to \infty} X_{\mathrm{D}}(\tau; a) = G \ .$$

In conclusion, the properties of Remark 3.2.1 and Remark 3.2.26 reflect the natural behavior that we expect from our abstract experimental setup. This reassures us in our selection of equations to describe the experimental setup.

3.2.3 Improved theoretical bounds for antibody depletion

Unfortunately, the properties of Remark 3.2.26 do not provide much information about the shape of the depletion accumulation dose-response curve. They only state that the dose-response curve is a strictly monotonically increasing function, limited by the amount of antibodies and the amount of epitopes.

Of course, we can always resort to numerical solutions if we want to plot a depletion accumulation dose-response curve. Since numerical solution methods for differential equations are not the focus of this dissertation, we may use the automatic solver selection and sensitivity analysis of the "DifferentialEquations.jl" package [RN17; RN19; Ma+21]. We may justify this black-box approach with the general interest in numerical solutions of differential equations that has led to decades of research into robust algorithms with automatic detection of numerical instabilities.

Nevertheless, including additional checks is always a good idea. Especially in the case of dose-response curves, where it does not suffice to solve a single initial value problem. Instead, for each antibody concentration, the depletion accumulation IVP needs to be solved numerically and only the time point $t = \tau$ is used.

To check that a numerically calculated dose-response curve $X_{\mathrm{N}}(a)$ is not completely unrealistic, we should derive theoretical bounds for the true depletion accumulation dose-response curve $X_{\mathrm{D}}(a)$. If sufficiently strong, these bounds could determine the rough shape of the depletion accumulation dose-response curve, so that we can base our observations on analytical results. The numerical solution would then serve as an indication of the detailed shape of the dose-response curve. And the bounds would corroborate this indication if the numerical dose-response curve remains within the bounds over the entire range of initial antibody concentrations.

We have already derived theoretical bounds for the depletion accumulation dose-response curve with Corollary 3.2.21:

$$X_{\mathrm{R}}(a_*(a)) \leq X_{\mathrm{D}}(a) \leq X_{\mathrm{R}}(a) \ .$$

However, these bounds were only intended as an intermediate result to prove the limit behavior of the depletion accumulation dose-response curve (Theorem

3.2.23 and Corollary 3.2.25). Hence, it is not surprising that these bounds are rather weak and can become useless for unfavorable system parameters. For example, the bounds in Figure 3.6 do not even determine the rough shape of the depletion accumulation dose-response curve.

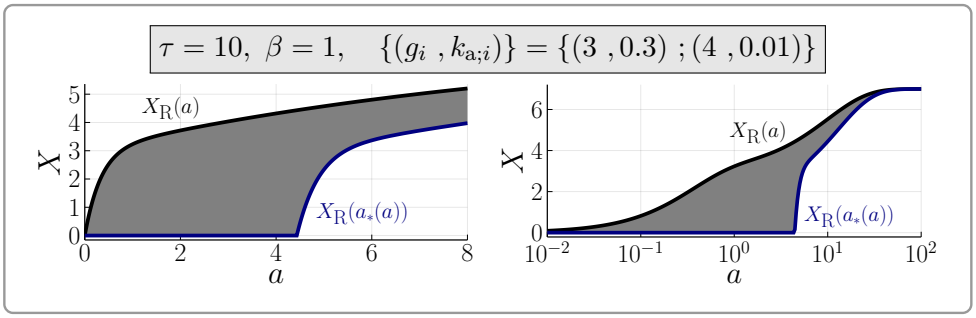

Figure 3.6: {Adapted from [Theory-Preprint]} Graphs for the bounds $X_{\mathrm{R}}(a)$ (black, solid) and $X_{\mathrm{R}}(a_*(a))$ (blue, solid) of Corollary 3.2.21, using exemplary system parameters. The bounds determine the region (gray surface) to which the depletion dose-response curve is confined. However, the bounds are not strong enough to estimate the rough shape of the depletion accumulation dose-response curve.

As a first step towards improved theoretical bounds, we should analyze the reasons why $X_{\mathrm{R}}(a)$ and $X_{\mathrm{R}}(a_*(a))$ fail. For the upper bound $X_{\mathrm{R}}(a)$, which is just the reservoir accumulation dose-response curve, this is quite easy. Since the reservoir case does, by definition, not contain any information about antibody depletion, it cannot be used to estimate the shape of the depletion accumulation dose-response curve when substantial antibody depletion occurs.

The lower bound $X_{\mathrm{R}}(a_*(a))$ becomes useless when the reservoir depleted concentration $a_*(a)$ is zero for a large part of the initial antibody concentration range. By the definition of the reservoir depleted concentration (Definition 3.2.18), the inequality $X_{\mathrm{R}}(a) \leq G$ of Remark 3.2.1 yields $a_*(a) > 0$ only when $a \geq \beta G$. For lower initial antibody concentrations, the condition $a_*(a) > 0$ is equivalent to $a > \beta X_{\mathrm{R}}(a)$. Unfortunately, we cannot solve this inequality analytically to investigate when exactly the lower bound fails.

However, using the closed-form expression for the solution of the reservoir accumulation IVP (3.2), we can calculate

$$\frac{d}{da} X_{\mathrm{R}}(a) = \frac{d}{da} \sum_{i=1}^{N} g_i \left(1 - e^{-k_{\mathrm{a};i} a \tau}\right) = \sum_{i=1}^{N} k_{\mathrm{a};i} \tau g_i e^{-k_{\mathrm{a};i} \tau a} \ .$$

This is a monotonically decreasing function of the initial antibody concentra-

tion. Thus, if

$$\beta \frac{dX_{\mathrm{R}}}{da}(0) = \beta \sum_{i=1}^{N} k_{\mathrm{a};i} \tau g_i < \left. \frac{d}{da} \right|_{a=0} a = 1 \ ,$$

then the reservoir depleted concentration $a_*(a)$ is nowhere zero, and $X_{\mathrm{R}}(a_*(a))$ might be a good lower bound. Otherwise, $a_*(a)$ is zero until the initial antibody concentration is large enough. Although we cannot give the exact initial antibody concentration when $a_*(a)$ becomes non-zero, we know that it is zero for all initial antibody concentrations with

$$\beta \frac{d}{da} X_{\mathrm{R}}(a) \leq \frac{d}{da} a \qquad \Leftrightarrow \qquad \beta \sum_{i=1}^{N} k_{\mathrm{a};i} \tau g_i e^{-k_{\mathrm{a};i} \tau a} \leq 1 \ . \tag{3.5}$$

Since exponential functions grow faster than finite polynomials, the last condition boils down to the following heuristic: *For sufficiently large depletion factors β and/or sufficiently large amounts of epitopes g_i, the reservoir depleted concentration $a_*(a)$ is zero for small initial antibody concentration range. Then the lower bound $X_{\mathrm{R}}(a_*(a))$ can be useless as a tool to estimate the depletion accumulation dose-response curve.*

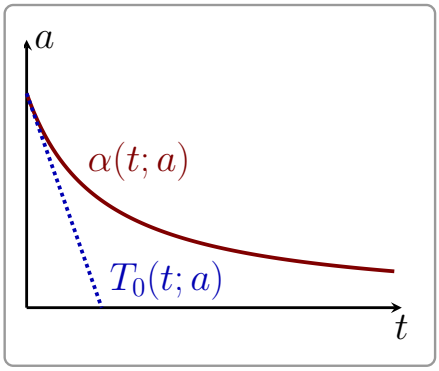

Figure 3.7: Illustration of the tangent line $T_0(t;a)$ at $t = 0$ to the effective antibody concentration $\alpha(t;a)$ of the depletion accumulation IVP.

Now that we understand the reasons why the bounds $X_{\mathrm{R}}(a)$ and $X_{\mathrm{R}}(a_*(a))$ became useless in Figure 3.6, we can improve them. First, the upper bound should reflect the antibody depletion. This can easily be achieved with the natural bound $X_{\mathrm{D}}(a) \leq \beta^{-1} a$ of Remark 3.2.26. Second, we need to prevent the lower bound from becoming zero for low initial antibody concentrations. Especially when the depletion factors β and/or the amounts of epitopes g_i are large. Unfortunately, we have no apparent candidate in our previous results, so we need to construct a new bound.

Among our results, Corollary 3.2.12 has received the least attention so far. Together with Theorem 3.2.7, it states that the solution components $x_{\mathrm{D};i}(t;a)$ of the depletion accumulation IVP are strictly concave and strictly monotonically increasing functions of time t. Thus, the effective antibody concentration of

the depletion accumulation IVP,

$$\alpha(t;a) = a - \beta \sum_{j=1}^{N} x_{\mathrm{D};j}(t) \ ,$$

is a strictly convex, strictly monotonically decreasing function of time t.

In particular, this means that the tangent line $T_0(t;a)$ at $t = 0$ is always below the effective antibody concentration $\alpha(t;a)$ of the depletion accumulation IVP:

$$T_0(t;a) \leq \alpha(t;a) \qquad \forall\ t \geq 0, \forall\ a > 0 \ .$$

See Figure 3.7 for an illustration.

Since we can easily integrate a linear function, we can use $T_0(t;a)$ as an effective antibody concentration for a generalized accumulation model, which should define a lower bound for the depletion accumulation dose-response curve.

Our proposed theoretical bounds for the depletion accumulation dose-response curve are formalized in the following theorem.

Theorem 3.2.27 ({Adapted from [Theory-Preprint]}).
Let $\{(g_i, k_{\mathrm{a};i})\}_{i=1}^{N}$ be epitope classes, $\tau > 0$ be an incubation time, and $\beta > 0$ be a depletion factor. Define

$$\widetilde{A}(\tau;a) := \begin{cases} a\tau\left(1 - \frac{1}{2}\tau\beta\sum_{i=1}^{N} k_{\mathrm{a};i}g_i\right) & , \ \tau \leq \frac{1}{\beta\sum_{i=1}^{N} k_{\mathrm{a};i}g_i} \\ \frac{a}{2\beta\sum_{i=1}^{N} k_{\mathrm{a};i}g_i} & , \textit{otherwise} \end{cases}$$

and

$$Y(a) := Y(\tau;a) := \sum_{i=1}^{N} g_i(1 - e^{-k_{\mathrm{a};i}\widetilde{A}(\tau;a)}) \ .$$

Then the inequalities

$$\max\{Y(a), X_{\mathrm{R}}(a_*(a))\} \leq X_{\mathrm{D}}(a) \leq \min\{\beta^{-1}a, X_{\mathrm{R}}(a)\}$$

hold for all initial antibody concentrations $a > 0$.

Proof 3.2.28 (**Proof idea** (detailed proof in Appendix B.2.4)).
Except for $Y(a)$ the bounds follow from Theorem 3.2.9 and Corollary 3.2.21.

For $Y(a)$ we construct the tangent line of $\alpha(t;a)$ at $t=0$, which is given by

$$T_0(t;a) := a + t\frac{d\alpha}{dt}(0;a) = a - a\beta t\sum_{i=1}^{N} k_{\mathrm{a};i} g_i \ .$$

Since $\alpha(t;a) > 0$ is a strictly convex function, it can be shown that

$$\widetilde{\alpha}(t;a) := \max\{0, T_0(t;a)\} \leq \alpha(t;a) \ ,$$

which shows that $Y(a) \leq X_{\mathrm{D}}(a)$ for $\widetilde{A}(t;a) := \int_{0,t} \widetilde{\alpha}(s;a)\, ds$.

The expression for $\widetilde{A}(t;a)$ is obtained by evaluating the integral.

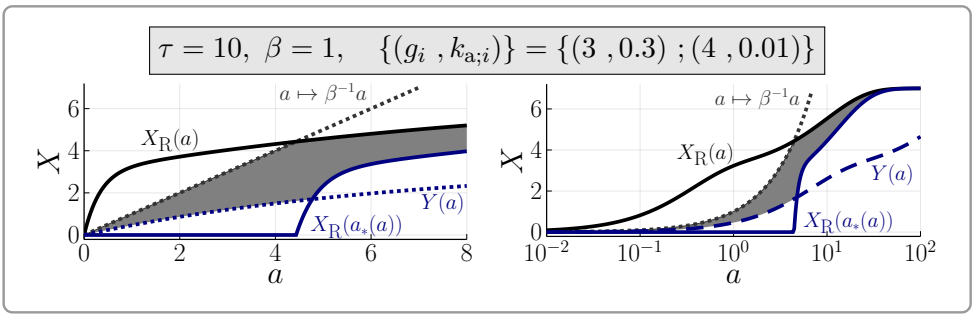

Figure 3.8: {Adapted from [Theory-Preprint]} Graphs for the improved bounds of Theorem 3.2.27, using the system parameters from Figure 3.6. As in Figure 3.6, the depletion accumulation dose-response curve is confined to the gray area. In addition, the individual parts that define the bounds are plotted to illustrate how the bounds of Theorem 3.2.27 improve the bounds of Corollary 3.2.21.

Figure 3.8 shows how the bounds of Theorem 3.2.27 improve the bounds of Corollary 3.2.21. Now, we can at least estimate what the shape of the depletion accumulation dose-response curve could look like. In particular, we know the weakest possible depletion effect because of the upper bound $a \mapsto \beta^{-1}a$. And we know the strongest possible depletion effect for low initial antibody concentration because of the lower bound $Y(a)$. Thus, we can begin to consider the numerical solution $X_{\mathrm{N}}(a)$ of the depletion accumulation dose-response curve and check if it abides by the theoretical bounds. Unsurprisingly, Figure 3.9 shows that the numerical solution remains within the theoretical bounds, corroborating the automatic solvers of the "DifferentialEquations.jl" package [RN17; RN19; Ma+21].

To investigate the behavior of the theoretical bounds and the depletion

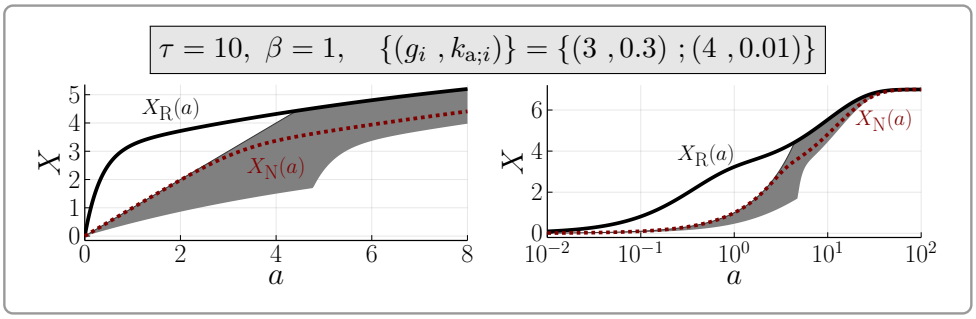

Figure 3.9: Graphs of the numerical solution $X_{\mathrm{N}}(a)$ (red, dashed), the theoretical bounds (gray area), and the reservoir accumulation dose-response curve $X_{\mathrm{R}}(a)$ (black, solid). The numerical solution remains within the theoretical bounds, corroborating its validity.

accumulation dose-response curve, we should consider different combinations of system parameters. Accordingly, Figure 3.10 shows plots for an increased binding rate constant.

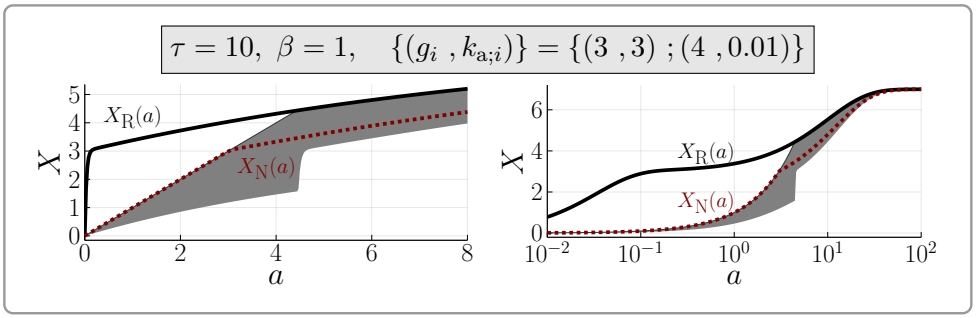

Figure 3.10: Graphs of the numerical solution $X_{\mathrm{N}}(a)$ (red, dashed), the theoretical bounds (gray surface), and the reservoir accumulation dose-response curve $X_{\mathrm{R}}(a)$ (black, solid). The bounds of Theorem 3.2.27 do not adapt to an increase in the highest binding rate constant ($0.3 \rightsquigarrow 3$).

Interestingly, the improved bounds of Theorem 3.2.27 have not changed much, as can be inferred from the shape of the gray area. However, this is not a general property of the bounds but an artifact of the system parameters. Already the parameters of Figure 3.9,

$$(g_1, k_{\mathrm{a};1}) = (3, 0.3) \qquad \text{and} \qquad (g_2, k_{\mathrm{a};2}) = (4, 0.01),$$

show a strong imbalance. While $g_1 \approx g_2$, the rate constant $k_{\mathrm{a};1}$ is 30-times larger than $k_{\mathrm{a};2}$. Increasing $k_{\mathrm{a};1}$, as done for Figure 3.10, only exacerbates this

imbalance.

Since the upper bound improvement $a \mapsto \beta^{-1}a$ of Theorem 3.2.27 does not depend on the epitope classes, it seems reasonable that the epitope classes are irrelevant for the upper bound. However, $a \mapsto \beta^{-1}a$ improves the bound only if $\beta^{-1}a \leq X_{\mathrm{R}}(a)$, which depends on the epitope classes.

Nevertheless, the contribution of the first epitope class $(g_1, k_{\mathrm{a};1}) = (3, 0.3)$ already saturates before $\beta^{-1}a$ intersects $X_{\mathrm{R}}(a)$. And the second epitope class only contributes significantly after this intersection point, which we can easily observe in the logarithmic plot of Figure 3.9. Increasing the binding rate constant k_1 shifts the saturation point to lower initial antibody concentrations, while leaving the contribution of the second epitope class unchanged. Thus, the intersection point of $a \mapsto \beta^{-1}a$ and $X_{\mathrm{R}}(a)$ does not change. Hence, the upper bound of Figure 3.10 closely resembles the upper bound of Figure 3.9.

With some minor calculations, we can also see why the lower bound improvement $Y(a)$ does not differ between Figure 3.10 and Figure 3.9. First, we observe that $\tau = 10$ and $\beta = 1$ yield

$$\tau \geq \frac{1}{\beta \sum_{i=1}^{N} k_{\mathrm{a};i} g_i} \qquad \Rightarrow \qquad \widetilde{A}(\tau, a) = \frac{a}{2\beta \sum_{i=1}^{N} k_{\mathrm{a};i} g_i}$$

for the system parameters used in Figure 3.9. Since $g_1 \approx g_2$ and $k_{\mathrm{a};1} \gg k_{\mathrm{a};2}$, we can approximate the sum over the epitope classes as

$$\sum_{i=1}^{N} k_{\mathrm{a};i} g_i \approx k_{\mathrm{a};1} g_1 \qquad \Rightarrow \qquad \widetilde{A}(\tau; a) \approx \frac{a}{2\beta k_{\mathrm{a};1} g_1} \,.$$

This implies

$$Y(a) \approx g_1 \left(1 - e^{-\frac{a}{2\beta g_1}}\right) + g_2 \left(1 - e^{-\frac{k_{\mathrm{a};2}}{k_{\mathrm{a};1}} \frac{a}{2\beta g_1}}\right) \,. \tag{3.6}$$

Finally, since $k_{\mathrm{a};1} \gg k_{\mathrm{a};2}$, it follows that $\frac{k_{\mathrm{a};2}}{k_{\mathrm{a};1}} \ll 1$, such that the second term of (3.6) affects the shape of $Y(a)$ only for high initial antibody concentrations, where $X_{\mathrm{R}}(a_*(a))$ is already the better lower bound. Thus, the relevant part of $Y(a)$ is determined only by $g_1(1 - e^{-\frac{a}{2\beta g_1}})$, which does not depend on the binding rate constants.

In summary, the improvements $a \mapsto \beta^{-1}a$ and $Y(a)$ of Theorem 3.2.27 are not affected by the increase of $k_{\mathrm{a};1}$, since $k_{\mathrm{a};1}$ is already much larger than $k_{\mathrm{a};2}$. On the other hand, this means that the improvements $a \mapsto \beta^{-1}a$ and $Y(a)$ should adapt if we reduce $k_{\mathrm{a};1}$, which is exactly what happens in Figure 3.11.

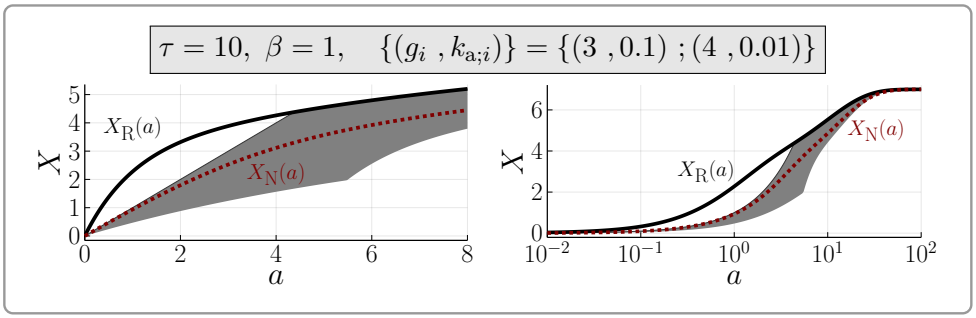

Figure 3.11: Graphs of the numerical solution $X_{\mathrm{N}}(a)$ (red, dashed), the theoretical bounds (gray surface), and the reservoir accumulation dose-response curve $X_{\mathrm{R}}(a)$ (black, solid). The bounds of Theorem 3.2.27 adapt to a decrease in the highest binding rate constant ($0.3 \rightsquigarrow 0.1$).

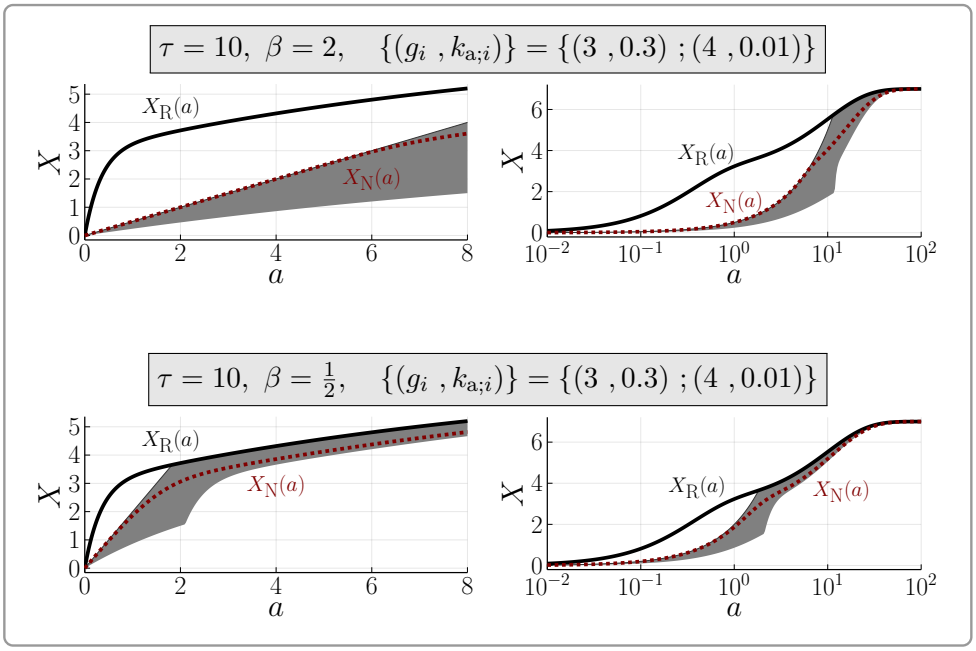

Figure 3.12: Graphs of the numerical solution $X_{\mathrm{N}}(a)$ (red, dashed), the theoretical bounds (gray area), and the reservoir accumulation dose-response curve $X_{\mathrm{R}}(a)$ (black, solid). The bounds of Theorem 3.2.27 depend on the depletion factor.

Unsurprisingly, the depletion factor β directly affects $a \mapsto \beta^{-1}a$ (Figure 3.12). However, the lower bound is also affected since the depletion factor is part of condition (3.5), which describes the domain where $X_{\mathrm{R}}(a_*(a)) = 0$.

3.2.4 Dose-response behavior

The theoretical bounds are ultimately just a tool for us. The real aspects of interest are the dose-response behavior of the accumulation models in general and the depletion effect in particular.

Let us first restrict our attention to the reservoir accumulation dose-response curve. In Figure 3.10, we can see that the dose-response curve has an intermediate plateau on the logarithmic scale. Such a plateau appears when

- the epitopes of an epitope class saturate at an initial antibody concentration $\widehat{a}$,
- and significant binding to the epitopes of the next epitope class (next higher rate constant) occurs only for initial antibody concentrations larger than $\widehat{a}$.

Hence, intermediate plateaus are a definite sign that there must be more than one epitope class.

However, the opposite direction is not true. In Figure 3.9, the intermediate plateau is less pronounced, and in Figure 3.11, there remains only a bump in the dose-response curve. In general, plateaus disappear when the rate constants of the epitope classes are similar enough. Consequently, multiple epitope classes with similar rate constants might not be discernible from the dose-response curve.

A similar behavior can be observed for the depletion accumulation dose-response curve. Two epitope classes create a bump in the dose-response curve. Interestingly, the depletion effect prevents a plateau. Thus, a lack of a plateau/bump does not necessarily mean that all epitope classes have similar rate constants. Instead, antibody depletion can completely mask the existence of multiple epitope classes.

Regarding antibody depletion, Figures 3.9–3.12 illustrate the behavior of antibody depletion quite well. Antibody depletion mostly affects the lower initial antibody concentrations and becomes negligible in the limit $a \to \infty$.

Both observations agree with the theoretical bounds. The behavior at high initial antibody concentrations follows immediately from $X_{\mathrm{R}}(a_*(a)) \to X_{\mathrm{R}}(a)$ as $a \to \infty$, which shows that the depletion effect converges to zero, irrespective of the epitope classes or the depletion factor.

At low initial antibody concentrations, the depletion accumulation dose-response curve is bounded by $a \mapsto \beta^{-1}a$, which does not depend on the epitope classes. In contrast, the reservoir accumulation dose-response curve is only bounded by the amount of epitopes. Thus, sufficiently many epitopes with sufficiently large rate constants lead to a large amount of bound antibodies, thus creating a large relative depletion (the difference between $X_{\mathrm{R}}(a)$ and $X_{\mathrm{D}}(a)$ relative to $X_{\mathrm{R}}(a)$).

In other words, we can understand the rate constant as a prerequisite for antibodies to bind to the respective epitope at low initial antibody concentrations (see Figures 3.10 and 3.11). The corresponding amount of epitopes with that rate constant then determines the magnitude of the relative depletion (see Figures 3.10 and 3.13).

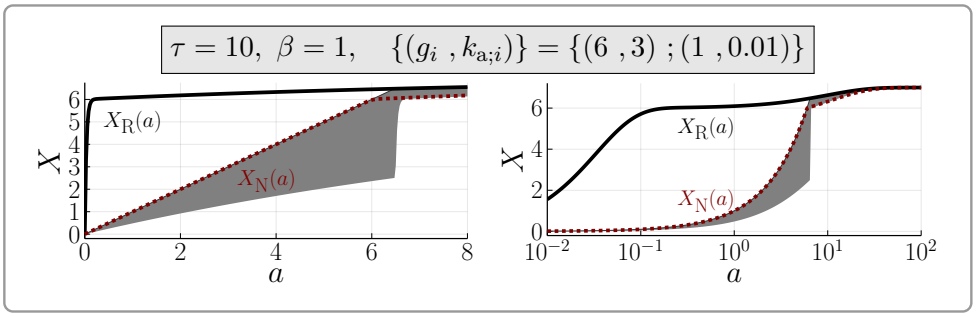

Figure 3.13: Graphs of the numerical solution $X_{\mathrm{N}}(a)$ (red, dashed), the theoretical bounds (gray surface), and the reservoir accumulation dose-response curve $X_{\mathrm{R}}(a)$ (black, solid). Increasing the amount of epitopes for the first epitope class ($3 \rightsquigarrow 6$) increases the relative depletion, compared to Figure 3.11. (The decrease in epitopes for the second epitope class retains the vertical axis scaling.)

Finally, the relative depletion depends on the depletion factor, as the name "depletion factor" already suggests. Increasing the depletion factor increases the relative depletion, while decreasing the depletion factor decreases the relative depletion (see Figures 3.9 and 3.12). Again, this behavior follows from the theoretical bound $a \mapsto \beta^{-1}a$, which depends reciprocally on the depletion factor.

3.3 Multiple antibody types

Up to this point, we have only considered a homogeneous antibody. Unlike epitope heterogeneity that is inevitable for apparent rate constants, **monoclonal antibodies** can at least approach the idealized setting of a homogeneous antibody. To achieve this goal, monoclonal antibodies are produced from clones of a single B cell [Lip+05] [Cam+15, Section 44.3.5].

As the name "monoclonal" suggests, there is at least a second type of antibodies. **Polyclonal antibodies** are derived from multiple B cells. Thus, they are heterogeneous [Lip+05] [Cam+15, Section 44.3.5]. Essentially, we can understand polyclonal antibodies as a mixture of monoclonal antibodies. These clones can have different binding properties or even different target epitopes.

Unfortunately, we cannot easily generalize our results to heterogeneous antibodies, so we might have to restrict our model to monoclonal antibodies. In fact, we have already suggested this restriction by defining epitope classes and the accumulation model (Definitions 3.1.3, 3.1.4 and 3.1.5) only for the special case of homogeneous antibodies. And most of the experimental dose-response curves that we will analyze in Chapter 5 use monoclonal antibodies.

However, to validate applications of the accumulation model, we will analyze data from a mixture of monoclonal antibodies against different proteins. Obviously, such a mixture violates the assumption that all individual antibodies are identical. Thus, we need to find arguments that justify the use of the accumulation model.

3.3.1 Definitions for multiple antibody types

Although we are interested in a mixture of monoclonal antibodies against different targets, it is much easier to introduce the accumulation model for generic heterogeneous antibodies first. Then, once we understand the underlying equations, we can formulate the special case of monoclonal antibodies against different targets mathematically.

In essence, we have already seen in Subsection 2.2.2 how to include antibody heterogeneity, albeit for the Langmuir model, where we called the binding molecules "particles". Nevertheless, the principle remains the same. We consider a mixture of M different antibody types and express the initial concentrations of the antibody types as $a_\mu = f_\mu a$, where f_μ denotes the fraction of antibodies that belong to the antibody type $\mu \in \{1, \dots, M\}$.

Definition 3.3.1.
We call a set of fractions $\{f_\mu\}_{\mu=1}^M$ **antibody-mix fractions** if

$$f_\mu > 0 \quad \forall\ \mu \in \{1, \dots, M\} \quad \text{and} \quad \sum_{\nu=1}^{M} f_\nu = 1\ .$$

Since we now consider different types of antibodies, we need to distinguish epitopes by their binding behavior with respect to each antibody type.

Definition 3.3.2.
Let $\{f_\mu\}_{\mu=1}^M$ be antibody mix-fractions. An **antibody-mix epitope class** is a tuple $(g, k_{\mathrm{a};1}, \dots, k_{\mathrm{a};M})$, where

i) $g > 0$,

ii) $k_{\mathrm{a};\mu} \geq 0$ for all $\mu \in \{1, \dots, M\}$,

iii) and there is at least one $\mu \in \{1, \dots, M\}$ such that $k_{\mathrm{a};\mu} > 0$.

Here g denotes the amount of epitopes, and $k_{\mathrm{a};\mu}$ denotes the binding rate constant for antibodies of type μ.

Although antibody-mix epitope classes already specify the number of antibody types, we will have to provide the antibody-mix fractions to specify a system anyway. So we might as well define the shorthand notation

$$\{f_\mu; (g_i, k_{\mathrm{a};i\mu}, \dots)\}_{i,\mu}^{N,M}$$

to specify both antibody-mix fractions $\{f_\mu\}_{\mu=1}^M$ and antibody-mix epitope classes $\{(g_i, k_{\mathrm{a};i1}, \dots, k_{\mathrm{a};iM})\}_{i=1}^N$. For short, we may call this the **antibody-mix configuration**.

Note that we arrange the indices so that the first index corresponds to the epitope class, while the second index corresponds to the antibody type. Furthermore, we follow our convention from the Langmuir model to use Roman letters as index variables for epitope classes and Greek letters as index variables for antibody types.

Unlike the definition of epitope classes for a homogeneous antibody (Definition 3.1.3), we allow some rate constants to be zero, as we cannot assume that all antibody types bind to all epitope classes. However, we want to consider only epitopes that allow the binding of antibodies. Hence, we require that at least one of the rate constants be non-zero.

Furthermore, we do not want to describe antibodies that cannot bind to anything. That is not to say that we exclude mixtures containing antibody types that cannot bind. We just do not describe the properties of those antibodies. After all, if they cannot bind, they will be washed away and cannot be measured in the context of antibody-stainings. Formally, regarding only antibodies that can bind to epitopes means that for each antibody type μ, there is at least one epitope class i_μ with $k_{\mathrm{a};i_\mu\mu} > 0$.

Definition 3.3.3.
We call an antibody-mix configuration $\{f_\mu; (g_i, k_{\mathrm{a};i\mu}, \ldots)\}_{i,\mu}^{N,M}$ **non-degenerate** if

$$\forall\ \mu \in \{1, \ldots, M\} \quad \exists\ i_\mu \in \{1, \ldots, N\} :\ k_{\mathrm{a};i_\mu\mu} > 0\ .$$

In the same way that we distinguish the binding rate constants $k_{\mathrm{a};i\mu}$ by the epitope class $i \in \{1, \ldots, N\}$ and the antibody type $\mu \in \{1, \ldots, M\}$, we also distinguish the amount of bound antibodies $x_{i\mu}$ by the epitope class and the antibody type. The amount of vacant epitopes of class i is now given by

$$g_i(t) = g_i - \sum_{\nu=1}^{M} x_{i\nu}(t)\ ,$$

because the occupancy of an epitope does not depend on the type of the individual antibody that is bound to it. Similarly, we need to sum over all epitope classes to obtain the concentration of free antibodies (of type μ) for the depletion case:

$$a_\mu(t) = a_\mu - \beta \sum_{j=1}^{N} x_{j\mu}(t) = f_\mu a - \beta \sum_{j=1}^{N} x_{j\mu}(t)\ .$$

Finally, we obtain the following accumulation IVPs for antibody mixtures.

Definition 3.3.4.
Let $\{f_\mu; (g_i, k_{\mathrm{a};i\mu}, \ldots)\}_{i,\mu}^{N,M}$ be a non-degenerate antibody-mix configuration, let $a > 0$ be an initial antibody concentration, and let $\beta > 0$ be a depletion factor. The **antibody-mix reservoir accumulation**

IVP is given by

$$\begin{cases} \dfrac{d}{dt}x_{\mathrm{R};i\mu}(t) = k_{\mathrm{a};i\mu}f_\mu a\left(g_i - \displaystyle\sum_{\nu=1}^{M} x_{\mathrm{R};i\nu}(t)\right) , \\ x_{i\mu}(0) = 0 \end{cases}$$

for all $i \in \{1,\dots,N\}$ and all $\mu \in \{1,\dots,M\}$. The **antibody-mix depletion accumulation IVP** is given by

$$\begin{cases} \dfrac{d}{dt}x_{\mathrm{D};i\mu}(t) = k_{\mathrm{a};i\mu}\left(f_\mu a - \beta\displaystyle\sum_{j=1}^{N} x_{\mathrm{D};j\mu}(t)\right)\left(g_i - \displaystyle\sum_{\nu=1}^{M} x_{\mathrm{D};i\nu}(t)\right) , \\ x_{i\mu}(0) = 0 \end{cases}$$

for all $i \in \{1,\dots,N\}$ and all $\mu \in \{1,\dots,M\}$.

The accumulation models and dose-response curves for multiple antibody types can be defined as before (Definition 3.1.5); we just need to sum over two indices.

Definition 3.3.5.
Let $\tau \geq 0$ denote an incubation time. If the antibody-mix reservoir/depletion accumulation IVP has a unique solution $x\colon [0,\tau] \longrightarrow \mathbb{R}^{NM}$ for all initial antibody concentrations $a \in I \subseteq \mathbb{R}_{>0}$, we call $a \mapsto x(\tau;a)$ the **antibody-mix reservoir/depletion accumulation model** over I. Furthermore, we call

$$a \longmapsto X(a) \coloneqq X(\tau;a) \coloneqq \sum_{i=1}^{N}\sum_{\mu=1}^{M} x_{i\mu}(\tau;a)$$

the **dose-response curve** over I.

Unsurprisingly, the antibody-mix accumulation IVPs are still autonomous systems,

$$\frac{d}{dt}x_{\mathrm{R}}(t) = h(x_{\mathrm{R}}(t)) \qquad \text{and} \qquad \frac{d}{dt}x_{\mathrm{D}}(t) = \ell(x_{\mathrm{D}}(t)) ,$$

for the functions $h, \ell \colon \mathbb{R}^{NM} \to \mathbb{R}^{NM}$, given by

$$h(x) = \begin{pmatrix} k_{\mathrm{a};11} f_1 a \left(g_1 - \sum_{\nu=1}^{M} x_{1\nu} \right) \\ \vdots \\ k_{\mathrm{a};NM} f_M a \left(g_N - \sum_{\nu=1}^{M} x_{N\nu} \right) \end{pmatrix}$$

and

$$\ell(x) = \begin{pmatrix} k_{\mathrm{a};11} \left(f_1 a - \beta \sum_{j=1}^{N} x_{j1} \right) \left(g_1 - \sum_{\nu=1}^{M} x_{1\nu} \right) \\ \vdots \\ k_{\mathrm{a};NM} \left(f_M a - \beta \sum_{j=1}^{N} x_{jM} \right) \left(g_N - \sum_{\nu=1}^{M} x_{N\nu} \right) \end{pmatrix} .$$

And since the components are still polynomials, the same arguments as in the proof of Lemma 3.1.9 yield that h and ℓ are Lipschitz continuous. Thus, Proposition 3.1.8 ensures the local existence and uniqueness of solutions. As before, we denote the **maximal existence time** of the solutions by T, suppressing the dependence on the system parameters in the notation.

3.3.2 Separated antibody-mix configurations

Having defined the accumulation IVPs and accumulation models for heterogeneous antibodies, we can consider mixtures of monoclonal antibodies against different targets. By "different targets" we essentially mean that the antibodies do not compete for epitopes. Formulated more abstractly, we mean that no antibody type can bind to an epitope class to which another antibody type can already bind.

Definition 3.3.6.
We call an antibody-mix configuration $\{f_\mu; (g_i, k_{\mathrm{a};i\mu}, \ldots)\}_{i,\mu}^{N,M}$ **separated** if

$$\forall\, i \in \{1, \ldots, N\} \quad \exists!\, \gamma(i) \in \{1, \ldots, M\} \,:\, k_{\mathrm{a};i\gamma(i)} > 0 \,.$$

Furthermore, we call $\gamma(i)$ the **associated antibody index** for $i \in \{1, \ldots, N\}$.

The name "separated" already suggests the consequence of separated antibody-mix configurations. The differential equations for the different antibody types become independent of each other, i.e., they become separated.

Before we prove this claim, we should define additional concepts and notations to keep track of the unique antibody types that correspond to the epitope classes.

Definition and Lemma 3.3.7.
Let $\{f_\mu; (g_i, k_{\mathrm{a};i\mu}, \dots)\}_{i,\mu}^{N,M}$ be a non-degenerate, separated antibody-mix configuration. We define the **antibody-type relation** $i \sim j$ for the epitope class indices by their associated antibody indices

$$i \sim j \qquad \Leftrightarrow \qquad \gamma(i) = \gamma(j)$$

and denote the set of related indices as

$$[i] \coloneqq \{j \in \{1, \dots, N\} \mid j \sim i\} \ .$$

Then, $\sim$ is an equivalence relation and $[i]$ is an equivalence class. Furthermore, the equivalence classes are a partition of the epitope class indices. We call this partition **antibody-type partition**.

Proof 3.3.8.
The antibody-type relation satisfies the properties of an equivalence relation because equality $(=)$ is an equivalence relation.

$\gamma(i) = \gamma(i)$	$i \sim i$
$\gamma(i) = \gamma(j) \ \Leftrightarrow \ \gamma(j) = \gamma(i)$	$i \sim j \ \Leftrightarrow \ j \sim i$
$\gamma(i) = \gamma(j) \ \wedge \ \gamma(j) = \gamma(k) \ \Rightarrow \ \gamma(i) = \gamma(k)$	$i \sim j \ \wedge \ j \sim k \ \Rightarrow \ i \sim k$

The set of related indices $[i]$ is just the definition of an equivalence class, since $\sim$ is an equivalence relation. Finally, the partition property follows from the fundamental theorem of equivalence relations (see, e.g., [Joh23, Theorem 2.1.12]). □

Now we can prove the independence of the differential equations when the antibody-mix configuration is separated. Note that the actual statement of the theorem and its proof will be rather simple, but setting up the notation for the conditions will result in a long theorem that appears more complicated than it actually is.

Theorem 3.3.9.
Let $\{f_\mu; (g_i, k_{\mathrm{a};i\mu}, \ldots)\}_{i,\mu}^{N,M}$ *be a non-degenerate, separated antibody-mix configuration, let* $a > 0$ *be an initial antibody concentration, and let* $\beta > 0$ *be a depletion factor. Let* T_{R} *and* T_{D} *denote the corresponding maximal existence times for the antibody-mix reservoir accumulation IVP and the antibody-mix depletion accumulation IVP, respectively.*

Furthermore, let $x_{\mathrm{R}} \colon [0, T_{\mathrm{R}}) \to \mathbb{R}^{NM}$ *denote the solution of the antibody-mix reservoir accumulation IVP and let* $x_{\mathrm{D}} \colon [0, T_{\mathrm{D}}) \to \mathbb{R}^{NM}$ *denote the solution of the antibody-mix depletion accumulation IVP.*

Finally, let $J_1, \ldots, J_L$ *denote the equivalence classes of the antibody-type partition for the antibody-mix configuration, let* $\gamma(J_1), \ldots, \gamma(J_L)$ *denote the associated antibody indices that define the equivalence classes, and let* $|J_1|, \ldots, |J_L|$ *denote the number of elements in the equivalence classes.*

Then *the antibody-mix accumulation IVPs can be decomposed into*

$$\frac{d}{dt}\begin{pmatrix} v^{(1)}(t) \\ \vdots \\ v^{(L)}(t) \\ \vec{0} \end{pmatrix} = \begin{pmatrix} h^{(1)}(v^{(1)}(t)) \\ \vdots \\ h^{(L)}(v^{(L)}(t)) \\ \vec{0} \end{pmatrix}, \qquad \vec{0} \in \mathbb{R}^{NM-(|J_1|+\ldots+|J_L|)}, \quad (3.7)$$

where $v^{(\ell)} \colon [0, T_\bullet) \to \mathbb{R}^{|J_\ell|}$ *and* $h^{(\ell)} \colon \mathbb{R}^{|J_\ell|} \to \mathbb{R}^{|J_\ell|}$ *for all* $\ell \in \{1, \ldots, L\}$.

For the ***reservoir case****, the terms are given by*

$$v_i^{(\ell)}(t) = x_{\mathrm{R};i\gamma(J_\ell)}(t), \quad h_i^{(\ell)}(v^{(\ell)}(t)) = k_{\mathrm{a};i\gamma(J_\ell)} f_{\gamma(J_\ell)} a \left(g_i - v_i^{(\ell)}(t)\right)$$

for all $i \in J_\ell$ *and all* $\ell \in \{1, \ldots, L\}$.

For the ***depletion case****, the terms are given by*

$$v_i^{(\ell)}(t) = x_{\mathrm{D};i\gamma(J_\ell)}(t),$$

$$h_i^{(\ell)}(v^{(\ell)}(t)) = k_{\mathrm{a};i\gamma(J_\ell)} \left(f_{\gamma(J_\ell)} a - \sum_{k \in J_\ell} v_k^{(\ell)}(t)\right) \left(g_i - v_i^{(\ell)}(t)\right)$$

for all $i \in J_\ell$ *and all* $\ell \in \{1, \ldots, L\}$.

Proof 3.3.10.
From the definition of separated antibody-mix configurations (Definition 3.3.6), we know that $k_{\mathrm{a};i\mu} = 0$ if $\mu \neq \gamma(i)$. It follows for all $i \in \{1, \ldots, N\}$ and all $\mu \neq \gamma(i)$ that

$$\frac{d}{dt} x_{\mathrm{R};i\mu}(t) = 0 \quad \Rightarrow \quad x_{\mathrm{R};i\mu}(t) = 0 \qquad \forall\, t \in [0, T_{\mathrm{R}})$$

and

$$\frac{d}{dt} x_{\mathrm{D};i\mu}(t) = 0 \quad \Rightarrow \quad x_{\mathrm{D};i\mu}(t) = 0 \qquad \forall\, t \in [0, T_{\mathrm{R}}) \ .$$

Thus, all $x_{\mathrm{R};i\mu}(t)$ and all $x_{\mathrm{D};i\mu}(t)$ for $\mu \neq \gamma(i)$ constitute the zero $\vec{0}$ of (3.7). Each equivalence class J_ℓ defines $|J_\ell|$ combinations that do not belong to $\vec{0}$, namely

$$\{(i, \gamma(J_\ell)) \mid i \in J_\ell\} \ .$$

The remaining cases all belong to $\vec{0}$. Since there are NM combinations of indices and $|J_1| + \ldots + |J_L|$ combinations that do not belong to $\vec{0}$, it follows that $\vec{0} \in \mathbb{R}^{NM-(|J_1|+\ldots+|J_L|)}$.

Let now $\ell \in \{1, \ldots, L\}$ and $i \in J_\ell$ be arbitrary, then

$$\sum_{\nu=1}^{M} x_{\mathrm{R};i\nu}(t) = x_{\mathrm{R};i\gamma(J_\ell)}(t) + \sum_{\nu \neq \gamma(J_\ell)} x_{\mathrm{R};i\nu}(t) = x_{\mathrm{R};i\gamma(J_\ell)}(t)$$

and

$$\sum_{\nu=1}^{M} x_{\mathrm{D};i\nu}(t) = x_{\mathrm{D};i\gamma(J_\ell)}(t) + \sum_{\nu \neq \gamma(J_\ell)} x_{\mathrm{D};i\nu}(t) = x_{\mathrm{D};i\gamma(J_\ell)}(t) \ ,$$

since $\gamma(i) = \gamma(J_\ell)$ for all $i \in J_\ell$. Furthermore, this also implies that

$$\sum_{k=1}^{N} x_{\mathrm{D};k\gamma(J_\ell)}(t) = \sum_{k \in J_\ell} x_{\mathrm{D};k\gamma(J_\ell)}(t) \ .$$

For the antibody-mix accumulation differential equations, this leads to

$$\frac{d}{dt} x_{\mathrm{R};i\gamma(J_\ell)}(t) = k_{\mathrm{a};i\gamma(J_\ell)} f_{\gamma(J_\ell)} a \left(g_i - \sum_{\nu=1}^{M} x_{\mathrm{R};i\nu}(t) \right)$$

$$= k_{\mathrm{a};i\gamma(J_\ell)} f_{\gamma(J_\ell)} a \left(g_i - x_{\mathrm{R};i\gamma(J_\ell)}(t) \right) \tag{3.8}$$

and

$$\begin{aligned} \frac{d}{dt} x_{\mathrm{D};i\gamma(J_\ell)}(t) &= k_{\mathrm{a};i\gamma(J_\ell)} \left(f_{\gamma(J_\ell)} a - \beta \sum_{k=1}^{N} x_{\mathrm{D};k\gamma(J_\ell)}(t) \right) \left(g_i - \sum_{\nu=1}^{M} x_{\mathrm{D};i\nu}(t) \right) \\ &= k_{\mathrm{a};i\gamma(J_\ell)} \left(f_{\gamma(J_\ell)} a - \beta \sum_{k \in J_\ell} x_{\mathrm{D};k\gamma(J_\ell)}(t) \right) \left(g_i - x_{\mathrm{D};i\gamma(J_\ell)}(t) \right) \end{aligned} \tag{3.9}$$

In both cases, the couplings become confined to a single antibody type $\gamma(J_\ell)$ and to the epitope classes belonging to J_ℓ. Thus, the system of differential equations can be decomposed into independent systems, one for each equivalence class of the antibody-type partition.

Finally, we observe that plugging the definition

$$v_i^{(\ell)}(t) = x_{\mathrm{R};i\gamma(J_\ell)}(t)$$

into (3.8) yields

$$\frac{d}{dt} v^{(\ell)}(t) = k_{\mathrm{a};i\gamma(J_\ell)} f_{\gamma(J_\ell)} a \left(g_i - v_i^{(\ell)}(t) \right) = h_i^{(\ell)}(v^{(\ell)}(t)) \ .$$

In the same way, plugging the definition

$$v_i^{(\ell)}(t) = x_{\mathrm{D};i\gamma(J_\ell)}(t) \ ,$$

into (3.9) yields

$$\begin{aligned} \frac{d}{dt} v_i^{(\ell)}(t) &= k_{\mathrm{a};i\gamma(J_\ell)} \left(f_{\gamma(J_\ell)} a - \sum_{k \in J_\ell} v_k^{(\ell)}(t) \right) \left(g_i - v_i^{(\ell)}(t) \right) \\ &= h_i^{(\ell)}(v^{(\ell)}(t)) \ . \end{aligned}$$

□

In essence, the theorem simply states that antibody types that do not compete for epitopes are independent of each other. Thus, for a mixture of monoclonal antibodies against different targets, the differential equations of

the accumulation IVPs decompose into independent differential equations for each antibody type:

$$\frac{d}{dt}v^{(\ell)}(t) = h^{(\ell)}(v^{(\ell)}(t)) \ .$$

Corollary 3.3.11.
The $\{v^{(\ell)}\}_{\ell=1}^{L}$ of Theorem 3.3.9 are solutions of reservoir/depletion accumulation IVPs for homogeneous antibodies with initial antibody concentrations $f_{\gamma(J_\ell)}a$ and epitope classes $\{(g_i, k_{\mathrm{a};i\gamma(J_\ell)})\}_{i\in J_\ell}$.

Proof 3.3.12.
By definition of $v^{(\ell)}$, we have

$$v_i^{(\ell)}(0) = x_{i\gamma(J_\ell)}(0) = 0 \quad \forall\ i \in J_\ell \qquad \Rightarrow \qquad v^{(\ell)}(0) = 0$$

for both the reservoir case $x_{i\gamma(J_\ell)}(t) = x_{\mathrm{R};i\gamma(J_\ell)}(t)$ and the depletion case $x_{i\gamma(J_\ell)}(t) = x_{\mathrm{D};i\gamma(J_\ell)}(t)$. Thus, $v^{(\ell)}$ satisfies the initial value condition of the accumulation IVPs. Finally, we observe that the expressions for $h_i^{(\ell)}(v^{(\ell)}(t))$ in Theorem 3.3.9 are precisely the differential equation terms of the reservoir/depletion accumulation IVPs (Definition 3.1.4) for the initial antibody concentration $f_{\gamma(J_\ell)}a$ and the epitope classes $\{(g_i, k_{\mathrm{a};i\gamma(J_\ell)})\}_{i\in J_\ell}$. □

3.3.3 Reservoir case

Unlike the reservoir accumulation IVP for a homogeneous antibody, the antibody-mix reservoir accumulation IVP is a system of coupled differential equations. Thus, we cannot solve the components individually. However, the reservoir case has been well-behaved so far. And it does not disappoint us here. Although we cannot solve the initial value problem directly, we can find a reservoir accumulation IVP for a homogeneous antibody that behaves similarly, even without requiring separated antibody-mix configurations.

Theorem 3.3.13.
Let $\{f_\mu; (g_i, k_{\mathrm{a};i\mu}, \ldots)\}_{i,\mu}^{N,M}$ be a non-degenerate antibody-mix configuration and let $a > 0$ be an initial antibody concentration. Then there is a

unique solution $x_{\mathrm{R}}\colon [0,\infty) \to \mathbb{R}^{NM}$ *for the corresponding antibody-mix reservoir accumulation IVP. And the sums over the antibody types*

$$y_i(t) \coloneqq \sum_{\mu=1}^{M} x_{\mathrm{R};i\mu}(t) \qquad \forall\, i \in \{1,\dots,N\}$$

are the components of the unique solution $y\colon [0,\infty) \to \mathbb{R}^N$ *of a reservoir accumulation IVP for the epitope classes*

$$\{(g_i, \mathfrak{K}_{\mathrm{a};i})\}_{i=1}^{N} \ , \qquad \textit{where} \qquad \mathfrak{K}_{\mathrm{a};i} = \sum_{\mu=1}^{M} f_\mu k_{\mathrm{a};i\mu} \ .$$

Proof 3.3.14.
Because of Proposition 3.1.8, there is a unique solution $x_{\mathrm{R}}\colon [0,T) \to \mathbb{R}^{NM}$ of the antibody-mix reservoir accumulation IVP for a maximal existence time T. Since the components of x_{R} are the unique solution of the antibody-mix reservoir accumulation IVP, they satisfy

$$\frac{d}{dt} x_{\mathrm{R};i\mu}(t) = k_{\mathrm{a};i\mu} f_\mu a \left(g_i - \sum_{\nu=1}^{M} x_{\mathrm{R};i\nu}(t) \right) \ .$$

It follows for all $i \in \{1,\dots,N\}$ that

$$\begin{aligned}
\frac{d}{dt} y_i(t) &= \frac{d}{dt} \sum_{\mu=1}^{M} x_{\mathrm{R};i\mu}(t) = \sum_{\mu=1}^{M} \frac{d}{dt} x_{\mathrm{R};i\nu}(t) \\
&= \sum_{\mu=1}^{M} k_{\mathrm{a};i\mu} f_\mu a \left(g_i - \sum_{\nu=1}^{M} x_{\mathrm{R};i\nu}(t) \right) \\
&= \left(\sum_{\mu=1}^{M} k_{\mathrm{a};i\mu} f_\mu \right) a \left(g_i - \sum_{\nu=1}^{M} x_{\mathrm{R};i\nu}(t) \right) \\
&= \mathfrak{K}_{\mathrm{a};i} a \left(g_i - y_i(t) \right) \ ,
\end{aligned}$$

where we have defined $\mathfrak{K}_{\mathrm{a};i} \coloneqq \sum_{\mu=1}^{M} k_{\mathrm{a};i\mu} f_\mu$ in the last step.

Thus, the y_i satisfy the reservoir accumulation differential equations. And since $x_{\mathrm{R};i\mu}(0) = 0$ for all $i \in \{1, \ldots, N\}$ and $\mu \in \{1, \ldots, M\}$, by definition of the antibody-mix reservoir accumulation IVP, $y_i(0) = 0$ holds for all $i \in \{1, \ldots, N\}$. In summary, this means that the y_i are the components of the unique solution of a reservoir accumulation IVP with the epitope classes $\{(g_i, \mathfrak{K}_{\mathrm{a};i})\}_{i=1}^{N}$.

It remains to show that $T = \infty$, or more precisely, to show that there is a compact set $K \subset \mathbb{R}^{NM}$ with $x_{\mathrm{R}}([0, T)) \subset K$, since $T = \infty$ then follows from Proposition 3.1.8.

Because y is the solution of the reservoir accumulation IVP, $0 \leq y_i(t) \leq g_i$ holds for all $t \in [0, \infty)$ and all $i \in \{1, \ldots, N\}$. However, this does not yet restrict the individual components $x_{\mathrm{R};i\mu}(t)$. Only the sums are bounded:

$$0 \leq \sum_{\nu=1}^{M} x_{\mathrm{R};i\nu}(t) = y_i(t) \leq g_i \ .$$

But these bounds yield

$$\frac{d}{dt} x_{\mathrm{R};i\mu}(t) = k_{\mathrm{a};i\mu} f_\mu a \left(g_i - \sum_{\nu=1}^{M} x_{\mathrm{R};i\nu}(t) \right) = k_{\mathrm{a};i\mu} f_\mu a \left(g_i - y_i(t) \right) \geq 0 \ ,$$

since all system parameters are positive by definition. In consequence, all $x_{\mathrm{R};i\mu}(t)$ are non-negative for all $t \in [0, T)$. Thus, the sum $\sum_{\nu=1}^{M} x_{\mathrm{R};i\nu}(t)$ comprises only non-negative terms, which implies that the individual terms are also bounded:

$$0 \leq x_{\mathrm{R};i\mu}(t) \leq g_i \qquad \forall\ i \in \{1, \ldots, N\},\ \forall\ \mu \in \{1, \ldots, M\},\ \forall\ t \in [0, T) \ .$$

This concludes the proof. □

Theorem 3.3.13 does not solve the antibody-mix reservoir accumulation IVP. We still do not know the shape of the individual components $x_{\mathrm{R};i\mu}(t)$, but we can interpret heterogeneous antibodies as a homogeneous antibody for modified epitope classes. This means that

$$\sum_{\mu=1}^{M} x_{\mathrm{R};i\mu}(t) = g_i \left(1 - e^{-\sum_{\mu=1}^{M} f_\mu k_{\mathrm{a};i\mu} a t} \right) \ , \tag{3.10}$$

which allows us to calculate at least the dose-response curves analytically.

For the special case of separated antibody-mix configurations, Theorem 3.3.9 and Corollary 3.3.11 even allow us to write down the analytical solution

of the antibody-mix reservoir accumulation IVP.

Corollary 3.3.15.
Let $\{f_\mu; (g_i, k_{\mathrm{a};i\mu}, \ldots)\}_{i,\mu}^{N,M}$ *be a non-degenerate, separated antibody-mix configuration and let* $a > 0$ *be an initial antibody concentration. Then the solution of the corresponding antibody-mix reservoir accumulation IVP is given by*

$$x_{\mathrm{R};i\mu}(t) = \begin{cases} g_i \left(1 - e^{-k_{\mathrm{a};i\mu} f_\mu a t}\right) & , \quad \mu = \gamma(i) \\ 0 & , \quad \mu \neq \gamma(i) \end{cases} .$$

Proof 3.3.16.
Because of Theorem 3.3.13, there is a unique solution $x_{\mathrm{R}} \colon [0, \infty) \to \mathbb{R}^{NM}$ for the antibody-mix reservoir accumulation IVP.

Theorem 3.3.9 now states that we can arrange the components $x_{\mathrm{R};i\mu}(t)$ into $(v^{(1)}(t), \ldots, v^{(L)}(t), 0)$, based on the antibody-type partition $J_1, \ldots, J_L$. By Corollary 3.3.11, the $v^{(\ell)}(t)$ are solutions of reservoir accumulation IVPs with initial antibody concentrations $f_{\gamma(J_\ell)} a$ and epitope classes $\{(g_i, k_{\mathrm{a};i\gamma(J_\ell)})\}_{i \in J_\ell}$. Thus,

$$x_{\mathrm{R};i\gamma(J_\ell)}(t) = v_i^{(\ell)}(t) = g_i \left(1 - e^{-k_{\mathrm{a};i\mu} f_\mu a t}\right)$$

for all $t \geq 0$, all $\ell \in \{1, \ldots, L\}$ and all $i \in J_\ell$.

For the remaining components $x_{\mathrm{R};k\nu}(t)$, where $k \in \{1, \ldots, N\}$ and $\nu \neq \gamma(k)$, Theorem 3.3.9 also states that $x_{\mathrm{R};k\nu}(t) = 0$ for all $t \geq 0$, which completes the proof. □

3.3.4 Depletion case

The depletion case has been more difficult to handle than the reservoir case. And the antibody-mix depletion accumulation IVP does not appear to be different any in that regard. In fact, we will not be able to apply the ideas of Section 3.2 to the antibody-mix depletion accumulation IVP with generic heterogeneous antibodies. See Appendix B.2.5 for more information.

However, for mixtures of monoclonal antibodies against different targets, i.e., separated antibody-mix configurations, we can retrieve most of the deple-

tion accumulation properties (Remark 3.2.26).

Theorem 3.3.17.
Let $\{f_\mu; (g_i, k_{\mathrm{a};i\mu}, \dots)\}_{i,\mu}^{N,M}$ be a non-degenerate, separated antibody-mix configuration, let $a > 0$ be an initial antibody concentration, let $\beta > 0$ be a depletion factor, and let $\tau > 0$ be an incubation time. Then there is a unique solution $x_{\mathrm{D}} \colon [0, \infty) \to \mathbb{R}^{NM}$ for the corresponding antibody-mix depletion accumulation IVP with the following properties:

i) ***Accumulation principle***
The antibodies accumulate over time, i.e.,

$$\frac{d}{dt} x_{\mathrm{D};i\mu}(t) \geq 0$$

for all $t \geq 0$, all $i \in \{1, \dots, N\}$, and all $\mu \in \{1, \dots, M\}$.

ii) ***Natural bounds***
The amount of bound antibodies can only be positive and can neither exceed the initial amount of antibodies nor the amount of available epitopes. That is,

$$0 \leq x_{\mathrm{D};i\mu}(\tau; a) < \min\{\beta^{-1} f_\mu a, g_i\}$$

for all $i \in \{1, \dots, N\}$ and all $\mu \in \{1, \dots, M\}$, as well as

$$0 \leq X_{\mathrm{D}}(\tau; a) < \min\{\beta^{-1} a, G\} \ .$$

iii) ***Natural dose-response behavior***
Higher initial antibody concentrations imply larger amounts of bound antibodies. For $0 < a < b$ we have

$$x_{\mathrm{D};i\mu}(\tau; a) \leq x_{\mathrm{D};i\mu}(\tau; b)$$

for all $i \in \{1, \dots, N\}$ and all $\mu \in \{1, \dots, M\}$, as well as

$$X_{\mathrm{D}}(\tau; a) < X_{\mathrm{D}}(\tau; b) \ .$$

iv) ***Limit behavior***
Without antibodies, no binding occurs. That is,

$$\lim_{a \to 0} x_{\mathrm{D};i\mu}(\tau; a) = 0 \qquad \text{and} \qquad \lim_{a \to 0} X_{\mathrm{D}}(\tau; a) = 0$$

for all $i \in \{1, \dots, N\}$ and all $\mu \in \{1, \dots, M\}$. Furthermore, for an infinitly high initial antibody concentration, epitope saturation is reached, which means

$$\lim_{a\to\infty} x_{\mathrm{D};i\mu}(\tau; a) = \begin{cases} g_i & , \ \mu = \gamma(i) \\ 0 & , \ \mu \neq \gamma(i) \end{cases} \quad \text{and} \quad \lim_{a\to\infty} X_{\mathrm{D}}(\tau; a) = G$$

for all $i \in \{1, \dots, N\}$ and all $\mu \in \{1, \dots, M\}$.

v) ***Improved bounds***
The dose-response curve satisfies

$$X_{\mathrm{D}}(\tau; a) \leq \min\{\beta^{-1}a, X_{\mathrm{R}}(\tau; a)\} \ ,$$

where $X_{\mathrm{R}}(\tau; a)$ is the dose-response curve of the antibody-mix reservoir accumulation model for the same system parameters.

Proof 3.3.18 (**Proof idea** (detailed proof in Appendix B.2.6))**.**
As in the proof of Theorem 3.3.13, local existence and uniqueness of a solution follows from Proposition 3.1.8. Then, Theorem 3.3.9 and Corollary 3.3.11 can be used to separate this solution of the antibody-mix depletion accumulation IVP into components that are just solutions of some depletion accumulation IVPs (for homogeneous antibodies). For these separated components, the depletion accumulation properties (Remark 3.2.26) apply, which suffices to extend the depletion accumulation properties to the antibody-mix depletion accumulation IVP. In most cases, these extensions are trivial or just require keeping track of indices.

4

Accumulation model and parameter estimation

In the last chapter, we have developed the accumulation model, focusing on the theoretical aspects of the model, which allow us to determine the dose-response behavior, given the system parameters. However, calculating the effects from known parameters will rarely be relevant for applications. Most of the time, the dose-response behavior can be measured, at least up to proportionality, while the epitope classes and the depletion factor are unknown. So for this chapter, we want to shift the focus to the estimation of epitope classes from dose-response data.

This chapter uses content that I contributed to [Methods-Paper] and [Theory-Preprint]:

- Section 4.1 discusses the limitations of experimental data and the use of experimental units that are outlined in [Methods-Paper]. Here, experimental units and the limitations of experimental data are discussed in greater detail.
- Section 4.2 introduces the parameter estimation model, its interpretation, and its unit invariance, which are also described in [Methods-Paper]. However, these aspects are formulated more rigorously and in the context of proper densities.
- Subsection 4.3.2 explains in greater detail the visualization of epitope densities in the form of accessibility histograms, which are briefly described in [Methods-Paper].
- Subsection 4.3.3 and Subsection 4.3.4 motivate and explain curve fitting, the objective function, and the adaptive refinement strategy, which are only briefly stated in [Methods-Paper].
- Subsection 4.3.5 contains the worst-case depletion correction of [Methods-Paper].

The respective (sub)sections, in particular, and this chapter in general, contain additional new content beyond the highlighted differences.

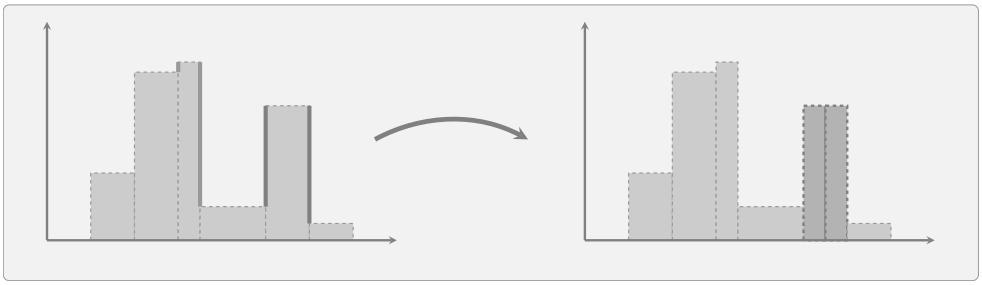

4.1 Experimental data and measurement limitations

Before we address how to estimate epitope classes from dose-response data, we should familiarize ourselves with experimental dose-response data and its shortcomings. For this purpose, let us focus in particular on the data that we will analyze in the next chapter.

Note that we have already described the abstract experimental setting of antibody-staining (Subsection 3.1.1). And the outlined experimental steps, including the time point of the actual measurement, have led us to develop the accumulation model. However, we have stopped short of describing the whole experimental process by considering the exact amounts of bound antibodies, instead of outlining a measurement process. Our main motivation was to focus on the behavior of the accumulation model rather than to describe a complete list of steps required to obtain experimental data. But there is a second reason for this approach. We do not want to restrict the abstract experimental system any more than necessary. Although the data that we will analyze in the next chapter is obtained with fluorescence microscopy, there might be other measurement techniques that achieve the same or better results in the future.

Irrespective of the measurement principle and potential advances therein, the non-zero antibody incubation time τ implies that only a finite number n of initial antibody concentrations can be prepared experimentally in a finite amount of time. Thus, **dose-response data** consists of discrete points

$$D \coloneqq \{(a_i, X_i)\}_{i=1}^{n} \ . \tag{4.1}$$

Here, a_i denotes the initial antibody concentration, and X_i denotes the corresponding amount of bound antibodies. As required by the definition of the accumulation model (Definition 3.1.5), the same incubation time τ must be used for each data point of the data D.

Despite potential improvements in measurement techniques, measurements up to proportionality are usually easier to obtain. That is, instead of the actual initial antibody concentration a and the actual number (amount) of bound antibodies X, only proportional quantities

$$\mathcal{A} = \gamma a \qquad \text{and} \qquad \mathcal{X} = \xi X \qquad \text{where} \qquad \gamma, \xi > 0 \ , \tag{4.2}$$

are measured, often without knowledge about the proportionality factors γ and ξ. Since these proportionalities are essentially just unit transformations (see Appendix C.2), we can understand them as **experimental units**. In

case of experimental units, the dose-response data is given by

$$\mathcal{D} = \{(\mathcal{A}_i, \mathcal{X}_i)\}_{i=1}^{n} \ . \tag{4.3}$$

To illustrate the need for experimental units, we should consider some experimental limitations of the data that we will analyze in the next chapter. However, since the experimental details are not our primary interest, we should introduce the limitations in a conceptual order instead of a procedural order. In other words, we should consider one limitation at a time, starting from the most general aspects.

4.1.1 Initial antibody concentration

Let us assume that we have already prepared the cells for the antibody-staining dose-response experiment. Our next step would be to prepare different initial antibody concentrations. From a purely theoretical perspective, we would simply add the required number of antibodies to the chosen liquid to achieve the desired antibody concentration. However, this is far from experimental reality.

Usually, antibodies are either dissolved in a solution with a certain concentration, or they are freeze-dried and need to be redissolved before application. But even in the freeze-dried state, one does not have pure antibodies, since additional substances are required to prevent the denaturation of the antibodies [Joh12; MÓO20]. In either case, one starts with a stock solution that has a certain antibody concentration. From there, this stock solution is diluted to obtain antibody solutions with lower antibody concentrations.

When the antibody concentration of the stock solution is known, it is trivial to calculate the concentration of a dilution. And antibody vendors usually provide antibody concentrations for their products, albeit in terms of mass concentrations, which can easily be converted to the number concentrations that we have considered so far. Thus, we might expect that it is quite easy to prepare specific initial antibody concentrations for dose-response experiments.

Unfortunately, the situation is not that simple. Knowing the concentration of antibodies in a solution is not the same as knowing the concentration of active antibodies, that is, undamaged antibodies that can bind to the target epitope. Even assuming that vendors managed to produce only active antibodies does not mean that an antibody solution will contain only active antibodies during the experiment. It is reasonable to assume that some antibodies denature during shipping and storage, given the concern about storage methods (cf. [Joh12; MÓO20]). Not to mention that the assumption of vendors producing only active antibodies was just an idealization for the sake of argument.

As a result, the concentration of active antibodies in a stock solution should be determined prior to a dose-response experiment. However, measuring active antibody concentrations requires specialized setups that are not available in all laboratories [Wel16; Kar16]. This could explain why dilutions (and sometimes lot numbers to identify a specific antibody batch) are commonly reported instead of antibody concentrations. This can also be observed in publications that focus on antibody validation or the optimization of concentrations for antibody-staining [Bor+10; Pil+20; Smi13; Dud+22].

In summary, the initial antibody concentration is usually unknown. Only the **dilution quotient** can be determined, which we define as the fraction of stock solution present in the diluted antibody solution. For example, mixing 1 part (certain volume) of the stock solution with 1 part of the diluent (filler, like water, buffer, etc.) leads to a dilution quotient of $1/2$, since 1 part of the stock solution now belongs to 2 parts in total. In this way, the dilution quotient constitutes a measurement up to proportionality, where the unknown concentration of the stock solution acts as the proportionality factor γ between the actual concentration a and the dilution quotient $\mathcal{A}$.

Following the concept of experimental units, we may define **dilution quotient** ($\mathrm{D_q}$) as a unit of concentration. The numerical value in this unit is just the dilution quotient itself. Of course, this unit relies on the concentration of a particular stock solution, such that dilution-quotient values cannot be compared when different stock solutions are used.

Remark 4.1.1 (**Dilution quotient and dilution ratio**).
Note that the dilution quotient is not the only way to express dilutions. Instead of the fraction of stock solution in the diluted solution, we could describe the mixing ratios, that is, how many parts n of the stock solution are mixed with how many parts m of the diluent. Unfortunately, the common notation for this ratio is $n : m$, which could be confused with a division. Thus, the ratio can easily be confused with the dilution quotient, despite yielding different concentrations. For example, in our explanation above, we have created a $1 : 1$ dilution, which has a dilution quotient of $1/2$.

The dilution ratio is ill-defined as a unit ($\mathrm{D_r}$) of concentration. Take, for example, the $1 : 1$ dilution, i.e, a solution with dilution quotient $1/2 = 0.5$. Using "dilution quotient" as a unit behaves perfectly well. Doubling the concentration of a $0.5\,\mathrm{D_q}$ solution (multiplying the quantity by 2) yields a $1\,\mathrm{D_q}$ solution, which is indeed twice as concentrated as a $0.5\,\mathrm{D_q}$

solution. The same calculation fails for the dilution-ratio. Neither defining $2:1\,\mathrm{D_r}$ nor $1:2\,\mathrm{D_r}$ for the multiplication by 2 would result in a solution with double the concentration of a $1:1\,\mathrm{D_r}$ solution.

Of course, one could object that $n:m$ is not a real number. But simply defining n/m or m/n as numerical value of $n:m$ would fail, as we have just seen. The correct way to obtain a well-behaved real number from the dilution ratio is the formula $n/n+m$, which simply yields the dilution quotient.

4.1.2 Fluorescence microscopy and bound antibodies

Suppose that we have already applied the antibody dilutions and that we have already washed the cells after the antibody incubation. Now, it would remain to measure the number of bound antibodies. But that is, again, easier said than done. We cannot simply count or weigh the antibodies, especially with the commonly available instruments in the context of antibody-staining.

However, the original purpose of antibody-staining — an observable staining of biological structures — can be used to estimate the number of bound antibodies. This requires a stain that can easily be separated from unrelated signals. For example, fluorescent molecules are a popular choice because of their specific emission frequency, which can be isolated with optical filters (see, e.g., [San+14] for a brief overview or [Mon14] for a textbook on the physical principles). These molecules, sometimes referred to as (fluorescent) labels or tags, need to be chemically attached to the antibodies.

Let us ignore the problem of attaching labels to antibodies for the moment, and let us focus solely on the measurement of already labeled antibodies. By the very principle of fluorescence, the labels emit photons that can be captured with an image sensor. The resulting image, or rather the total pixel intensity (sum of all pixel values), should then be a numerical representation that is proportional to the number of fluorescence photons collected by the sensor during the image exposure.

Unfortunately, the image sensor cannot distinguish the sources of photons. Although optical filters are used to single out the wavelength of the fluorescence signal (often completely blocking stray excitation light), any source that emits photons of wavelengths similar to those of the fluorescence signal will contribute to the final image. For example, some biological structures are naturally fluorescent and could contribute to the fluorescence signal. To mitigate these unwanted contributions, negative controls are performed, which

are usually just measurements of cells without fluorescent labels. Subtracting the total pixel intensity of the negative control from the total pixel intensity of the actual measurement should, on average, yield the total pixel intensity corresponding to the photons emitted by the fluorescent labels.

Because the number of emitted fluorescence photons is proportional to the number of fluorescent labels, the total pixel intensity is proportional to the number of fluorescent labels in the image. Thus, when the number of fluorescent molecules is the same for each individual antibody, at least on average, the total pixel intensity $\mathcal{X}$ of a fluorescence-microscopy image is proportional to the number of bound antibodies X in the image. In summary, we can define **intensity** as an experimental unit for the amount of bound antibodies.

Of course, the measured intensity values depend on imaging parameters such as the excitation source, the fluorescent label, and the image exposure settings. In other words, intensity as an experimental unit relies on imaging parameters in the same way that the dilution quotient relies on a specific stock solution. However, unlike the dilution quotient, there is a simple solution to compare intensities across different imaging parameters. We can use normalized intensities, where we express all intensities as multiples of another intensity that we fix as a reference point.

Since multiplication by a positive constant value is a proper unit transformation, we can also define **normalized intensity** ($\mathrm{I_n}$) as an experimental unit for the amount of bound antibodies.

The normalization of intensities also reveals a rather obvious method to obtain the actual amount of bound antibodies from the measured intensity value. One can simply compare the measured intensity to the intensity of a reference system with a known amount of antibodies [CW12]. This approach has the advantage that the reference system can be measured at any time.

Although the concept of a reference system is quite easy, obtaining such a system is often difficult. The reference system must use the same fluorescent labels, and the average number of labels per individual antibody must be the same as in the experiment of interest. And since measuring the concentration of (active) antibodies is already difficult, as discussed in the last subsection, good reference systems are usually out of reach for most laboratories.

In addition to reference systems, the bleaching behavior of fluorescent labels can be used to estimate at least the amount of fluorescent labels in a system. The idea is to exploit the loss of fluorescence after several excitation-emission cycles, known as photobleaching. Counting the discrete bleaching events might be the most straightforward approach [CW12]. However, this requires a low

number of labels to reduce the risk of undercounting simultaneous bleaching events, is time-consuming, and needs to be repeated for each measurement. These limitations can be avoided by exploiting the stochastic behavior of photobleaching [NR11; BS19].

Unfortunately, bleaching approaches only provide information about the number of fluorescent labels, not about the number of bound antibodies. Furthermore, both the bleaching approaches and comparisons with reference systems add additional uncertainties. Finally, in all cases, the intensity needs to be measured anyway. Thus, simply using (normalized) intensity as an experimental unit is definitely easier.

4.1.3 Secondary antibodies

We have already considered how to measure antibodies if fluorescent labels are attached to them. But how do fluorescent labels get attached to the antibodies in the first place?

For our purposes, it suffices to distinguish between two approaches: **direct staining** and **indirect staining**, as explained in [Piñ+22; Par+25]. Direct staining means that the fluorescent labels are chemically attached to the antibodies before these labeled antibodies are applied to the cells. Following this logic, indirect staining would just mean that the labels are attached after the antibodies have been applied to the cells. However, in most cases, indirect staining refers more specifically to the use of **secondary antibodies**, which are pre-labeled antibodies that detect the unmodified antibodies of interest, called **primary antibodies** in this context.

The concept of secondary antibodies seems counterproductive. If commercially available secondary antibodies are labeled anyway, why do manufacturers not provide labeled primary antibodies?

There are two advantages of secondary antibodies that can be inferred from the short description of [Par+25]. First, producing only a handful of secondary antibodies can be standardized to ensure a high quality product. This is possible because secondary antibodies detect specific regions of primary antibodies that depend on the host organism from which the primary antibodies were obtained. Second, when the secondary antibody is polyclonal, multiple individual secondary antibodies can bind to a single primary antibody, which amplifies the staining result.

The underlying biological details are well described in the literature and are mostly irrelevant to us. However, using secondary antibodies to detect the primary antibodies, whose dose-response behavior we want to describe, skews the measured data. Secondary antibodies introduce their own binding

behavior on top of the binding behavior of the primary antibodies. Thus, the final staining originates from the combined properties of primary and secondary antibodies.

At this point, it helps to recall the antibody-staining context of the accumulation model. Intrinsic properties of different antibody types, together with associated biological questions, do not necessarily concern us. Our main focus is the behavior of the staining result, so we should describe the staining that appears as a result of the whole staining experiment, including the use of secondary antibodies.

One might argue that indirect staining should be avoided, as direct staining would not alter the epitope classes. However, data obtained by direct staining could also be skewed, since attaching a label to an antibody could alter its binding behavior. This is not just a theoretical concern. For example, using label-free detection methods, [Sun+08] and [Yin+15] demonstrate that unlabeled proteins show different kinetics compared to their labeled counterparts.

In summary, there is no way around the effects of direct labeling and secondary antibodies, since either labels or secondary antibodies must be used to measure antibodies in the context of antibody-staining. We can express this as a general observation.

Remark 4.1.2 (**Staining context**)**.**
Whenever we infer epitope classes from antibody-staining data, we obtain epitope classes for the staining results, not for the actual (primary/ unlabeled) antibody.

Although the bias introduced by secondary antibodies is inevitable, it should be reduced as much as possible. There are some experimental considerations to achieve this goal, some of which may be regarded as requirements for the accumulation model.

Washing steps after primary and secondary antibodies

Requirement: The incubation of primary and secondary antibodies must be performed one after another. Furthermore, washing steps must be performed after each antibody incubation.

Since the incubation of primary antibodies is finished before secondary antibodies are added, the binding of primary antibodies cannot be affected by

secondary antibodies. The washing steps in between ensure that the secondary antibodies only encounter bound primary antibodies. Thus, the binding of secondary antibodies does not depend on the binding dynamics of primary antibodies, but only on the eventual locations of bound primary antibodies. Finally, the binding of secondary antibodies could, in theory, affect the paratopes of the primary antibody, leading to the detachment of the primary-secondary-antibody complexes. Thus, the final washing steps do not only remove unbound secondary antibodies but also detached primary-secondary-antibody complexes.

However, there is a final hypothetical scenario in which the secondary antibodies could alter the binding properties of the primary antibodies. When the binding of secondary antibodies affects the paratopes of the primary antibody such that the primary-secondary-antibody complexes detach from the original cellular epitope and bind permanently to another cellular epitope, the secondary antibodies would retroactively affect the binding of primary antibodies. On the other hand, this re-binding behavior could not be observed by antibody-staining, nor could antibody-staining data be used to infer properties of this behavior. Furthermore, it is not clear if this re-binding occurs sufficiently often to matter at all.

In summary, we may understand the final staining result as follows. First, the primary antibodies bind, reflecting the raw interaction between their paratopes and epitopes, but also additional effects that constitute the apparent binding rates; among others, the location of the epitope together with diffusion limitations, as discussed in Section 3.1. The location of the epitopes also affects the binding of secondary antibodies that must reach the bound primary antibodies before they can attach to them. In this way, the location effect of epitopes becomes more important. Finally, once the secondary antibodies have reached the primary antibodies, the binding is mainly determined by the interaction between the primary and secondary antibodies.

Consistent application of secondary antibodies

> **Requirement:** The volume and antibody concentration of the secondary antibody solution, as well as the incubation time, must be the same for all experiments, i.e., for all initial primary antibody concentrations.

A consistent application of secondary antibodies reduces confounding effects that skew the dose-response relationship of the primary antibody. In fact, any

independent variable other than the initial concentration of primary antibodies should be avoided, as it would not be reflected in the accumulation model. This includes, for example, the temperature or the use of additional chemicals, etc. All aspects other than the concentration of primary antibodies should remain constant.

High concentration and large volume for the secondary antibody solution

> **Suggestion:** A highly concentrated secondary antibody solution should be applied at a large volume.

A sufficiently high concentration leads to a fast binding rate, and a sufficiently large volume reduces the depletion of secondary antibodies such that the fast binding rate is maintained throughout the incubation phase. In consequence, a high concentration and a large volume increase the chance that the secondary antibodies bind to all primary antibodies.

Unfortunately, this recommendation can be quite expensive. The same concentration and volume of secondary antibodies must be used for all experimental conditions (see above). This is less of a problem for primary antibodies, where all conditions, except for the highest antibody concentration, are obtained by dilutions, as described in Subsection 4.1.1.

4.1.4 Regions of interest

So far, we have simply assumed that we can compare the effects of different initial antibody concentrations in the same biological sample, or at least in identical samples; but that again is far from reality. Using the same sample for different antibody concentrations would require that we could remove bound antibodies that have already withstood several washing steps. In addition, this removal of antibodies would need to be gentle enough so that it does not damage the biological sample or the epitopes. Finally, applying different initial antibody concentrations one after another would be very time-consuming.

In practice, different initial antibody concentrations are usually applied to different samples. This has the advantage that multiple conditions can be created in parallel. However, it also has the significant disadvantage that the resulting antibody-stainings cannot be compared directly.

For example, the number and size of cells in an image greatly influence the total intensity of the image. Hence, to avoid any bias that could occur when different images are compared, the intensity value should not be calculated as the sum over all pixels, where some pixels could correspond to regions without cells, but as the average value of pixels that belong to regions of interest.

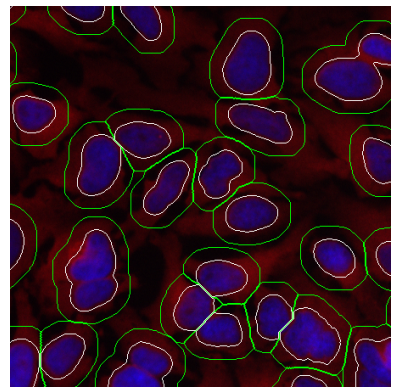

Figure 4.1: {Adapted from [Methods-Paper], raw data from [Momina Saeed; Raw-Data]} Example for regions of interest (green circles) from stained cell nuclei (stain in blue, identification in white).

Regions of interest can be defined in many ways. For example, additional fluorescent labels with distinct fluorescence wavelengths can be used to stain and identify the nuclei of cells in an image. Then, one can define the regions of interest by enlarging the areas that have been identified as cell nuclei, to include only the pixels that correspond to cells. Figure 4.1 illustrates this approach.

Remark 4.1.3 (**Multiplexing**).
Using multiple different fluorescent labels in a single sample is sometimes referred to as **multiplexing**. In principle, all fluorescence signals could be captured simultaneously by using a color-resolving image sensor. However, color filters are necessary to filter out the excitation light. Furthermore, the excitation wavelength of one label can overlap with the emission wavelength of another label. Thus, repeated illuminations with different excitation wavelengths and color filters are commonly used to capture all fluorescence signals.

In consequence, multicolor images like Figure 4.1 are often artificially created by superimposing the individual staining signals as different digital colors. Thus, arbitrary colors that do not need to correspond to the emission wavelengths can be used for the composites. Especially for far-red wavelengths beyond the range of human vision, this is inevitable.

Evaluating only pixels in regions of interest does not alter the binding

behavior of antibodies, but it does affect the data that is obtained. As with the unobservable temporary binding of antibodies, we can regard all effects that occur outside the regions of interest as binding obstructions for the epitopes within the regions of interest. Unfortunately, this means that the depletion factor can no longer be calculated from the system properties. As problematic as this sounds, the same is true for experimental units, where the unit conversion factors are unknown. In either case, the depletion factor becomes an additional parameter that needs to be estimated from the data.

4.1.5 Measurement uncertainty

Given the variability of biological systems, it is hardly surprising that dose-response data includes measurement uncertainties. However, this is not a special property of biological systems. In fact, even measurements for highly controlled physics experiments have uncertainties, such that some courses on experimental physics discuss measurement uncertainties in their introductory chapters [Dem08, Section 1.8] [Mes15, Section 0.3].

Before we discuss the measurement uncertainty for dose-response data, it is helpful to define and discuss the terms "measurement error" and "measurement uncertainty" in general. For this purpose, we may follow the terminology introduced in [Rab05, Section 1.1].

Assume that we have prepared an experimental system and that we want to measure a specific quantity of this system. Let us assume the perspective of classical physics, which simply means assuming that the quantity has a definite (true) value q_t at the time of measurement. Then we define the **measurement error** as the difference between the true value q_t and the measured value q, i.e., $\delta q = q - q_\mathrm{t}$.

There can be many reasons for measurement errors. Perhaps the most obvious reasons are mistakes made by the experimenter and issues with faulty instruments. But even in the case of flawless execution, every measurement instrument has a limited resolution beyond which no differences can be discerned. Finally, systems that may appear identical on the macroscopic scale might differ on the microscopic scale. These differences can lead to measurement errors that appear to be stochastic in nature because the underlying microscopic states are unknown.

Pursuing the idea of stochastic measurement errors further, we can model a measurement as a sample drawn from a probability distribution. Using probability distributions to describe measurements naturally leads to the concept of measurement uncertainty. In [Rab05, Section 1.1] measurement uncertainty is defined as "an interval within which a true value of a measurand

lies with a given probability". We deviate from this concept and consider the **measurement uncertainty distribution** instead, which we define as the probability distribution for obtaining a certain value q as the result of a measurement. In this way, the interval-definition is just a special case with less information, as the distribution allows us to calculate the probabilities for all intervals. Furthermore, we retain measurement uncertainty as a generic term to express a lack of knowledge about the true value.

Note that the definition of a measurement uncertainty distribution is more akin to the Bayesian interpretation of probability[1], which we will use in this dissertation. In that regard, we may understand the measurement uncertainty distribution as our lack of knowledge about the true value.

In general, the measurement uncertainty distribution is unknown, as is the true value. This does not only mean that some statistics of the distribution are unknown. Even the type of distribution is unknown.

A common approach to estimate the distribution is to collect samples from the distribution, i.e., to repeat the measurement $\{q_\ell\}_{\ell=1}^{r}$. However, in most cases, the number of measurements is severely limited, such that the samples alone do not suffice to determine the shape of the distribution. In this case, additional assumptions about the general type of the distribution become necessary. The most common assumption is probably that measurement errors are normally distributed, i.e., that the measurement uncertainty distribution is a normal distribution[2] [Mes15, Subsection 0.3.1] [Dem06, Subsection 1.8.4].

A normal distribution, often denoted as $\mathcal{N}(\mu, \sigma^2)$, is given by the probability density function

$$p(q \mid \mu, \sigma) = \frac{1}{\sqrt{2\pi\sigma^2}} e^{-\frac{(q-\mu)^2}{2\sigma^2}} \quad , \tag{4.4}$$

where μ denotes the mean value and σ denotes the standard deviation. Since the normal distribution is fully characterized by the mean value and the standard deviation, only these two parameters need to be estimated from

[1] See [For+22] for a short overview of Bayesian and frequentist statistics and their methods, or [Mac03, Section 37] for a comparison that favors the Bayesian approach. In summary, *frequentist statistics* considers probabilities as limits of relative frequencies that can only be assigned to repeatable events. Thus, it is not possible to speak about the probability that the true value is in a given interval, for example. In contrast, *Bayesian statistics* employs probability as a degree of certainty/uncertainty.

[2] Although normal distributions are commonly assumed, there is no mathematical or natural law that this is always the case. Depending on the measurement principle and the underlying microscopic processes that cause stochastic measurement errors, other distributions are more suitable. For example, [Dem06, Subsection 1.8.4] remarks that radioactive decay has Poisson-distributed measurement errors.

samples. Common point estimators[3] (cf. [Dem08, Equation (1.13)], [Mes15, Equation (6)] and [Mac03, Subsection 24.1]) for these parameters are

$$\mu = \frac{1}{r}\sum_{\ell=1}^{r} q_\ell \qquad \text{and} \qquad \sigma = \sqrt{\frac{\sum_{\ell=1}^{r}(q_\ell - \mu)^2}{r-1}}\,, \tag{4.5}$$

which we call **sample mean** and **corrected sample standard deviation**, respectively.

Returning to the measurement uncertainty of dose-response data, we can easily identify sources of measurement errors that cannot be avoided. For example, pipettes have certain tolerances, which leads to small variations in the volumes obtained through pipetting. For the dilution series that are necessary to obtain the initial antibody concentrations, these volume variations can accumulate in the worst case. Another example is the measurement principle of the staining result. The emission of fluorescence photons, the detection with a camera sensor, and the conversion from electrical to digital signals, are all processes governed by quantum mechanics, which leads to random fluctuations from a macroscopic perspective. But perhaps even more important is the fact that different biological samples are used for each experimental condition.

In summary, dose-response data is clearly affected by measurement uncertainty that needs to be estimated. Unfortunately, repeating the experiment from scratch to obtain independent measurements, also known as creating **replicates** in biological sciences, is quite laborious. Although dozens of replicates could be achieved with enough patience, hundreds or thousands of dose-response experiments are out of reach in most cases. Thus, we adopt the assumption that the measurement uncertainty distribution is a normal distribution, so that we only need to calculate the sample mean and the sample standard deviation.

However, there is a problem that we have not addressed so far. We do not measure the antibody concentration. All we do is follow instructions that will lead to a specific antibody dilution if everything is done with absolute precision. In that sense, initial antibody concentrations are nothing more than labels for the experimental conditions. Since these labels do not vary between replicates, we cannot use replicates to estimate the uncertainties of initial antibody concentrations.

[3] In a fully Bayesian treatment, point estimates may not always be the best solution (cf. [Mac03, Subsection 22.4]). However, we intend to allocate computational resources to the estimation of epitope classes (see Subsection 4.3.4). Hence, we prefer simple estimates for the measurement uncertainty.

At this point, we could guesstimate the uncertainties, e.g., by theoretical considerations about the antibody distribution in solutions and pipette tolerances; but the usefulness of this approach remains questionable. Instead, we may treat the initial antibody concentration as a label without uncertainty. Then, differences in the actual antibody concentration will be part of the measurement uncertainty of the resulting amount of bound antibodies. And since the amount of bound antibodies is actually measured (in terms of signal intensities), it is possible to estimate the measurement uncertainty distribution from replicates.

We can summarize our discussion about measurement uncertainties and dose-response data with the following definition.

Definition 4.1.4.
Experimental dose-response data is a set of tuples

$$\mathcal{D} \coloneqq \{(\mathcal{A}_i, \mathcal{X}_i, \Delta\mathcal{X}_i)\}_{i=1}^{n} \ ,$$

where each tuple consists of:

i) The initial antibody concentration $\mathcal{A}_i$, as an uncertainty-free label, measured in units of dilution quotient ($\mathrm{D_q}$).

ii) The amount of bound antibodies $\mathcal{X}_i$, as the sample mean of replicates, measured in units of normalized intensity ($\mathrm{I_n}$).

iii) The corrected sample standard deviation $\Delta\mathcal{X}_i$ of the replicates, measured in units of normalized intensity ($\mathrm{I_n}$).

In this context, we call $\mathcal{X}_i$ **response value** and $\Delta\mathcal{X}_i$ **response spread**.

4.2 Epitope density as an estimation tool

With our basic understanding of experimental data and its limitations, we can consider the estimation process. Our goal is to infer the underlying epitope classes, given some experimental dose-response data. However, we face two major problems. First, we only have an analytical solution for the reservoir case. Second, we have no idea about the number of epitope classes in a system.

Of course, we could use numerical solutions of the depletion accumulation IVP to estimate epitope classes. After all, numerical solutions worked quite well to plot the depletion accumulation dose-response curves in Figures 3.9–3.13.

But, as argued in Subsection 3.2.3, we must calculate numerical solutions from scratch for each individual initial antibody concentration of the dose-response curve. Even worse, if the estimation is an iterative process, the numerical calculations need to be repeated for each initial antibody concentration and each iteration step. This quickly becomes computationally expensive, especially when there is a large number of epitope classes, which leads to high-dimensional coupled differential equations.

Since we used apparent rate constants for the accumulation model, the dimensionality problem leads to conceptual conflicts. On the one hand, we should expect quite a large number of epitope classes, given the heterogeneity of epitope locations, for example, in complex cellular structures. On the other hand, we need to minimize the number of epitope classes to reduce the computational cost of numerical solutions.

These limitations of the depletion model motivate us to favor the reservoir model. Although depletion may still play a major role in the actual experiment, we may regard these effects as an additional aspect that contributes to the apparent rate constants. After all, the accumulation model is just an empirical model, not a mechanistic model. But we need not ignore depletion effects completely. In Subsection 4.3.5, we will develop methods to investigate the severity of depletion and to correct the data accordingly.

In the meantime, we benefit from the well-behavedness of the reservoir accumulation model. We have analytical solutions that are valid for mixtures of monoclonal antibodies against different targets (Corollary 3.3.15), and we can even re-interpret epitope classes in order to apply the reservoir model to generic mixtures and polyclonal antibodies (Theorem 3.3.13).

However, before we address the unknown number of epitope classes, there is a slight modification that will allow us to disregard the incubation time. We can absorb the incubation time into the rate constants if we define characteristic constants.

Definition 4.2.1.
Let $\{(g_i, k_{\mathrm{a};i})\}_{i=1}^{N}$ be epitope classes. We call

$$K_{\tau;i} \coloneqq \frac{1}{k_{\mathrm{a};i}\tau}$$

obstruction constant and its inverse value $K_i = K_{\tau;i}^{-1}$ **accessibility constant**[4].

In terms of accessibility constants, the epitope classes are given by $\{(g_i, K_i)\}_{i=1}^N$ and the reservoir accumulation model reads

$$X(a) = \sum_{i=1}^{N} g_i \left(1 - e^{-K_i a}\right) \ . \tag{4.6}$$

In terms of obstruction constants, the epitope classes become $\{(g_i, K_{\tau;i})\}_{i=1}^N$ and the reservoir accumulation model reads

$$X(a) = \sum_{i=1}^{N} g_i \left(1 - e^{-\frac{a}{K_{\tau;i}}}\right) \ . \tag{4.7}$$

Note that we prefer the obstruction constants, as they have the same dimension/ unit as the antibody concentration, which will lead to more intuitive plots.

In either case, the accessibility/obstruction constants act as system parameters that implicitly depend on the incubation time. Expressing the system constants in this form allows us to compare experiments with different incubation times and to analyze data where the incubation time is unknown. The incubation time simply becomes an implicit part of the estimation process.

4.2.1 The epitope density

Despite the well-behavedness of the reservoir model, the conceptual conflict regarding the number of epitope classes remains. To address this issue, [Svi+03] proposed continuous densities for the description of epitopes in the context of the Langmuir model. This approach was subsequently applied and improved, e.g., by [Svi+03; Svi+07; Gor+08; Zha+13; Zha+18; For+18; Zha+19; Mal+20].

We can easily adapt the density approach to the reservoir accumulation model. For this purpose, we consider densities (odd/twisted differential forms) of the form

$$\eta(K_\tau) = g(K_\tau)|dK_\tau| \ ,$$

where the function $g(K_\tau) \geq 0$ describes the proportion of epitopes that have the obstruction constant K_τ (see Appendix C.6 for an intuitive introduction

[4] In [Methods-Paper], K_τ is called *accessibility constant*. Here, we call $K = K_\tau^{-1}$ accessibility constant and call K_τ obstruction constant. The reason for this discrepancy is the limited scope of a paper. In the paper, only K_τ was used, because it has the same dimension/unit as the antibody concentration, leading to more intuitive plots. And since accessibility is a major concept of the accumulation model, K_τ was called accessibility constant. Here, we have a broader scope, allowing us to consider both K_τ and K.

to densities). Then, the response value is given by the integral of the **accumulation model function** $F(K_\tau, a) = (1 - e^{-\frac{a}{K_\tau}})$ against the epitope density over the set of valid obstruction constants $\mathbb{K} = (0, \infty)$,

$$X(a) = \int_{\mathbb{K}} F(K_\tau, a)\, \eta(K_\tau) \;= \int_{(0,\infty)} g(K_\tau) \left(1 - e^{-\frac{a}{K_\tau}}\right) \; |dK_\tau| \; .$$

And the total amount of epitopes is given by the integral of the epitope density,

$$G = \int_{\mathbb{K}} \eta(K_\tau) \;= \int_{(0,\infty)} g(K_\tau) \; |dK_\tau| \; .$$

Unfortunately, an epitope density $\eta(K_\tau) = g(K_\tau) \; |dK_\tau|$ is not a generalization of the model, as it cannot describe discrete epitope classes. Since the discrete case is the natural one (there are only finitely many epitopes in a real system), we should consider the epitope density as a convenient approximation.

If we want to retrieve (4.7), we could allow sums of delta functions in the density:

$$\eta_\delta(K_\tau) = \sum_{i=1}^{N} g_i \delta(K_\tau - K_{\tau;i}) \; |dK_\tau| \; .$$

Then, using the defining property of delta functions (see, e.g., [AD19, Section C6.1]),

$$\int_{(a,b)} \delta(x - c) f(x) \; |dx| = f(c) \qquad \text{if} \qquad c \in (a, b) \; ,$$

we obtain

$$\begin{aligned} X(a) &= \int_{\mathbb{K}} F(K_\tau, a)\, \eta_\delta(K_\tau) \\ &= \int_{(0,\infty)} \sum_{i=1}^{N} g_i \delta(K_\tau - K_{\tau;i}) \left(1 - e^{-\frac{a}{K_\tau}}\right) \; |dK_\tau| \\ &= \sum_{i=1}^{N} \; g_i \left(1 - e^{-\frac{a}{K_{\tau;i}}}\right) \; . \end{aligned}$$

It should be noted that delta functions are not proper functions and that η_δ is not a valid density in the sense of twisted/odd differential forms. The use of delta functions can be made rigorous, either by considering measure theory or by using de Rham currents (see [Rha84, Chapter III]). Following

the latter approach, we would need to consider double currents for a rigorous formulation. However, that much formalism could hardly be justified for an empirical model that should just be a sum over finite epitope classes. Thus, we will stick to proper densities[5]. The takeaway of this reference to rigorous formalisms should be that the epitope density η is a proper object by itself that exists beyond integration.

In itself, densities do not help us estimate epitope classes from experimental data. Determining an unknown density is even more difficult than determining a finite set of epitope classes. Thus, we should express the density in terms of a sum of ansatz functions, which are uniquely characterized by a few parameters.

Maybe the simplest approach that does not presume a certain shape of density is a sum of piece-wise-constant functions. This approach was already used by [Svi+03] for the equilibrium dose-response curve of the Langmuir model. Thus, let us consider a bounded right-open interval $I \subset \mathbb{K}$ and a partition of the interval, i.e., a finite set of points $P = \{q_1, \dots, q_{m+1}\} \subset I$, such that

$$q_1 = \min(I) \ , \quad q_{m+1} = \sup(I) \qquad \text{and} \qquad q_i < q_j \quad \forall \ i < j \ .$$

The partition defines m non-empty right-open subintervals $I_j = [q_j, q_{j+1})$ of I for all $j \in \{1, \dots, m\}$. Furthermore, let χ_{I_j} denote the characteristic functions of the subintervals, that is,

$$\chi_{I_j}(K_\tau) = \begin{cases} 1 & , \quad K_\tau \in I_j \\ \\ 0 & , \quad K_\tau \notin I_j \end{cases} \ .$$

Next, let us assume that the epitope density is given by $\eta = g(K_\tau) \ |dK_\tau|$, where $g(K_\tau)$ is a proper function that has compact support in I. The compact support assumption can be justified by the requirement that all rate constants, and thus all obstruction constants, should be non-zero and finite. Now, we can approximate the density function as

$$g(K_\tau) \approx \sum_{j=1}^{m} g(\xi_j)\chi_{I_j}(K_\tau) \qquad \Rightarrow \qquad \eta(K_\tau) \approx \sum_{j=1}^{m} g(\xi_j)\chi_{I_j}(K_\tau) \ |dK_\tau| \ ,$$

by choosing $\xi_j \in I_j$ for all $j \in \{1, \dots, m\}$. Since we have essentially followed the construction of a Riemann sum (see Figure 4.2), we may call this approximation **Riemann-sum approximation**.

[5]When η is a proper density, it can be identified with a current by $\eta[F] = \int_{\mathbb{K}} \eta F = \int_{\mathbb{K}} F\eta$.

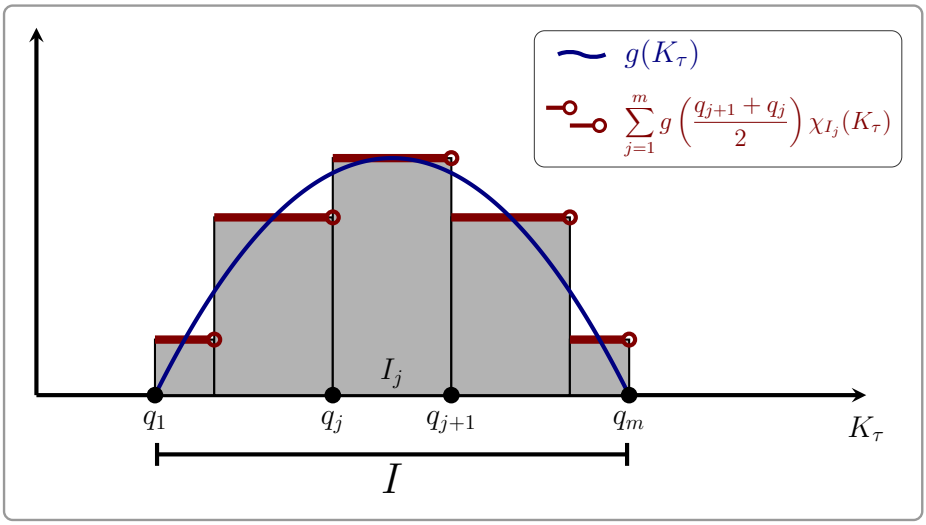

Figure 4.2: Illustration of the Riemann-sum approximation of a density function. Here, the evaluation points ξ_j are the centers $\frac{q_{j+1}+q_j}{2}$ of the intervals $I_j = [q_j, q_{j+1})$. The gray rectangles correspond to the surface areas that would be summed up in a corresponding Riemann sum. This illustrates the similarity between Riemann sums and Riemann-sum approximations.

The true density function $g(K_\tau)$ is still unknown, so we have to replace the values $g(\xi_j)$ with parameters λ_j that need to be estimated. For the interpretation of the parameters λ_j, it is convenient to divide them by $q_{j+1} - q_j$.

Definition 4.2.2.
Let $I \subset \mathbb{K} = (0, \infty)$ be a bounded right-open interval, let $P = \{q_1, \ldots, q_{m+1}\}$ be a partition of I, and let

$$F(K_\tau, a) = 1 - e^{-\frac{a}{K_\tau}}$$

be the accumulation model function. Then we call

$$\left(\eta_{\{P,\lambda\}}(K_\tau),\ F(K_\tau, a)\right)$$

with

$$\lambda \in \mathbb{R}^m\ , \qquad \eta_{\{P,\lambda\}}(K_\tau) = \sum_{j=1}^{m} \frac{\lambda_j}{q_{j+1} - q_j} \chi_{I_j}(K_\tau)\ |dK_\tau|$$

accumulation estimation model. Furthermore, we refer to $\lambda \in \mathbb{R}^m$ as **parameters** of the accumulation estimation model and call the epitope density **estimation epitope density**.

At first glance, it seems that we have come full circle. We started with an estimation problem for a finite set of parameters (the epitope classes $\{(g_i, K_{\tau;i})\}_{i=1}^N$). Then we introduced densities, which are even harder to estimate. Finally, we used the Riemann-sum approximation, just to end up again with a finite set of parameters $\lambda = (\lambda_1, \ldots, \lambda_m)$ that we need to estimate.

However, there is a small but important difference. While the number of epitope classes is unknown, we can freely choose the number of parameters for the accumulation estimation model by using different partitions. Essentially, this choice allows us to control the coarseness of the approximation.

Observe that dividing the parameters λ_j by $q_{j+1} - q_j$ gives them an intuitive interpretation. To see that, let us calculate the response value for $\eta_{\{P,\lambda\}}(K_\tau)$:

$$\begin{aligned} X(a) &= \int_{\mathbb{K}} F(K_\tau, a)\, \eta_{\{P,\lambda\}}(K_\tau) \\ &= \int_{(0,\infty)} \left(1 - e^{-\frac{a}{K_\tau}}\right) \sum_{j=1}^{m} \frac{\lambda_j}{q_{j+1} - q_j} \chi_{I_j}(K_\tau)\ |dK_\tau| \\ &= \sum_{j=1}^{m} \frac{\lambda_j}{q_{j+1} - q_j} \int_{I_j} \left(1 - e^{-\frac{a}{K_\tau}}\right)\ |dK_\tau| \ . \end{aligned}$$

Since $1 - e^{-\frac{a}{K_\tau}}$ is smooth on $(0, \infty)$ as a function of K_τ, it is Riemann integrable for each compact interval in $(0, \infty)$. It follows that the improper integral over the bounded right-open intervals I_j is equal to the integral over the closures $\overline{I}_j$ with respect to the standard topology of $\mathbb{R}$:

$$\int_{I_j} \left(1 - e^{-\frac{a}{K_\tau}}\right)\ |dK_\tau| = \int_{\overline{I}_j} \left(1 - e^{-\frac{a}{K_\tau}}\right)\ |dK_\tau| \ .$$

Now we can apply the first mean value theorem of integral calculus (see, e.g., [KW13, Theorem 5.2.1]) to the right-hand side of the equation, leading to

$$\int_{I_j} \left(1 - e^{-\frac{a}{K_\tau}}\right)\ |dK_\tau| = \left(1 - e^{-\frac{a}{\xi_j}}\right) (q_{j+1} - q_j)$$

for some $\xi_j \in \overline{I}_j$.

In fact, since $a > 0$, the expression $1 - e^{-\frac{a}{K_\tau}}$ is strictly monotonically decreasing on $(0, \infty)$ as a function of K_τ, which can easily be seen by differentiation. Thus,

$$1 - e^{-\frac{a}{q_{j+1}}} < 1 - e^{-\frac{a}{K_\tau}} \qquad \forall\ K_\tau \in I_j = [q_j, q_{j+1}) \ ,$$

which yields $\xi_j \in I_j$.

For the response value, we obtain

$$\begin{aligned} X(a) &= \sum_{j=1}^{m} \frac{\lambda_j}{q_{j+1} - q_j} \int_{I_j} \left(1 - e^{-\frac{a}{K_\tau}}\right) \ |dK_\tau| \\ &= \sum_{j=1}^{m} \frac{\lambda_j}{q_{j+1} - q_j} \left(1 - e^{-\frac{a}{\xi_j}}\right) (q_{j+1} - q_j) = \sum_{j=1}^{m} \lambda_j \left(1 - e^{-\frac{a}{\xi_j}}\right) \ , \end{aligned}$$

where $\xi_j \in I_j$ for all $j \in \{1, \ldots, m\}$. Comparing the last term with (4.7) reveals that λ_j may be interpreted as an amount of epitopes. More precisely, λ_j is the amount of epitopes with $K_\tau \in I_j$.

We can confirm this interpretation of the model parameters λ by calculating the total amount of epitopes G for the accumulation estimation model:

$$\begin{aligned} G &= \int_{\mathbb{K}} \eta_{\{P,\lambda\}}(K_\tau) = \int_{\mathbb{K}} \sum_{j=1}^{m} \frac{\lambda_j}{q_{j+1} - q_j} \chi_{I_j}(K_\tau) \ |dK_\tau| \\ &= \sum_{j=1}^{m} \frac{\lambda_j}{q_{j+1} - q_j} \int_{\mathbb{K}} \chi_{I_j}(K_\tau) \ |dK_\tau| = \sum_{j=1}^{m} \frac{\lambda_j}{q_{j+1} - q_j} \int_{I_j} \ |dK_\tau| \\ &= \sum_{j=1}^{m} \frac{\lambda_j}{q_{j+1} - q_j} (q_{j+1} - q_j) = \sum_{j=1}^{m} \lambda_j \ . \end{aligned}$$

In summary, when we estimate epitope classes using the accumulation estimation model, we estimate **approximate epitope classes**

$$\{(\lambda_j, [q_j, q_{j+1}))\}_{j=1}^{m} \ ,$$

where $[q_j, q_{j+1})$ is the interval of possible obstruction-constant values for the approximated epitope class, and λ_j is the amount of epitopes with obstruction constant $K_\tau \in [q_j, q_{j+1})$.

4.2.2 Coordinate transformations and unit invariance

Experimental dose-response data is often measured in terms of experimental units (see Section 4.1), so we should investigate how epitope densities and the accumulation estimation model behave when the units are changed.

Formally, we can understand a change of units as a coordinate transformation (see Appendix C). Assuming that we transform both arguments of the accumulation model function F with the same coordinate transformation, i.e., $\phi_2 = \phi \times \phi$, the function transformation is given by

$$\widetilde{F}(\widetilde{K_\tau}, \widetilde{a}) = F\left(\phi^{-1}(\widetilde{K_\tau}), \phi^{-1}(\widetilde{a})\right) \ . \tag{4.8}$$

And the epitope density transformation is given by

$$\widetilde{\eta}(\widetilde{K_\tau}) = g\left(\phi^{-1}(\widetilde{K_\tau})\right) \left| \frac{d}{d\widetilde{K_\tau}} \phi^{-1}(\widetilde{K_\tau}) \right| \ |d\widetilde{K_\tau}| \ , \tag{4.9}$$

which agrees with integration by substitution over a set $M \subset \mathbb{K}$:

$$\begin{aligned} \int_M \eta(K_\tau) = \int_M g(K_\tau) \ |dK_\tau| &= \int_{\phi(M)} g\left(\phi^{-1}(\widetilde{K_\tau})\right) \left| \frac{d}{d\widetilde{K_\tau}} \phi^{-1}(\widetilde{K_\tau}) \right| \ |d\widetilde{K_\tau}| \\ &= \int_{\widetilde{M}} \widetilde{\eta}(\widetilde{K_\tau}) \ . \end{aligned} \tag{4.10}$$

See Appendix C.4 and Appendix C.6 for further information on the transformation behavior.

There is a final transformation rule that we need before we can consider the accumulation estimation model. For a coordinate transformation $\phi \colon M \to M$, we have

$$\chi_I(\phi^{-1}(x)) = \chi_{\phi(I)}(x) \qquad \forall \ I \subseteq M \ , \ x \in \phi(I) \ , \tag{4.11}$$

which follows immediately from the definition of characteristic functions (see Appendix B.3.1).

Now, we can consider unit transformations and their effects on the accumulation estimation model.

Theorem 4.2.3.
Let $\phi\colon \mathbb{K} \to \mathbb{K}\ , a \mapsto \gamma a$ be a unit transformation ($\gamma > 0$). In the new units $\mathcal{K}_\tau = \phi(K_\tau)$ and $\mathcal{A} = \phi(a)$, the accumulation estimation model is given by

$$\left(\eta_{\{\mathcal{P},\lambda\}}(\mathcal{K}_\tau), F(\mathcal{K}_\tau, \mathcal{A})\right) \ ,$$

where

$$\mathcal{P} = \{\phi(q_1), \ldots, \phi(q_{m+1})\} \ .$$

Furthermore,

$$\int_{\mathbb{K}} F(K_\tau, a)\, \eta_{\{P,\lambda\}}(K_\tau) = \int_{\mathbb{K}} F(\mathcal{K}_\tau, \mathcal{A})\, \eta_{\{\mathcal{P},\lambda\}}(\mathcal{K}_\tau)$$

and

$$\int_{\mathbb{K}} \eta_{\{P,\lambda\}}(K_\tau) = \int_{\mathbb{K}} \eta_{\{\mathcal{P},\lambda\}}(\mathcal{K}_\tau) \ .$$

Proof 4.2.4.
In the coordinates $\mathcal{K}_\tau = \phi(K_\tau)$ and $\mathcal{A} = \phi(a)$, the accumulation estimation model is given by

$$\left(\widetilde{\eta}_{\{P,\lambda\}}(\mathcal{K}_\tau), \widetilde{F}(\mathcal{K}_\tau, \mathcal{A})\right) \ .$$

According to (4.8), the accumulation model function in the new coordinates $\mathcal{K}_\tau$ and $\mathcal{A}$ is given by

$$\widetilde{F}(\mathcal{K}_\tau, \mathcal{A}) = F(\phi^{-1}(\mathcal{K}_\tau), \phi^{-1}(\mathcal{A})) = F\left(\tfrac{1}{\gamma}\mathcal{K}_\tau, \tfrac{1}{\gamma}\mathcal{A}\right)$$

$$= 1 - \exp\left(-\frac{\frac{1}{\gamma}\mathcal{A}}{\frac{1}{\gamma}\mathcal{K}_\tau}\right) = 1 - \exp\left(-\frac{\mathcal{A}}{\mathcal{K}_\tau}\right) = F(\mathcal{K}_\tau, \mathcal{A}) \ .$$

And according to (4.9) and (4.11), the epitope density in the new coordinates is given by

$$\widetilde{\eta}_{\{P,\lambda\}}(\mathcal{K}_\tau) = g(\phi^{-1}(\mathcal{K}_\tau)) \left|\frac{d}{d\mathcal{K}_\tau}\phi^{-1}(\mathcal{K}_\tau)\right| |d\mathcal{K}_\tau|$$

$$= \sum_{j=1}^{m} \frac{\lambda_j}{q_{j+1} - q_j} \chi_{I_j}(\phi^{-1}(\mathcal{K}_\tau)) \left|\frac{d}{d\mathcal{K}_\tau}\phi^{-1}(\mathcal{K}_\tau)\right| |d\mathcal{K}_\tau|$$

$$= \sum_{j=1}^{m} \frac{\lambda_j}{q_{j+1} - q_j} \chi_{\phi(I_j)}(\mathcal{K}_\tau) \frac{1}{\gamma} |d\mathcal{K}_\tau|$$

$$= \sum_{j=1}^{m} \frac{\lambda_j}{\phi(q_{j+1}) - \phi(q_j)} \chi_{\phi(I_j)}(\mathcal{K}_\tau) |d\mathcal{K}_\tau|$$

$$= \eta_{\{\mathcal{P},\lambda\}}(\mathcal{K}_\tau) \ ,$$

Note that we have implicitly used $[\phi(q_{j+1}), \phi(q_j)) = \phi([q_{j+1}, q_j)) = \phi(I_j)$ in the last step.

In summary, the accumulation estimation model in the coordinates $\mathcal{K}_\tau$ and $\mathcal{A}$ is given by

$$\Big(\eta_{\{\mathcal{P},\lambda\}}(\mathcal{K}_\tau), F(\mathcal{K}_\tau, \mathcal{A})\Big) \ .$$

It remains to prove the integral equations. For the first equation, we use (4.10) to calculate

$$\int_{\mathbb{K}} F(\mathcal{K}_\tau, \mathcal{A})\, \eta_{\{\mathcal{P},\lambda\}}(\mathcal{K}_\tau)$$

$$= \int_{\mathbb{K}} \sum_{j=1}^{m} \frac{\lambda_j}{\phi(q_{j+1}) - \phi(q_j)} \chi_{\phi(I_j)}(\mathcal{K}_\tau) \left(1 - e^{-\frac{\mathcal{A}}{\mathcal{K}_\tau}}\right) |d\mathcal{K}_\tau|$$

$$= \sum_{j=1}^{m} \frac{\lambda_j}{\gamma q_{j+1} - \gamma q_j} \int_{\phi(I_j)} \left(1 - e^{-\frac{\mathcal{A}}{\mathcal{K}_\tau}}\right) |d\mathcal{K}_\tau|$$

$$= \sum_{j=1}^{m} \frac{\lambda_j}{q_{j+1} - q_j} \frac{1}{\gamma} \int_{\phi^{-1}(\phi(I_j))} \left(1 - e^{-\frac{\mathcal{A}}{\phi(K_\tau)}}\right) |d\phi(K_\tau)|$$

$$= \sum_{j=1}^{m} \frac{\lambda_j}{q_{j+1} - q_j} \frac{1}{\gamma} \int_{I_j} \left(1 - e^{-\frac{\frac{1}{\gamma}\mathcal{A}}{K_\tau}}\right) \gamma |dK_\tau|$$

$$= \sum_{j=1}^{m} \frac{\lambda_j}{q_{j+1} - q_j} \int_{I_j} \left(1 - e^{-\frac{a}{K_\tau}}\right) |dK_\tau|$$

$$= \int_{\mathbb{K}} \sum_{j=1}^{m} \frac{\lambda_j}{q_{j+1} - q_j} \chi_{I_j}(K_\tau) \left(1 - e^{-\frac{a}{K_\tau}}\right) \, |dK_\tau|$$

$$= \int_{\mathbb{K}} F(K_\tau, a)\, \eta_{\{P,\lambda\}}(K_\tau) \; .$$

For the second integral equation, we observe that $\widetilde{\mathbb{K}} = \phi(\mathbb{K}) = \mathbb{K}$. Thus, using $\widetilde{\eta}_{\{P,\lambda\}}(\mathcal{K}_\tau) = \eta_{\{\mathcal{P},\lambda\}}(\mathcal{K}_\tau)$ and (4.10) yields

$$\int_{\mathbb{K}} \eta_{\{P,\lambda\}}(K_\tau) = \int_{\widetilde{\mathbb{K}}} \widetilde{\eta}_{\{P,\lambda\}}(\mathcal{K}_\tau) = \int_{\mathbb{K}} \eta_{\{\mathcal{P},\lambda\}}(\mathcal{K}_\tau) \; .$$

□

Despite its technical appearance, the last theorem has a simple yet important interpretation. When we use the same unit for the obstruction constant as for the initial antibody concentration, the shape of the accumulation estimation model, the dose-response value, and the amount of epitopes do not depend on the unit. This means that we can use experimental units for the initial antibody concentration. Furthermore, the estimation parameters are the same for each unit. Thus, we always estimate the same parameters, irrespective of the unit of the initial antibody concentration.

In addition to the unit for the initial antibody concentration, experimental dose-response data also carries a unit for the response value. Unlike the initial antibody concentration and the obstruction constant, the response value is not an argument of the epitope density or of the accumulation model function. Thus, we have to change the function values instead of the function arguments. For the response value, a unit change is given by

$$X(a) \longmapsto \xi X(a) \qquad \forall\, \xi > 0 \; .$$

We have argued in Subsection 2.1.3 that epitopes (binding sites) and bound antibodies (bound particles) should have the same dimension/unit, so the epitope density should carry the unit of the response value.

Since the product of densities with real values (and functions in general) is a valid operation, we can define a change of units for the epitope density as

$$\eta(K_\tau) \longmapsto \xi \eta(K_\tau) \qquad \forall\, \xi > 0 \; .$$

Theorem 4.2.5.
Let $\xi > 0$ be a unit conversion factor, let $\eta(K_\tau)$ be an epitope density, and let $F(a, K_\tau)$ be the accumulation model function. Then

$$\xi X(a) = \int_{\mathbb{K}} F(K_\tau, a)\xi\eta(K_\tau)$$

and

$$\xi G = \int_{\mathbb{K}} \xi\eta(K_\tau) \ .$$

Furthermore,

$$\xi\eta_{\{P,\lambda\}}(K_\tau) = \eta_{\{P,\xi\lambda\}}(K_\tau)$$

for every estimation epitope density $\eta_{\{P,\lambda\}}(K_\tau)$.

Proof 4.2.6.
The integral equations follow immediately from the linearity of integration. For the estimation epitope density, we calculate

$$\begin{aligned}\xi\eta_{\{P,\lambda\}}(K_\tau) &= \xi \sum_{j=1}^{m} \frac{\lambda_j}{q_{j+1} - q_j} \chi_{I_j}(K_\tau) \ |dK_\tau| \\ &= \sum_{j=1}^{m} \frac{\xi\lambda_j}{q_{j+1} - q_j} \chi_{I_j}(K_\tau) \ |dK_\tau| = \eta_{\{P,\xi\lambda\}}(K_\tau) \ .\end{aligned}$$

□

Together, Theorem 4.2.3 and Theorem 4.2.5 show that we can use experimental dose-response data $\{(\mathcal{A}_i, \mathcal{X}_i, \Delta\mathcal{X}_i)\}_{i=1}^n$ to estimate approximate epitope classes $\{(\Lambda_j, [\mathcal{Q}_j, \mathcal{Q}_{j+1}))\}_{j=1}^m$ with the accumulation estimation model, whose construction is the same for all units. Furthermore, the approximate epitope classes have the same units as the experimental dose-response data, i.e.,

$$\{(\mathcal{A}_i, \mathcal{X}_i, \Delta\mathcal{X}_i)\}_{i=1}^n = \{(\gamma a_i, \ \xi X_i, \ \gamma\Delta X_i)\}_{i=1}^n$$

and

$$\{(\Lambda_j, \ [\mathcal{Q}_j, \mathcal{Q}_{j+1}) \ )\}_{j=1}^m = \{(\xi\lambda_j, \ [\gamma q_j, \gamma q_{j+1}) \ )\}_{j=1}^m \ .$$

4.3 Accessibility analysis

There are additional aspects that we need to discuss before we can apply established methods to estimate parameters with the accumulation estimation model. For example, we need to choose an objective function and an algorithm to optimize the objective function. Furthermore, we should develop a visualization of estimated epitope densities to facilitate an intuitive interpretation. Hence, this section focuses on practical aspects of the accumulation estimation model, parameter estimation, and the visualization of estimation epitope densities. Together, these aspects will define the *accessibility analysis*.

4.3.1 Obstruction constant vs accessibility constant

In Definition 4.2.1, we have introduced the obstruction constant K_τ and the accessibility constant K. However, we have only used the obstruction constant for the accumulation estimation model. Among others, we prefer the obstruction constant, as it has the same unit as the initial antibody concentration.

Accumulation estimation ansatz for the accessibility constant

Nevertheless, we can construct an accumulation estimation ansatz

$$\Big(\rho_{\{P',\lambda\}}(K), H(K,a)\Big)$$

by defining

$$\rho_{\{P',\lambda\}}(K) = \sum_{j=1}^{m} \frac{\lambda_j}{q'_{j+1} - q'_j} \chi_{[q'_j, q'_{j+1})}(K)\ |dK| \ , \quad H(K,a) = \Big(1 - e^{-Ka}\Big) \ .$$

The unit invariance of Theorem 4.2.3 still holds when we transform K with the inverse map; that is, $\widetilde{K} = \phi^{-1}(K) = \frac{1}{\gamma}K$, whereas $\widetilde{a} = \phi(a) = \gamma a$. The inverse map is used because the unit of the accessibility constant is the reciprocal unit of the initial antibody concentration.

For the discrete models (4.7) and (4.6), the relationship $K_{\tau;i} = K_i^{-1}$ between the obstruction constants and the accessibility constants ensures that the models yield the same result:

$$\sum_{i=1}^{N} g_i \left(1 - e^{-K_i a}\right) = \sum_{i=1}^{N} g_i \left(1 - e^{-\frac{a}{K_{\tau;i}}}\right) \ .$$

Thus, one might think that obstruction constants and accessibility constants lead to equivalent accumulation estimation models. Unfortunately, this is not the case.

Considering the relationship between obstruction constants and accessibility constants as coordinate transformations $K_i = \psi(K_{\tau;i})$ and $K_{\tau;i} = \psi^{-1}(K_i)$, where

$$\psi\colon \mathbb{K} \to \mathbb{K},\ x \mapsto \frac{1}{x} \qquad \Leftrightarrow \qquad \psi^{-1} = \psi\colon \mathbb{K} \to \mathbb{K},\ y \mapsto \frac{1}{y}\ ,$$

we can transform the epitope densities $\eta_{\{P,\lambda\}}(K_\tau)$ and $\rho_{\{P',\lambda\}}(K)$. This allows us to calculate that the constructions of the accumulation estimation models do not agree, i.e.,

$$\widetilde{\eta}_{\{P,\lambda\}}(K) \neq \rho_{\{\psi^{-1}(P),\lambda\}}(K) \qquad \text{and} \qquad \widetilde{\rho}_{\{P',\lambda\}}(K_\tau) \neq \eta_{\{\psi(P'),\lambda\}}(K_\tau)\ .$$

To verify this claim, we calculate

$$\begin{aligned}
\widetilde{\eta}_{\{P,\lambda\}}(K) &= \sum_{j=1}^{m} \frac{\lambda_j}{q_{j+1} - q_j} \chi_{[q_j,q_{j+1})}(\psi(K)) \left| \frac{d}{dK}\psi(K) \right| \ |dK| \\
&= \sum_{j=1}^{m} \frac{\lambda_j}{q_{j+1} - q_j} \chi_{[\psi^{-1}(q_j),\psi^{-1}(q_{j+1}))}(K) \frac{1}{K^2} \ |dK| \\
&\neq \rho_{\{\psi^{-1}(P),\lambda\}}(K) \\
&= \sum_{j=1}^{m} \frac{\lambda_j}{\psi^{-1}(q_{j+1}) - \psi^{-1}(q_j)} \chi_{[\psi^{-1}(q_j),\psi^{-1}(q_{j+1}))}(K) \ |dK|\ .
\end{aligned}$$

Finally, we calculate

$$\begin{aligned}
\widetilde{\rho}_{\{P',\lambda\}}(K_\tau) &= \sum_{j=1}^{m} \frac{\lambda_j}{q'_{j+1} - q'_j} \chi_{[q'_j,q'_{j+1})}(\psi^{-1}(K_\tau)) \left| \frac{d}{dK_\tau}\psi^{-1}(K_\tau) \right| \ |dK_\tau| \\
&= \sum_{j=1}^{m} \frac{\lambda_j}{q'_{j+1} - q'_j} \chi_{[\psi(q'_j),\psi(q'_{j+1}))}(K_\tau) \frac{1}{K_\tau^2} \ |dK_\tau| \\
&\neq \eta_{\{\psi(P'),\lambda\}}(K_\tau) \\
&= \sum_{j=1}^{m} \frac{\lambda_j}{\psi(q'_{j+1}) - \psi(q'_j)} \chi_{[\psi(q'_j),\psi(q'_{j+1}))}(K_\tau) \ |dK_\tau|\ .
\end{aligned}$$

In itself, this disagreement is not problematic. It just shows that using the accessibility constant instead of the obstruction constant corresponds to a different ansatz for the estimation. Naturally, this poses the question: what ansatz is better suited?

Analytical solutions of the integrals

As mentioned above, we prefer the obstruction constant, as it has the same unit as the initial antibody concentration; but the accessibility constant ansatz has its merits, too. Note that we have not solved the integral

$$\int_{I_j} 1 - e^{-\frac{a}{K_\tau}} \, |dK_\tau| = \int_{q_j}^{q_{j+1}} 1 - e^{-\frac{a}{K_\tau}} \, dK_\tau \tag{4.12}$$

that appears in the accumulation estimation model:

$$X(a) = \int_{\mathbb{K}} F(K_\tau, a)\, \eta_{\{P,\lambda\}}(K_\tau) = \sum_{j=1}^{m} \frac{\lambda_j}{q_{j+1} - q_j} \int_{I_j} \left(1 - e^{-\frac{a}{K_\tau}}\right) \, |dK_\tau| \; .$$

The reason for the missing solution is that it cannot be expressed in terms of elementary functions. Here, the accessibility constant is superior. Calculating the response value of the accumulation estimation ansatz for the accessibility constant, we obtain (see Appendix B.3.2, page 189)

$$\int_{\mathbb{K}} H(K, a)\, \rho_{\{P',\lambda\}}(K) = \sum_{j=1}^{m} \lambda_j \left(1 + \frac{1}{a(q'_{j+1} - q'_j)} \left(e^{-q'_{j+1}a} - e^{-q'_j a}\right)\right) \; .$$

However, using the exponential integral (cf. [GR09, Subsection 8.21]), given by

$$\mathrm{Ei}(x) = -\int_{-x}^{\infty} \frac{e^{-t}}{t} \, dt \qquad \forall\, x < 0 \; , \tag{4.13}$$

we can solve the integral (4.12) that appears in the accumulation estimation model (see Appendix B.3.2, page 190 ff.):

$$X(a) = \sum_{j=1}^{m} \frac{\lambda_j}{q_{j+1} - q_j} \left[K_\tau \left(1 - e^{-\frac{a}{K_\tau}}\right) - a\, \mathrm{Ei}\left(-\frac{a}{K_\tau}\right)\right]_{K_\tau = q_j}^{K_\tau = q_{j+1}} \tag{4.14}$$

$$= \sum_{j=1}^{m} \frac{\lambda_j}{q_{j+1} - q_j} \left(q_{j+1}\left(1 - e^{-\frac{a}{q_{j+1}}}\right) - a\, \mathrm{Ei}\left(-\frac{a}{q_{j+1}}\right)\right.$$

$$\left. - q_j \left(1 - e^{-\frac{a}{q_j}}\right) + a\, \mathrm{Ei}\left(-\frac{a}{q_j}\right)\right) \; .$$

And although the exponential integral is not an elementary function, it is still a standard function in the sense that it is available in many programming languages[6].

Furthermore, because of Theorem 4.2.3 and Theorem 4.2.5, we can also use experimental units,

$$\mathcal{X}(\mathcal{A}) = \sum_{j=1}^{m} \frac{\Lambda_j}{\mathcal{Q}_{j+1} - \mathcal{Q}_j} \left[\mathcal{K}_\tau \left(1 - e^{-\frac{\mathcal{A}}{\mathcal{K}_\tau}}\right) - \mathcal{A}\,\mathrm{Ei}\left(-\frac{\mathcal{A}}{\mathcal{K}_\tau}\right) \right]_{\mathcal{K}_\tau = \mathcal{Q}_j}^{\mathcal{K}_\tau = \mathcal{Q}_{j+1}} , \quad (4.15)$$

to estimate approximate epitope classes $\{(\Lambda_j, [\mathcal{Q}_j, \mathcal{Q}_{j+1}))\}_{j=1}^{m}$ in experimental units.

4.3.2 Visualization of estimation epitope densities

The estimation epitope density $\eta_{\{P,\lambda\}}(K_\tau)$ is fully characterized by the partition P and the model parameters λ. However, a list of numbers is not a human-friendly representation that can be understood intuitively. Thus, we should visualize epitope densities in a plot. A straightforward approach would be a histogram, where the bar widths are given by the sub-intervals of the partition P and the bar heights are the parameters λ. Figure 4.3 illustrates such a histogram.

Alternatively, we can visualize the estimation epitope density $\eta_{\{P,\lambda\}}(K_\tau)$ by plotting the density function

$$g(K_\tau) = \sum_{j=1}^{m} \frac{\lambda_j}{q_{j+1} - q_j} \chi_{I_j}(K_\tau) \ .$$

Figure 4.4 shows the resulting plot.

Unlike the histogram visualization, individual intervals I_j are not highlighted by borders around the bars. But more importantly, observe that the shape of the density (Figure 4.4) differs from the shape of the histogram (Figure 4.3) because the bar height in the histogram is the parameter value λ_j, while the "bar" height in the density plot is the normalized parameter value $\lambda_j / (q_{j+1} - q_j)$.

The density visualization does not directly show the amount of epitopes with K_τ in a given interval; but it allows us to see the amount of epitopes for arbitrary regions across multiple intervals, since the surface area corresponds 1 : 1 to the amount of epitopes. This immediately follows from the fact that the

[6] However, in many cases, additional libraries or packages are necessary.

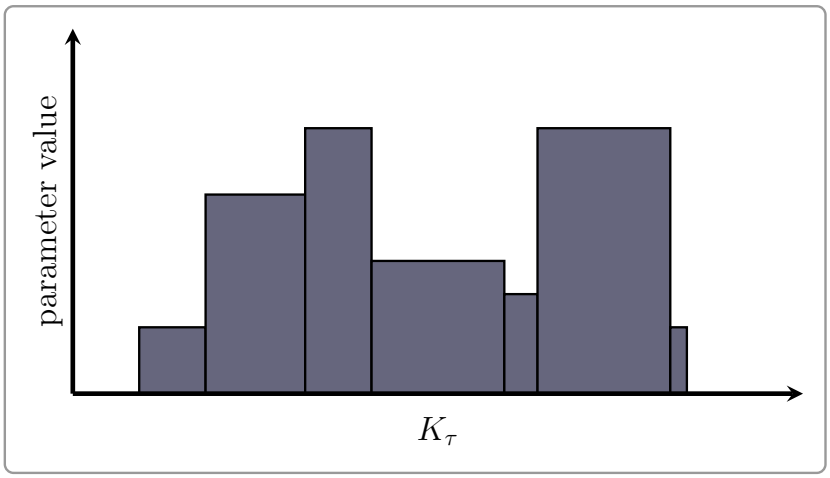

Figure 4.3: Illustration of the visualization of epitope densities $\eta_{\{P,\lambda\}}(K_\tau)$ as histogram, where the bar widths are defined by the partition P and the bar heights are the parameters λ.

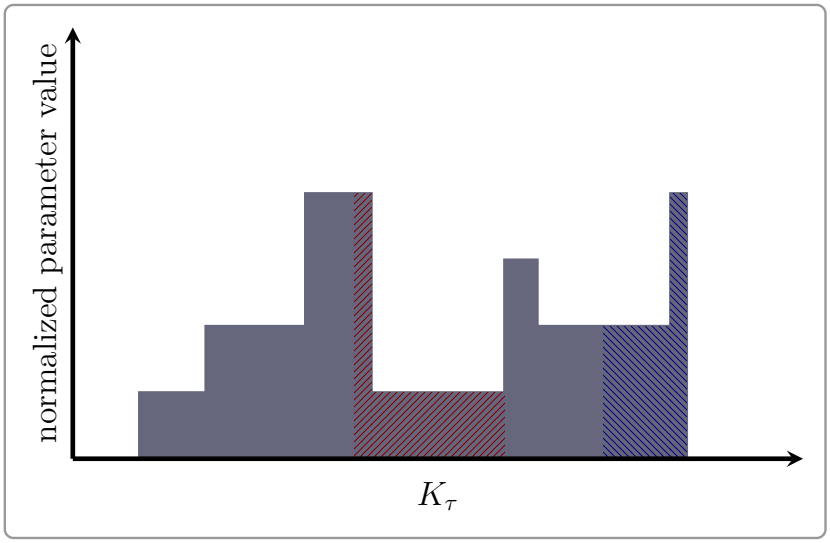

Figure 4.4: Illustration of the visualization of epitope densities $\eta_{\{P,\lambda\}}(K_\tau)$ as density. The hatched areas (left, red) and (right, blue) correspond to the same amount of epitopes.

area under the density function is just the integral of the estimation epitope density, which was defined to be the amount of epitopes.

The correspondence between the visual area and the amount of epitopes will be especially useful for fine partitions. Figure 4.5b shows an example, where the bars become indiscernible. Hence, we prefer the visualization as density.

Unfortunately, we have not yet completed our discussion of the visualization. Since concentrations for dose-response data often span several orders of magnitude, we will use logarithmic scales for the plots. And the support of the estimation epitope density should span a range similar to the concentration range of the dose-response data, because the accumulation model function $F(K_\tau, a)$ has an inflection point on a logarithmic scale at $a = K_\tau$ (see Appendix B.3.3).

Loosely speaking, we can understand the integration of the accumulation model function against the estimation epitope density as a combination of inflection point slopes. Of course, not only the inflection point slopes but the entire shapes of the accumulation model functions are combined for each K_τ value. Nevertheless, the argument still holds that the support of the epitope density needs to cover the concentration range of the dose-response curve.

To find a useful visualization for logarithmic scales, we may construct a density function, approximate it with an estimation epitope density $\eta_{\{P,\lambda\}}(K_\tau)$, and then calculate the dose-response curves. Thus, comparing different visualizations of $\eta_{\{P,\lambda\}}(K_\tau)$ with the corresponding dose-response curve will allow us to select a useful visualization.

Let us consider the example density function from [Methods-Paper], i.e., the sum of the normal distributions $\mathcal{N}(10^{-6}, (3 \cdot 10^{-7})^2)$ and $\mathcal{N}(10^{-5}, (3 \cdot 10^{-6})^2)$:

$$g(K_\tau) = \frac{1}{3{\cdot}10^{-7}{\cdot}\sqrt{2\pi}}\, e^{-\frac{1}{2}\left(\frac{K_\tau - 10^{-6}}{3{\cdot}10^{-7}}\right)^2} + \frac{1}{3{\cdot}10^{-6}{\cdot}\sqrt{2\pi}}\, e^{-\frac{1}{2}\left(\frac{K_\tau - 10^{-5}}{3{\cdot}10^{-6}}\right)^2} .$$

Figure 4.5a shows a plot of the density function on a logarithmic scale, where we refer to the individual bell curves as peak A and peak B.

For the partition, we choose

$$\begin{aligned} P = &\left\{10^x \;\middle|\; x = -10 + \tfrac{-6-(-10)}{24} n \quad , n = 0, \ldots, 24\right\} \\ &\cup \left\{10^x \;\middle|\; x = -6 + \tfrac{-5-(-6)}{49} n \quad , n = 0, \ldots, 49\right\} \\ &\cup \left\{10^x \;\middle|\; x = -5 + \tfrac{-2-(-5)}{99} n \quad , n = 0, \ldots, 99\right\} , \end{aligned}$$

i.e., 25 logarithmically spaced points from 10^{-10} to 10^{-6}, 50 logarithmically spaced points from 10^{-6} to 10^{-5}, and finally 100 logarithmically spaced points from 10^{-5} to 10^{-2}.

Next, we approximate the density function $g(K_\tau)$ as

$$\eta_{\{P,\lambda\}} = \sum_{j=1}^{m} g\left(\tfrac{q_{j+1}-q_j}{2}\right) \chi_{I_j}(K_\tau)\ |dK_\tau| \quad \Rightarrow \quad \lambda_j = g\left(\tfrac{q_{j+1}-q_j}{2}\right)(q_{j+1}-q_j)\ .$$

Observe the additional factors $(q_{j+1} - q_j)$ for the parameters λ_j that appear because we have defined the estimation epitope density (Definition 4.2.2) with the factors $1/(q_{j+1}-q_j)$. This is the reason why the histogram visualization does not agree with the shape of density functions, in general (see Figure 4.5a and Figure 4.5b). Of course, the density visualization (Figure 4.6b) agrees with the plot of the density function.

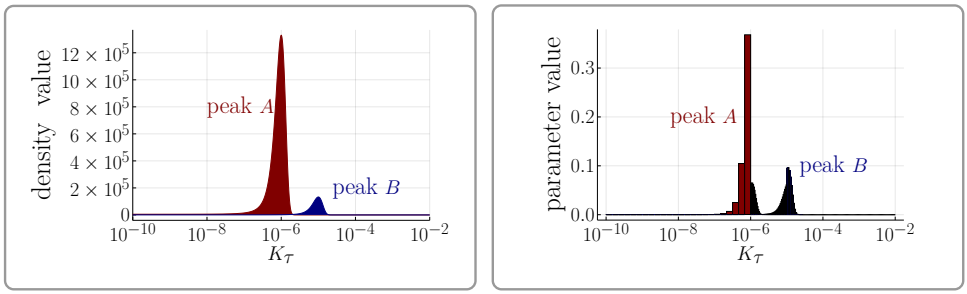

(a) True density plot

(b) $\eta_{\{P,\lambda\}}(K_\tau)$ – Histogram visualization

Figure 4.5: {Adapted from [Methods-Paper]}
Plot of (**a**) the density function $g(K_\tau)$ and (**b**) the histogram visualization of the estimation epitope density $\eta_{\{P,\lambda\}}(K_\tau)$ that approximates the density function.

By definition, the individual normal distributions of our density function are both normalized to 1, such that they correspond to equal amounts of epitopes. However, the logarithmic scale hides this property. Nevertheless, we can easily check that the amount of epitopes is the same for both peaks by calculating the dose-response curve. More precisely, we calculate the dose-response curves for the individual peaks, which constitute the contributions of the peaks to the overall dose-response curve. Figure 4.6a shows the resulting dose-response curves, confirming that both peaks contribute equally.

Since the density visualization does not produce plots where the visual area corresponds to the amount of epitopes — the peaks have different visual areas — we need to modify the visualization for logarithmic scales.

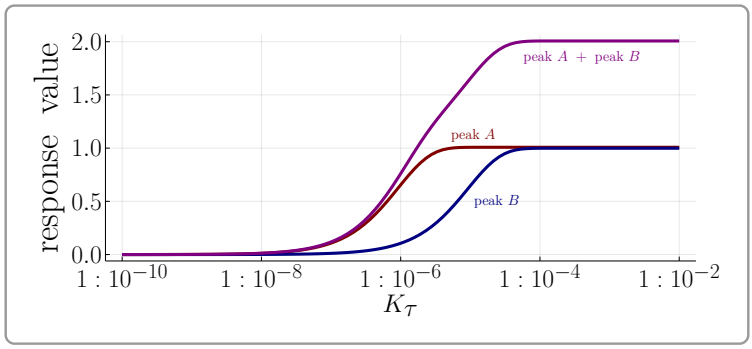

(a) Dose-response curve and contributions of the individual peaks

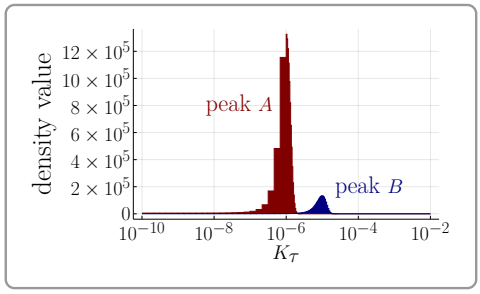

(b) $\eta_{\{P,\lambda\}}(K_\tau)$ – Density visualization

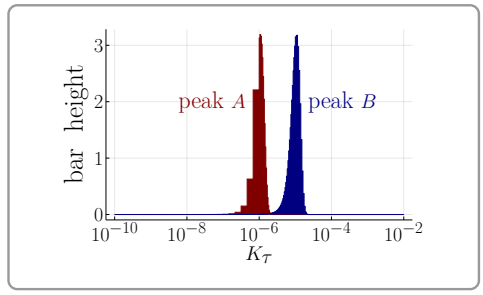

(c) $\eta_{\{P,\lambda\}}(K_\tau)$ – Accessibility histogram

Figure 4.6: {Adapted from [Methods-Paper]}
Dose-response curve and the individual contributions of peak A and peak B, as well as two visualizations for the estimation epitope density $\eta_{\{P,\lambda\}}(K_\tau)$. The density visualization (**b**) agrees with the graph of the density function (Figure 4.5a), but the visual peak sizes do not correspond to the contributions of the peaks to the dose-response curve (**a**). Normalizing the parameters to the visual length (here $\log_{10}(q_{j+1}) - \log_{10}(q_j)$) leads to the accessibility histogram (**c**), where both peaks have the same surface area.

Here, it helps to recall the difference between the histogram visualization and the density visualization. Apart from omitting the borders, the density visualization is the same as the histogram visualization, except for the bar heights, which are $\lambda_j/q_{j+1}-q_j$ instead of λ_j. Thus, for the logarithmic scale, we could try a different normalization of the parameters. Instead of normalizing the parameter values λ_j to their interval lengths $q_{j+1} - q_j$, we should consider the visual lengths $\widetilde{L}_j$ of the intervals on a logarithmic scale (with base c)

$$\widetilde{L}_j = \widetilde{q}_{j+1} - \widetilde{q}_j = \log_c(q_{j+1}) - \log_c(q_j) \ ,$$

which define the normalized parameters

$$\widetilde{\lambda}_j = \frac{\lambda_j}{\log_c(q_{j+1}) - \log_c(q_j)} \ . \tag{4.16}$$

We call the resulting visualization for $c = 10$ the **accessibility histogram** (histogram with normalized parameters, plotted without borders around the bars) and call the normalized parameters **accessibility bar heights**.

Figure 4.6c shows this accessibility histogram for our example epitope density, where we can see that both peaks have the same visual area, as desired.

4.3.3 Estimation of model parameters

We constructed the accumulation estimation model to estimate epitope classes from experimental dose-response data. However, we have not yet described how to obtain the model parameters from the data, as other aspects of the accumulation estimation model needed to be discussed first. Now, we can focus on the estimation process itself.

Since parameter estimation is a common problem that is not the focus of this dissertation, we do not need to develop a new approach. We can simply use one of the available approaches that best suits our needs. For our use case, the approach of choice is simple curve fitting. We have a closed form expression for the model (4.14), and experimental dose-response data describes a curve: the dose-response curve.

The idea behind curve fitting is quite simple. First, we need a method to compare the data curve with a theoretical curve obtained from the model for a given parameter configuration. This comparison method is called **objective function** and should return a real number (or a value in a set with total order). Second, we need a method to select parameter configurations for the comparison. Ideally, this should be done in a way that leads to better fitting parameter configurations over time.

For the selection of parameter configurations, we can simply use one of the many well-established iterative optimization algorithms provided by the Julia-native "Optim.jl" package [MR18]. In particular, we will use the gradient-free Nelder-Mead algorithm and the limited-memory Broyden-Fletcher-Goldfarb-Shanno (LBFGS) algorithm with numerical gradients (see Subsection 4.3.6).

Although there are also predefined curve-fitting packages, we will benefit from constructing our own objective function, albeit only for the motivation of the regularization method. The rest of the objective function will essentially be just a weighted least-squares objective.

Construction of the objective function

Recall that we described measurement uncertainty as an uncertainty distribution in the Bayesian context. Thus, it makes sense to use a posterior density function as an objective function. For this purpose, we can follow the illustrative examples of [Mac03, Chapter 3] and include ideas from the unpublished article [Jay99]. In our case, we are interested in the conditional probability density function[7]

$$p(\Lambda \mid \mathcal{D}, \mathcal{P}, F) \ ,$$

which expresses the probability of a parameter configuration Λ, given the dose-response data $\mathcal{D} = \{(\mathcal{A}_i, \mathcal{X}_i, \Delta\mathcal{X}_i)\}_{i=1}^n$, the partition $\mathcal{P} = \{\mathcal{Q}_1, \ldots, \mathcal{Q}_{m+1}\}$, and the accumulation model function $F(\mathcal{K}_\tau, \mathcal{A})$ of the accumulation estimation model[8], all in experimental units.

Before we can apply Bayes' theorem, we have to change the notation slightly. So far, we have denoted the data as tuples $(\mathcal{A}_i, \mathcal{X}_i, \Delta\mathcal{X}_i)$ to highlight the connection between the initial antibody concentration $\mathcal{A}_i$, the resulting response value $\mathcal{X}_i$, and the corresponding response spread $\Delta\mathcal{X}_i$. However, each value can be regarded as an individual condition for the conditional probability:

$$\begin{aligned} p(\Lambda \mid \mathcal{D}, \mathcal{P}, F) &\coloneqq p(\Lambda \mid \mathcal{A}_1, \ldots, \mathcal{A}_N, \mathcal{X}_1, \ldots, \mathcal{X}_N, \Delta\mathcal{X}_1, \ldots, \Delta\mathcal{X}_N, \mathcal{P}, F) \\ &=: p(\Lambda \mid \{\mathcal{A}_i\}, \{\mathcal{X}_j\}, \{\Delta\mathcal{X}_k\}, \mathcal{P}, F) \ . \end{aligned}$$

Now, we can use Bayes' theorem to obtain

$$p(\Lambda \mid \mathcal{D}, \mathcal{P}, F) \sim p(\{\mathcal{X}_j\} \mid \Lambda, \{\mathcal{A}_i\}, \{\Delta\mathcal{X}_k\}, \mathcal{P}, F) \cdot p(\Lambda \mid \{\mathcal{A}_i\}, \{\Delta\mathcal{X}_k\}, \mathcal{P}, F) \ .$$

Assuming, as is commonly done, that individual measurement tuples $(\mathcal{A}_i, \mathcal{X}_i, \Delta\mathcal{X}_i)$ are statistically independent, we can express the likelihood as

$$p(\{\mathcal{X}_j\} \mid \Lambda, \{\mathcal{A}_i\}, \{\Delta\mathcal{X}_k\}, \mathcal{P}, F) = \prod_{i=1}^{n} p(\mathcal{X}_i \mid \Lambda, \mathcal{A}_i, \Delta\mathcal{X}_i, \mathcal{P}, F) \ .$$

[7] Although we distinguish between densities and density functions and have explicitly constructed the epitope density as a proper density, we follow the common practice and consider probability density functions. Furthermore, we assume the pragmatic approach/ notation of elementary probability courses, as we do not benefit from introducing measure-theoretic approaches. For a rigorous formulation of conditional density functions, see, e.g., [Çin11, Chapter 4, Section 2].

[8] Note that $\widetilde{F}(\mathcal{K}_\tau, \mathcal{A}) = F(\mathcal{K}_\tau, \mathcal{A})$ for the accumulation model function, which follows from Theorem 4.2.3.

Note that stochastic independence also implies that $\mathcal{A}_j$ and $\Delta\mathcal{X}_j$ do not impose any conditions unless $j = i$, which we used for the right-hand side of the equation.

It remains to observe that the conditional probability density function $p(\mathcal{X}_i \mid \Lambda, \mathcal{A}_i, \Delta\mathcal{X}_i, \mathcal{P}, F)$ describes the uncertainty in obtaining a measurement value $\mathcal{X}_i$, given the initial antibody concentration $\mathcal{A}_i$, the model parameters Λ, and the response value spread $\Delta\mathcal{X}_i$ (among others). Thus, as discussed in Subsection 4.1.5, we assume a normal distribution of the form

$$p(\mathcal{X}_i \mid \Lambda, \mathcal{A}_i, \Delta\mathcal{X}_i, \mathcal{P}, F) = \frac{1}{\sqrt{2\pi\Delta\mathcal{X}_i^2}} \exp\left(-\frac{(\mathcal{X}_i - \mu(\Lambda, \mathcal{P}, \mathcal{A}_i))^2}{2\Delta\mathcal{X}_i^2}\right) ,$$

where $\mu(\Lambda, \mathcal{P}, \mathcal{A}_i)$ is the theoretical mean value, given by

$$\mu(\Lambda, \mathcal{P}, \mathcal{A}_i) = \int_{\mathbb{K}} F(\mathcal{K}_\tau, \mathcal{A}_i)\, \eta_{\{\mathcal{P},\Lambda\}}(\mathcal{K}_\tau) \, . \tag{4.17}$$

Since we can essentially choose the **prior** (i.e., the prior probability density function)

$$p_0(\Lambda) \coloneqq p(\Lambda \mid \{\mathcal{A}_i\}, \{\Delta\mathcal{X}_k\}, \mathcal{P}, F)$$

to express our general knowledge about the parameters, and since we can calculate the theoretical value $\mu(\Lambda, \mathcal{P}, \mathcal{A}_i)$ with (4.15), we have obtained a computable expression (up to proportionality) for the conditional probability density function of interest:

$$p(\Lambda \mid \mathcal{D}, \mathcal{P}, F) \sim p_0(\Lambda) \prod_{i=1}^{n} \frac{1}{\sqrt{2\pi\Delta\mathcal{X}_i^2}} \exp\left(-\frac{(\mathcal{X}_i - \mu(\Lambda, \mathcal{P}, \mathcal{A}_i))^2}{2\Delta\mathcal{X}_i^2}\right) . \tag{4.18}$$

For a fully Bayesian treatment, we would need to obtain the shape of the posterior density function $p(\Lambda \mid \mathcal{D}, \mathcal{P}, F)$. Unfortunately, this is computationally expensive because we cannot expect a standard distribution for the posterior density function, such that we need sufficiently many parameter configurations Λ to estimate its shape. And depending on the partition, Λ can be high-dimensional, requiring even more parameter configurations to explore the shape of the posterior density function. However, since we want to use computational resources to refine the partition adaptively (see Subsection 4.3.4), we only consider the posterior density function as an objective function that we want to maximize.

But we will not directly use (4.18) as the objective function because the floating point representation of real numbers has finite precision. Numbers

close to zero, smaller than the smallest representable positive number, are rounded down to zero (floating underflow) [Bee17, Section 4.11]. Hence, we use the logarithm of the posterior density function, as maximizing the logarithm of a positive function is mathematically equivalent to maximizing the function.

Let Z denote the proportionality factor for which

$$p(\Lambda \mid \mathcal{D}, \mathcal{P}, F) = Z p_0(\Lambda) \prod_{i=1}^{n} \frac{1}{\sqrt{2\pi\Delta\mathcal{X}_i^2}} \exp\left(-\frac{(\mathcal{X}_i - \mu(\Lambda, \mathcal{P}, \mathcal{A}_i))^2}{2\Delta\mathcal{X}_i^2}\right) .$$

Taking the natural logarithm then yields

$$\begin{aligned}\ln(p(\Lambda \mid \mathcal{D}, \mathcal{P}, F)) = \ln(p_0(\Lambda)) &- \sum_{i=1}^{n} \left(\frac{(\mathcal{X}_i - \mu(\Lambda, \mathcal{P}, \mathcal{A}_i))^2}{2\Delta\mathcal{X}_i^2}\right) \\ &+ \ln(Z) - \sum_{i=1}^{n} \ln\left(\sqrt{2\pi\Delta\mathcal{X}_i^2}\right) .\end{aligned}$$

Note that the terms in the second line are just constant values that do not depend on the parameters Λ. So we can ignore them for the maximization of the logarithmic posterior density function. Finally, we observe that maximizing a function $f(\Lambda)$ is the same as minimizing $-f(\Lambda)$. Hence, we define the objective function as

$$\operatorname{obj}(\Lambda \mid \mathcal{D}, \mathcal{P}, F) \coloneqq \sum_{i=1}^{n} \left(\frac{(\mathcal{X}_i - \mu(\Lambda, \mathcal{P}, \mathcal{A}_i))^2}{2\Delta\mathcal{X}_i^2}\right) + \ell_0(\Lambda \mid \{\mathcal{A}_i\}, \{\Delta\mathcal{X}_k\}, \mathcal{P}, F) , \tag{4.19}$$

where

$$\ell_0(\Lambda \mid \{\mathcal{A}_i\}, \{\Delta\mathcal{X}_k\}, \mathcal{P}, F) = -\ln(p_0(\Lambda)) = -\ln(p(\Lambda \mid \{\mathcal{A}_i\}, \{\Delta\mathcal{X}_k\}, \mathcal{P}, F))$$

denotes the sign-flipped logarithmic prior of the parameters.

Defining an objective function that is to be minimized instead of maximized has two reasons. The first is rather mundane. The "Optim.jl" package only provides algorithms for function minimization. For the second reason, observe that our objective function is just a weighted least squares objective with a regularization term $\ell_0(\Lambda \mid \{\mathcal{A}_i\}, \{\Delta\mathcal{X}_k\}, \mathcal{P}, F)$. Thus, up to our choice of the prior, we use a tried and true method, yet with the ability to use the Bayesian interpretation.

We have not yet seen any data, that is, we have no experience, so we could simply use uninformative priors. For example, we could fix a finite domain of

permissible parameters Λ and set $\ell_0(\Lambda \mid \{\mathcal{A}_i\}, \{\Delta\mathcal{X}_k\}, \mathcal{P}, F) = 0$ in this domain (which leads to a weighted least squares objective). However, [Svi+03] describes that unregularized least squares fitting suffers from overfitting artifacts due to noise (cf. [Pro82]).

Choice of the prior

For the accumulation estimation model, we should assume similar problems. Among others, our construction of the accumulation estimation model was heavily inspired by the density approach of [Svi+03]. Thus, we should choose a prior that reduces individual singular features (e.g., sharp peaks) to avoid overfitting in the case of noisy data. In fact, since we will mostly consider the accessibility histogram of the resulting epitope density, we should construct the prior so that it reduces singular features in the accessibility histogram.

We can reduce sharp peaks by penalizing the difference between the weights for neighboring intervals. Recalling the accessibility bar heights (4.16), we could use

$$\sum_{j=1}^{m-1} |\widetilde{\Lambda}_{j+1} - \widetilde{\Lambda}_j| = \sum_{j=1}^{m-1} \left| \frac{\Lambda_{j+1}}{\log_{10}(\mathcal{Q}_{j+2}) - \log_{10}(\mathcal{Q}_{j+1})} - \frac{\Lambda_j}{\log_{10}(\mathcal{Q}_{j+1}) - \log_{10}(\mathcal{Q}_j)} \right|$$

for the sign-flipped logarithmic prior. However, let us choose

$$\ell_0(\Lambda \mid \{\mathcal{A}_i\}, \{\Delta\mathcal{X}_k\}, \mathcal{P}, F) = \frac{\varrho}{m} \sum_{j=1}^{m-1} (\widetilde{\Lambda}_{j+1} - \widetilde{\Lambda}_j)^2 =$$

$$= \frac{\varrho}{m} \sum_{j=1}^{m-1} \left(\frac{\Lambda_{j+1}}{\log_{10}(\mathcal{Q}_{j+2}) - \log_{10}(\mathcal{Q}_{j+1})} - \frac{\Lambda_j}{\log_{10}(\mathcal{Q}_{j+1}) - \log_{10}(\mathcal{Q}_j)} \right)^2 . \tag{4.20}$$

Here, $\varrho \geq 0$ is just a scaling parameter that allows us to control the strength/importance of the sign-flipped logarithmic prior, e.g., to adapt the prior to specific data. And the factor $1/m$ simply normalizes the scaling parameter to the number of parameters, which will become relevant only for the adaptive refinement of the partition (Subsection 4.3.4).

Using squared differences $\Delta\widetilde{\Lambda}_j^2 \coloneqq (\widetilde{\Lambda}_{j+1} - \widetilde{\Lambda}_j)^2$ can be motivated by the interpretation of ℓ_0 as sign-flipped logarithmic prior. Converting (4.20) back

to the linear scale, we obtain

$$p_0(\Lambda \mid \{\mathcal{A}_i\}, \{\Delta\mathcal{X}_k\}, \mathcal{P}, F) = \prod_{j=1}^{m-1} \exp\left(-\frac{\widetilde{\Delta\Lambda_j}^2}{m/\varrho}\right)$$

$$\sim \prod_{j=1}^{m-1} \frac{1}{\sqrt{2\pi\frac{1}{2}\frac{m}{\varrho}}} \exp\left(-\frac{\widetilde{\Delta\Lambda_j}^2}{m/\varrho}\right) .$$

Thus, our chosen prior is essentially a product of normal distributions $\mathcal{N}(0, m/2\varrho)$ for the differences between the accessibility bar heights $\Delta\widetilde{\Lambda}_j$. In particular, this means that we assume, before seeing any data, that the differences are most likely zero (flat histogram) and that the differences are statistically independent.

Remark 4.3.1 (**Scaling parameter ϱ and objectivity**).
Although we can motivate our choices, every prior is subjective, at least to some degree. This also extends to the choice of the scaling parameter ϱ. However, the same holds true for any choice regarding the fitting objective and the regularization. Or, to quote [Mac03, Chapter 3, p. 51]: "you can't do inference — or data compression — without making assumptions". The objectivity lies in the fact that all assumptions for the curve fitting are clearly stated in (4.17)-(4.20) and their derivation.

With the interpretation of (4.20) as a product of normal distributions, we have provided a rationale for the general shape of the prior. For the scaling parameter ϱ, we will test a range of values, aiming for strong and weak smoothing of the accessibility histogram.

4.3.4 Adaptive refinement of the partition

With the accumulation estimation model, we have gained control over the coarseness of the epitope class estimation, since we can freely choose the partition P. However, this poses a dilemma. On the one hand, we would like to use a fine partition to cover the underlying details of the epitope classes. On the other hand, a finer partition means more parameters, which makes the optimization of the objective function harder. Among others, iterative methods, like those of "Optim.jl", will require much more time and become more sensitive to the starting position for the iteration.

This dilemma is not specific to the accumulation estimation model but affects discretization approaches for Fredholm integral equations[9] in general. To solve this dilemma, adaptive finite element methods can be used [AE94; KB13]. For example, [Zha+18] and [Zha+19] apply this approach to the rate constant distribution model of [Svi+03].

Since we only have one-dimensional integrals, we can reduce the formalism and consider only the adaptive refinement aspect. Thus, let us use the following steps.

Algorithm 4.3.2 (**Adaptive partition refinement**).

1) Start with a coarse partition $\mathcal{P}^{(m+1)} = \{\mathcal{Q}_1, \ldots, \mathcal{Q}_{m+1}\}$ and initial parameters $\{\Lambda_j\}_{j=1}^{m}$.

2) Construct the accumulation estimation model and optimize the parameters $\{\widehat{\Lambda_j}\}_{j=1}^{m}$ with respect to the objective function (4.19).

3) Refine the partition ($\mathcal{P}^{(m+1)} \rightsquigarrow \mathcal{P}^{(m+2)}$) by subdividing one interval, i.e., by inserting an additional point $\mathcal{Q}^*$ between $\mathcal{Q}_{j^*}$ and $\mathcal{Q}_{j^*+1}$ for some appropriately chosen $j^* \in \{1, \ldots, m+1\}$:

$$\mathcal{P}^{(m+2)} = \{\mathcal{Q}_1, \ldots, \mathcal{Q}_{j^*}, \mathcal{Q}^*, \mathcal{Q}_{j^*+1}, \ldots, \mathcal{Q}_{m+1}\} \ .$$

4) Adapt the optimized parameters $\{\widehat{\Lambda}_j\}_{j=1}^{m} \rightsquigarrow \{\widehat{\Lambda}_j\}_{j=1}^{m+1}$ to the refined partition.

5) If the partition is not fine enough, return to step 2 with the refined partition $\mathcal{P}^{(m+2)}$ and the adapted optimal parameters $\{\Lambda_j\}_{j=1}^{m+1}$ as initial parameters (understanding $m+1$ as the new m, of course).

Using this adaptive partition refinement has three advantages compared to a fixed, fine partition. First, starting with few parameters is computationally

[9] The accumulation estimation model is essentially a discretized Fredholm equation of the first kind. By construction (in experimental units), the estimation epitope density can only be non-zero on $I = [\mathcal{Q}_1, \ldots, \mathcal{Q}_{m+1})$, such that we can write the integral as a Fredholm integral

$$\mathcal{X}(\mathcal{A}) = \int_{\mathbb{K}} F(\mathcal{K}_\tau, \mathcal{A})\, \eta_{\{\mathcal{P},\Lambda\}}(\mathcal{K}_\tau) = \int_{\mathcal{Q}_1}^{\mathcal{Q}_{m+1}} F(\mathcal{K}_\tau, \mathcal{A}) g_{\{\mathcal{P},\Lambda\}}(\mathcal{K}_\tau)\ d\mathcal{K}_\tau \ ,$$

where $g(K_\tau)$ denotes the coefficient (function) of $\eta_{\{\mathcal{P},\Lambda\}}(\mathcal{K}_\tau)$.

less demanding. Carrying over the optimized parameters as initial parameters for the refined partition then provides a good starting point for the next optimization. Second, although the adaptive refinement does not remove the dependence of iterative optimization on the initial parameter configuration, it at least reduces our choices to a few parameter values. Then, the subsequent initial configurations are determined automatically by the refinement algorithm and iterative optimizations. Finally, the adaptive refinement leads to a locally fine partition instead of a globally fine partition. Thus, it focuses computational resources on important regions instead of wasting computation time on unimportant regions that could be well described by only a few intervals.

To apply the adaptive refinement, it remains to specify which interval is subdivided and how it is subdivided (construction of $\mathcal{Q}^*$), as well as how parameters are adapted to the refined partition.

For the subdivision rule, it makes sense to select the interval by selecting the parameter that differs the most compared to its neighboring parameters:

$$j^* = \operatorname*{arg\,max}_{j\in\{1,\dots,m\}} \begin{cases} |\Lambda_{j+1} - \Lambda_j| & , \quad j = 1 \\ |\Lambda_j - \Lambda_{j-1}| & , \quad j = m \\ \frac{1}{2}|\Lambda_{j+1} - \Lambda_j| + \frac{1}{2}|\Lambda_j - \Lambda_{j-1}| & , \quad 1 < j < m \end{cases} .$$

This is because a large parameter difference produces a sudden jump, which indicates that a finer resolution is needed to capture the proper shape of the density function in that region. Here, we use the average parameter difference of both neighbors to prioritize singular peaks, where both sides exhibit sudden jumps, over one-sided "cliffs".

However, as for the choice of the prior, we should consider the accessibility histogram, which is our primary way to interpret estimation epitope densities. Thus, let us use the accessibility bar heights

$$\widetilde{\Lambda}_j = \frac{\Lambda_j}{\log_{10}(\mathcal{Q}_{j+1}) - \log_{10}(\mathcal{Q}_j)}$$

for the selection rule to determine the interval that will be refined:

$$j^* = \operatorname*{arg\,max}_{j\in\{1,\dots,m\}} \begin{cases} |\widetilde{\Lambda}_{j+1} - \widetilde{\Lambda}_j| & , \quad j = 1 \\ |\widetilde{\Lambda}_j - \widetilde{\Lambda}_{j-1}| & , \quad j = m \\ \frac{1}{2}|\widetilde{\Lambda}_{j+1} - \widetilde{\Lambda}_j| + \frac{1}{2}|\widetilde{\Lambda}_j - \widetilde{\Lambda}_{j-1}| & , \quad 1 < j < m \end{cases} . \tag{4.21}$$

Since we use the accessibility histogram to select the interval that will be refined, we should also construct the refinement, i.e., the point $\mathcal{Q}^*$ that we

insert, from the accessibility histogram. Thus, we choose

$$\log_{10}(\mathcal{Q}^*) = \frac{(\log_{10}(\mathcal{Q}_{j^*+1}) + \log_{10}(\mathcal{Q}_{j^*}))}{2} \,, \tag{4.22}$$

so that $\mathcal{Q}^*$ is the midpoint between $\mathcal{Q}_{j^*+1}$ and $\mathcal{Q}_{j^*}$ on a logarithmic scale.

Finally, the adaptation of the parameters to the refined partition is quite straightforward. Since the accessibility histogram was constructed so that the visual area of a bar corresponds to its dose-response contribution, subdividing an interval/bar should preserve the overall visible area. In other words, splitting up a bar should not affect the accessibility bar heights:

$$\{\widetilde{\Lambda}^*_j\}_{j=1}^{m+1} = \{\widetilde{\Lambda}_1, \dots \widetilde{\Lambda}_{j^*}, \widetilde{\Lambda}_{j^*}, \dots, \widetilde{\Lambda}_m\} \,.$$

Here, we just repeated the bar height $\widetilde{\Lambda}_{j^*}$ to assign the bar height of the original interval/bar to both subdividing intervals/bars. Figure 4.7 illustrates our choices for the refinement process.

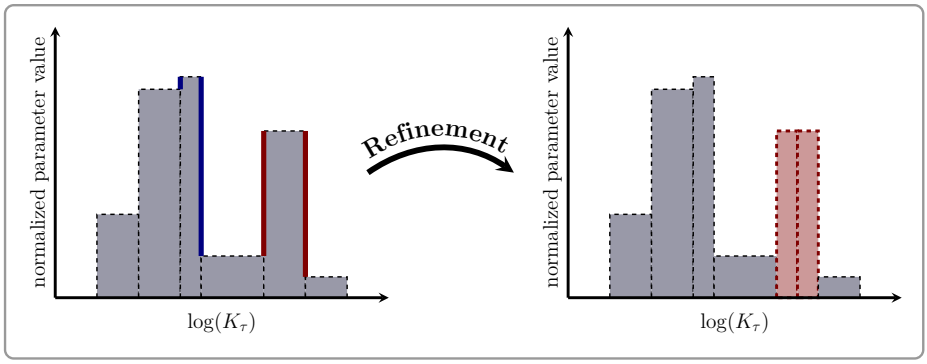

Figure 4.7: Illustration of the partition refinement strategy, based on the accessibility histogram. The interval/bar with the largest average bar-height-difference to its neighbors is refined. This prioritizes sharp peaks, where both sides show large differences (red edges, right bar), over "cliffs", where only one side shows a large difference (blue edges, left bar). For the refinement, the bar is bisected (on the logarithmic scale), preserving the original bar heights.

The parameters that we need for the actual calculations require additional attention, as the refinement changes the lengths of the intervals, and thus the relationship between the bar heights and the parameters. Of course, for $j \neq j^*$, the intervals do not change, such that

$$\Lambda^*_j = \Lambda_j \qquad \forall\, j \neq j^* \,.$$

For the subdividing intervals, we have to normalize the parameters to the new visual lengths in the accessibility histogram after the refinement. The corresponding normalization factors are

$$\mathcal{V}_{\mathrm{L}} \coloneqq \frac{\log_{10}(\mathcal{Q}^*) - \log_{10}(\mathcal{Q}_{j^*})}{\log_{10}(\mathcal{Q}_{j^*+1}) - \log_{10}(\mathcal{Q}_{j^*})} \tag{4.23}$$

for the left subdividing interval and

$$\mathcal{V}_{\mathrm{R}} \coloneqq \frac{\log_{10}(\mathcal{Q}_{j^*+1}) - \log_{10}(\mathcal{Q}^*)}{\log_{10}(\mathcal{Q}_{j^*+1}) - \log_{10}(\mathcal{Q}_{j^*})} \tag{4.24}$$

for the right subdividing interval. In summary, this means that the adapted parameters are given by

$$\{\Lambda_j^*\}_{j=1}^{m+1} = \{\Lambda_1, \ldots, \Lambda_{j^*-1},\ \mathcal{V}_{\mathrm{L}}\Lambda_{j^*},\ \mathcal{V}_{\mathrm{R}}\Lambda_{j^*}\ , \Lambda_{j^*+1}, \ldots, \Lambda_m\}\ . \tag{4.25}$$

Remark 4.3.3 (**Normalization of the scaling parameter ϱ**). For a single optimization run, the normalization factor $1/m$ in the logarithmic prior (4.20) did not make a difference, as it could easily be absorbed into the scaling parameter ϱ. However, when we use the adaptive refinement, the number of parameters increases after each refinement. Here, the normalization factor $1/m$ normalizes the scaling parameter ϱ across the different optimization runs during the adaptive partition refinement algorithm (Algorithm 4.3.2). It approximately rescales the sum of squared bar-height differences to the average squared bar-height difference (approximately, since there are only $m-1$ differences for m parameters).

4.3.5 Depletion corrections

Because of the lack of an analytical solution for the depletion accumulation model, we have developed parameter estimation based on the reservoir accumulation model. In this way, depletion effects are implicitly contained in the apparent rate constants.

However, conflating depletion effects with binding properties is not always desirable. Since we cannot recreate the accumulation estimation model for the depletion case, we must approach depletion effects from the other side: the data. Our goal in this subsection is to correct the dose-response data for depletion effects, i.e., to transform the data $\mathcal{D} \mapsto \mathcal{D}_{\mathrm{cor}}$ so that depletion effects

are removed, or at least reduced. Then, we can continue using the reservoir model that assumes the absence of depletion effects.

For the depletion correction, we have two options. First, we can increase the response values to the amount of bound antibodies that would have accumulated if the effective antibody concentration had not decreased over time. Alternatively, we can reduce the initial antibody concentrations to the concentrations that would have sufficed for a system without depletion to produce the same response values.

Worst-case correction

A simple approach to correct the dose-response data is a worst-case antibody-concentration correction along the lines of the correction presented by [Edw+98].

First, we recall the conservation of antibodies ((2.4) and Subsection 3.1.1), which expresses the effective antibody concentration as the difference between the initial antibody concentration and the amount of bound antibodies:

$$a(t) = a - \beta X(t; a) \ .$$

The idea of [Edw+98] is now to replace the initial antibody concentrations $\mathcal{A}_i$ with the depleted antibody concentration $\mathcal{A}_i - \widetilde{\beta}\mathcal{X}_i$, yielding

$$\{(\mathcal{A}_i - \widetilde{\beta}\mathcal{X}_i, \mathcal{X}_i, \Delta\mathcal{X}_i)\}_{i=1}^n$$

as corrected data.

However, using experimental units (with unknown conversion factors) means that we do not know the depletion factor $\widetilde{\beta}$ in these units. Thus, we have to make a worst-case assumption for the depletion factor, i.e., the largest possible depletion factor β^*, which leads to the strongest corrections. This largest possible depletion factor is given by

$$\beta^* \coloneqq \max\{\phi \geq 0 \mid \mathcal{A}_i - \phi\mathcal{X}_i \geq 0 \quad \forall\, i \in \{1, \ldots, n\}\} \ . \tag{4.26}$$

For monoclonal antibodies and mixtures of monoclonal antibodies against different targets, the condition $\mathcal{A}_i - \phi\mathcal{X}_i \geq 0$ follows from Theorem 3.2.9 and Theorem 3.3.17, respectively. And since $\beta^* \geq \widetilde{\beta}$ by construction, the correction $\mathcal{A}_i - \beta^*\mathcal{X}_i$ is stronger than the correction $\mathcal{A}_i - \widetilde{\beta}\mathcal{X}_i$. Hence, the corrected data

$$\mathcal{D}_{\widehat{\text{cor}}} \coloneqq \{(\mathcal{A}_i - \beta^*\mathcal{X}_i, \mathcal{X}_i, \Delta\mathcal{X}_i)\}_{i=1}^n \tag{4.27}$$

is a candidate for a worst-case correction, which probably overcorrects but never undercorrects the data.

We call $\mathcal{D}_{\widehat{\text{cor}}}$ candidate, as there is another aspect that we need to consider. Unlike the Langmuir isotherm considered by [Edw+98], we do not have an equilibrium state, but an arbitrary stopping point of the accumulation kinetics. While the Langmuir equilibrium state does not depend on the time development that led to the equilibrium state, the finite-time accumulation of antibodies does depend on the time development. Thus, correcting the antibody concentration only with the final amount of bound antibodies might not suffice.

Fortunately, Theorem 3.2.7 and Theorem 3.3.17 ensure that the amount of bound antibodies is monotonically increasing over time, which implies that the effective antibody concentration is monotonically decreasing over time. In other words, $\mathcal{A}_i - \widetilde{\beta}\mathcal{X}_i$ are lower bounds for the actual effective antibody concentrations $\mathcal{A}_i(t)$. This means that the depletion model with an initial antibody concentration $\mathcal{A}_i$ yields a larger response value than the reservoir model for $\mathcal{A}_i - \widetilde{\beta}\mathcal{X}_i$. Hence, $\mathcal{A}_i - \widetilde{\beta}\mathcal{X}_i$ is an overcorrection, and so is $\mathcal{A}_i - \beta^*\mathcal{X}_i \leq \mathcal{A}_i - \widetilde{\beta}\mathcal{X}_i$, which confirms that $\mathcal{D}_{\widehat{\text{cor}}}$ is a worst-case correction.

Remark 4.3.4 (**Generic antibody mixtures**).
Since we have only proven the necessary properties for monoclonal antibodies and mixtures of monoclonal antibodies against different targets, the worst-case correction (4.27) is only valid for those cases. However, the properties that we have used to derive the worst-case correction are quite natural:

1) The amount of bound antibodies cannot exceed the total (initial) amount of antibodies.

2) When measurable antibodies bind permanently, the amount of bound antibodies can only increase over time.

Since these properties are natural, we may assume them as axioms for practical applications, allowing us to use the worst-case correction (4.27) for arbitrary mixtures of antibodies.

Numerical solutions and corrections for monoclonal antibodies

Considering only monoclonal antibodies, we can provide a better data correction for depletion effects. In Subsection 3.2.3, we plotted the results of numerical solutions from the "DifferentialEquations.jl" package [RN17; RN19; Ma+21] to analyze the theoretical bounds for the depletion accumulation dose-response curve. Hence, we can obtain numerical solutions, at least for a few discrete epitope classes.

Since we have combined the rate constant and the incubation time into a single constant (Definition 4.2.1), we should do the same for the numerical model. Furthermore, we are interested in a data correction for data in experimental units, so we should also express the depletion accumulation IVP (Definition 3.1.4) in experimental units. In summary, we obtain (see Appendix B.3.4)

$$\begin{cases} \dfrac{d}{dT}\widetilde{\mathcal{X}}_{\mathrm{D};i}(T;\mathcal{A}) = \dfrac{1}{\mathcal{K}_{\tau;i}}\left(\mathcal{A} - \widetilde{\beta}\sum_{j=1}^{N}\widetilde{\mathcal{X}}_{\mathrm{D};j}(T;\mathcal{A})\right)\left(\mathcal{G}_i - \widetilde{\mathcal{X}}_{\mathrm{D};i}(T;\mathcal{A})\right) \\ \widetilde{\mathcal{X}}_{\mathrm{D};i}(0;\mathcal{A}) = 0 \end{cases} \tag{4.28}$$

for all $i \in \{1,\ldots,N\}$. Here, $\widetilde{\beta}$ denotes the depletion factor in experimental units and $T = {}^{t}/_{\tau}$ is the time, normalized to the incubation time. This means that the depletion accumulation model is given by

$$\mathcal{A} \longmapsto \widetilde{\mathcal{X}}_{\mathrm{D};i}(1;\mathcal{A}) \ .$$

Hence, the initial value problem can always be solved for the same time $T = 1$.

We can use the automatic numerical solvers from the "DifferentialEquations.jl" package to construct the following data correction method (see Figure 4.8 for a visualization).

Algorithm 4.3.5 (Numerical depletion correction).

1) Calculate the largest possible depletion factor β^* in experimental units (see (4.26)).

2) Fit the depletion accumulation model (simple least squares fit) to the dose-response data, using the numerical solvers from the "DifferentialEquations.jl" package to obtain epitope classes $\{(\mathcal{G}_i, \mathcal{K}_{\tau;i})\}_{i=1}^{N}$ in experimental units.

3) Calculate the theoretical depletion accumulation dose-response curve and the theoretical reservoir accumulation dose-response curve for the epitope classes $\{(\mathcal{G}_i, \mathcal{K}_{\tau;i})\}_{i=1}^{N}$.

4) Calculate the difference between the reservoir accumulation dose-response curve and the depletion accumulation dose-response curve to obtain a correction curve.

5) Increase the response values according to the correction curve.

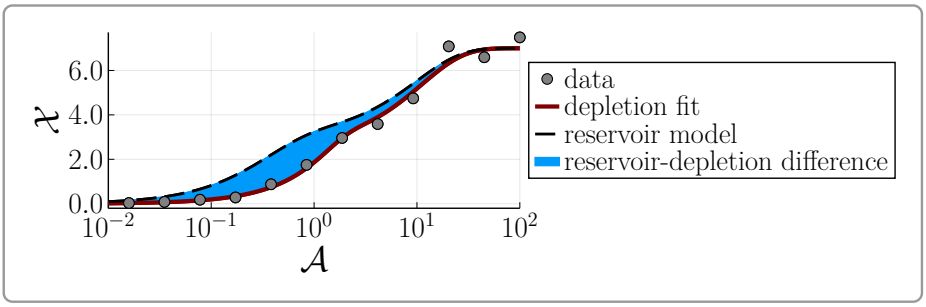

(a) Fitting the depletion accumulation model with numerical solutions

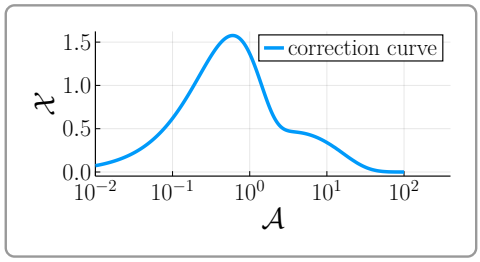

(b) Correction curve

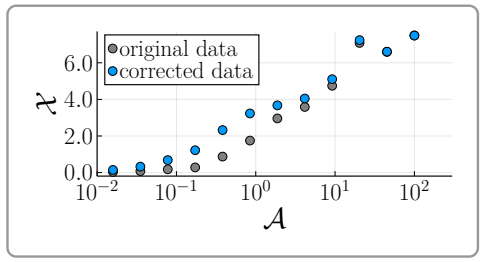

(c) Data correction

Figure 4.8: Illustration of the numerical depletion correction (Algorithm 4.3.5) using simulated data.

Before we conclude this Subsection, there are two things to observe. First, note that we still use the largest possible depletion factor $\widetilde{\beta} = \beta^*$, which we could equally well estimate using curve fitting. However, when the accumulation estimation model without depletion can fit the data well, it can happen that the depletion accumulation model (for a few epitope classes) could fit the data equally well for multiple values of the depletion factor, even $\widetilde{\beta} = 0$. In this case, the estimated depletion factor would be arbitrary, depending only

on the initial parameter configuration and the optimization algorithm. Thus, to ensure a meaningful depletion correction, we should use the largest possible depletion factor β^*.

Second, note that we do not change the response spreads for the depletion correction. This follows from

$$\sum_{\ell=1}^{r}\left((q_\ell + c) - \frac{1}{r}\sum_{\ell=1}^{r}(q_\ell + c)\right) = \sum_{\ell=1}^{r}\left(q_\ell - \frac{1}{r}\sum_{\ell=1}^{r} q_\ell\right) \ ,$$

which shows that a constant offset c does not change the corrected sample standard deviation (4.5). In fact, this is a general property of variance and standard deviation [Geo08, Theorem 4.23 (a)].

4.3.6 Accessibility analysis and default analysis setup

We call the estimation process that we have described in this section **accessibility analysis**. More precisely, accessibility analysis refers to the estimation of the parameters for the accumulation estimation model, using the objective function (4.19)-(4.20) and the adaptive partition refinement (Algorithm 4.3.2). Since the accessibility histogram visualizes the estimation epitope density, which is the result of the accessibility analysis, we can also understand the accessibility histogram as a part of the accessibility analysis.

The accessibility analysis is implemented and published in the form of Julia packages [AMDRC.jl; AMDRR.jl; ADMR.jl; ADA.jl; ADAR.jl; FOF.jl]. These Julia packages are also used for the data analysis in the next chapter. If not specified otherwise, the accessibility analysis will use the following default setup throughout this dissertation.

- The adaptive partition refinement (Algorithm 4.3.2) is used for 50 iterations.
- The initial partition is $\{\mathcal{A}_{\min}, p, \mathcal{A}_{\max}\}$, where $\mathcal{A}_{\min}$ is the lowest non-zero initial antibody concentration, $\mathcal{A}_{\max}$ is the largest initial antibody concentration, and p is their midpoint on a logarithmic scale, given by

$$\log_{10}(p) = \frac{\log_{10}(\min\{\mathcal{A}_{\min}\}) + \log_{10}(\max\{\mathcal{A}_{\max}\})}{2} \ .$$

- For each (new/refined) partition, the accumulation estimation model (Definition 4.2.2) and the objective function (defined by (4.19)-(4.20)) are constructed.

- The parameters are optimized using the Nelder-Mead algorithm from the "Optim.jl" package [MR18], with the box constraints $0 \leq \Lambda_j < \infty$, a relative tolerance of `1e-12`, and `2000` iterations.
- The first initial parameter configuration is $\Lambda = (1, 1)$. Afterward, the adapted optimal parameter configuration from the previous iteration of the adaptive partition refinement is used.
- After optimizing the parameters, the adaptive partition refinement (Algorithm 4.3.2 and (4.21)-(4.25)) is applied.
- After the 50th iteration of the adaptive partition refinement, the parameters are optimized once more using the LBFGS algorithm from the "Optim.jl" package, with the box constraints $0 \leq \Lambda_j < \infty$, numerically calculated gradients, a relative tolerance of `1e-12`, and `2000` iterations.

Note that we do not specify the default scaling parameter ϱ, as different analyses in this dissertation will use different scaling parameters, or compare multiple scaling parameters (see Remark 4.3.1).

Comparison to [Methods-Paper]

The analyses in this dissertation differ in some details from the analyses of [Methods-Paper], despite using the same data.[10]

In [Methods-Paper], the approximation

$$\begin{aligned}\mathcal{X}(\mathcal{A}) &= \sum_{j=1}^{m} \frac{\Lambda_j}{\mathcal{Q}_{j+1} - \mathcal{Q}_j} \int_{I_j} \left(1 - e^{-\frac{\mathcal{A}}{\mathcal{K}_\tau}}\right) \, |d\mathcal{K}_\tau| \\ &\approx \sum_{j=1}^{m} \frac{\Lambda_j}{\mathcal{Q}_{j+1} - \mathcal{Q}_j} \left(1 - e^{-\frac{2\mathcal{A}}{\mathcal{Q}_{j+1} + \mathcal{Q}_j}}\right) (\mathcal{Q}_{j+1} - \mathcal{Q}_j) \\ &= \sum_{j=1}^{m} \Lambda_j \left(1 - e^{-\frac{2\mathcal{A}}{\mathcal{Q}_{j+1} + \mathcal{Q}_j}}\right)\end{aligned}$$

is used, instead of the analytical solution (4.15), to simplify the calculations. Furthermore, the normalization factor for the scaling parameter is $1/m^2$ in

[10] For [Methods-Paper], the choices were based on early trial and error experience and were kept the same for later revisions. In this dissertation, we took our time to motivate all our decisions, leading to natural choices that slightly differ from those of [Methods-Paper].

[Methods-Paper]. Thus, the strength/importance of the logarithmic prior decreased during the adaptive partition refinement.[11] Finally, the intervals were not split on the logarithmic scale but on the linear scale by setting $\mathcal{Q}^* = (Q_{j^*+1}+Q_{j^*})/2$.

However, the results remain almost identical, which indicates that aforementioned differences do not strongly alter the analysis results.

[11] Since we determine the scaling parameter ϱ only by its effect on the final accessibility histogram, the normalization parameter affects only the intermediate calculations during the adaptive partition refinement. For example, we generally use scaling parameters 50-times lower than [Methods-Paper], which counteracts the additional factor $1/m = 1/52$ in the last optimization.

5

Experimental validation and applications

So far, we have not yet validated the accumulation principle, which is central for the accumulation model. The same holds true for the accessibility analysis, which we have described but not tested. Thus, this chapter focuses on experimental validations and potential applications. For this purpose, we can use the [Raw-Data] from [Methods-Paper].

This chapter analyzes the same [Raw-Data] as [Methods-Paper] using similar methods. And despite the minor differences in the analysis details (see Subsection 4.3.6), the results remain almost identical. Thus, this chapter will necessarily contain similar descriptions and conclusions as [Methods-Paper], but presented in a slightly different order.

I did not conduct the actual experiments that resulted in the raw data. All experiments used in this chapter were conducted by [Momina Saeed] and [Maike Siobal]. Hence, the data will always be referenced in this chapter. In addition, Tim Hucho provided the idea to mix antibodies and suggested the first application: the optimization of initial antibody concentrations.

However, I designed the requirements, including the selection of antibodies and cells, for the experiments used in this chapter. In addition, I developed and implemented the analysis methods, conducted the data analysis, evaluated the results, and created the figures. Hence, the inclusion of the experiments and their results in this chapter.

Since I did not optimize or conduct the experiments, technical and biological details of the experiments will not be included here (all details are published in [Methods-Paper]). Instead, the experiments will be described abstractly to focus on the relevant validation aspects.

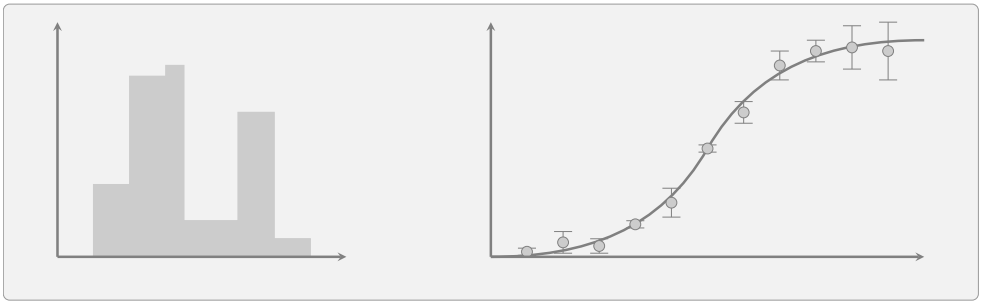

5.1 Validations

Before we can discuss potential applications of the accessibility analysis, we have to validate the accumulation model first. For this purpose, we will consider data and dose-response curves in this section. In each plot, the error bars will represent the corrected standard deviations (4.5) of the replicates.

5.1.1 Cell system and antibodies

As a first step for the validation, we should get acquainted with the experimental system. For each experiment, HeLa cells were used. Using this cell line was just a matter of convenience, as HeLa cells could be prepared repeatedly with little effort. In particular, there were no other biological considerations involved in this choice.

The same applies to the antibodies. The only biological considerations were the requirements that the antibodies must be monoclonal, from different host organisms (see Subsection 4.1.3), and against targets on different proteins. From trial and error with respect to the dose-response behavior, the following primary antibodies were selected among the antibodies that were readily available in the laboratory at the time:

- A monoclonal mouse antibody (Sigma-Aldrich, N0142-.2ML) against an epitope on a neurofilament (neurofilament 200). Let us call the antibody **NF200 antibody** for short.
- A monoclonal rabbit antibody (Abcam, ab175213) against an epitope on ribosomes (protein S11). Let us call the antibody **RPS11 antibody** for short.

As explained in Subsection 4.1.4, cell nuclei were stained to define regions of interest for the measurement of staining results.

Since these primary antibodies are from different host-organisms, secondary antibodies with different fluorescent labels were used to individually quantify the intensities of the NF200 antibody and the RPS11 antibody.

5.1.2 Incubation-time experiment

There is a simple experiment to check whether the accumulation principle applies. We can repeat dose-response experiments for different incubation times τ. When the accumulation principle applies, longer incubation times should result in higher staining intensities.

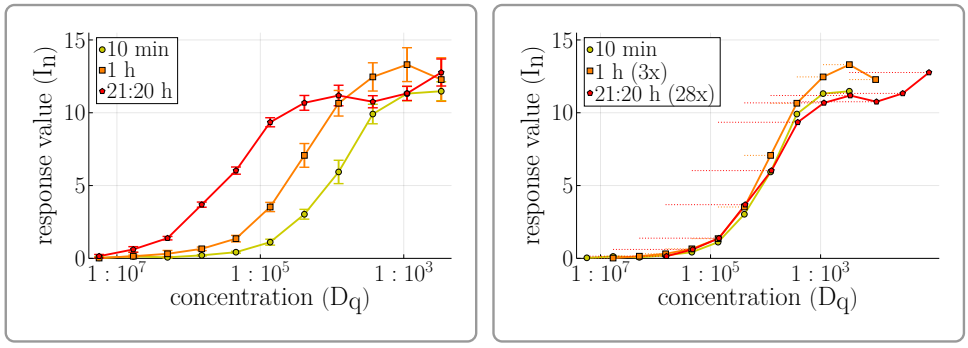

(a) Original dose-response curves **(b)** Shifted dose-response curves

Figure 5.1: {Adapted from [Methods-Paper], raw data from [Maike Siobal; Raw-Data]} Dose-response curves (**a**) for the NF200 antibody incubated for 10 mins, 1 h and 21:20 h respectively. For the shifted dose-response curves (**b**) all concentration values were multiplied with constant factors (3 for the 1 h incubation and 28 for the 21:20 h incubation), which leads to a translation/shift on the logarithmic scale.

Figure 5.1a shows the results of a dose-response experiment [Maike Siobal; Raw-Data], where the NF200 antibody was incubated for 10 mins, 1 h, and 21:20 h, respectively. As predicted, longer incubation times produce larger response values, provided that a shorter incubation time did not already reach saturation for a given initial antibody concentration. This hints at the predicted similarity between the effects of incubation time and initial antibody concentration. In fact, with minimal analysis effort, we can even verify this similarity.

Let us assume for the moment that the incubation time has the same effect as the initial antibody concentration. In other words, let us consider the reservoir model, where the incubation time τ and the initial antibody concentration a always appear in the form of a product $a\tau$. This means that doubling the incubation time should have the same effect as doubling the initial antibody concentration. Or, to put it differently, increasing the incubation time by a factor ϑ can be counteracted by reducing the initial antibody concentration by the factor $1/\vartheta$. For example, the 1 h-incubation dose-response curve should reach a certain response value at $1/6$ of the concentration

needed for the 10 min-incubation dose-response curve.

So, for a proper validation, we would repeat the 1 h-incubation dose-response curve with concentrations reduced by a factor of $1/6$. Then we would compare the corresponding response values. That is, we would compare the response values for the highest concentrations, the response values for the second-highest concentrations, and so forth. A plot of these response values would then use categorical values like "1st-highest", "2nd-highest", etc. Equivalently, we could multiply all concentrations of the 1 h-incubation by 6 before plotting the dose-response curve. This would equalize the concentrations for the plot, placing the response values that would belong to the same categorical label next to each other.

Fortunately, there is no need for additional experiments, as we have dose-response curves. Using interpolation, we have response values for the concentrations reduced by a factor of $1/6$. In fact, we have response values for arbitrary factors $1/\vartheta$ within a certain range.

Figure 5.1b shows the dose-response curves, where we multiplied the concentrations by constant factors[1], so that the dose-response curves overlap. The fact that constant factors could be found such that the dose-response curves become almost identical, within the margins of experimental variability, confirms the accumulation principle. For all incubation times, the dose-response curve is the same, just at different concentrations.

Before we can conclude the validation of the accumulation principle, there is a last important detail to address. Instead of a factor of 6, the 1 h-incubation dose-response curve uses a factor of 3. And instead of a factor of 128, the 21:20 h-incubation dose-response curve uses a much smaller factor of 28. Thus, not only is the factor smaller than expected from the incubation time, but it also needs to be decreased even further for longer incubation times, which implies that the relationship between incubation time and initial antibody concentration is non-linear.

This non-linear relationship is not concerning, as we have already speculated about potential reasons in Subsection 3.1.3. Once we have tested the accessibility analysis, we can further investigate differences in the dose-response curves for different incubation times.

[1] resulting in a translation/shift on logarithmic scales (see Appendix C.7).

5.1.3 Antibody-mix experiment

Having validated the fundamental principle of the accumulation model, we can consider the accessibility analysis.

Antibody-mix idea

Since apparent rate constants, and by extension obstruction constants, comprise multiple unobservable effects, it is difficult to construct systems with known epitope densities. Consequently, we cannot easily verify or falsify estimated epitope densities.

At this point, we could use simulations for the validation of the accessibility analysis. However, this would only demonstrate the consistency of the proposed method. It would not show that the estimated densities reflect the binding behavior of antibodies in a real antibody-staining experiment.

Fortunately, there is a compromise between simulation and purely experimental validation that was devised by Tim Hucho. We can analyze the dose-response curves of two different antibodies. If the respective target epitopes belong to separate structures, we may assume that the antibodies do not interfere with each other. Thus, applying both antibodies simultaneously should lead to a perfect superposition of the dose-response curves. The corresponding epitope density should then be the sum of the epitope densities of the individual antibodies. At least if epitope densities really correspond to dose-response behavior.

The compromise of this antibody-mix approach is that the true epitope densities remain unknown. We only obtain a consistency validation similar to a simulation. In other words, we only check that the accessibility analysis consistently produces epitope densities for certain dose-response features and their superposition.

Using experimental data for this consistency check has some advantages over mere simulations. First, we do not need to assume that the model is true in order to generate data. Thus, we can demonstrate that the consistency applies to real dose-response data. Second, we can use any knowledge gained about the system to construct additional experiments that demonstrate potential applications.

The ideal antibody pair for the antibody-mix experiment would comprise antibodies with dose-response curves whose features do not overlap. That is, the response values of one antibody reach saturation at concentrations that do not yet produce measurable responses for the other antibody. For later reference, we may call the point where responses become non-zero the

response onset.

Unfortunately, it is very difficult to obtain two ideal antibodies. Often, the response onsets are too close together. Fortunately, the problem can be alleviated by varying the relative concentration of the antibodies in the mixture. Increasing the concentration of one antibody means that the response onset of this antibody occurs at a lower dilution quotient of the mixture. In this way, the response onsets can at least be moved further apart if a complete separation of the dose-response features is not possible.

Experimental realization

In the actual antibody-mix experiment [Momina Saeed; Raw-Data], the NF200 antibody was used at higher concentrations than the RPS11 antibody. While the RPS11 antibody was diluted 1 to 100 from the vendor stock, the NF200 antibody was only diluted 1 to 20. The resulting mixture was treated as a new stock solution with concentration $1 : 100\,\mathrm{D_q}$. We call this setup **antibody-mix system** in the following.

At this point, we could keep track of the relative concentrations, i.e., the antibody-mix fractions (Definition 3.3.1). However, since we constructed the accumulation estimation model (Definition 4.2.2) from the reservoir model, we can use Theorem 3.3.13 and interpret the antibody mixture as a solution that contains only a single antibody type.

For a sensible comparison between the antibody mixture and the individual antibodies, the dose-response curves need to be expressed in the same units. By definition of the unit "dilution quotient" (see Subsection 4.1.1), this means that we have to construct stock solutions with identical antibody concentrations for the individual antibodies. Hence, the stock solution for the NF200 antibody consists of a 1 to 20 dilution of the vendor stock, whereas the stock solution for the RPS11 antibody consists of a 1 to 100 dilution of the vendor stock. In both cases, these stock solutions have the concentration $1 : 100\,\mathrm{D_q}$.

There is a last peculiarity of this antibody-mix system that needs to be addressed: the use of different secondary antibodies. It would certainly be desirable to use primary antibodies derived from the same host organism, so that a single secondary antibody could be used for both antibodies. This would reduce the potential bias of secondary antibodies, which we have considered in Subsection 4.1.3. On the other hand, the experimental system was constructed to serve as a showcase system for potential applications, which requires that different primary antibodies be distinguishable in microscopy images. Hence, primary antibodies from different host organisms and corresponding secondary antibodies with different fluorescent labels were used. Let us abstractly name

the labels L_{NF} for the NF200 antibody and L_{RP} for the RPS11 antibody.

As described in Remark 4.1.3, multiplexing allows the acquisition of individual antibody signals. Since multiplexing produces two response values, one for each label, the total response value for the antibody mixture is defined as the sum of both label signals. However, the signals from the labels need to be normalized to a common standard, as the fluorescent labels could produce different response values for the same amount of bound antibodies[2].

To normalize the label signals, two secondary antibodies against the NF200 antibody were used simultaneously as a control condition. One secondary antibody had the label L_{NF}, while the other secondary antibody had the label L_{RP}. On average, both secondary antibodies should bind in equal amounts. Thus, the signals of the control condition could be used as normalization values for the signals of the dose-response curves.

Dose-response data

Figure 5.2 shows the resulting dose-response curves. For each dose-response curve, both label signals were measured and the sum of both signals was calculated. This allows us to test the optical filters that were used to isolate the signals of the labels. Furthermore, we can check that the antibodies do not influence each other in the mixture.

Although the difference is very small, we can see that for the NF200 antibody the dose-response curve of the summed-signal diverges from the dose-response curve of the L_{NF} signal (see Figure 5.2a). To find the reason for this difference, we should compare the L_{NF} signal and the L_{RP} signal. Figure 5.2d shows that the L_{RP} signal and the L_{NF} signal behave similarly for high initial antibody concentrations. The signal intensity of the L_{RP} label maintains 5% to 10% of the signal intensity of the L_{NF} label. The initial fluctuation of the $(L_{\mathrm{RP}}/L_{\mathrm{NF}})$-graph can be explained by noise governing the signal, since the dose-response curves are close to zero for low initial antibody concentrations.

In summary, this indicates that a small but constant percentage of the L_{NF} signal passes through the L_{RP} filter. Interestingly, this does not happen for the opposite direction. The L_{RP} signal appears to be reliably blocked by the L_{NF} filter, since the dose-response curves (summed signal and L_{RP} signal) agree for the RPS11 antibody (see Figure 5.2b).

[2]For example, the response values differ when there are differences in the emission intensities of the fluorescent labels, differences in the transmittance of the respective optical filters, or when the detection efficiency of the imaging sensor depends on wavelength.

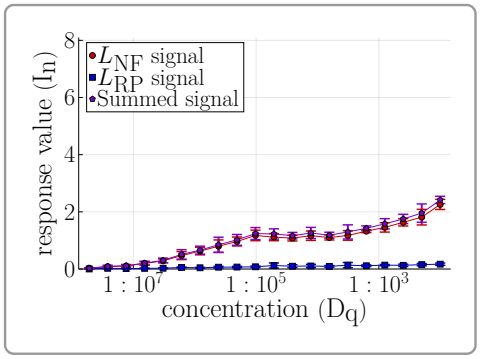

(a) NF200 antibody

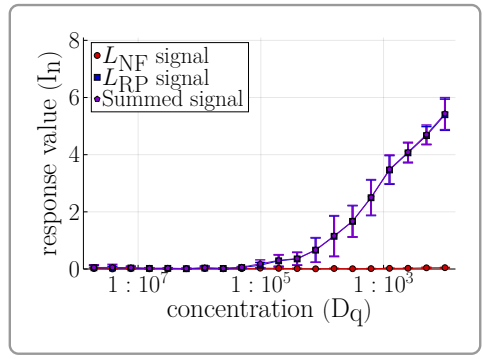

(b) RPS11 antibody

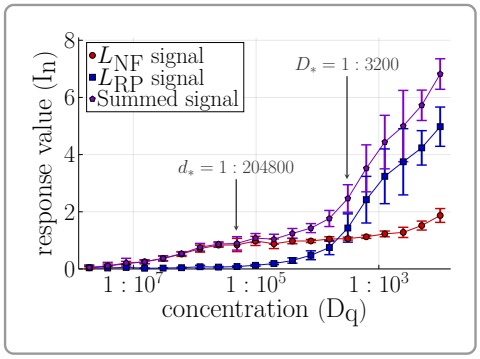

(c) Antibody mixture

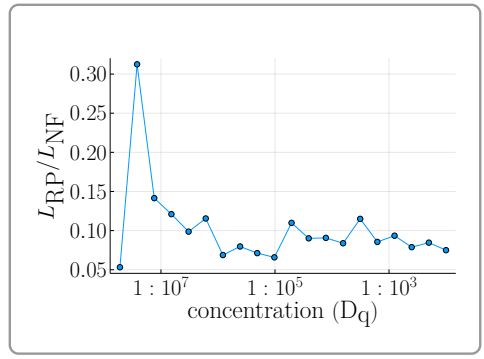

(d) NF200 antibody, L_{RP}/L_{NF}-plot

Figure 5.2: {Adapted from [Methods-Paper], raw data from [Momina Saeed; Raw-Data]} Dose-response curves for the individual antibodies and the antibody mixture (**a-c**). For each antibody solution, the signals of both labels and the sum of the signals were evaluated. In addition, the quotient of the L_{RP} signal and the L_{NF} signal is plotted (**d**), which shows that some of the L_{NF} signal passes through the L_{RP} filter. The annotations in (**c**) are needed for another validation (see Subsection 5.2.1).

Next, we observe that the dose-response curves for the individual antibodies (for their respective labels) closely resemble the L_{NF}-signal dose-response curve and the L_{RP}-signal dose-response curve of the antibody mixture (see Figure 5.2c). This reassures us in our assumption that the antibodies do not influence each other, regarding their dose-response behavior.

Finally, Figure 5.2 shows that the choice of relative concentrations for the individual antibodies separates their dose-response features. The NF200 antibody reaches a plateau roughly at the concentration of the response onset of the RPS11 antibody. However, the plateau of the NF200 antibody is not the saturation of the dose-response curve. Nevertheless, the antibody-mix system fulfills the requirements of our theoretical considerations for the validation of the accessibility analysis.

Validation

The final step is the estimation of epitope densities. Figure 5.3 shows the accessibility histograms and the fitted dose-response curves, obtained from the accessibility analysis using the scaling parameter $\varrho = 1$. See Figures A.1–A.3 for different scaling parameters.

As required for the consistency verification of the accessibility analysis, the epitope density of the antibody mixture (Figure 5.3c) is the sum of the epitope densities of the individual antibodies (Figures 5.3a and 5.3b). The peaks at $K_\tau < 10^{-5}$ of the NF200 antibody also appear in the accessibility histogram of the antibody mixture, albeit mirrored; but they are not present in the accessibility histogram of the RPS11 antibody. Similarly, the double peak of the RPS11 antibody is also present in the accessibility histogram of the antibody mixture. In fact, for the antibody mixture, the peaks at $K_\tau > 10^{-4}$ of the NF200 antibody are added on top of the double peak of the RPS11 antibody. All of these aspects, except for the shape of the peaks, do not depend on the scaling parameter (see Figures A.1–A.3). Hence, we may conclude that the accessibility analysis is consistent.

Since the antibody-mix system uses a mixture of two monoclonal antibodies, we cannot use the numerical depletion correction. However, we can use the worst-case depletion correction (see Figure A.7). All in all, we find that the accessibility histograms do not differ much, indicating that potential depletion effects do not severely affect the estimated epitope densities. The only noteworthy differences are that the peak between $K_\tau = 10^{-7}$ and $K_\tau = 10^{-5}$ disperses slightly into two separate peaks and that the peak at $K_\tau < 10^{-7}$ is shifted to the left edge of the histogram. Since these peaks belong to the NF200 antibody, we can explore the effects of the depletion correction in the

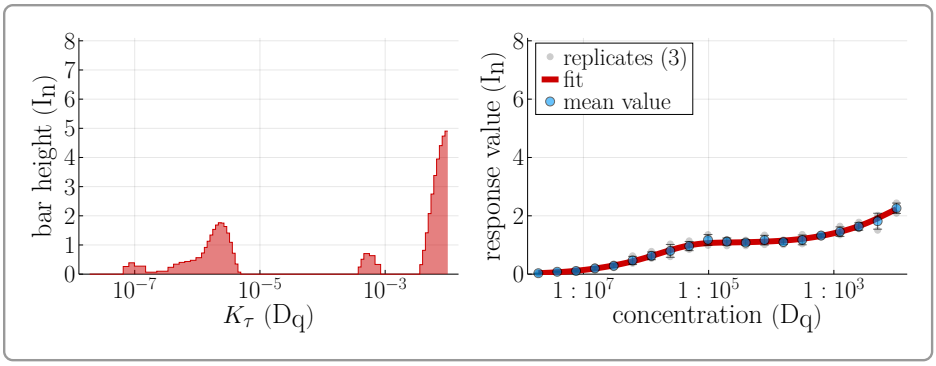

(a) NF200 antibody, L_{NF} signal

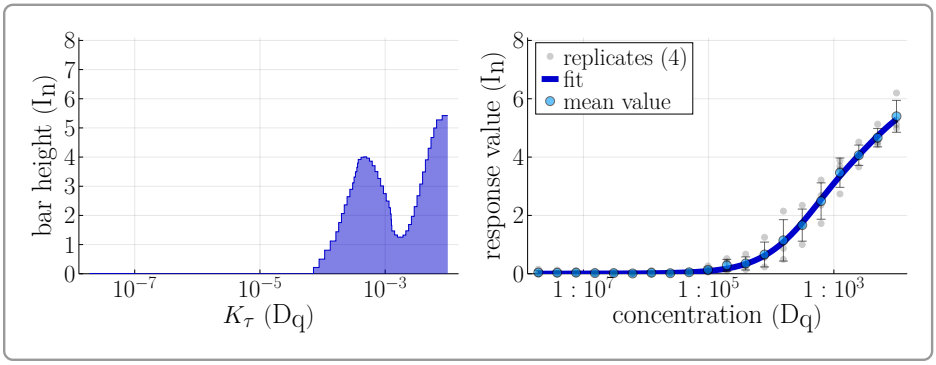

(b) RPS11 antibody, L_{RP} signal

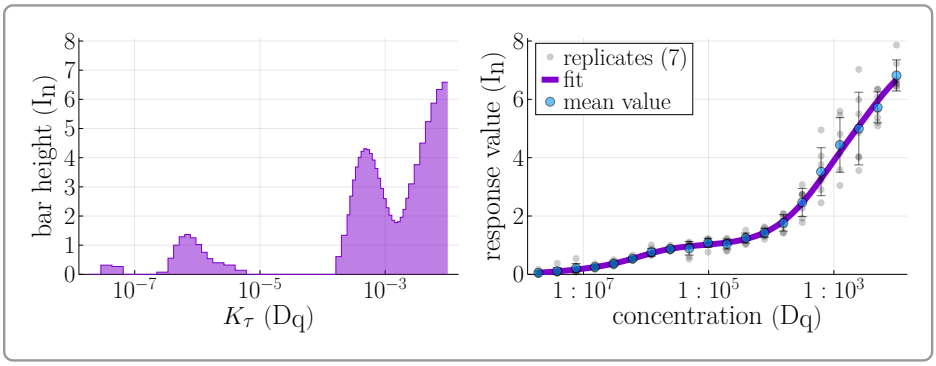

(c) Antibody mixture, summed signal

Figure 5.3: {Adapted from [Methods-Paper], raw data from [Momina Saeed; Raw-Data]} Accessibility analysis of the antibody-mix system using the scaling parameter $\varrho = 1$.

next Subsection, when we analyze the NF200 antibody in detail for different incubation times.

5.1.4 Incubation-time experiment revisited

Now that we have reassured ourselves about the consistency of the accessibility analysis, we may also analyze the dose-response curves of the incubation-time experiment. Accordingly, Figure 5.4 shows the accessibility histograms and the fitted models for the dose-response curves of the incubation-time experiment.

Here, we can clearly see the correspondence between the initial antibody concentration and the obstruction constant, which was merely an argument for the logarithmic scale in Subsection 4.3.2. The position (obstruction constant K_τ) of the peak in the accessibility histogram corresponds to the location (initial antibody concentration a) of the non-constant regions of the dose-response curve. As the dose-response curves move to the left (on the logarithmic scale) due to the increased incubation times, so do the peaks in the accessibility histograms.

More important, however, is the dispersion of the peak for longer incubation times. This confirms our random-walk description of the unobserved microscopic binding behavior from Subsection 3.1.3. Longer incubation times lead to a stronger distinction of the accessibility of epitopes.

At this point, it could be argued that the dispersion of the peak is just an artifact of the scaling parameter $\varrho = 1$. And indeed, larger scaling parameters seem to reduce this effect, as the resulting smoothing reduces the individual features/distinct peaks (see Figures A.5–A.6). But there are limits to how large the scaling parameter can become before the fitted models fail to agree with the data. Taking this into account, the dispersion remains valid for all reasonable scaling parameters.

The dispersion becomes even more pronounced when we account for potential depletion effects. For the worst-case correction (Figures A.8a–A.8c), the peak even dispersed into two separate peaks for the 21:20 h incubation. For the numerical depletion correction (Figures A.13–A.14), which is less extreme, the dispersion is still more pronounced than for the uncorrected data.

Finally, we can observe two aspects of the depletion correction that we have already observed in the last Subsection. First, both depletion correction methods affect only the low-K_τ part of the histogram. Second, low-K_τ-peaks are slightly shifted leftwards. Put differently, the K_τ-values of these peaks have decreased.

At this point, we can easily explain both aspects. In Subsection 3.2.4, we observed that antibody depletion affects the dose-response curve mainly at low

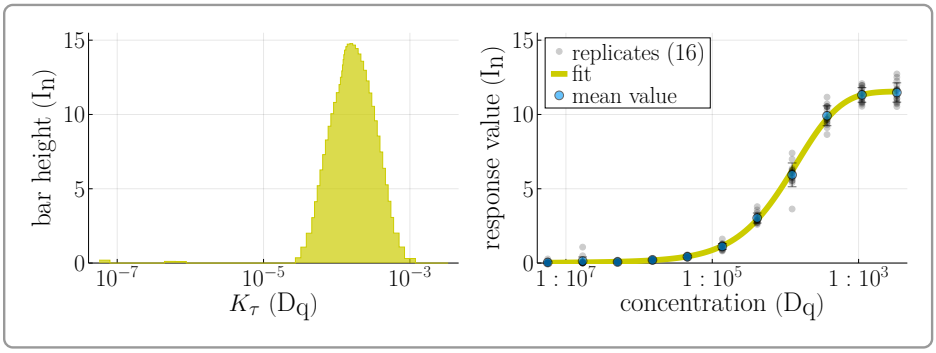

(a) 10 min incubation

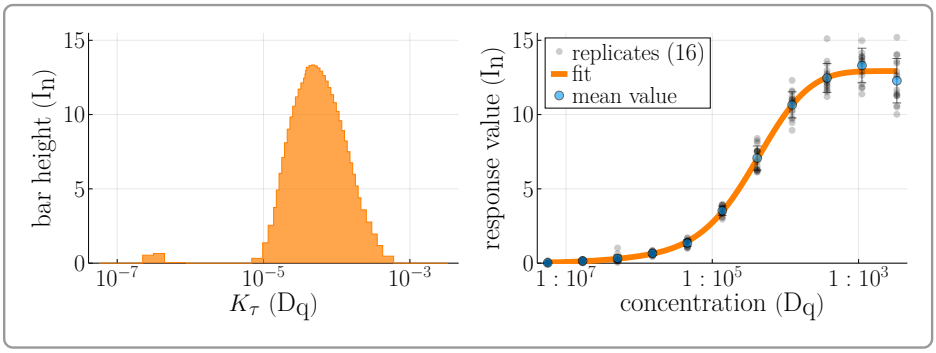

(b) 1 h incubation

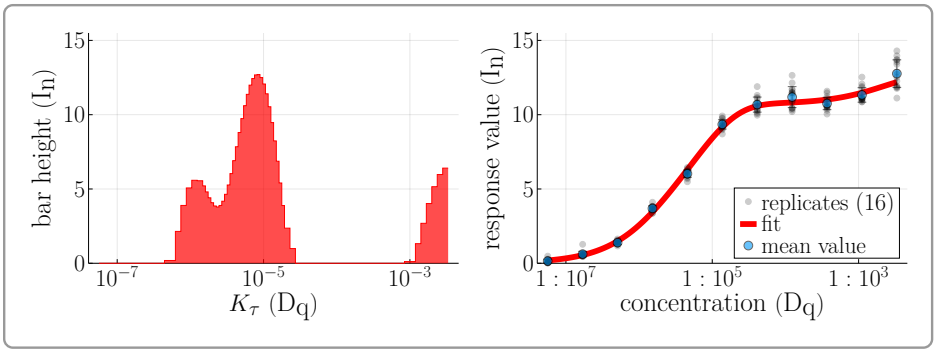

(c) 21:20 h incubation

Figure 5.4: {Adapted from [Methods-Paper], raw data from [Maike Siobal; Raw-Data]} Accessibility analysis of the incubation-time experiment using the scaling parameter $\varrho = 1$.

initial antibody concentrations. Thus, because of the correspondence between the initial antibody concentration and the obstruction constant, depletion corrections should mainly affect the low-K_τ part of the histogram. And since both correction methods aim to undo the depletion effect, higher response values are assigned to lower initial antibody concentrations in the corrected dose-response curves. Hence, the correspondence between initial antibody concentrations and obstruction constants explains the decrease in K_τ-values.

5.2 Applications

Provided with the confidence gained from the validation experiments, we can consider potential applications of the accessibility analysis.

5.2.1 Selection of antibody concentrations

During the analysis of the accessibility histograms for the incubation-time data (Subsection 5.1.4), we could observe that the location of a peak in the accessibility histogram corresponds to the non-constant region of the dose-response curve. Thus, low-K_τ peaks lead to a response increases at low initial antibody concentrations, and high-K_τ peaks lead to a response increases at high initial antibody concentrations.

Since high antibody concentrations are commonly reported to cause non-specific staining [Pil+20; Dud+22; Par+25] and cross-reactions [Lip+05], Tim Hucho suggested using the accessibility histogram for the optimization of initial antibody concentrations. In essence, the idea is to maximize signal contributions belonging to low-K_τ peaks while minimizing signal contributions belonging to high-K_τ peaks.

To realize such a selection criterion for initial antibody concentrations, let us define the concept of K_τ-optimal initial antibody concentrations. We call an initial antibody concentration **K_τ-optimal** for a peak, when it maximizes the response contribution of signals belonging to the considered peak while minimizing the response contributions belonging to peaks with larger K_τ values.

Fortunately, determining K_τ-optimal initial antibody concentrations is quite easy. After all, we have determined the epitope density by calculating the resulting dose-response curve for multiple possible epitope densities (see Subsection 4.3.3). So, we can also evaluate the individual dose-response curves for each part of the accessibility histogram. The respective contributions to the overall dose-response curve can then be visualized by adding the individual

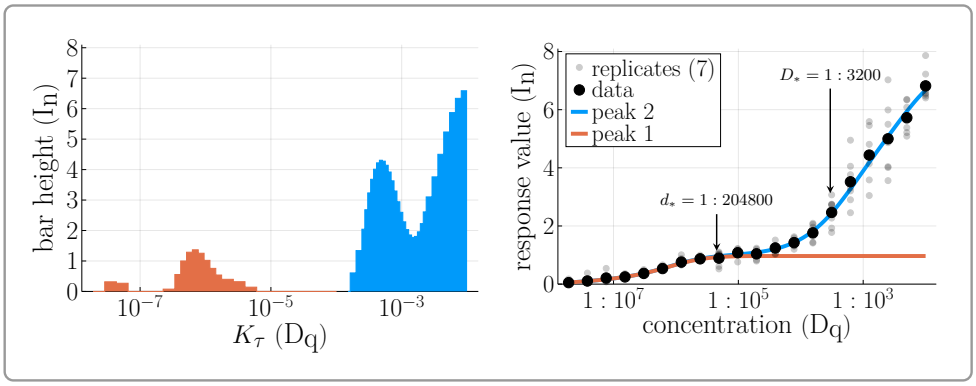

(a) Response contributions of the peaks (color matched)

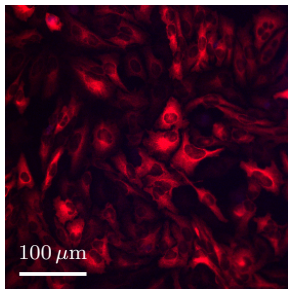

(b) d_* : Composite

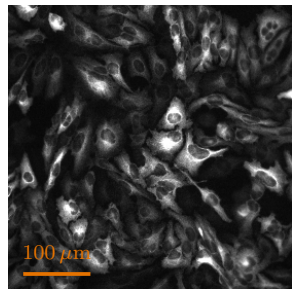

(c) d_* : L_{NF} signal

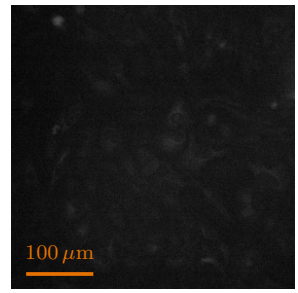

(d) d_* : L_{RP} signal

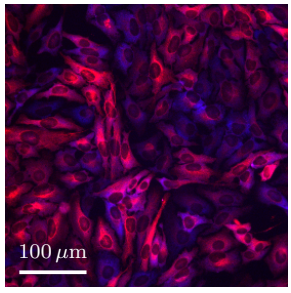

(e) D_* : Composite

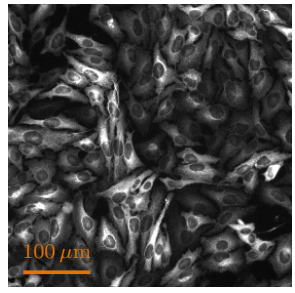

(f) D_* : L_{NF} signal

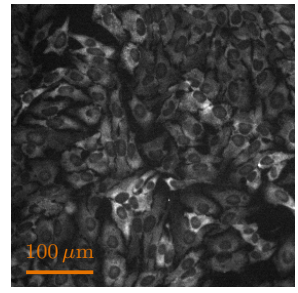

(g) D_* : L_{RP} signal

Figure 5.5: {Adapted from [Methods-Paper], raw data from [Momina Saeed; Raw-Data]} **(a)** shows the response contributions of low-K_τ peaks (orange) and high-K_τ peaks (azure) for the antibody mixture (see Figure 5.3c). d_* is the K_τ-optimal initial antibody concentration, whereas D_* leads to equal contributions from low-K_τ peaks and high-K_τ peaks.**(b)-(g)** show the corresponding microscopy images (label signals normalized as for the response values; uniformly increased brightness for better visibility) for both labels and the composite (red = L_{NF}, blue = L_{RP}).

dose-response curves on top of each other.[3] The K_τ-optimal initial antibody concentration is then given by the point where the dose-response contributions diverge.

We can illustrate and validate the principle of K_τ-optimal initial antibody concentrations with data from the antibody-mix experiment [Momina Saeed; Raw-Data]. By construction of the antibody mixture, the NF200 antibody mimics a specific signal that appears at low initial antibody concentrations (of the mixture), whereas the RPS11 antibody mimics a nonspecific staining signal that appears only at high initial antibody concentrations.

Figure 5.5a shows these response contributions for the antibody mixture of the antibody-mix system. Here, we have distinguished between the peaks at $K_\tau < 10^{-5}$ and the peaks at $K_\tau > 10^{-5}$. The K_τ-optimal initial antibody concentration is at the location where the contributions diverge ($d_* = 1 : 204800$). By design of the antibody mixture, this is also the initial antibody concentration at which the dose-response curve for the low-K_τ peaks reaches its saturation.

The microscopy images[4] (Figures 5.5b–5.5d) for the K_τ-optimal initial antibody concentration d_* show that the majority of the signal comes from the L_{NF} label. The weak L_{RP} signal can be attributed to the L_{NF} signal passing through the L_{RP} filter (see Figure 5.2) because the L_{RP}-signal image is just a faint copy of the L_{NF}-signal image. The response values in Figure 5.2c confirm our visual inspection.

By construction of the antibody-mix system, the low-K_τ peaks correspond solely to the NF200 antibody. Hence, the lack of L_{RP} signal for the initial antibody concentration d_* validates the selection approach for K_τ-optimal initial antibody concentrations. In fact, we can validate the selection approach further, by considering an initial antibody concentration D_*, where both low-K_τ peaks and high-K_τ peaks contribute equally. This is around $D_* = 1 : 3200$. And indeed, both the L_{NF} signal and the L_{RP} signal are observable in the microscopy images (Figures 5.5e–5.5g). As before, the visual inspection is confirmed by the response values in Figure 5.2c.

Although the antibody-mix system demonstrates and validates the selection of K_τ-optimal initial antibody concentrations, we cannot draw decisive conclusions about the use of K_τ-optimal antibody concentrations to reduce nonspecific signals or cross-reactions. The underlying assumption that nonspe-

[3] Because low obstruction constants correspond to low initial antibody concentrations, the order of the dose-response curves must be: first low K_τ contributions, then high K_τ contributions.

[4] Microscopy images were obtained along with the response values for the antibody-mix experiment

cific signals and cross-reactions appear at high initial antibody concentrations was not addressed by us. Quite the opposite, we constructed the antibody-mix system to fulfill this assumption, so that we could validate the selection process of K_τ-optimal initial antibody concentrations.

Hence, we need to be cautious about premature interpretations of peaks in the accessibility histogram. The location of a peak in the accessibility histogram does not tell us much about the specificity of the corresponding signal; at least not on its own. The obstruction constants, and thus the accessibility histogram, depend on apparent rate constants. These apparent rate constants can include many effects apart from the raw paratope-epitope interaction. In theory, the same biological type of epitope could have vastly different obstruction constants, depending on its location within the cell. Thus, high-K_τ peaks should only be viewed as candidates for potentially nonspecific signals, and conclusions should only be drawn after additional experiments and analyses.

Finally, we must note that the concentration heuristic regarding nonspecific binding can only be applied to monoclonal antibodies. In fact, the antibody-mix system provides the perfect example of this restriction. By varying the mixing ratios of the antibodies, we could arrange that the RPS11 antibody contributes to the staining signal only at high initial antibody concentrations of the antibody mixture. The same could happen for a polyclonal antibody, where a rare antibody type in the polyclonal mixture might only contribute to the signal at high initial antibody concentrations. However, this contribution would not need to be any less specific than the signal contributions of the other antibody types.

5.2.2 Multi-staining multiplexing

The last subsection suggested an important question. What structures cause distinct peaks in an accessibility histogram? Answering this question would help determine whether a K_τ-optimal initial antibody concentration reduces nonspecific staining or cross-reactions in a given system.

Unsurprisingly, the accessibility histogram cannot answer this question on its own, since the underlying epitope density is estimated solely from a dose-response curve. Hence, we need to construct additional experiments.

Motivation for the multi-staining idea

The working principle of the K_τ-optimal initial antibody concentration might be the best tool to analyze peaks in the accessibility histogram, as it allows us to isolate the signal contributions of the peaks. Even better, this principle does not require monoclonal antibodies, so we can also analyze peaks for polyclonal antibodies.

However, there is a problem. A K_τ-optimal initial antibody concentration can only isolate the contributions of peaks with low K_τ-values (from the contribution of peaks with high K_τ values). Signals that already appear at low initial antibody concentrations will continue to appear at high initial antibody concentrations. In other words, there is no single initial antibody concentration that isolates the signals belonging to high-K_τ peaks.

But why should we restrict ourselves to a single staining? We could stain and image the same biological sample repeatedly with the same antibodies at increasing initial antibody concentrations (**multi-staining**), similar to [Smi13].

Hence, we can isolate the signals from a low-K_τ peak with the first staining and include the signals from a high-K_τ peak with a second staining, using a higher initial antibody concentration. The signal difference between two staining images should then correspond to the signals of the high-K_τ peak.

In itself, subtracting images from each other is not difficult. After all, an image is just a matrix of RGB values. However, subtracting arbitrary pixels (the components of the image matrix) from each other produces meaningless results. We must ensure that we only subtract pixels that belong to the same structure, captured at different time points. Hence, the same region of the biological sample must be imaged after each staining. Furthermore, a perfect alignment is impossible in practice, requiring image registration[5], which is a common problem that can be solved by additional packages/libraries available for most programming languages.

Remark 5.2.1 (**Double-application correction**).
In our discussion about secondary antibodies (Subsection 4.1.3), we noted that the accumulation model describes the final staining result, including the properties of secondary antibodies. Contrary to the dose-response experiment used to determine the K_τ-optimal initial antibody concentrations, we must apply secondary antibodies twice for the multi-

[5]Transformation of images to align the structures digitally.

staining. During the second staining, this has the side effect that secondary antibodies could bind to primary antibodies from the first staining, where the secondary antibodies did not attach in the first attempt.

To correct for this double-application effect of secondary antibodies, we can add a control condition in which only secondary antibodies are used during the second staining. The resulting response increase can then be used as a correction factor by which the pixel intensities of the first-staining image need to be increased for the calculation of the difference image.

Experimental realization to validate the multi-staining idea

The antibody-mix system is again a solid choice to illustrate and validate the multi-staining idea, but it will begin to show its limitations.

Remark 5.2.2 (**Label information**).
For a generic antibody from a single host organism, there would only be a single label, in general. Thus, when we use the antibody-mix system for the validation of the multi-staining, we need to toss additional information provided by the distinct antibody labels (L_{NF} and L_{RP}). As with the response values, this can be achieved by summing the individual images for the antibody labels. Note that the label signals are not normalized in this subsection.

Considering the peak analysis of the accessibility histogram for the antibody mixture (see Figure 5.5a), we would select two initial antibody concentrations for the multi-staining. First, the K_τ-optimal initial antibody concentration $\mathcal{A}_1 = d_* = 1 : 204800$ for the peaks at $K_\tau \leq 10^{-5}$. Second, the K_τ-optimal initial antibody concentration for the peaks at $K_\tau > 10^{-5}$, which is $\mathcal{A}_2 = 1 : 100$ (or higher).

Following the multi-staining idea, we would obtain two images of interest: the first staining image corresponding to the peaks at $K_\tau < 10^{-5}$ and the difference image corresponding to the peaks at $K_\tau > 10^{-5}$. A validation would then involve comparing these images with images of the antibody labels L_{NF} and L_{RP}, since the peaks at $K_\tau < 10^{-5}$ belong solely to the NF200 antibody, by construction of the antibody-mix system. However, although the RPS11 antibody constitutes the majority of the peaks at $K_\tau > 10^5$, there is also

some contribution from the NF200 antibody (see Figure 5.3). Hence, a second staining image with initial antibody concentration $\mathcal{A}_2 = 1:100$ would contain a signal increase from the L_{NF} label that would appear in the difference image.

To retain the antibody-mix system for the validation, we need to compromise the initial antibody concentration for the second staining. The response onset of the RPS11 antibody (in the antibody mixture) occurs at lower initial antibody concentrations than the second response increase of the NF200 antibody (see Figure 5.3). Thus, we can use a lower initial antibody concentration for the second staining to avoid a response increase from the NF200 antibody.

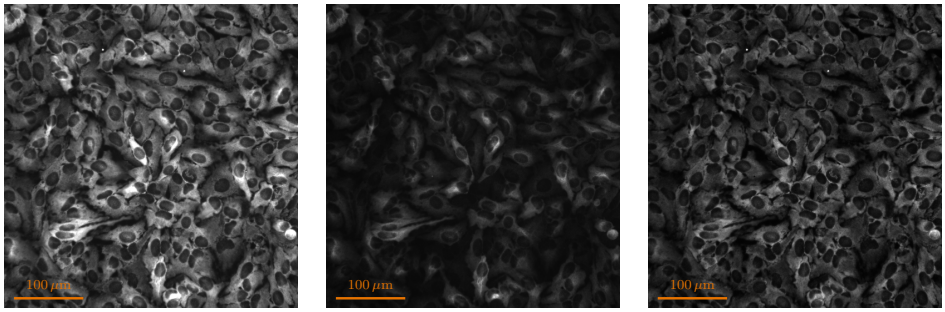

(a) Second staining image **(b)** First staining image **(c)** Difference image

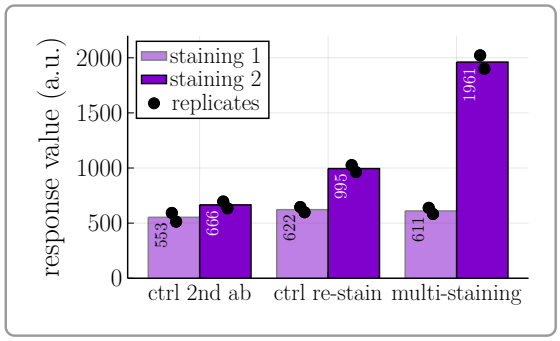

(d) Response values (multi-staining and controls)

Figure 5.6: {Adapted from [Methods-Paper], raw data from [Momina Saeed; Raw-Data]} Illustration and result of the multi-staining principle: second staining (**a**) − corrected first staining = difference image (**c**). Subfigure **(b)** shows the uncorrected first staining image. The brightness of all images was equally increased for better visibility. The response values (**d**) of the control condition "ctrl 2nd ab" are used for the double-application correction. The second control condition,"ctrl re-stain", serves as additional validation of the accumulation principle (see Remark 5.2.3). The response values for the "multi-staining" condition are added as a reference point.

For the experimental realization [Momina Saeed; Raw-Data], $\mathcal{A}_2 = 1:6400$ was used as initial antibody concentration for the second staining. Furthermore, the initial antibody concentration for the first staining was not the K_τ-optimal initial antibody concentration d_*, but a slightly higher concentration $\mathcal{A}_1 = 1:102400$ to ensure saturation of the contributions from the low-K_τ peaks. Figure 5.6 shows the resulting images.

Aside from the control for the double-application correction (ctrl 2nd ab), Figure 5.6d also contains the response values[6] for the multi-staining condition and an additional control (ctrl re-stain), where the first staining was repeated. Additional response values for the individual antibody labels can be found in Figure A.15.

Remark 5.2.3 (**Accumulation model effect**).
Regarding the response values for the controls and the multi-staining condition in Figure 5.6d, we can observe a last interesting property that corroborates the accumulation model. Simply repeating the first staining increases the response value. With the accumulation model in mind, this is hardly surprising. Applying the primary antibodies a second time essentially means replenishing depleted antibodies. Furthermore, even if depletion effects are negligible, repeating the staining doubles the incubation time, which also increases the amount of bound antibodies, as demonstrated in Subsection 5.1.2.

Validation of multi-staining multiplexing

The difference image (Figure 5.6c) should contain only signals belonging to the high-K_τ peaks of the antibody-mix system, and should be identical to the L_{RP}-signal image, by construction of the validation experiment. In the same way, the first-staining image (Figure 5.6b) should contain only signals belonging to the low-K_τ peaks of the antibody-mix system. That is, it should be identical to the L_{NF}-signal image.

However, since we will consider the L_{NF}-signal image from the second staining, to illustrate deficiencies of the multi-staining approach, we need to take the double-incubation of secondary antibodies into account. Hence, we will compare the L_{NF}-signal image from the second staining to the total-signal image from the first staining, where we increase the brightness according to the double-application correction.

[6] The response values are obtained in the same way as for the dose-response experiments, i.e., by analyzing regions of interest (see Subsection 4.1.4).

To ease the comparison between the multi-staining results and the images for the antibody labels, we can construct color-composites, as commonly done for multiplexing (see Remark 4.1.3). This allows us to focus only on two images, where the respective peak signals /label signals are represented by the pixel color. We may use **red** for the signals corresponding to the low-K_τ peaks /the L_{NF} label and **blue** for the signals corresponding to the high-K_τ peaks /the L_{RP} label.

Let us call the composite of the multi-staining images **multi-staining composite** and the composite of the antibody-label images **label composite**. Since the label composite is obtained with common label multiplexing, we call the multi-staining approach **multi-staining multiplexing**.

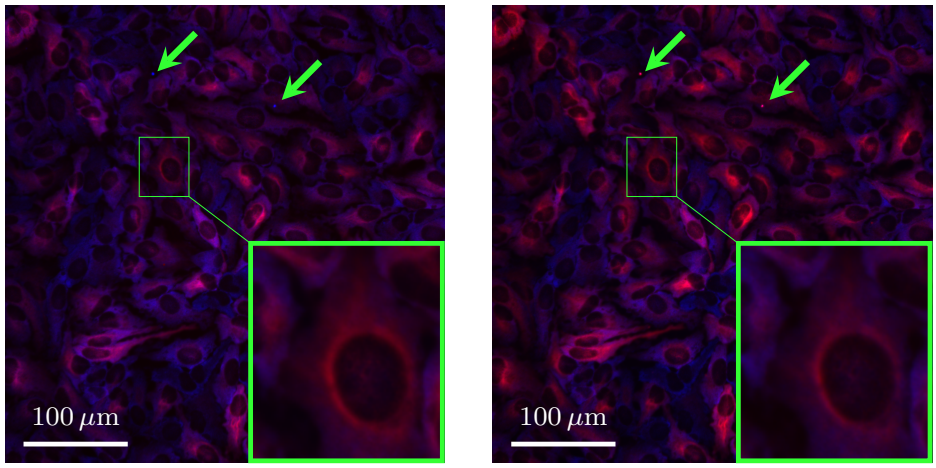

(a) Multi-staining composite **(b)** Label composite

Figure 5.7: {Adapted from [Methods-Paper], raw data from [Momina Saeed; Raw-Data]} Color composite for the multi-staining images (**a**) and the antibody-label images (**b**). Red is used for the double-application corrected first-staining image and for the L_{NF}-signal image after the second staining. Blue is used for the difference image and for the L_{RP}-signal image after the second staining. The brightness of all images was equally increased for better visibility. The green arrows indicate dust/debris that was misattributed by the multi-staining multiplexing.

The multi-staining composite (Figure 5.7a) and the label composite (Figure 5.7b) look very similar, which generally validates multi-staining multiplexing. A complete repetition of the experiment (see Figure A.18) corroborates this validation.

Since the repeated staining of multi-staining multiplexing does not depend

on the accessibility analysis, we should verify that arbitrary initial antibody concentrations for the first staining lead to arbitrary results. Hence, the multi-staining experiments [Momina Saeed; Raw-Data] also contained conditions for an initial antibody concentration that is lower than the K_τ-optimal initial antibody concentration (Figures A.16, A.19, A.20, using $1:1638400$ instead of $1:102400$) and for an initial antibody concentration that higher than the K_τ-optimal initial antibody concentration (Figures A.17, A.21, A.22, using $1:25600$ instead of $1:102400$).

In summary, a too low initial antibody concentration leads to signals belonging to low-K_τ peaks being falsely attributed to high-K_τ peaks, which can be observed by the lack of red in Figures A.19 and A.20. Conversely, using too high initial antibody concentrations leads to signals belonging to high-K_τ peaks being falsely attributed to low-K_τ peaks. However, the lack of blue in Figures A.21 and A.22 is only minimal, as the initial antibody concentration for the first staining was constrained by the already low initial antibody concentration for the second staining ($1:6400$).

Limitations

Let us conclude this chapter by observing the limitations of multi-staining multiplexing. Most obviously, multi-staining multiplexing is limited to immobilized biological samples, as the same region needs to be aligned and imaged twice. Any partial movement of structures that cannot be fixed with image registration will lead to a misattribution of signals. This includes dust and debris, as shown by the green arrows in Figure 5.7.

Furthermore, multi-staining multiplexing requires sufficiently separated peaks in the accessibility histogram. More precisely, the dose-response curve of the low-K_τ peak must reach saturation at concentrations lower than the concentration for the response onset of the high-K_τ peaks. Thus, multi-staining multiplexing would not be of much use for the 10 min incubation or the 1 h incubation of the incubation-time experiment.

6
Conclusion

In this dissertation, we have set out to achieve two major goals. First, we wanted to describe the binding of antibodies that can be measured in a generic antibody-staining experiment, using only macroscopic observables and model parameters. Second, we wanted to develop a method to characterize antibody-staining systems with the accumulation model. To conclude the dissertation, let us summarize and discuss our results in the context of our initial goals.

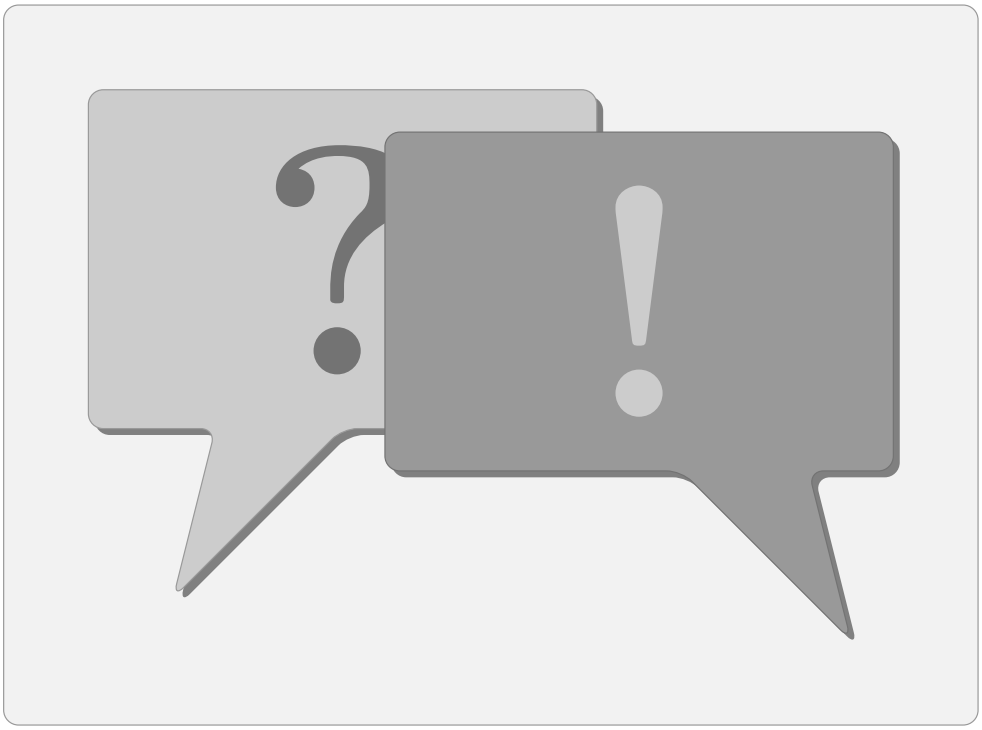

6.1 Summary

In antibody-staining experiments, the antibodies are only incubated for a finite amount of time before washing steps remove all antibodies that have not bound during that time. Since washing is a disruptive process, the antibodies that remain observable at the end of the staining experiment must be strongly attached to the epitopes to withstand washing. Thus, the unbinding of these antibodies during the incubation time is unlikely, leading to an accumulation of bound antibodies during the incubation phase. Based on these observations, we defined the accumulation IVPs and the accumulation models (Subsection 3.1.2).

A simple consequence of the accumulation model is the accumulation principle, which predicts that the amount of bound antibodies depends both on the initial antibody concentration and on the incubation time. Speculating about the unobservable microscopic behavior of the antibodies allowed us to specify how the amount of bound antibodies changes when the antibody concentration and the incubation time are increased (Subsection 3.1.3). Both the prediction of the accumulation principle and the effects of the unobservable microscopic behavior could be observed in experimental data (Subsections 5.1.2 and 5.1.4), validating the accumulation model in general.

While the reservoir accumulation IVP can be solved analytically, there does not seem to be a general closed-form expression for the solution of the depletion accumulation IVP. However, we could show that both cases have similar properties (Remarks 3.2.1 and 3.2.26). Although these properties seem to be obvious from the construction of the initial value problems, the coupling of epitope classes in the depletion case could have led to pathological solutions. Proving that this is not the case corroborated the accumulation model. Furthermore, the properties even extend to mixtures of monoclonal antibodies against different targets (Section 3.3). In fact, the reservoir case is well-behaved enough to retain the properties for arbitrary antibody mixtures, and the dose-response behavior can be reinterpreted as the behavior of a monoclonal antibody in a modified system (Subsection 3.3.3).

Based on the well-behavedness of the reservoir case, we reformulated the accumulation model in terms of epitope densities and defined the accumulation estimation model to estimate epitope classes (Section 4.2) from limited experimental dose-response data (Section 4.1). For the estimation process, we adapted established methods (Subsections 4.3.3–4.3.6) and defined accessibility histograms to interpret estimated epitope densities (Subsection 4.3.2). Together, the accumulation estimation model, the estimation process and the

accessibility histogram define the accessibility analysis that can be used for the characterization of antibody-staining systems. Since the accumulation estimation model relies on the reservoir case, we also proposed two depletion correction methods (Subsection 4.3.5).

Using experimental data from [Methods-Paper; Momina Saeed; Maike Siobal; Raw-Data], we could verify the model assumptions, as mentioned above, and demonstrate the applicability of the accessibility analysis (Section 5.1), which is implemented and published in the form of Julia packages [AMDRC.jl; AMDRR.jl; ADMR.jl; ADA.jl; ADAR.jl; FOF.jl]. Furthermore, we provided two potential applications for the accessibility analysis (Section 5.2): K_τ-optimal initial antibody concentrations as selection criterion for staining concentrations and multi-staining multiplexing.

6.2 Discussion and outlook

The accumulation model is an empirical model that relies on apparent rate constants, which comprise many unobserved effects. This is a consequence of our goal to describe general antibody-staining experiments. Hence, the accumulation model cannot provide deep insights into antibody binding. Nevertheless, the accumulation principle provides an explanation for the commonly observed dose-response behavior in antibody-staining experiments. Furthermore, some papers warn about incubation time as a potential source of nonspecific binding [Pil+20; Par+25], which can also be explained by the accumulation principle.

Even as an empirical model, the accumulation model and the resulting accessibility analysis have practical utility for the analysis of specific antibody-staining experiments. The antibody-mix experiments show that accessibility histograms can be estimated consistently and that the accessibility histogram characterizes the dose-response curve. Since the dose-response behavior is a consequence of the antibody binding properties in an antibody-staining system, the accessibility histogram also characterizes the binding properties indirectly.

At this point, it is important to remember that the accessibility histogram characterizes the entire staining protocol. The results obtained for one staining protocol and one sample type do not necessarily carry over to other protocols and other sample types. In this regard, one should be careful not to interpret the results of the accessibility analysis as a description of the antibody without reference to the experimental setup.

However, this warning does not affect the proposed applications of the accessibility analysis. The K_τ-optimal initial antibody concentration as a selection criterion for staining concentrations should be obtained for the experi-

mental setup of interest. The same applies to multi-staining multiplexing. The concentrations for the multi-staining must be chosen with dose-response data from the same experimental setup in which the multi-staining is performed.

Unfortunately, it is not yet clear whether K_τ-optimal initial antibody concentrations can reduce nonspecific staining or cross-reactions, in practice. The connection between nonspecific staining/cross-reactions and high antibody concentrations is only a heuristic for monoclonal antibodies. Verifying this heuristic would require proper antibody validation, since specific and nonspecific staining/cross-reactions must be discernible in some way. However, there does not appear to be universal agreement on antibody validation [Bor+10; Uhl+16; Edf+18; Pil+20; Kah+24].

But even without verification of the heuristic, it can be viewed as good practice to avoid too high antibody concentrations [Pil+20; Dud+22; Par+25]. Thus, K_τ-optimal initial antibody concentrations could be used as an objective way to determine what "too high" means; at least for monoclonal antibodies.

By using the principle of K_τ-optimal initial antibody concentrations, multi-staining multiplexing produces staining images where the contributions of different peaks in an accessibility histogram become discernible. This could be used to investigate whether an K_τ-optimal initial antibody concentration reduces nonspecific staining and cross-reactions. However, multi-staining multiplexing could also be useful for the investigation of general epitope heterogeneity in biological samples, since epitopes with distinct binding behavior lead to distinct peaks in the accessibility histogram.

Finally, the accessibility analysis might be useful for the research on multi-specific antibodies. These antibodies are particularly interesting for medical applications because of their ability to bind to two (or more) different epitopes simultaneously [CB09; Run+18; Seg+23]. Multi-staining multiplexing could be used to distinguish bound multi-specific antibodies, e.g., in microscopy images of biological samples, based on the epitope type to which the antibodies have bound.

A

Additional figures for Chapter 5

For the validations and applications presented in Chapter 5, there are additional analysis variations, leading to numerous figures that would clutter the main part of the dissertation. As for the main part, all error bars represent the corrected standard deviations (4.5) of the respective replicates.

A.1 Scaling parameters

For the comparison of different scaling parameters, we define the mean squared error (of a parameter configuration λ) in resemblance to the objective function (4.19) as

$$\mathrm{MSE}(\Lambda \mid \mathcal{D}, \mathcal{P}, F) \coloneqq \frac{1}{n} \sum_{i=1}^{n} (\mathcal{X}_i - \mu(\Lambda, \mathcal{P}, \mathcal{A}_i))^2 \ . \tag{A.1}$$

As for the objective function, $\mu(\Lambda, \mathcal{P}, \mathcal{A}_i)$ denotes the theoretical mean (4.17), i.e., the theoretical value of the accumulation estimation model at $\mathcal{A}_i$.

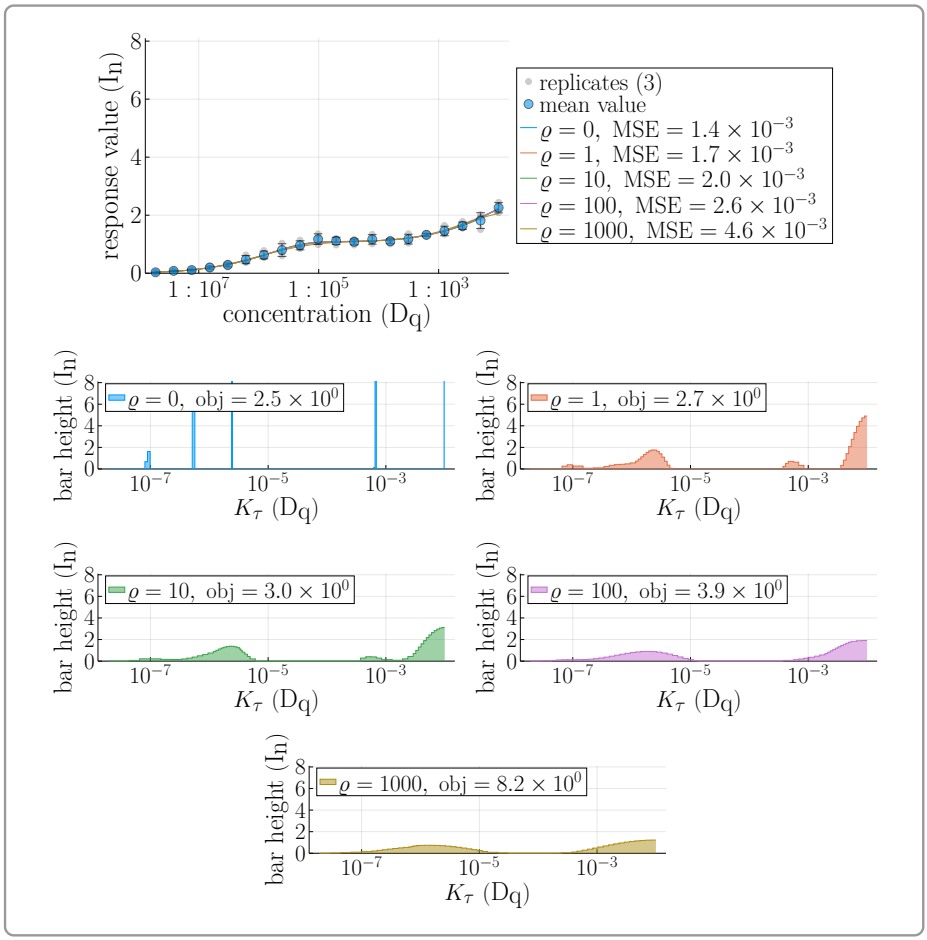

Figure A.1: {Adapted from [Methods-Paper], raw data from [Momina Saeed; Raw-Data]} **Antibody-mix experiment, NF200 antibody:** Accessibility analysis for different values of the scaling parameter ϱ. "obj" refers to the objective function value (4.19) and "MSE" refers to the mean squared error (A.1) of the fitted model.

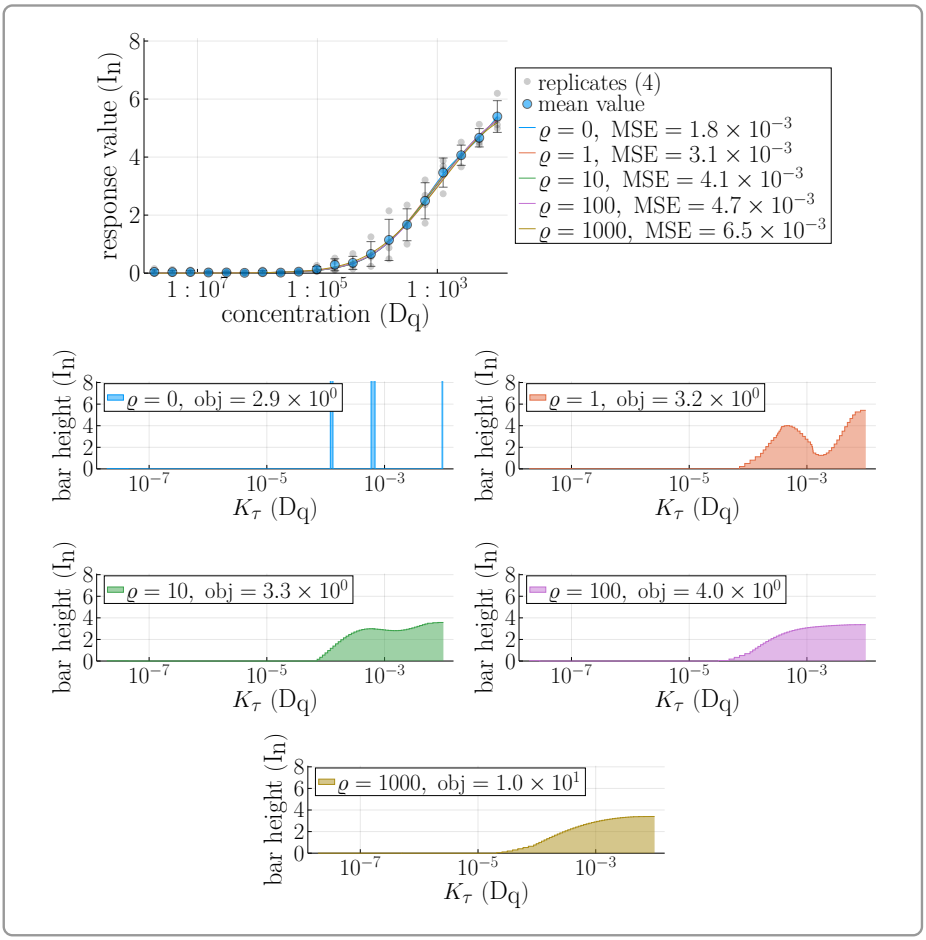

Figure A.2: {Adapted from [Methods-Paper], raw data from [Momina Saeed; Raw-Data]} **Antibody-mix experiment, RPS11 antibody:** Accessibility analysis for different values of the scaling parameter ϱ. "obj" refers to the objective function value (4.19) and "MSE" refers to the mean squared error (A.1) of the fitted model.

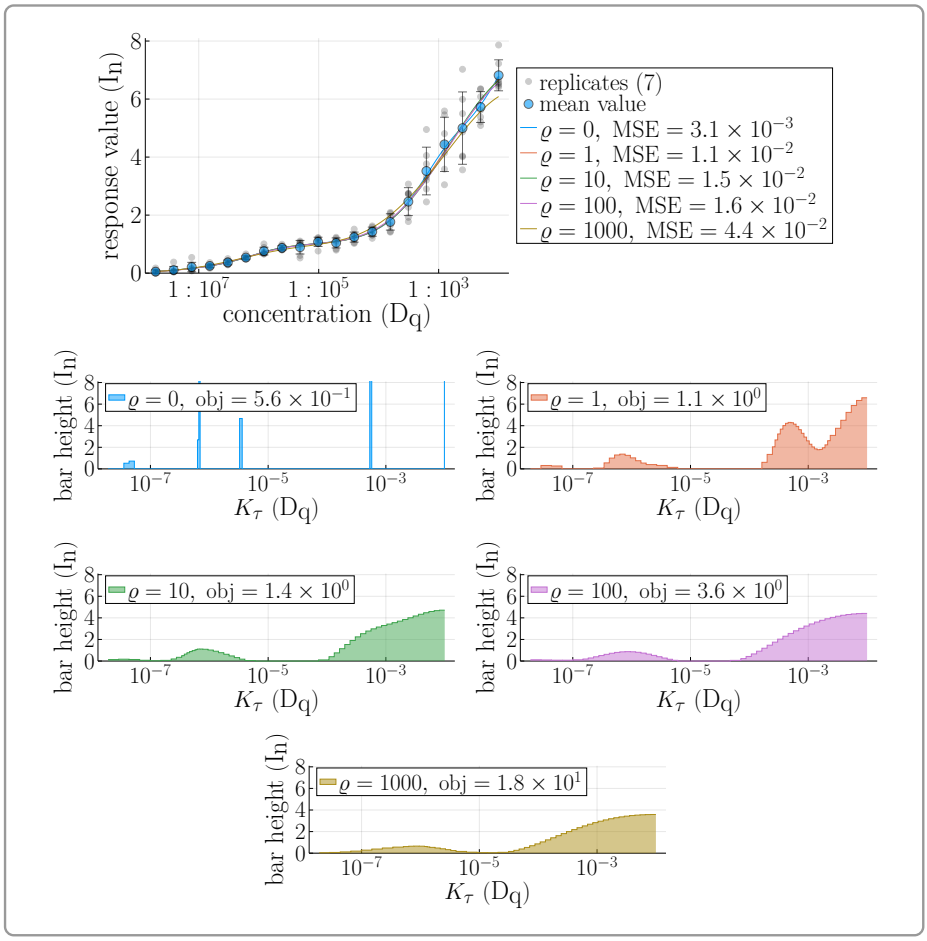

Figure A.3: {Adapted from [Methods-Paper], raw data from [Momina Saeed; Raw-Data]} **Antibody-mix experiment, antibody mixture:** Accessibility analysis for different values of the scaling parameter ϱ. "obj" refers to the objective function value (4.19) and "MSE" refers to the mean squared error (A.1) of the fitted model.

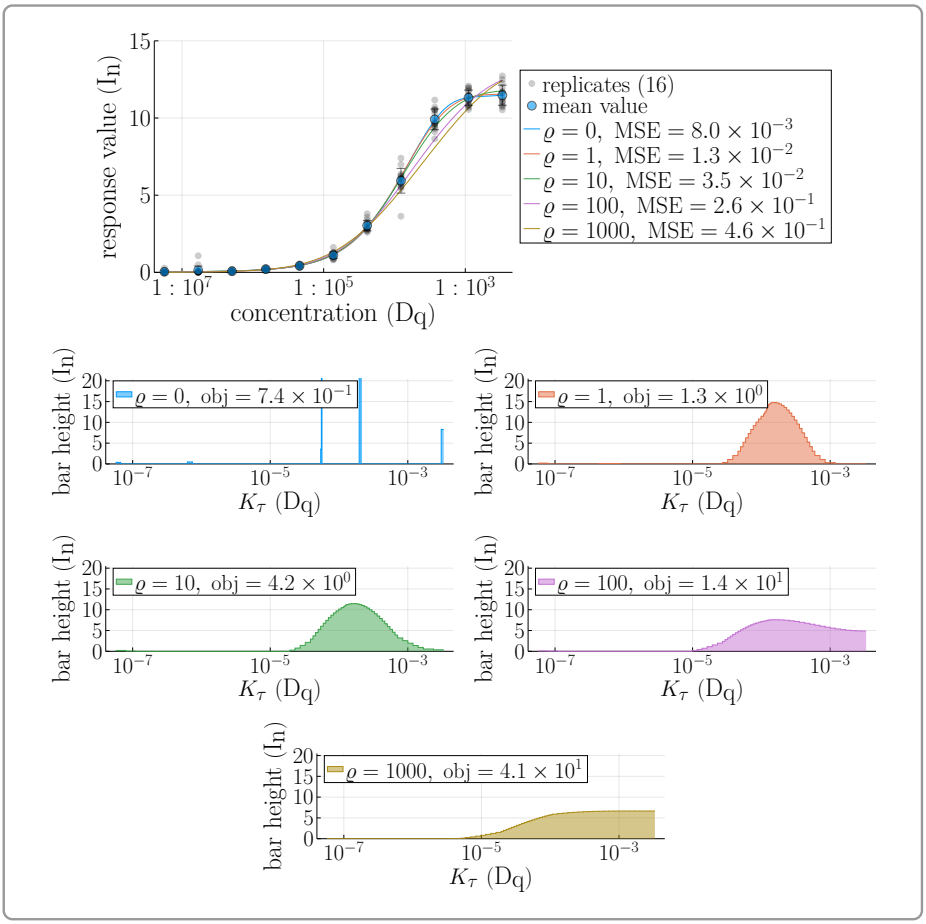

Figure A.4: {Adapted from [Methods-Paper], raw data from [Maike Siobal; Raw-Data]} **Incubation-time experiment, 10 min:** Accessibility analysis for different values of the scaling parameter ϱ. "obj" refers to the objective function value (4.19) and "MSE" refers to the mean squared error (A.1) of the fitted model.

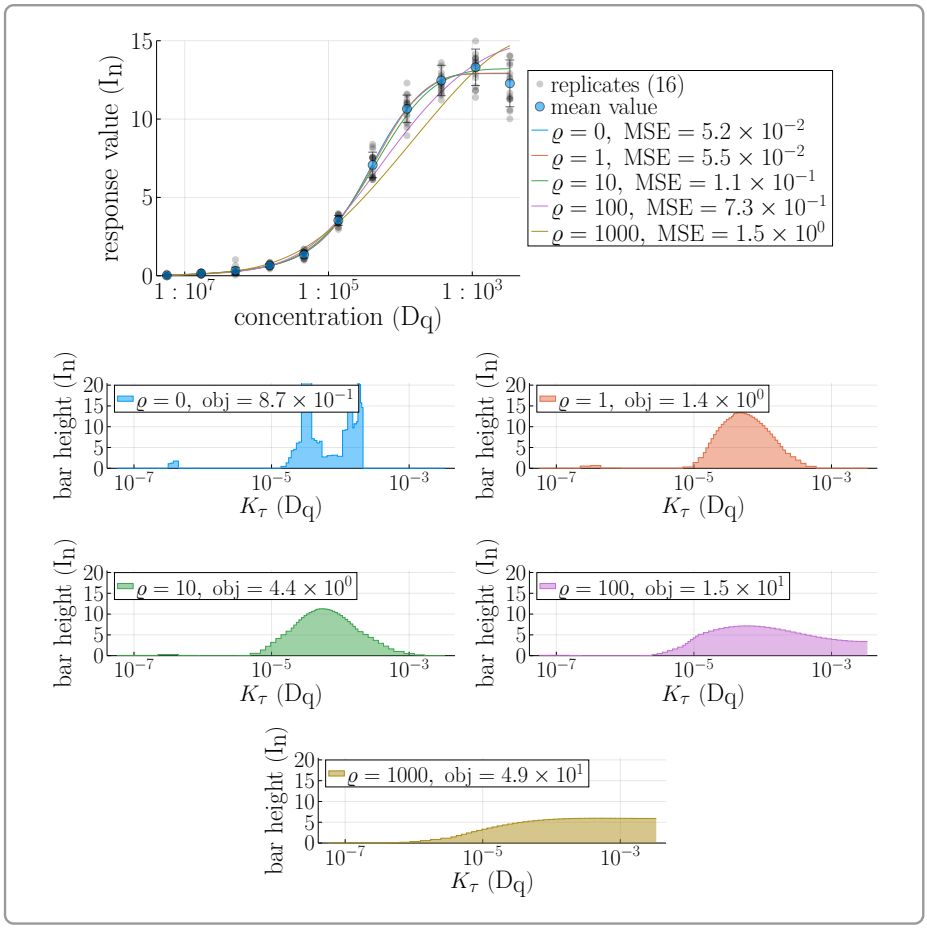

Figure A.5: {Adapted from [Methods-Paper], raw data from [Maike Siobal; Raw-Data]} **Incubation-time experiment, 1 h:** Accessibility analysis for different values of the scaling parameter ϱ. "obj" refers to the objective function value (4.19) and "MSE" refers to the mean squared error (A.1) of the fitted model.

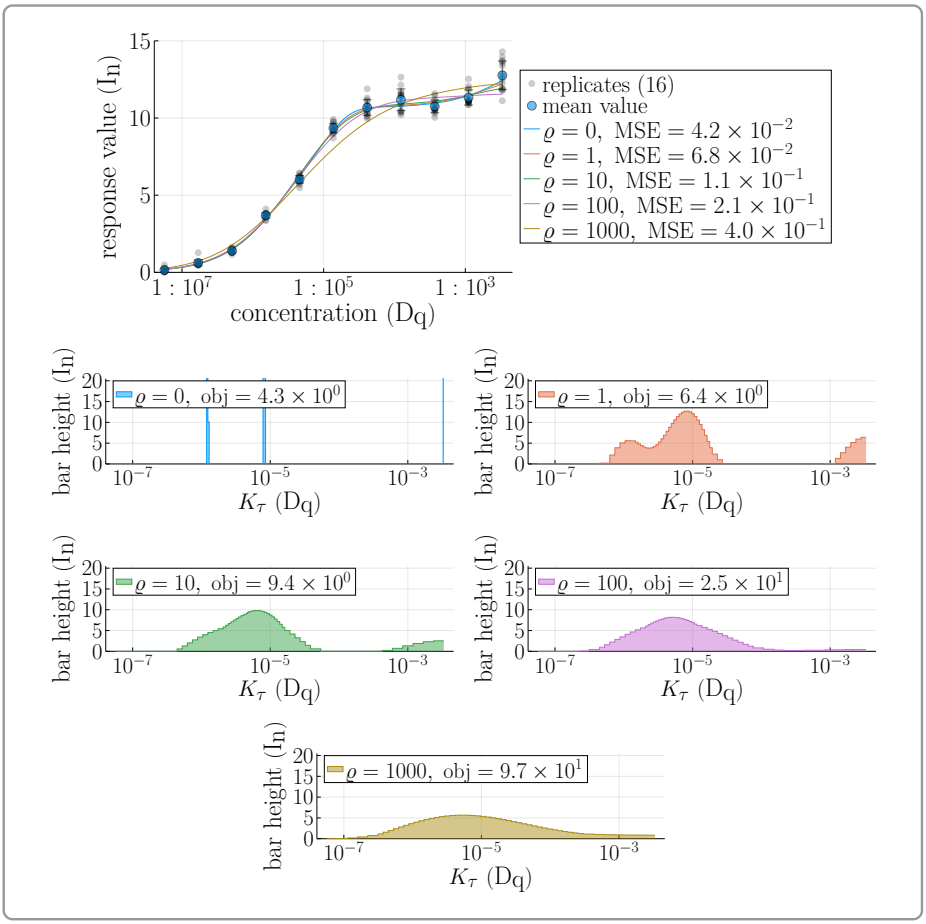

Figure A.6: {Adapted from [Methods-Paper], raw data from [Maike Siobal; Raw-Data]} **Incubation-time experiment, 21:20 h:** Accessibility analysis for different values of the scaling parameter ϱ. "obj" refers to the objective function value (4.19) and "MSE" refers to the mean squared error (A.1) of the fitted model.

A.2 Worst-case depletion correction

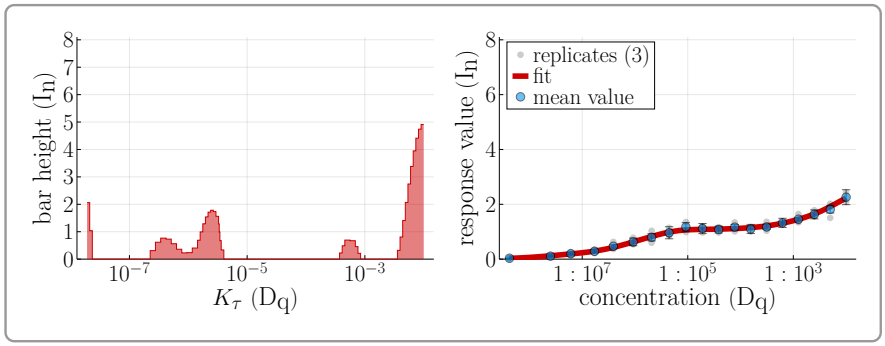

(a) NF200 antibody

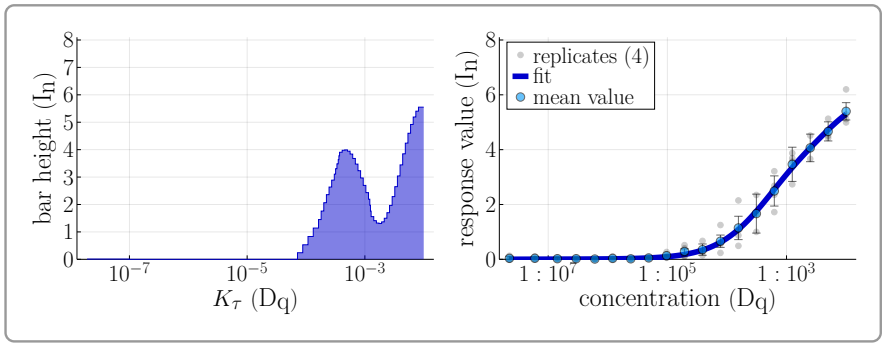

(b) RPS11 antibody

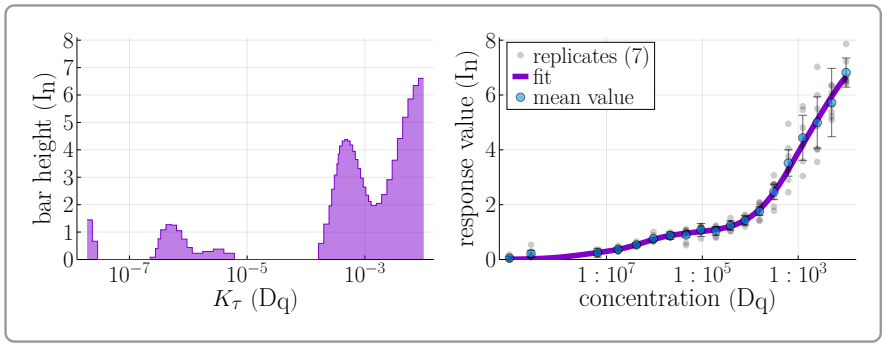

(c) Antibody mixture

Figure A.7: {Adapted from [Methods-Paper], raw data from [Momina Saeed; Raw-Data]} **Antibody-mix experiment:** Accessibility analysis of data corrected with the worst-case depletion correction (4.27), using the scaling parameter $\varrho = 1$.

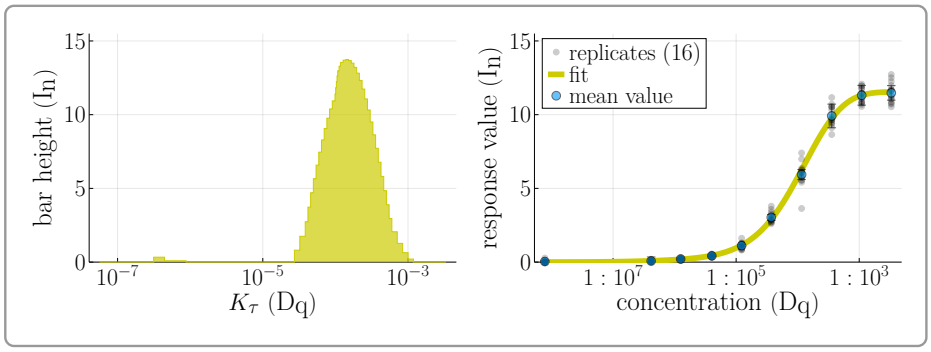

(a) 10 min incubation

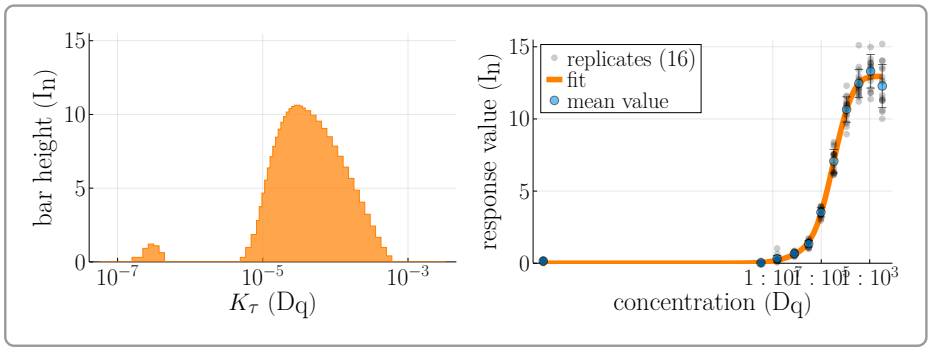

(b) 1 h incubation

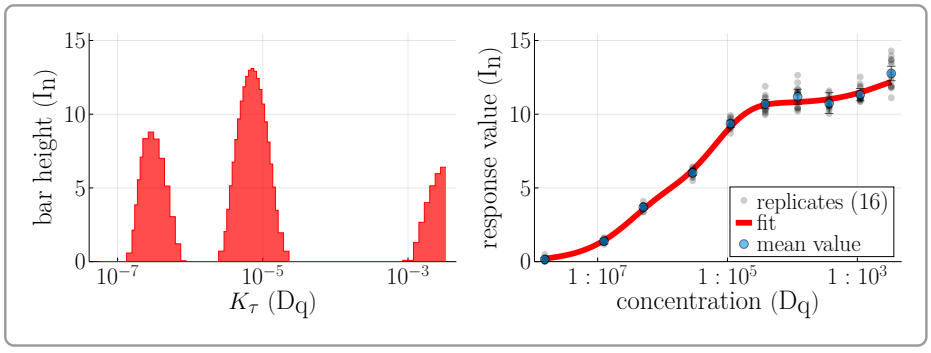

(c) 21:20 h incubation

Figure A.8: {Adapted from [Methods-Paper], raw data from [Momina Saeed; Raw-Data]} **Incubation-time experiment:** Accessibility analysis of data corrected with the worst-case depletion correction (4.27), using the scaling parameter $\varrho = 1$.

A.3 Numerical depletion correction

A.3.1 Curve fitting for numerical models

All analyses in this subsection use the following setup.

- The model $\mathcal{M}(\mathcal{A}, \{(\mathcal{G}_i, \mathcal{K}_{\tau;i})\}_{i=1}^N)$ is the numerical solution of the depletion accumulation IVP in experimental units (4.28), using the automatic numerical solvers from the "DifferentialEquations.jl" package [RN17; RN19; Ma+21].
- For each initial antibody concentration $\mathcal{A}_i$ and each epitope class configuration $\{(\mathcal{G}_i, \mathcal{K}_{\tau;i})\}_{i=1}^N$ during the optimization, numerical solutions need to be calculated from scratch.
- The objective function for the curve fitting is a weighted least squares objective

$$\text{obj}(\{(\mathcal{G}_i, \mathcal{K}_{\tau;i})\}) = \sum_{i=1}^{n} \frac{(\mathcal{X}_i - \mathcal{M}(\mathcal{A}, \{(\mathcal{G}_i, \mathcal{K}_{\tau;i})\}_{i=1}^N))^2}{2\Delta\mathcal{X}_i^2} \ .$$

- For the optimization of the epitope class configuration, the box-constrained Nelder-Mead algorithm from the "Optim.jl" package [MR18] is used with `3000` iterations and a time-limit of `120` seconds. The constraints are $0 < \mathcal{G}_i < \infty$ and $0 < \mathcal{K}_{\tau;i} < 10^{-1}$.
- Despite overfitting, the numerical depletion correction always uses the results for 4 epitope classes to ensure that the fitted models agree with the data as much as possible.

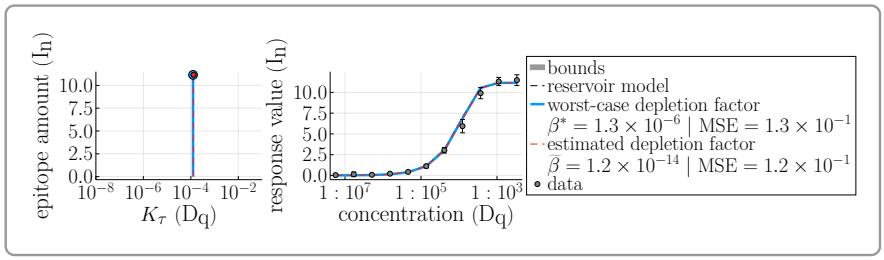

(a) 1 epitope class

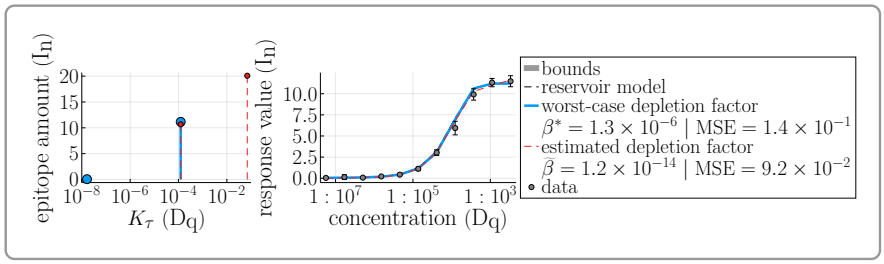

(b) 2 epitope classes

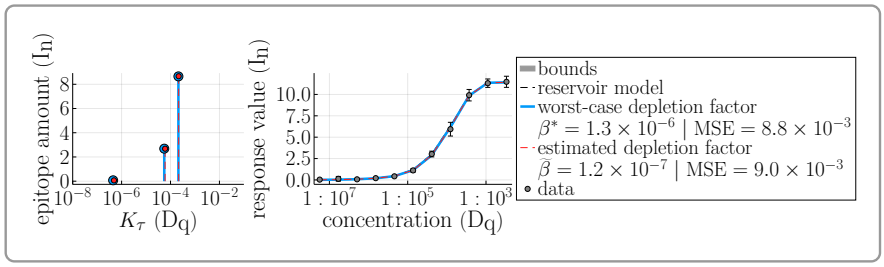

(c) 3 epitope classes

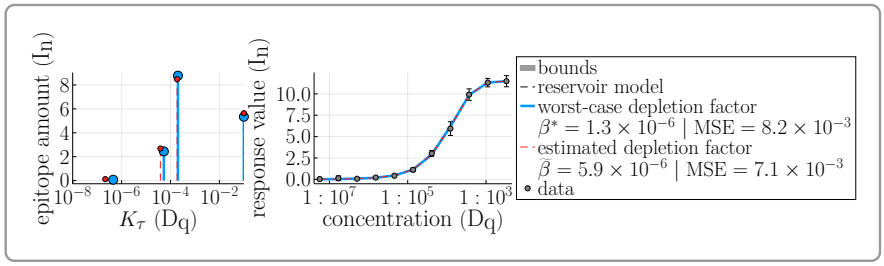

(d) 4 epitope classes

Figure A.9: Incubation-time experiment, 10 min incubation: Curve fitting of the depletion accumulation model (numerical solutions) with discrete epitope classes.

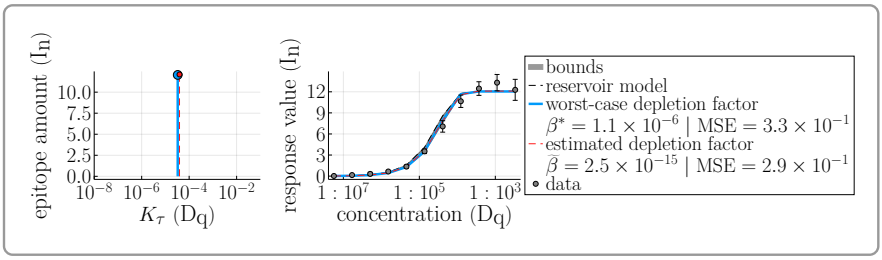

(a) 1 epitope class.

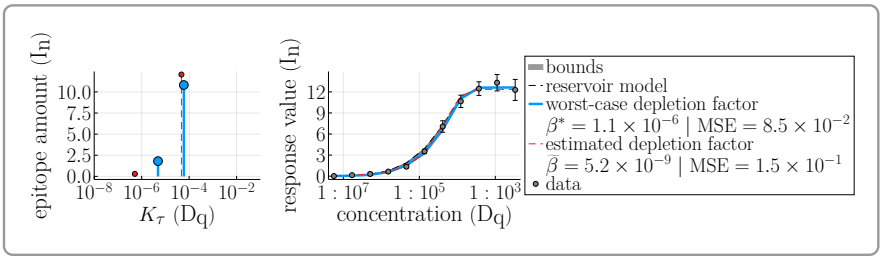

(b) 2 epitope classes

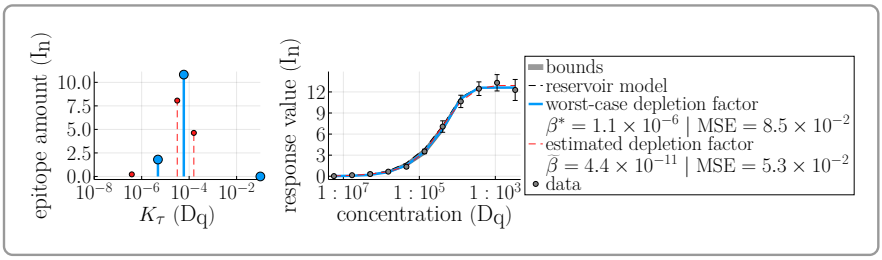

(c) 3 epitope classes

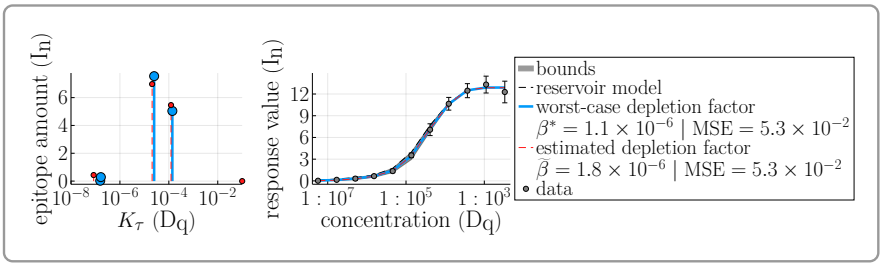

(d) 4 epitope classes

Figure A.10: Incubation-time experiment, 1 h incubation: Curve fitting of the depletion accumulation model (numerical solutions) with discrete epitope classes.

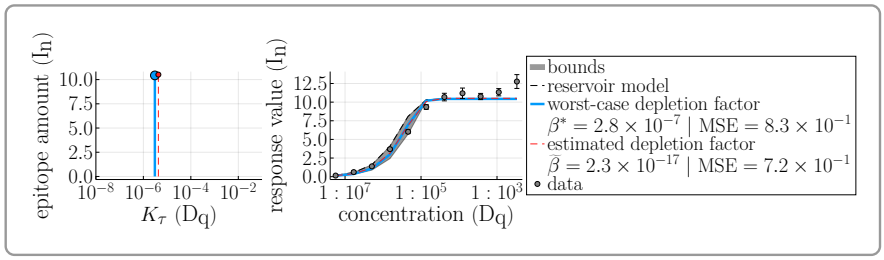

(a) 1 epitope class

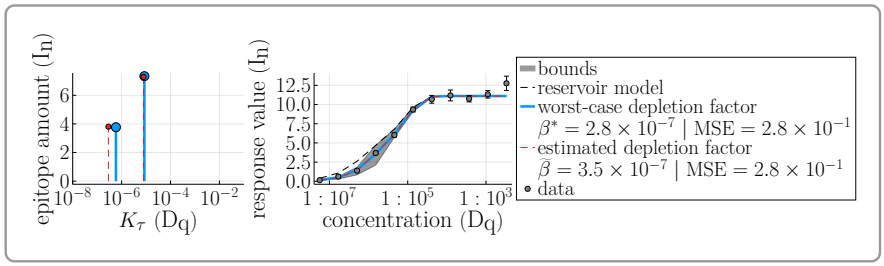

(b) 2 epitope classes

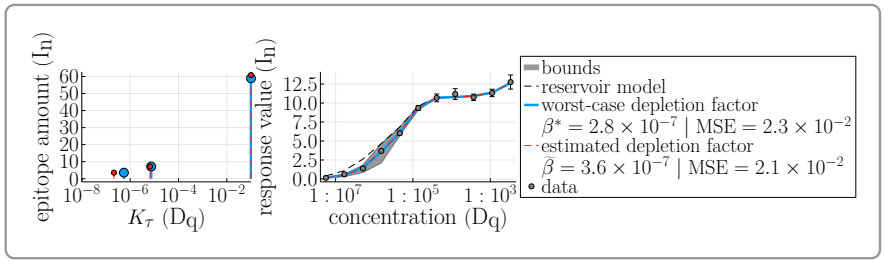

(c) 3 epitope classes

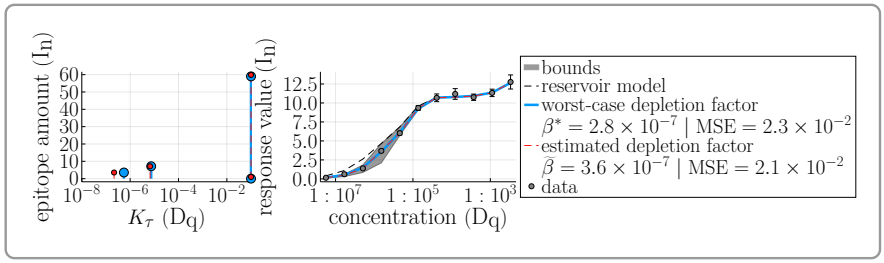

(d) 4 epitope classes

Figure A.11: Incubation-time experiment, 21:20 h incubation: Curve fitting of the depletion accumulation model (numerical solutions) with discrete epitope classes.

A.3.2 Depletion corrections

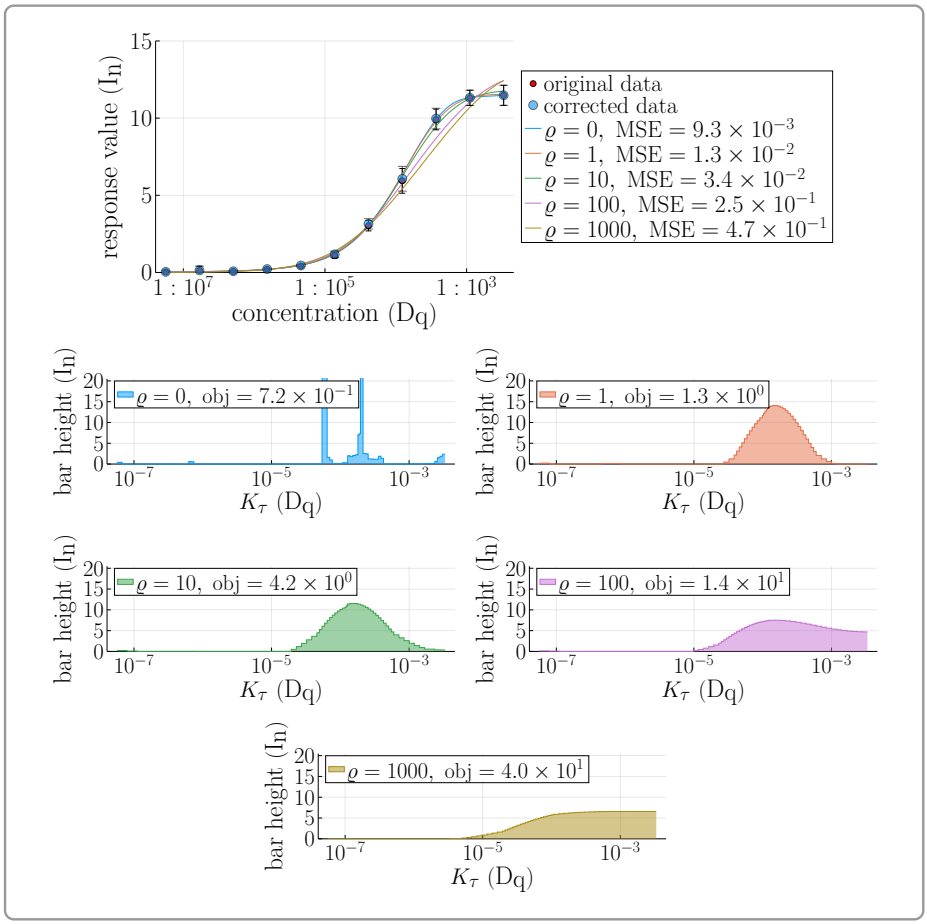

Figure A.12: Incubation-time experiment, 10 min incubation: Accessibility analysis for data corrected with the numerical depletion correction (Algorithm 4.3.5) using various scaling parameters (color matched).

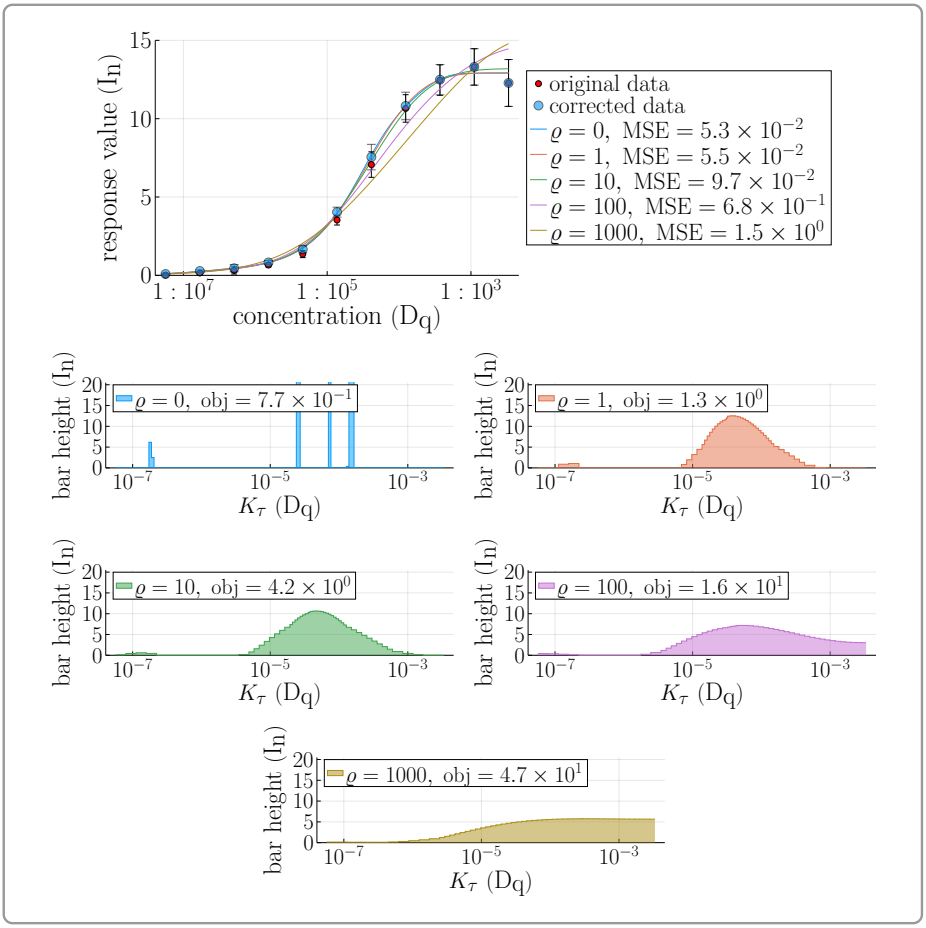

Figure A.13: Incubation-time experiment, 1 h incubation: Accessibility analysis for data corrected with the numerical depletion correction (Algorithm 4.3.5) using various scaling parameters (color matched).

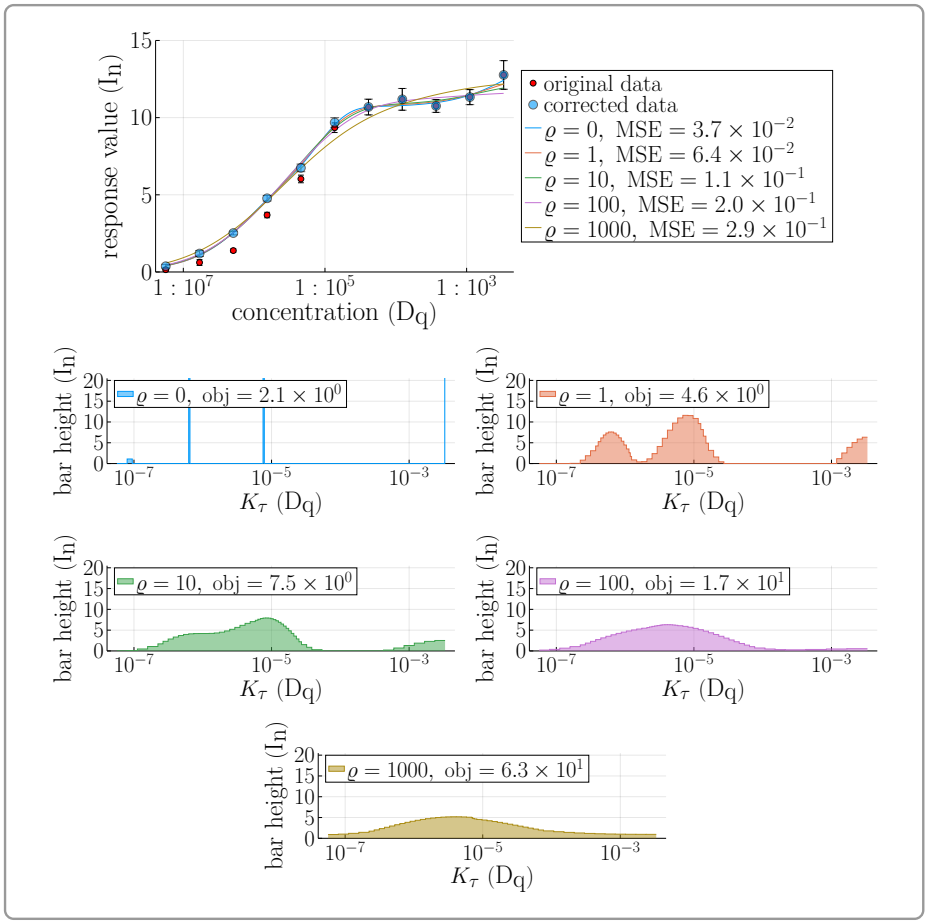

Figure A.14: Incubation-time experiment, 21:20 h incubation: Accessibility analysis for data corrected with the numerical depletion correction (Algorithm 4.3.5) using various scaling parameters (color matched).

A.4 Multi-staining

A.4.1 Metrics

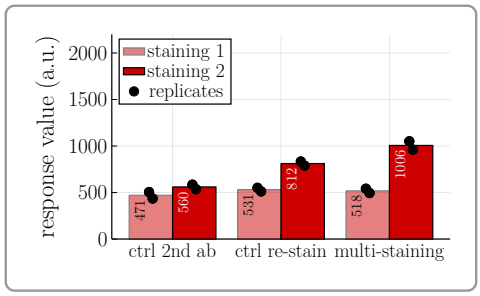

(a) NF200 channel, experiment 1

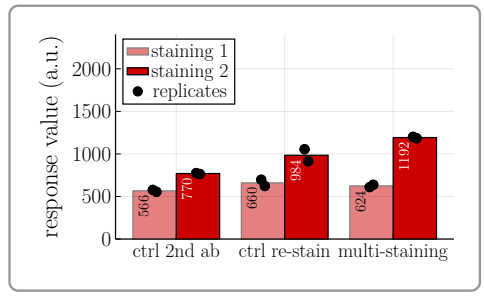

(b) NF200 channel, experiment 2

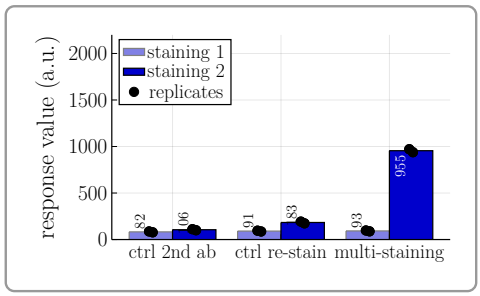

(c) RPS11 channel, experiment 1

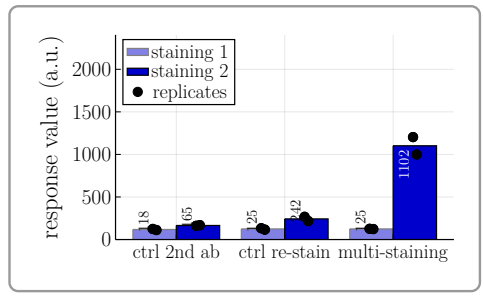

(d) RPS11 channel, experiment 2

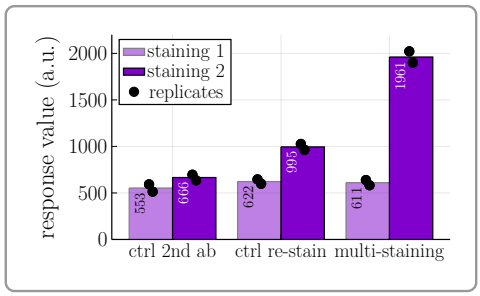

(e) Summed channels, experiment 1

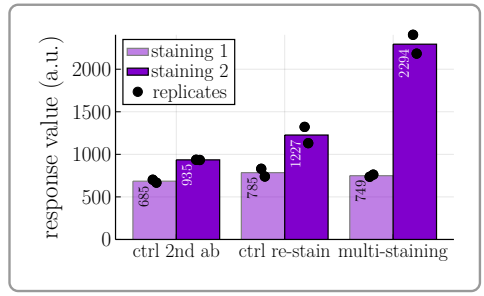

(f) Summed channels, experiment 2

Figure A.15: {Adapted from [Methods-Paper], raw data from [Momina Saeed; Raw-Data]} Metrics for the multi-staining experiments with the K_τ**-optimal initial antibody concentration for the first staining.**

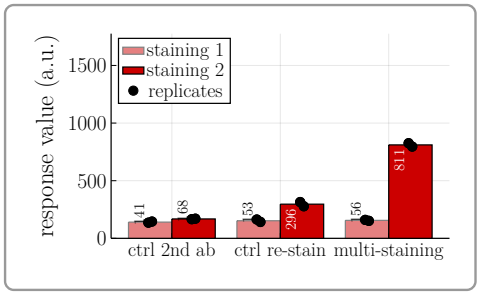

(a) NF200 channel, experiment 1

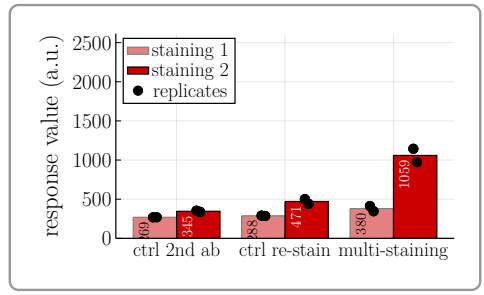

(b) NF200 channel, experiment 2

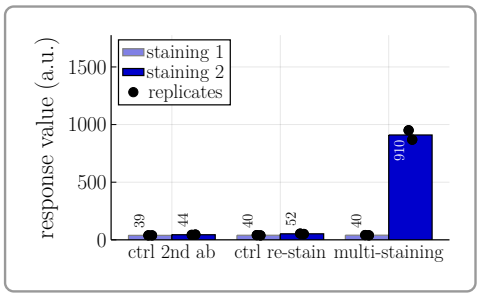

(c) RPS11 channel, experiment 1

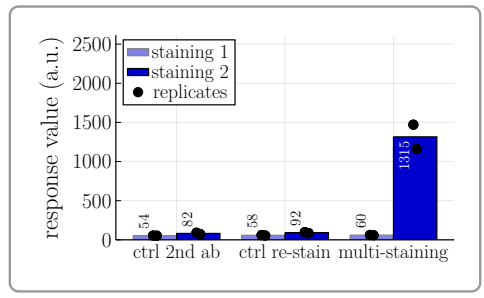

(d) RPS11 channel, experiment 2

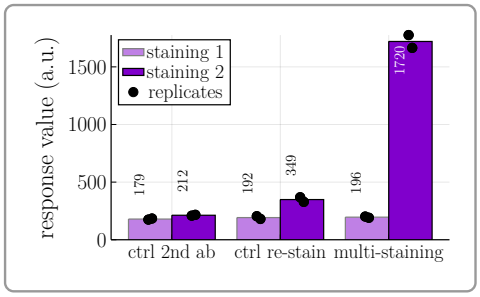

(e) Summed channels, experiment 1

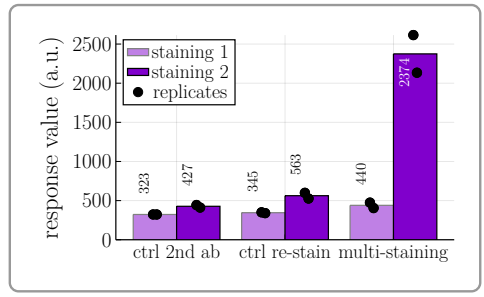

(f) Summed channels, experiment 2

Figure A.16: {Adapted from [Methods-Paper], raw data from [Momina Saeed; Raw-Data]} Metrics for the multi-staining experiments with an **initial antibody concentration too low for the first staining** (1 : 1638400 instead of 1 : 102400).

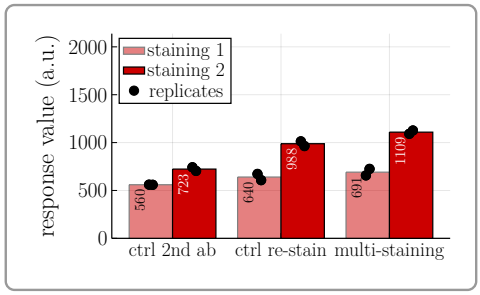

(a) NF200 channel, experiment 1

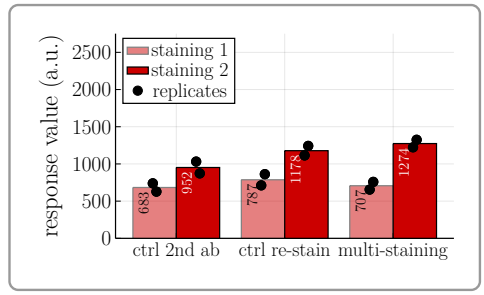

(b) NF200 channel, experiment 2

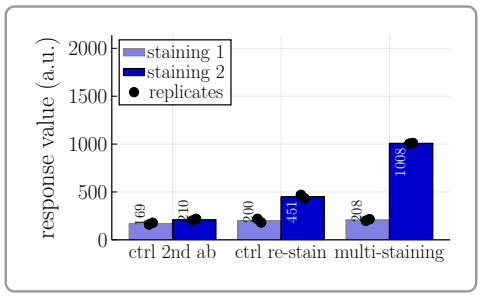

(c) RPS11 channel, experiment 1

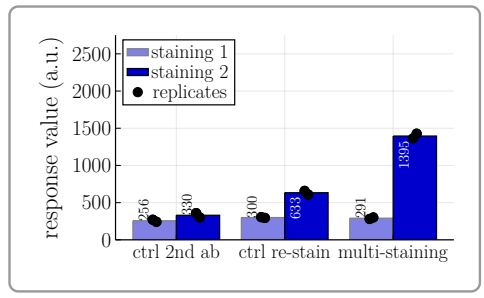

(d) RPS11 channel, experiment 2

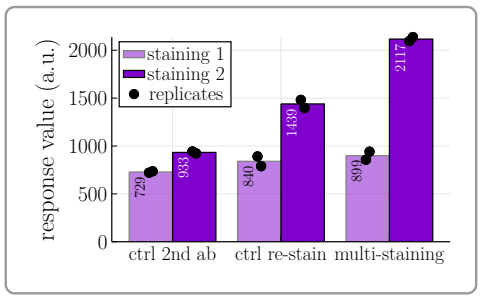

(e) Summed channels, experiment 1

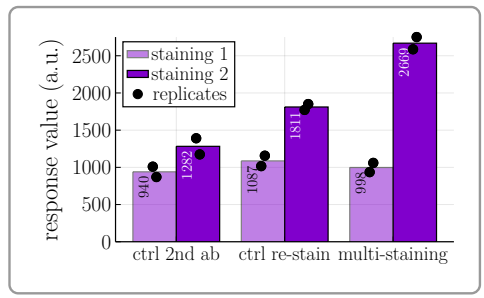

(f) Summed channels, experiment 2

Figure A.17: {Adapted from [Methods-Paper], raw data from [Momina Saeed; Raw-Data]} Metrics for the multi-staining experiments with an **initial antibody concentration too high for the first staining** ($1:25600$ instead of $1:102400$).

A.4.2 Experiment 2

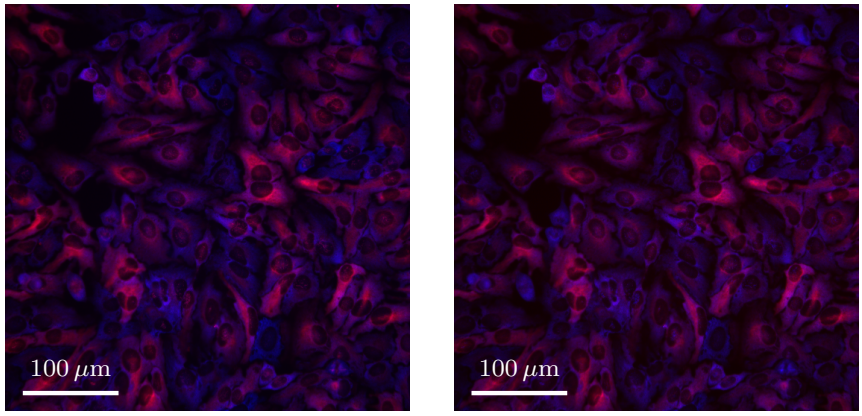

(a) Multi-staining composite **(b)** Label composite

Figure A.18: {Adapted from [Methods-Paper], raw data from [Momina Saeed; Raw-Data]} Replication of the multi-staining experiment with the $\boldsymbol{K_\tau}$**-optimal initial antibody concentration for the first staining**. The brightness of all images was equally increased for better visibility.

A.4.3 Too low concentration

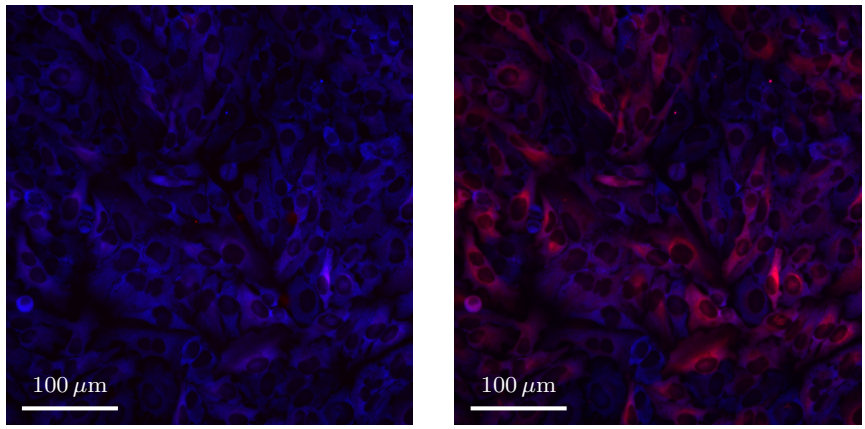

(a) Multi-staining composite **(b)** Label composite

Figure A.19: {Adapted from [Methods-Paper], raw data from [Momina Saeed; Raw-Data]} Multi-staining experiment with an **initial antibody concentration too low for the first staining** (1 : 1638400 instead of 1 : 102400). The brightness of all images was equally increased for better visibility.

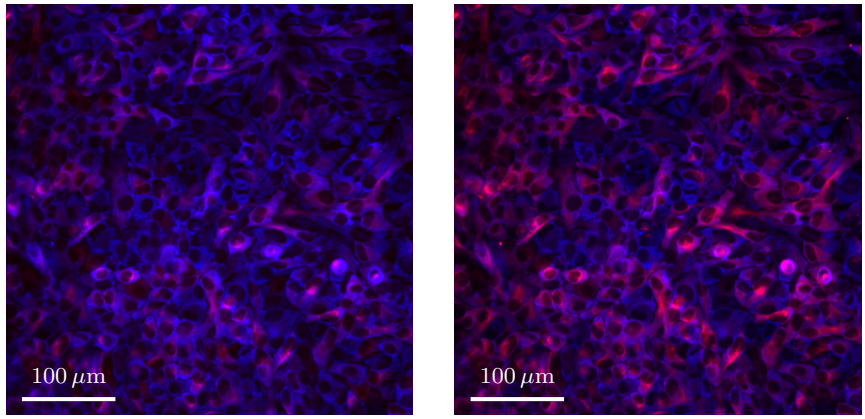

(a) Multi-staining composite **(b)** Label composite

Figure A.20: {Adapted from [Methods-Paper], raw data from [Momina Saeed; Raw-Data]} Replication of the multi-staining experiment with an **initial antibody concentration too low for the first staining** (1 : 1638400 instead of 1 : 102400). The brightness of all images was equally increased for better visibility.

A.4.4 Too high concentration

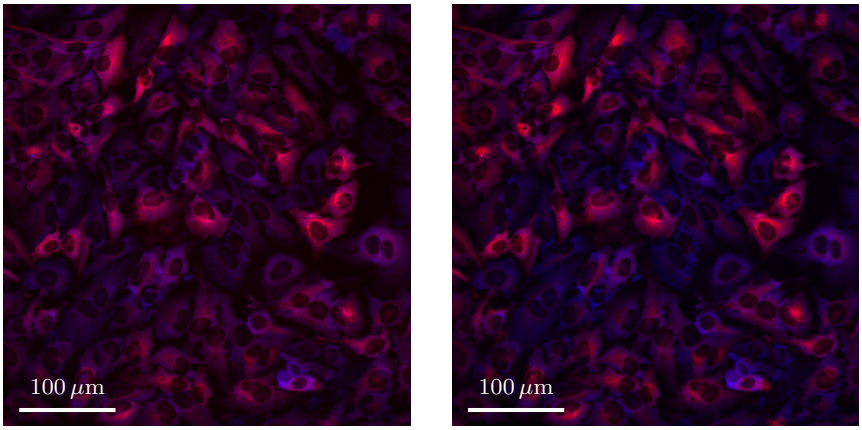

(a) Multi-staining composite **(b)** Label composite

Figure A.21: {Adapted from [Methods-Paper], raw data from [Momina Saeed; Raw-Data]} Multi-staining experiment with an **initial antibody concentration too high for the first staining** (1 : 25600 instead of 1 : 102400). The brightness of all images was equally increased for better visibility.

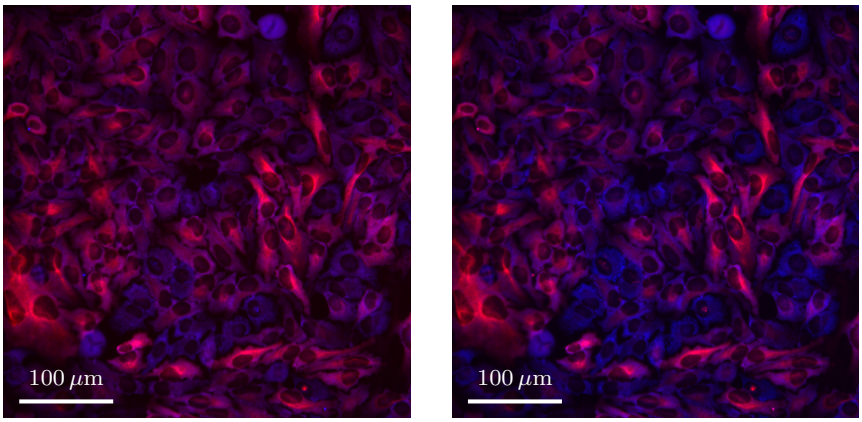

(a) Multi-staining composite **(b)** Label composite

Figure A.22: {Adapted from [Methods-Paper], raw data from [Momina Saeed; Raw-Data]} Replication of the multi-staining experiment with an **initial antibody concentration too high for the first staining** (1 : 25600 instead of 1 : 102400). The brightness of all images was equally increased for better visibility.

B Additional calculations

Some calculations and detailed proofs are skipped in the main part. Either because they are tedious but straightforward or because they do not provide additional insight. Nevertheless, they are necessary for formal proofs and arguments.

B.1 Additional calculations for Chapter 2

B.1.1 Solution of the Langmuir rate equation with depletion

Belonging to Subsection 2.1.4, page 13.

To solve the Langmuir rate equation for the depletion case,

$$\frac{d}{dt}x(t) = k_\mathrm{a}(a - \beta x(t))(g - x(t)) - k_\mathrm{d}x(t) \ , \tag{B.1}$$

we can follow [Edw+98] but with our notation. The essential idea is to use the zeros $z_{1,2}$ of

$$\begin{aligned} 0 &= k_\mathrm{a}(a - \beta x)(g - x) - k_\mathrm{d}x = \beta k_\mathrm{a}(\beta^{-1}a - x)(g - x) - k_\mathrm{d}x \\ &= \beta k_\mathrm{a}x^2 - (k_\mathrm{a}a + \beta k_\mathrm{a}g + k_\mathrm{d})x + k_\mathrm{a}ag \ , \end{aligned}$$

which are given by the quadratic formula

$$z_1 = \frac{(k_\mathrm{a}a + \beta k_\mathrm{a}g + k_\mathrm{d}) - \sqrt{(k_\mathrm{a}a + \beta k_\mathrm{a}g + k_\mathrm{d})^2 - 4\beta k_\mathrm{a}^2 ag}}{2\beta k_\mathrm{a}} \ .$$

$$z_2 = \frac{(k_\mathrm{a}a + \beta k_\mathrm{a}g + k_\mathrm{d}) + \sqrt{(k_\mathrm{a}a + \beta k_\mathrm{a}g + k_\mathrm{d})^2 - 4\beta k_\mathrm{a}^2 ag}}{2\beta k_\mathrm{a}} \ .$$

Using the zeros z_1 and z_2, the differential equation (B.1) can be rewritten as

$$\frac{d}{dt}x(t) = (z_1 - x(t))(z_2 - x(t)) \ ,$$

by factorization of the polynomial. Next, [Edw+98] solves this differential equation for the initial value $x(0) = 0$ using separation of variables. However, the differential equation can be solved for general initial values x_0.

Proposition B.1.1.
The function

$$x(t) = \frac{z_1 - z_2 \frac{x_0 - z_1}{x_0 - z_2} e^{(z_1 - z_2)(t - t_0)}}{1 - \frac{x_0 - z_1}{x_0 - z_2} e^{(z_1 - z_2)(t - t_0)}} \tag{B.2}$$

solves the initial value problem

$$\frac{d}{dt} x(t) = (z_1 - x(t))(z_2 - x(t)) \ , x(t_0) = x_0$$

for $0 < z_1 < z_2 < \infty$, $x_0 \neq z_1$ *and* $x_0 \neq z_2$.

Proof B.1.2.
To simplify the calculation, let us define

$$f \coloneqq \frac{x_0 - z_1}{x_0 - z_2} \qquad \text{and} \qquad E(t) = e^{(z_1 - z_2)(t - t_0)} \ ,$$

which simplifies the expression for $x(t)$:

$$x(t) = \frac{z_1 - z_2 f E(t)}{1 - f E(t)} \ .$$

Observing that $\frac{d}{dt} E(t) = (z_1 - z_2) E(t)$, we can calculate the derivative:

$$\frac{d}{dt} x(t) = \frac{-(z_1 - z_2) z_2 f E(t)}{1 - f E(t)} + (z_1 - z_2) f E(t) \frac{z_1 - z_2 f E(t)}{(1 - f E(t))^2}$$

$$\begin{aligned} &-z_1 z_2 f E(t) + z_2^2 f E(t) + \cancel{z_1 z_2 f^2 E^2(t)} - \cancel{z_2^2 f^2 E^2(t)} \\ = \ &\frac{+z_1^2 f E(t) - \cancel{z_1 z_2 f^2 E^2(t)} - z_1 z_2 f E(t) + \cancel{z_2^2 f^2 E^2(t)}}{(1 - f E(t))^2} \end{aligned}$$

$$= \frac{z_1^2 f E(t) - 2 z_1 z_2 f E(t) + z_2^2 f E(t)}{(1 - f E(t))^2} = \frac{(z_1 - z_2)^2 f E(t)}{(1 - f E(t))^2} \ .$$

Next, we calculate

$$(z_1 - x(t))(z_2 - x(t)) = z_1 z_2 - (z_1 + z_2)x(t) + x^2(t)$$

$$= z_1 z_2 - (z_1 + z_2)\frac{z_1 - z_2 f E(t)}{1 - f E(t)} + \frac{z_1^2 + z_2^2 f^2 E^2(t) - 2 z_1 z_2 f E(t)}{1 + f^2 E^2(t) - 2 f E(t)}$$

$$= \frac{\begin{array}{c} \cancel{z_1 z_2} + \cancel{z_1 z_2 f^2 E^2(t)} - 2 z_1 z_2 f E(t) - \cancel{z_1^2} + \cancel{z_1 z_2 f E(t)} \\ -\cancel{z_1 z_2} + z_2^2 f E(t) + z_1^2 f E(t) - \cancel{z_1 z_2 f^2 E^2(t)} + \cancel{z_1 z_2 f E(t)} \\ -\cancel{z_2^2 f^2 E^2(t)} + \cancel{z_1^2} + \cancel{z_2^2 f^2 E^2(t)} - 2\cancel{z_1 z_2 f E(t)} \end{array}}{1 + f^2 E^2(t) - 2 f E(f)}$$

$$= \frac{-2 z_1 z_2 f E(t) + z_2^2 f E(t) + z_1^2 f E(t)}{(1 + f E(t))^2}$$

$$= \frac{(z_1 - z_2)^2 f E(t)}{(1 - f E(t))^2} = \frac{d}{dt} x(t) \ ,$$

which shows that $x(t)$ solves the differential equation.

Finally, we check that $x(t)$ satisfies the initial value condition $x(t_0) = x_0$:

$$x(t = t_0) = \frac{z_1 - z_2 \frac{x_0 - z_1}{x_0 - z_2} e^{(z_1 - z_2)(t_0 - t_0)}}{1 - \frac{x_0 - z_1}{x_0 - z_2} e^{(z_1 - z_2)(t_0 - t_0)}}$$

$$= \frac{z_1 - z_2 \frac{x_0 - z_1}{x_0 - z_2}}{1 - \frac{x_0 - z_1}{x_0 - z_2}} = \frac{z_1(x_0 - z_2) - z_2(x_0 - z_1)}{(x_0 - z_2) - (x_0 - z_1)}$$

$$= \frac{z_1 x_0 - z_1 z_2 - z_2 x_0 + z_1 z_2}{z_1 - z_2} = \frac{(z_1 - z_2)x_0}{z_1 - z_2}$$

$$= x_0 \ .$$

□

B.2 Additional calculations for Chapter 3

B.2.1 Initial values for the accumulation IVPs

Belonging to Subsection 3.1.2, page 23.

Lemma B.2.1.
Let $\{(g_i, k_{\mathrm{a};i})\}_{i=1}^{N}$ *be epitope classes, let* $a > 0$ *be an initial antibody concentration, let* $\beta > 0$ *be a depletion factor, and let* $y_{0;i} > 0$ *be positive initial values for* $i \in \{1, \dots, N\}$.

When $x_{\mathrm{R}} \colon (p, q) \subset \mathbb{R}_{\geq 0} \longrightarrow \mathbb{R}^N$ *is a solution of the reservoir accumulation IVP, then*

$$y_{\mathrm{R}} \colon (p + t_0, q + t_0) \longrightarrow \mathbb{R}^N \ , \quad y_{\mathrm{R};i}(t) = x_{\mathrm{R};i}(t - t_0) + y_{0;i}$$

solves

$$\frac{d}{dt} y_{\mathrm{R};i}(t) = k_{\mathrm{a};i} a (\widetilde{g}_i - y_{\mathrm{R};i}(t)) \quad , \ y_{\mathrm{R};i}(t_0) = y_{0;i} \ ,$$

where $\widetilde{g}_i = g_i + y_{0;i}$.

Similarly, when $x_{\mathrm{D}} \colon (p, q) \subset \mathbb{R}_{\geq 0} \longrightarrow \mathbb{R}^N$ *is a solution of the depletion accumulation IVP, then*

$$y_{\mathrm{D}} \colon (p + t_0, q + t_0) \longrightarrow \mathbb{R}^N \ , \quad y_{\mathrm{D};i}(t) = x_{\mathrm{D};i}(t - t_0) + y_{0;i}$$

solves

$$\frac{d}{dt} y_{\mathrm{D};i}(t) = k_{\mathrm{a};i} \left(\widetilde{a} - \beta \sum_{j=1}^{N} y_{\mathrm{D};j}(t) \right) (\widetilde{g}_i - y_{\mathrm{D};i}(t)) \quad , \ y_{\mathrm{D};i}(t_0) = y_{0;i} \ ,$$

where $\widetilde{g}_i = g_i + y_{0;i}$ *and* $\widetilde{a} = a + \beta \sum_{j=1}^{N} y_{0;i}$.

Proof B.2.2.
Let us first consider the situation without time shift, that is, $t_0 = 0$.

Then, it follows that $y_{\mathrm{R};i}(0) = y_{0;i}$ and $y_{\mathrm{D};i}(0) = y_{0;i}$. Next, we calculate

$$\begin{aligned}\frac{d}{dt}y_{\mathrm{R};i}(t) &= \frac{d}{dt}(x_{\mathrm{R};i}(t) + y_{0;i}) = \frac{d}{dt}x_{\mathrm{R};i}(t) = k_{\mathrm{a};i}a(g_i - x_{\mathrm{R};i}(t)) \\ &= k_{\mathrm{a};i}a(g_i - (y_{\mathrm{R};i}(t) - y_{0;i})) = k_{\mathrm{a};i}a(g_i + y_{0;i} - y_{\mathrm{R};i}(t)) \\ &= k_{\mathrm{a};i}a(\widetilde{g}_i - y_{\mathrm{R};i}(t))\end{aligned}$$

for the reservoir case, and

$$\begin{aligned}\frac{d}{dt}y_{\mathrm{D};i}(t) &= \frac{d}{dt}(x_{\mathrm{D};i}(t) + y_{0;i}) = \frac{d}{dt}x_{\mathrm{D};i}(t) \\ &= k_{\mathrm{a};i}\left(a - \beta\sum_{j=1}^{N} x_{\mathrm{D};j}(t)\right)(g_i - x_{\mathrm{D};i}(t)) \\ &= k_{\mathrm{a};i}\left(a - \beta\sum_{j=1}^{N}(y_{\mathrm{D};j}(t) - y_{0;j})\right)(g_i - (y_{\mathrm{D};i}(t) - y_{0;i})) \\ &= k_{\mathrm{a};i}\left(a + \beta\sum_{j=1}^{N} y_{0;j} - \beta\sum_{j=1}^{N} y_{\mathrm{D};j}(t)\right)(g_i + y_{0;i} - y_{\mathrm{D};i}(t)) \\ &= k_{\mathrm{a};i}\left(\widetilde{a} - \beta\sum_{j=1}^{N} y_{\mathrm{D};j}(t)\right)(\widetilde{g}_i - y_{\mathrm{D};i}(t))\end{aligned}$$

for the depletion case.

Finally, we observe that the systems of differential equations, both for the reservoir case and for the depletion case, have no explicit time dependence. Thus, if $y_{\mathrm{R}}(t)$ is a solution, so is $z(t) = y_{\mathrm{R}}(t - t_0)$, since

$$\frac{d}{dt}y_{\mathrm{R}}(t - t_0) = \frac{d}{ds}y_{\mathrm{R}}(s)\Big|_{s=t-t_0}\frac{d}{dt}(t - t_0) = \frac{d}{ds}y_{\mathrm{R}}(s)\Big|_{s=t-t_0}.$$

The same argument applies to y_{D}. □

Note that the time-translation argument $t \mapsto t - t_0$ applies to autonomous systems in general (see [Wal98, chapter III, § 10, XI]).

B.2.2 Positive derivatives of positive functions

Belonging to Subsection 3.2.1, page 37.

Lemma B.2.3 ({Adapted from [Theory-Preprint]}).
Let $f\colon I \longrightarrow \mathbb{R}$ be a differentiable function on a non-empty interval I. If

$$\exists\, a \in I\colon f(a) \geq 0 \qquad \textit{and} \qquad \frac{d}{dt} f(t) \geq 0 \qquad \forall\, t \geq a$$

then $f(t) \geq 0$ for all $t \in I$ with $t \geq a$. If the derivative is strictly positive,

$$\frac{d}{dt} f(t) > 0 \qquad \forall\, t \geq a\ ,$$

then the strict inequality $f(t) > 0$ holds for all $t \in I$ with $t > a$.

Proof B.2.4 ({Adapted from [Theory-Preprint]}).
For $t = a$ the statement is obvious. If $a = \max\{I\}$ the statement is proven. Otherwise, let $t > a$. Then the mean value theorem implies that there is a $c \in [a, t]$ such that

$$\frac{f(t) - f(a)}{t - a} = \frac{df}{dt}(c)\ .$$

Since $t > a$ and $\frac{df}{dt}(c) \geq 0$, by the assumptions of the lemma, it follows that

$$f(t) - f(a) \geq 0 \qquad \Rightarrow \qquad f(t) \geq f(a) \quad \forall\, t > a\ .$$

For the strict inequality, repeat the argument with $\frac{df}{dt}(c) > 0$. □

B.2.3 Detailed proof of Lemma 3.2.14

Proof of Lemma 3.2.14, page 41.
{This proof is adapted from [Theory-Preprint].}

First, we recall from Definition 3.2.2 that

$$A(t;a) = \int_0^t \alpha(s;a)\ ds\ .$$

Thus, if we can show that $\alpha(t;b) > \alpha(t;a)$ for all $t \geq 0$, the inequality $A(t;b) > A(t_0;a)$ follows from the properties of integration. Hence, we will focus on $\alpha(t;b) > \alpha(t;a)$.

Since $x_{\mathrm{D}}(0;a) = 0$ and $b > a$, we have

$$\alpha(0;b) = b > a = \alpha(0;a) \qquad \Rightarrow \qquad \alpha(0;b) - \alpha(0;a) > 0\ .$$

And since the $x_{\mathrm{D};i}(t)$ are differentiable, so are $\alpha(t;a)$, $\alpha(t;b)$ and thus $\alpha(t;b) - \alpha(t;a)$. Our goal is now to show that $\alpha(t;b) - \alpha(t;a) > 0$ for all $t \geq 0$.

Let us assume that there is a $t_- > 0$ such that

$$\alpha(t_-;b) - \alpha(t_-;a) \leq 0\ .$$

Because of the continuity of $\alpha(t;b) - \alpha(t;a)$, there must be a smallest $t_0 > 0$ such that $\alpha(t_0;b) - \alpha(t_0;a) = 0$. If we can show that no such t_0 exists, then we will have proven that $\alpha(t;b) - \alpha(t;a) > 0$ for all $t \geq 0$.

Since $t_0 > 0$ and since by assumption t_0 is the smallest value such that $\alpha(t_0;b) - \alpha(t_0;a) = 0$, we know that

$$\alpha(t;b) - \alpha(t;a) > 0 \qquad \forall t \in [0, t_0)\ .$$

Thus,

$$A(t;b) = \int_0^t \alpha(s;b)\ ds > \int_0^t \alpha(s;a)\ ds = A(t;a)$$

for all $t \in [0, t_0]$. This also implies that

$$1 - e^{-k_{\mathrm{a};i} A(t;b)} > 1 - e^{-k_{\mathrm{a};i} A(t;a)}\ .$$

Because of Theorem 3.2.3 and Definition 3.2.2, it follows that

$$x_{\mathrm{D};i}(t;b) = g_i\left(1 - e^{-k_{\mathrm{a};i} \int_0^t \left(a - \beta \sum_{j=1}^N x_{\mathrm{D};j}(s;b)\right) ds}\right) = g_i(1 - e^{-k_{\mathrm{a};i} A(t;b)})$$

$$> g_i(1 - e^{-k_{\mathrm{a};i}A(t;a)}) = \ldots = x_{\mathrm{D};i}(t;a)$$

for all $t \in [0, t_0]$ and for all $i \in \{1, \ldots, N\}$. This implies that

$$\Gamma \coloneqq \min_{t\in[0,t_0], i\in\{1,\ldots,N\}} x_{\mathrm{D};i}(t;b) - x_{\mathrm{D};i}(t;a) > 0 \ .$$

Because of the bounds of Theorem 3.2.9, the inequalities $0 \leq x_{\mathrm{D};i}(t;b) < g_i$ hold for all $t \in [0, \infty)$ and for all $i \in \{1, \ldots, N\}$. Furthermore, the theorem states that $g_i - x_{\mathrm{D};i}(t;a) > 0$ and $a - \beta \sum_{j=1}^{N} x_{\mathrm{D};j}(t;a) > 0$, such that

$$\Psi \coloneqq \min_{t\in[0,t_0], i\in\{1,\ldots,N\}} \frac{1}{g_i - x_{\mathrm{D};i}(t;b)} > 0$$

is finite, and

$$\xi \coloneqq \min_{t\in[0,t_0]} \alpha(t;a) = \min_{t\in[0,t_0]} a - \beta \sum_{j=1}^{N} x_{\mathrm{D};j}(t;a) > 0 \ .$$

In summary, we have

$$0 < \Gamma\Psi\xi < \infty \ .$$

The difference $\alpha(t;b) - \alpha(t;a)$ is continuous and, by assumption, t_0 is the smallest value with $\alpha(t_0;b) - \alpha(t_0;a) = 0$, so there is an $\varepsilon > 0$ such that

$$\alpha(t;b) - \alpha(t;a) < \Gamma\Psi\xi \qquad \forall\ t \in (t_0 - \varepsilon, t_0] \ .$$

$$\Leftrightarrow \qquad \alpha(t;b) < \Gamma\Psi\xi + \alpha(t;a) \qquad \forall\ t \in (t_0 - \varepsilon, t_0] \ .$$

Now, since x_{D} is the solution of the depletion accumulation IVP it follows for all $i \in \{1, \ldots, N\}$ and all $t \in (t_0 - \varepsilon, t_0]$ that

$$\begin{aligned}
&\frac{1}{k_{\mathrm{a};i}} \left(\frac{d}{dt} x_{\mathrm{D};i}(t;a) - \frac{d}{dt} x_{\mathrm{D};i}(t;b) \right) \\
&\quad = \left(a - \sum_{j=1}^{N} x_{\mathrm{D};j}(t;a) \right) (g_i - x_{\mathrm{D};i}(t;a)) \\
&\qquad - \left(b - \beta \sum_{j=1}^{N} x_{\mathrm{D};j}(t;b) \right) (g_i - x_{\mathrm{D};i}(t;b)) \\
&\quad = \alpha(t;a)(g_i - \beta x_{\mathrm{D};i}(t;a)) - \alpha(t;b)(g_i - x_{\mathrm{D};i}(t;b))
\end{aligned}$$

$$
\begin{aligned}
&> \alpha(t;a)(g_i - x_{\mathrm{D};i}(t;a)) - (\alpha(t;a) + \Gamma\Psi\xi)(g_i - x_{\mathrm{D};i}(t;b)) \\
&= \alpha(t;a)(x_{\mathrm{D};i}(t;b) - x_{\mathrm{D};i}(t;a)) - \xi\Gamma\Psi(g_i - x_{\mathrm{D};i}(t;b)) \\
&\geq \alpha(t;a)(x_{\mathrm{D};i}(t;b) - x_{\mathrm{D};i}(t;a)) - \alpha(t;a)(x_{\mathrm{D};i}(t;b) - x_{\mathrm{D};i}(t;a)) \cdot 1 \\
&= 0 \ .
\end{aligned}
$$

Note that we have used the definitions of Γ, Ψ and ξ in the last step.

With the last calculation, we have obtained the statement

$$\frac{d}{dt}x_{\mathrm{D};i}(t;a) - \frac{d}{dt}x_{\mathrm{D};i}(t;b) > 0$$

for all $i \in \{1, \dots, N\}$ and all $t \in (t_0 - \varepsilon, t_0]$. For the time-derivatives of $\alpha(t;b)$ and $\alpha(t;a)$, this means that

$$\frac{d}{dt}\alpha(t;b) = -\beta \sum_{j=1}^{N} \frac{d}{dt}x_{\mathrm{D};j}(t;b) > -\beta \sum_{j=1}^{N} \frac{d}{dt}x(t;a) = \frac{d}{dt}\alpha(t;a)$$

for all $t \in (t_0 - \varepsilon, t_0]$, which is equivalent to

$$\frac{d}{dt}\alpha(t;b) - \frac{d}{dt}\alpha(t;a) > 0 \qquad \forall\, t \in (t_0 - \varepsilon, t_0] \ .$$

However, by definition of t_0, we have $\alpha(t;b) - \alpha(t;a) > 0$ for all $t \in [0, t_0)$. Since $\frac{d}{dt}\alpha(t;b) - \frac{d}{dt}\alpha(t;a) > 0$ for $t \in (t_0 - \varepsilon, t_0]$, it follows from (3.4) that $\alpha(t_0;b) - \alpha(t_0;a) > 0$. This contradicts the definition of t_0 to be the smallest value such that $\alpha(t_0;b) - \alpha(t_0;a) = 0$. Hence, there is no finite t_0 for which $\alpha(t_0;b) - \alpha(t_0;a) = 0$, which concludes the proof. □

B.2.4 Detailed proof of Theorem 3.2.27

Proof of Theorem 3.2.27, page 51.
{This proof is adapted from [Theory-Preprint].}

First, we observe that $\min\{\beta^{-1}a, X_{\mathrm{R}}(a)\}$ and $X_{\mathrm{R}}(a_*(a)) \leq X_{\mathrm{D}}(a)$ follow immediately from Theorem 3.2.9 and Corollary 3.2.21. Thus, it suffices to show $Y(a) \leq X_{\mathrm{D}}(a)$ for all initial antibody concentrations $a > 0$.

To prove $Y(a) \leq X_{\mathrm{D}}(a)$, let us begin by formally proving that the tangent line

$$T_0(t;a) \coloneqq a + t\frac{d\alpha}{dt}(0;a)$$

is below the effective antibody concentration $\alpha(t;a)$ of the depletion accumulation IVP. Theorem 3.2.7 and Corollary 3.2.12 state that the components $x_{\mathrm{D};i}(t;a)$ of depletion accumulation IVP solutions are strictly monotonically increasing and strictly concave as functions of t. Thus, $X_{\mathrm{D}}(t;a)$ is also strictly monotonically increasing and strictly concave as a function of t, which implies that the effective antibody concentration $\alpha(t;a) = a - \beta X_{\mathrm{D}}(t;a)$ is strictly monotonically decreasing and strictly convex as a function of t. This means that

$$\frac{d}{dt}\alpha(t;a) < 0 \qquad \text{and} \qquad \frac{d\alpha}{dt}(0;a) \leq \frac{d}{dt}\alpha(t;a)$$

for all $t \geq 0$. Now, (3.4) and $\alpha(0;a) = a$ imply that

$$\alpha(t;a) - \left(a + t\frac{d\alpha}{dt}(0;a)\right) \geq 0 \qquad \forall\ t \geq 0\ ,$$

which is equivalent to

$$\alpha(t;a) \geq a + t\frac{d\alpha}{dt}(0;a) \overset{\text{def}}{=} T_0(t;a) \qquad \forall\ t \geq 0\ .$$

In other words, the tangent line $T_0(t;a)$ is indeed below the effective antibody concentration of the depletion accumulation IVP.

Next, we construct the effective antibody concentration

$$\widetilde{\alpha}(t;a) \coloneqq \max\{0; T_0(t;a)\} = \max\left\{0; a + t\frac{d\alpha}{dt}(0;a)\right\}\ .$$

Since $\alpha(t;a) \geq 0$ by Theorem 3.2.9, it follows that $\widetilde{\alpha}(t;a) \leq \alpha(t;a)$ for all $t \geq 0$, which implies

$$\begin{aligned} Z(a) &\coloneqq \sum_{i=1}^{N} g_i \left(1 - e^{-k_{\mathrm{a};i}\int_0^\tau \widetilde{\alpha}(t;a)\ dt}\right) \\ &\leq \sum_{i=1}^{N} g_i \left(1 - e^{-k_{\mathrm{a};i}\int_0^\tau \alpha(t;a)\ dt}\right) = X_{\mathrm{D}}(a)\ . \end{aligned}$$

To conclude the proof, it remains to show that $Z(A) = Y(a)$, i.e., to show that

$$\int_0^\tau \widetilde{\alpha}(s;a)\ ds = \widetilde{A}(\tau;a)\ .$$

To solve this integral, we have to obtain the concrete expression for $\widetilde{\alpha}(t;a)$. First, we use that $x_{\mathrm{D}}(t;a)$ is the solution of the depletion accumulation IVP

to calculate $\frac{d\alpha}{dt}(0;a)$:

$$\begin{aligned}\frac{d\alpha}{dt}(0;a) &= \frac{d}{dt}\left(a - \beta\sum_{i=1}^{N} x_{\mathrm{D};i}(t;a)\right)\Bigg|_{t=0} \\ &= -\beta\sum_{i=1}^{N} k_{\mathrm{a};i}\left(a - \beta\sum_{j=1}^{N} x_{\mathrm{D};j}(0;a)\right)(g_i - x_i(0;a)) \\ &= -\beta\sum_{i=1}^{N} k_{\mathrm{a};i} a g_i = -a\beta\sum_{i=1}^{N} k_{\mathrm{a};i} g_i \ .\end{aligned}$$

For the tangent line $T_0(t;a)$, this leads to

$$T_0(t;a) = a - ta\beta\sum_{i=1}^{N} k_{\mathrm{a};i} g_i \ ,$$

which is negative when

$$t > \frac{1}{\beta\sum_{i=1}^{N} k_{\mathrm{a};i} g_i} =: t_0 \ .$$

Thus, we can express $\widetilde{\alpha}(t;a) = \max\{0, T_0(t;a)\}$ as

$$\widetilde{\alpha}(t;a) = \begin{cases} a - ta\beta\sum_{i=1}^{N} k_{\mathrm{a};i} g_i & , \ t \le t_0 \\ 0 & , \ \text{otherwise} \end{cases} \ .$$

For the integral, we have to distinguish between $\tau > t_0$ and $\tau \le t_0$. If $\tau > t_0$, then

$$\begin{aligned}\int_0^{\tau} \widetilde{\alpha}(t;a)\ dt &= \int_0^{t_0}\left(a - ta\beta\sum_{i=1}^{N} k_{\mathrm{a};i} g_i\right) dt + \int_{t_0}^{\tau} 0\ dt \\ &= \left[at - \frac{t^2}{2} a\beta\sum_{i=1}^{N} k_{\mathrm{a};i} g_i\right]_0^{t_0} = at_0\left(1 - \frac{t_0}{2}\beta\sum_{i=1}^{N} k_{\mathrm{a};i} g_i\right) \\ &= \frac{a}{\beta\sum_{i=1}^{N} k_{\mathrm{a};i} g_i}\left(1 - \frac{1}{2\beta\sum_{i=1}^{N} k_{\mathrm{a};i} g_i}\sum_{i=1}^{N}\beta k_{\mathrm{a};i} g_i\right)\end{aligned}$$

$$= \frac{a}{2\beta \sum_{i=1}^{N} k_{\mathrm{a};i} g_i} \ .$$

On the other hand, if $\tau \leq t_0$:

$$\int_0^\tau \widetilde{\alpha}(t;a)\ dt = \int_0^\tau \left(a - ta\beta \sum_{i=1}^{N} k_{\mathrm{a};i} g_i \right) dt$$

$$= a\tau \left(1 - \frac{\tau}{2} \beta \sum_{i=1}^{N} k_{\mathrm{a};i} g_i \right) \ .$$

Together, the integrals show that

$$\int_0^\tau \widetilde{\alpha}(t;a)\ dt = \widetilde{A}(\tau;a) \ ,$$

which concludes the proof. □

B.2.5 Depletion case for generic antibody-mix configurations

Belonging to Subsection 3.3.4, page 70.

In order to overcome problems associated with the coupling term of the depletion accumulation IVP, we have considered generic effective antibody concentrations $\alpha(t)$. This allowed us to replicate the structure of the reservoir case, leading to the integral equations of Theorem 3.2.3, which we used to derive properties of the depletion accumulation IVP.

However, for heterogeneous antibodies, we could not solve the antibody-mix reservoir accumulation IVP. Loosely speaking, we have only solved the problem for the sum over the antibody types. So we might consider the sum over the antibody types for the antibody-mix depletion accumulation IVP:

$$\frac{d}{dt} \sum_{\mu=1}^{M} x_{\mathrm{D};i\mu}(t) = \sum_{\mu=1}^{M} \frac{d}{dt} x_{\mathrm{D};i\mu}(t)$$

$$= \sum_{\mu=1}^{M} k_{\mathrm{a};i\mu} \left(f_\mu a - \beta \sum_{j=1}^{N} x_{\mathrm{D};j\mu}(t) \right) \left(g_i - \sum_{\nu=1}^{M} x_{\mathrm{D};i\nu}(t) \right)$$

$$= \left(\sum_{\mu=1}^{M} k_{\mathrm{a};i\mu} \left(f_\mu a - \beta \sum_{j=1}^{N} x_{\mathrm{D};j\mu}(t) \right) \right) \left(g_i - \sum_{\nu=1}^{M} x_{\mathrm{D};i\nu}(t) \right) \ .$$

Now, one might be inclined to replicate the integral equations of Theorem 3.2.3 by considering vector-valued functions $w\colon [0,T) \to \mathbb{R}^{NN}$ that satisfy the integral equations

$$\sum_{\mu=1}^{M} w_{i\mu}(t) = g_i \left(1 - e^{-\int_0^t \sum_{\mu=1}^{M} k_{\mathrm{a};i\mu}\left(f_\mu a - \beta \sum_{j=1}^{N} w_{j\mu}(t)\right)\, ds}\right) . \tag{B.3}$$

However, these vector-valued functions would only solve

$$\frac{d}{dt}\sum_{\mu=1}^{M} w_{i\mu}(t) = \left(\sum_{\mu=1}^{M} k_{\mathrm{a};i\mu}\left(f_\mu a - \beta \sum_{j=1}^{N} w_{j\mu}(t)\right)\right)\left(g_i - \sum_{\nu=1}^{M} w_{i\nu}(t)\right) , \tag{B.4}$$

which does not mean that the components $w_{i\mu}(t)$ also solve

$$\frac{d}{dt} w_{i\mu}(t) = k_{\mathrm{a};i\mu}\left(f_\mu a - \beta \sum_{j=1}^{N} w_{j\mu}(t)\right)\left(g_i - \sum_{\nu=1}^{M} w_{i\nu}(t)\right) .$$

In other words, it is not clear whether w solves the antibody-mix depletion accumulation IVP, so we cannot use the uniqueness of x_{D} to show that w and x_{D} are the same.

B.2.6 Detailed proof of Theorem 3.3.17

Proof of Theorem 3.3.17, page 71.

At first, we only know that there is a unique local solution $x_{\mathrm{D}}\colon [0,T) \to \mathbb{R}^{NM}$ for the antibody-mix depletion accumulation IVP.

According to Theorem 3.3.9, we can arrange the components $x_{\mathrm{D};i\mu}(t)$ into $(v^{(1)}(t), \dots, v^{(L)}(t), 0)$, based on the antibody-type partition $J_1, \dots, J_L$. Corollary 3.3.11 then states that the $\{v^{(\ell)}(t)\}_{\ell=1}^{L}$ are solutions of depletion accumulation IVPs for homogeneous antibodies, with initial antibody concentrations $f_{\gamma(J_\ell)}a$ and epitope classes $\{(g_i, k_{\mathrm{a};i\gamma(J_\ell)})\}_{i\in J_\ell}$.

As solutions of depletion accumulation IVPs, Theorem 3.2.9 applies, which means that

$$0 \le v_i^{(\ell)}(t) = x_{\mathrm{D};i\gamma(J_\ell)}(t) < \min\{\beta^{-1} f_{\gamma(J_\ell)} a, g_i\}$$

for all $\ell \in \{1, \dots, L\}$, all $i \in J_\ell$, and all $t \in [0,T)$. For the remaining components, i.e., for all combinations (k,ν) with $k \in \{1,\dots,N\}$ and $\nu \neq \gamma(k)$,

$x_{\mathrm{D};k\nu}(t) = 0$ for all $t \in [0, T)$. Thus, Proposition 3.1.8 applies and it follows that $T = \infty$.

Now, we can proceed to the list of properties given in the corollary. To keep things short, let us understand

$$a > 0 \,, \qquad \ell \in \{1, \dots, L\} \,, \qquad i \in J_\ell \,, \qquad t \geq 0$$

and

$$k \in \{1, \dots, N\} \,, \qquad \mu \in \{1, \dots, M\} \,, \qquad \nu \in \{1, \dots, M\} \setminus \{\gamma(k)\}$$

as arbitrary. In this way, we obtain the "for all ..." results without having to repeat the "for all ..." statements every time. Furthermore, since $t \geq 0$ is arbitrary, any result for $t \geq 0$ will also be valid for the incubation time $\tau > 0$.

Unfortunately, since $v^{(\ell)}(t)$ is the solution of a depletion accumulation IVP with initial antibody concentration $f_{\gamma(J_\ell)}a$, the notation $v^{(\ell)}(t; a)$ is ambiguous. Does it mean that $v^{(\ell)}$ is considered as solution for the initial antibody concentration a or does it imply the initial antibody concentration $f_{\gamma(J_\ell)}a$? Let us choose the former case: the argument denotes the initial antibody concentration as is, without any implicit transformation. Then

$$x_{\mathrm{D};i\gamma(J_\ell)}(t; a) = v_i^{(\ell)}(t; f_{\gamma(J_\ell)}a) \,.$$

i) The $\{v_i^{(\ell)}\}_{\ell=1}^{L}$ are solutions of depletion accumulation IVPs, thus Theorem 3.2.7 yields

$$\frac{d}{dt} x_{\mathrm{D};i\gamma(J_\ell)}(t) = \frac{d}{dt} v_i^{(\ell)}(t) > 0 \,.$$

For the components identically equal to zero, it is obvious that $\frac{d}{dt} x_{\mathrm{D};k\nu}(t) = 0$.

ii) We have already shown at the beginning of the proof above that

$$0 \leq x_{\mathrm{D};i\mu}(t) < \min\{\beta^{-1} f_{\gamma(J_\ell)}a, g_i\} \,.$$

Since $\sum_{\mu=1}^{M} f_\mu = 1$ by Definition 3.3.1, and since $x_{\mathrm{D};k,\nu}(t) \equiv 0$ by Definition 3.3.6, summation over all indices yields

$$0 \leq X_{\mathrm{D}}(t; a) < \min\{\beta^{-1} a, G\} \,.$$

iii) Because of Theorem 3.2.16, we have

$$x_{\mathrm{D};i\gamma(J_\ell)}(t; a) = v_i^{(\ell)}(t; f_{\gamma(J_\ell)}a) < v_i^{(\ell)}(t; f_{\gamma(J_\ell)}b) = x_{\mathrm{D};i\gamma(J_\ell)}(t; b)$$

for all $a < b$. And for the zero components,

$$x_{\mathrm{D};k\nu}(t;a) = 0 = x_{\mathrm{D};k\nu}(t;b)$$

is obvious. Summing over all indices thus yields

$$X_{\mathrm{D}}(t;a) < X_{\mathrm{D}}(t;b) \ .$$

iv) Because of Theorem 3.2.23, we have

$$\lim_{a\to 0} x_{\mathrm{D};i\gamma(J_\ell)}(t;a) = \lim_{a\to 0} v_i^{(\ell)}(t; f_{\gamma(J_\ell)}a) = 0 \ .$$

and

$$\lim_{a\to \infty} x_{\mathrm{D};i\gamma(J_\ell)}(t;a) = \lim_{a\to \infty} v_i^{(\ell)}(t; f_{\gamma(J_\ell)}a) = g_i \ .$$

For the zero components, the limits

$$\lim_{a\to 0} x_{\mathrm{D};k\nu}(t;a) = 0 \qquad \text{and} \qquad \lim_{a\to \infty} x_{\mathrm{D};k\nu}(t;a) = 0$$

are obvious. All in all, we have

$$\lim_{a\to 0} x_{\mathrm{D};k\mu}(t;a) = 0 \quad \text{and} \quad \lim_{a\to \infty} x_{\mathrm{D};k\mu}(t;a) = \begin{cases} g_k & , \ \mu = \gamma(k) \\ 0 & , \ \mu \neq \gamma(k) \end{cases} \ .$$

Summing over all indices then yields

$$\lim_{a\to 0} X_{\mathrm{D}}(t;a) = 0 \qquad \text{and} \qquad \lim_{a\to \infty} X_{\mathrm{D}}(t;a) = G \ .$$

v) First, Theorem 3.3.13 guarantees the existence and uniqueness of a solution $x_{\mathrm{R}} \colon [0,\infty) \to \mathbb{R}^{NM}$ for the antibody-mix reservoir accumulation IVP. Next, we recall that the separation theorem (Theorem 3.3.9) and its corollary (Corollary 3.3.11) apply to the reservoir case and the depletion case. Finally, the antibody-type partition is the same for both cases. Thus, the components $\{x_{\mathrm{R};k\mu}(t)\}_{k,\mu}$ can be arranged in the same way as the components $\{x_{\mathrm{D};k\mu}(t)\}_{k,\mu}$. That is,

$$v_i^{(\ell)}(t; f_{\gamma(J_\ell)}a) = x_{\mathrm{D};i\gamma(J_\ell)}(t;a) \quad \text{and} \quad w_i^{(\ell)}(t; f_{\gamma(J_\ell)}a) = x_{\mathrm{R};i\gamma(J_\ell)}(t;a) \ ,$$

as well as

$$x_{\mathrm{D};k\nu}(t) = 0 = x_{\mathrm{R};k\nu}(t) \ .$$

Note that we use $w^{(\ell)}$ for the decomposition of the reservoir case.

Corollary 3.3.11 now states that $v^{(\ell)}(t;a)$ is the solution of a depletion accumulation IVP and that $w^{(\ell)}(t;a)$ is the solution of a reservoir accumulation IVP. In both cases for the initial antibody concentration $f_{\gamma(J_\ell)}a$ and the epitope classes $\{(g_i, k_{\mathrm{a};i\gamma(J_\ell)})\}_{i\in J_\ell}$. Thus, Corollary 3.2.21 applies, which leads to

$$x_{\mathrm{D};i\gamma(J_\ell)}(t;a) = v_i^{(\ell)}(t; f_{\gamma(J_\ell)}a) \leq w_i^{(\ell)}(t; f_{\gamma(J_\ell)}a) = x_{\mathrm{R};i\gamma(J_\ell)}(t;a) \ .$$

With $x_{\mathrm{D};k\nu}(t) = 0 = x_{\mathrm{R};k\nu}(t)$, summing over all indices and choosing $t = \tau$, we obtain

$$X_{\mathrm{D}}(\tau;a) \leq X_{\mathrm{R}}(\tau;a) \ .$$

Finally, the inequality $X_{\mathrm{D}}(\tau;a) \leq \beta^{-1}a$ follows from the natural bounds that we have already proven above. Hence,

$$X_{\mathrm{D}}(\tau;a) \leq \min\{\beta^{-1}a, X_{\mathrm{R}}(\tau;a)\} \ .$$

□

B.3 Additional calculations for Chapter 4

B.3.1 Transformation of characteristic functions

Belonging to Subsection 4.2.2, page 95.

Lemma B.3.1.
Let $M \subseteq \mathbb{R}$ be a subset and let $\phi\colon M \to M$ be an invertible function. Then

$$\chi_I(\phi^{-1}(x)) = \chi_{\phi(I)}(x) \qquad \forall\ I \subseteq M\ ,\ x \in \phi(I)\ .$$

Proof B.3.2.
First, we observe that $\phi^{-1}(x) \in I$ is equivalent to $x \in \phi(I)$, since

$$\phi^{-1}(x) \in I \quad \Rightarrow \quad \phi(\phi^{-1}(x)) = x \in \phi(I)$$

and

$$x \in \phi(I) \quad \Rightarrow \quad \phi^{-1}(x) \in \phi^{-1}(\phi(I)) = I\ .$$

Then, by the definition of characteristic functions, it follows that

$$\chi_I(\phi^{-1}(x)) = \begin{cases} 1 & , \quad \phi^{-1}(x) \in I \\ 0 & , \quad \phi^{-1}(x) \notin I \end{cases}$$

$$= \begin{cases} 1 & , \quad x \in \phi(I) \\ 0 & , \quad x \notin \phi(I) \end{cases} = \chi_{\phi(I)}(x) \ .$$

□

B.3.2 Accumulation estimation integrals

Accumulation constant

Belonging to Subsection 4.3.1, page 102.

$$\int_{\mathbb{K}} H(K,a)\, \rho_{\{P',\lambda\}}(K) = \int_{\mathbb{K}} \sum_{j=1}^{m} \frac{\lambda_j}{q'_{j+1} - q'_j} \chi_{[q'_j, q'_{j+1})}(K) \left(1 - e^{-Ka}\right) \ |dK|$$

$$= \sum_{j=1}^{m} \frac{\lambda_j}{q'_{j+1} - q'_j} \int_{q'_j}^{q'_{j+1}} \left(1 - e^{-Ka}\right) \ dK$$

$$= \sum_{j=1}^{m} \frac{\lambda_j}{q'_{j+1} - q'_j} \left[K + \frac{1}{a} e^{-Ka}\right]_{q'_j}^{q'_{j+1}}$$

$$= \sum_{j=1}^{m} \lambda_j \left(1 + \frac{1}{a(q'_{j+1} - q'_j)} \left(e^{-q'_{j+1}a} - e^{-q'_j a}\right)\right) \ .$$

Obstruction constant

Belonging to Subsection 4.3.1, page 102.

First, we need a result from calculus.

Lemma B.3.3.
Let $f\colon (0,\infty) \to \mathbb{R}$ be a continuous function for which the improper integral

$$\int_a^\infty f(x)\ dx$$

exists for all $a > 0$. Then

$$\int_a^b f(x)\ dx = \int_a^\infty f(x)\ dx - \int_b^\infty f(x)\ dx \qquad \forall\ b \geq a\ .$$

Proof B.3.4.
By definition of improper integrals, we have

$$\begin{aligned}
\int_a^\infty f(x)\ dx &\coloneqq \lim_{T\to\infty} \int_a^T f(x)\ dx \\
&= \lim_{T\to\infty} \left(\int_a^b f(x)\ dx + \int_b^T f(x)\ dx \right) \\
&= \int_a^b f(x)\ dx + \lim_{T\to\infty} \int_b^T f(x)\ dx \\
&= \int_a^b f(x)\ dx + \int_b^\infty f(x)\ dx\ .
\end{aligned}$$

Rearranging the terms yields

$$\int_a^b f(x)\ dx = \int_a^\infty f(x)\ dx - \int_b^\infty f(x)\ dx\ .$$

□

Now we can solve the integral of the accumulation estimation model (4.12). First, using integration by parts, we find

$$\begin{aligned}
&\int_{q_j}^{q_{j+1}} 1 - e^{-\frac{a}{K_\tau}}\ dK_\tau = \\
&\quad = \left[K_\tau \left(1 - e^{-\frac{a}{K_\tau}}\right)\right]_{K_\tau=q_j}^{K_\tau=q_{j+1}} - \int_{q_j}^{q_{j+1}} K_\tau \frac{d}{dK_\tau}\left(1 - e^{-\frac{a}{K_\tau}}\right)\ dK_\tau \\
&\quad = \left[K_\tau \left(1 - e^{-\frac{a}{K_\tau}}\right)\right]_{K_\tau=q_j}^{K_\tau=q_{j+1}} + \int_{q_j}^{q_{j+1}} \frac{a}{K_\tau} e^{-\frac{a}{K_\tau}}\ dK_\tau\ .
\end{aligned}$$

Next, using integration by substitution and the orientation property of the Riemann integral, we obtain

$$\begin{aligned}
\int_{q_j}^{q_{j+1}} \frac{a}{K_\tau} e^{-\frac{a}{K_\tau}}\ dK_\tau &= \int_{a/q_j}^{a/q_{j+1}} \frac{a}{a/k} e^{-\frac{a}{a/k}} \frac{d}{dk}\left(\frac{a}{k}\right)\ dk \\
&= -a \int_{a/q_j}^{a/q_{j+1}} \frac{1}{k} e^{-k}\ dk = a \int_{a/q_{j+1}}^{a/q_j} \frac{1}{k} e^{-k}\ dk\ .
\end{aligned}$$

Finally, Lemma B.3.3 and the definition of the exponential integral (4.13) yield

$$\begin{aligned}
a \int_{a/q_{j+1}}^{a/q_j} \frac{1}{k} e^{-k}\ dk &= a \int_{-(-a/q_{j+1})}^{-(-a/q_j)} \frac{1}{k} e^{-k}\ dk \\
&= a \int_{-(-a/q_{j+1})}^{\infty} \frac{1}{k} e^{-k}\ dk - a \int_{-(-a/q_j)}^{\infty} \frac{1}{k} e^{-k}\ dk \\
&= -a\,\mathrm{Ei}\left(-\frac{a}{q_{j+1}}\right) + a\,\mathrm{Ei}\left(-\frac{a}{q_j}\right) = \left[-a\,\mathrm{Ei}\left(-\frac{a}{K_\tau}\right)\right]_{K_\tau=q_j}^{K_\tau=q_{j+1}}\ .
\end{aligned}$$

Plugging this term in, we have

$$\int_{q_j}^{q_{j+1}} 1 - e^{-\frac{a}{K_\tau}}\ dK_\tau = \left[K_\tau \left(1 - e^{-\frac{a}{K_\tau}}\right) - a\,\mathrm{Ei}\left(-\frac{a}{K_\tau}\right)\right]_{K_\tau=q_j}^{K_\tau=q_{j+1}}\ .$$

In summary, we have obtained an analytical solution for the response value

of the accumulation estimation model:

$$\begin{aligned} X(a) &= \int_{\mathbb{K}} F(K_\tau, a)\, \eta_{\{P,\lambda\}}(K_\tau) \\ &= \sum_{j=1}^{m} \frac{\lambda_j}{q_{j+1} - q_j} \int_{I_j} \left(1 - e^{-\frac{a}{K_\tau}}\right) \, |dK_\tau| \\ &= \sum_{j=1}^{m} \frac{\lambda_j}{q_{j+1} - q_j} \left[K_\tau \left(1 - e^{-\frac{a}{K_\tau}}\right) - a\, \mathrm{Ei}\left(-\frac{a}{K_\tau}\right)\right]_{K_\tau = q_j}^{K_\tau = q_{j+1}} . \end{aligned}$$

B.3.3 Inflection point of the accumulation model function

Belonging to Subsection 4.3.2, page 105.

Lemma B.3.5.
In logarithmic coordinates (with base c), the accumulation model function

$$\widetilde{F}(\widetilde{K_\tau}, \widetilde{a}) = 1 - \exp\left(-\frac{c^{\widetilde{a}}}{c^{\widetilde{K_\tau}}}\right) = 1 - \exp\left(-c^{\widetilde{a} - \widetilde{K_\tau}}\right)$$

has an inflection point at $\widetilde{a} = \widetilde{K_\tau}$ as a function of $\widetilde{a}$.

Proof B.3.6.
The second order derivative of $\widetilde{F}(\widetilde{K_\tau}, \widetilde{a})$ is given by

$$\frac{d^2}{d\widetilde{a}^2} \widetilde{F}(\widetilde{K_\tau}, \widetilde{a}) = \ln(c)^2 \exp\left(-c^{\widetilde{a} - \widetilde{K_\tau}}\right) c^{\widetilde{a} - 2\widetilde{K_\tau}} \left(c^{\widetilde{K_\tau}} - c^{\widetilde{a}}\right) .$$

We observe that

$$\frac{d^2}{d\widetilde{a}^2} \widetilde{F}(\widetilde{K_\tau}, \widetilde{a}) \begin{cases} > 0 & , \quad \widetilde{a} < \widetilde{K_\tau} \\ = 0 & , \quad \widetilde{a} = \widetilde{K_\tau} \\ < 0 & , \quad \widetilde{a} > \widetilde{K_\tau} \end{cases} .$$

Thus, $\widetilde{a} = \widetilde{K_\tau}$ is an inflection point of $\widetilde{F}(\widetilde{K_\tau}, \widetilde{a})$. □

B.3.4 IVP for the numerical depletion correction

Belonging to Subsection 4.3.5, page 120.

In the following, we always consider an arbitrary $i \in \{1, \dots, N\}$ so that the results hold for all $i \in \{1, \dots, N\}$.

Let us first consider the depletion accumulation differential equation (Definition 3.1.4) in terms of the normalized time $T = \frac{t}{\tau}$. Using the definition of the obstruction constant (Definition 4.2.1) together with the transformation behavior of functions (C.2) and of partial derivatives (C.4), for the coordinate transformation $T = \phi(t) = t/\tau$, we obtain

$$\begin{aligned}
\frac{1}{\tau}\frac{d}{dT}\widetilde{x}_{\mathrm{D};i}(T;a) = \frac{d}{dt}x_{\mathrm{D};i}(t;a) &= k_{\mathrm{a};i}\left(a - \beta\sum_{j=1}^{N} x_{\mathrm{D};j}(t;a)\right)\left(g_i - x_{\mathrm{D};i}(t;a)\right) \\
&= \frac{1}{K_{\tau;i}\tau}\left(a - \beta\sum_{j=1}^{N} \widetilde{x}_{\mathrm{D};i}(T;a)\right)\left(g_i - \widetilde{x}_{\mathrm{D};i}(T;a)\right) \\
\Rightarrow \qquad \frac{d}{dT}\widetilde{x}_{\mathrm{D};i}(T;a) &= \frac{1}{K_{\tau;i}}\left(a - \beta\sum_{j=1}^{N} \widetilde{x}_{\mathrm{D};j}(T;a)\right)\left(g_i - \widetilde{x}_{\mathrm{D};i}(T;a)\right) .
\end{aligned}$$

For the experimental units, we consider the coordinate transformation $\mathcal{A} = \psi(a) = \gamma a$ and define $\mathcal{G}_i = \xi g_i$, as well as $\widetilde{\mathcal{X}}_{\mathrm{D},i}(T;\mathcal{A}) = \xi\widetilde{x}_{\mathrm{D};i}(T;a)$. Then we find

$$\begin{aligned}
\frac{d}{dT}\widetilde{\mathcal{X}}_{\mathrm{D};i}(T;\mathcal{A}) &= \xi\frac{d}{dT}\widetilde{x}_{\mathrm{D};i}(T;a) \\
&= \xi\frac{1}{K_{\tau;i}}\left(a - \beta\sum_{j=1}^{N} \widetilde{x}_{\mathrm{D};j}(T;a)\right)\left(g_i - \widetilde{x}_{\mathrm{D};i}(T;a)\right) \\
&= \frac{1}{K_{\tau;i}}\left(a - \beta\sum_{j=1}^{N} \widetilde{x}_{\mathrm{D};j}(T;a)\right)\left(\xi g_i - \xi\widetilde{x}_{\mathrm{D};i}(T;a)\right) \\
&= \frac{1}{K_{\tau;i}}\left(a - \frac{\beta}{\xi}\sum_{j=1}^{N} \xi\widetilde{x}_{\mathrm{D};j}(T;a)\right)\left(\xi g_i - \xi\widetilde{x}_{\mathrm{D};i}(T;a)\right)
\end{aligned}$$

$$= \frac{1}{K_{\tau;i}\gamma}\left(\gamma a - \frac{\gamma\beta}{\xi}\sum_{j=1}^{N}\xi\widetilde{x}_{\mathrm{D};j}(T;a)\right)\left(\xi g_i - \xi\widetilde{x}_{\mathrm{D};i}(T;a)\right)$$

$$= \frac{1}{\mathcal{K}_{\tau;i}}\left(\mathcal{A} - \widetilde{\beta}\sum_{j=1}^{N}\widetilde{\mathcal{X}}_{\mathrm{D};j}(T;\mathcal{A})\right)\left(\mathcal{G}_i - \widetilde{\mathcal{X}}_{\mathrm{D};i}(T;\mathcal{A})\right) ,$$

where $\mathcal{K}_{\tau;i} = \gamma K_{\tau;i}$, as in Theorem 4.2.3, and $\widetilde{\beta} = \gamma\beta/\xi$.

In summary, we have obtained

$$\frac{d}{dT}\widetilde{\mathcal{X}}_{\mathrm{D};i}(T;\mathcal{A}) = \frac{1}{\mathcal{K}_{\tau;i}}\left(\mathcal{A} - \widetilde{\beta}\sum_{j=1}^{N}\widetilde{\mathcal{X}}_{\mathrm{D};j}(T;\mathcal{A})\right)\left(\mathcal{G}_i - \widetilde{\mathcal{X}}_{\mathrm{D};i}(T;\mathcal{A})\right)$$

for the differential equation. For the initial value, $T = t/\tau$ and $\widetilde{\mathcal{X}}_{\mathrm{D},i}(T;\mathcal{A}) = \xi\widetilde{x}_{\mathrm{D};i}(T;a)$ imply

$$\widetilde{\mathcal{X}}_{\mathrm{D};i}(0;\mathcal{A}) = 0 .$$

Finally, we observe that the depletion accumulation model is given by

$$\mathcal{A} \longmapsto \widetilde{\mathcal{X}}_{\mathrm{D};i}(1;\mathcal{A})$$

since we have normalized the time to the incubation time: $T = t/\tau$.

C

Units, logarithmic scales, and coordinates

In this dissertation, we use coordinate transformations to describe unit changes and logarithmic scales. Furthermore, we distinguish between density functions and proper densities, based on the coordinate transformation behavior. The underlying concepts should be familiar to most undergraduate physics students. Nevertheless, for the convenience of the reader, this chapter explains the connection between coordinates and units/logarithmic scales, starting from an intuitive description of units. Coordinate transformations are then properly defined, as well as the transformation behavior of functions, derivatives and densities, which leads to the distinction between density functions and proper densities. Finally, properties of plots on logarithmic scales are discussed (in the context of coordinate transformations) to collect the properties in one place.

C.1 Units and physical dimensions

Among the concepts listed at the beginning of the chapter, units may be the most familiar. We frequently encounter them in everyday life. Be it that we measure distances in centimeters, meters, etc., or time in seconds, minutes, hours, etc. As such, the idea behind units is intuitively clear. A unit sets a reference point to which a quantity is compared. In fact, any measurement is just a direct or indirect comparison of quantities (cf. [Dem08, Section 1.6]). As such, a quantity X consists of two aspects: a numerical value $\{X\}$ and the unit $\langle X \rangle$ to which the numerical value belongs. The **unit** describes which object or measurement method was used as a reference point. And the numerical value describes the proportionality relation to this object/method. For example, $X = 2.5\,\mathrm{m}$ means that a meter stick was set as the default object and X is 2.5 times longer than this stick. Accordingly, the numerical value of the standard object is set to 1.

Remark C.1.1 (**Arbitrariness of units**).
The standard quantity that defines a unit is completely arbitrary. Although many units are defined with respect to fundamental physical phenomena, there are often other phenomena that could be used, leading

to completely different numerical values. Furthermore, these definitions of units in terms of natural phenomena often include arbitrary numerical coefficients to retain historic definitions. For example, the meter was redefined by using the vacuum speed of light, which was fixed beforehand to 299792458 $^{m}/_{s}$ so that the original length of a meter remained unchanged (cf. [Dem08, section 1.6]).

Strictly speaking, a physical quantity X consists of three components: the numerical value X, the **physical dimension** $[X]$, and the unit $\langle X \rangle$. The measurement principle determines the physical dimension of a quantity. A unit is only the reference point for the numerical value of the measured quantity [Gib11, section 1.2]. In fact, even quantities that are commonly considered to be dimensionless can have a unit, such as angles [Dem08, section 1.6.10].

Especially in physics and engineering, dimensions are not defined in a mathematically rigorous formalism. Instead, two rules are usually applied (cf. [Mes15, Subsection 0.2.3]):

- Addition/Subtraction is only allowed for quantities with the same dimension.
- Multiplication/Division of dimensions defines a derived (new) dimension, following algebraic rules (e.g., cancellation of fractions).

Since we are not interested in mathematical models of physical dimensions, we adopt this practical approach to physical dimensions.

C.2 Unit changes and logarithmic scales as variable changes

Changing units means changing the reference point for the numerical value of a physical quantity. Thus, we can consider unit changes simply as changes of variables of the form $\widetilde{x} = \alpha x$, where $\alpha > 0$ is the unit conversion factor.

Remark C.2.1 (**Proper units**).
A unit, as we have introduced it, describes a reference object to which measured objects are compared. The resulting measurement value is the factor between the measured object and the reference object. Ignoring directionality, this means that negative measurement values cannot exist. Thus, all unit conversions between proper units have the form $\widetilde{x} = \alpha x$,

where $\alpha > 0$. A common example for an improper unit is the Celsius scale, where 0 °C is not the zero point of temperature.

Note that unit changes do not alter the physical dimension of a quantity. Only the numerical value is changed. Understanding that the numerical value is just a representation of a physical quantity for calculations, we can allow more general variable changes. For example, we can consider variable changes of the form $\widetilde{x} = \log_c(x)$, where $1 \neq c > 0$, to obtain logarithmic scales.

C.3 Coordinate transformations

We can formalize the notion of numerical representations and variable changes as coordinates and coordinate transformations. Coordinates, similar to units, define numerical representations for points in an abstract space. Changing the coordinates, similar to changing units, leads to different numerical representations. Furthermore, the relationships between different coordinates are not restricted to linear transformations but can involve differentiable, invertible functions, allowing the construction of logarithmic scales.

Coordinates and coordinate transformations are commonly used in mathematics and physics at different levels of abstraction, from undergraduate education to contemporary research. See, for example, [AD19, Section V2] for an introduction to coordinates as used in undergraduate physics or [Jän05, chapters 1-2] for an introduction to coordinates in the context of differentiable manifolds. Since there are many notations and abuses of notation, it is worthwhile for us to fix the notation before we consider the transformation behavior of functions, derivatives, and densities.

For our purposes, a **coordinate transformation** is a **diffeomorphism**, i.e., a bijective map[1] $\phi\colon U \subseteq \mathbb{R}^n \longrightarrow V \subseteq \mathbb{R}^n$, such that ϕ and ϕ^{-1} are infinitely differentiable. For example, we can express unit changes as coordinate transformations of the form

$$\phi\colon \mathbb{R}_{\geq 0} \longrightarrow \mathbb{R}_{\geq 0} \qquad x \longmapsto \alpha x \ ,$$

where $\alpha > 0$. The second example of interest, logarithmic scales, is given by coordinate transformations of the form

$$\phi\colon \mathbb{R}_{>0} \longrightarrow \mathbb{R} \qquad x \longmapsto \log_c(x) \ .$$

[1] Some authors prefer to distinguish functions from generic maps by understanding only maps with codomain $\mathbb{R}$ and/or $\mathbb{C}$ as functions. We do not follow such a methodical distinction between the terms but use them almost interchangeably, emphasizing either the pairing of elements of two sets or the functional relationship between, e.g., variables.

Because of the canonical basis of $\mathbb{R}^n$, we can express every point $x \in U \subseteq \mathbb{R}^n$ as a tuple

$$x = \begin{pmatrix} x_1 \\ \vdots \\ x_n \end{pmatrix}$$

of numbers $x_1, \ldots, x_n \in \mathbb{R}$. Thus, a coordinate transformation can be written as a tuple of functions $\phi_i \colon U \subseteq \mathbb{R}^n \to \mathbb{R}$:

$$\phi(x) = \begin{pmatrix} \phi_1(x) \\ \vdots \\ \phi_n(x) \end{pmatrix} = \begin{pmatrix} \phi_1(x_1, \ldots, x_n) \\ \vdots \\ \phi_n(x_1, \ldots, x_n) \end{pmatrix} .$$

Since $\phi_i(x)$ or even $\phi_i(x_1, \ldots, x_n)$ is cumbersome to write, we can define new variables $\widetilde{x}_i = \phi_i(x)$, leading to the *change of variables* from above. Thus, $(x_1, \ldots, x_n)$ are the coordinate values of x before the coordinate transformation and $(\widetilde{x}_1, \ldots, \widetilde{x}_n)$ are the coordinate values of x after the coordinate transformation.

Remark C.3.1 (**Abuse of notation**).
Note that we have already abused the notation here, using x_i for both the coordinate functions and the coordinate values of a point $x \in \mathbb{R}^n$. Given the canonical structure of $\mathbb{R}^n$, this is a common and convenient identification. And we would not benefit from the abstract notation/ formalism that is used for general manifolds. However, we can outline the rigorous notation to make the underlying concepts clear.

Coordinate functions x_i are the components of a *chart*, i.e., a map $x \colon M \subseteq \mathbb{R}^n \to x(M) \subseteq \mathbb{R}^n$. The *coordinate values* of a point $p \in M$ are then the result of that chart, applied to the point: $x(p) = (x_1(p), \ldots, x_n(p))$. This abstract formalism also agrees with the concept of units as a procedure to assign numbers to physical objects.

New coordinates are just another chart $\widetilde{x} \colon N \subseteq \mathbb{R}^n \to \widetilde{x}(N) \subseteq \mathbb{R}^n$. The coordinate transformation ϕ then describes the relationship between the charts. Formally, this coordinate transformation is called *transition map*, and is given by $\phi = \widetilde{x} \circ x^{-1}$ on the intersection $x(M \cap N)$. See, e.g., [Jän05, section 1.1] for further information.

C.4 Coordinate transformations of functions

To understand the transformation behavior of functions, we can consider a general vector-valued function $f\colon \mathbb{R}^n \to \mathbb{R}^k$. Here, we can change the coordinates for the domain $\phi\colon U \subseteq \mathbb{R}^n \to \phi(U) \subseteq \mathbb{R}^n$ and for the codomain $\psi\colon V \subseteq \mathbb{R}^k \to \psi(V) \subseteq \mathbb{R}^k$.

Of course, the relationship $y = f(x)$ between points of the domain x and points of the codomain y should not change when we change the coordinate representation to $\widetilde{x} = \phi(x)$ and $\widetilde{y} = \psi(y)$. However, since the numbers that describe the points change when we change coordinates, we have to adapt the calculation rules for the function f if we want to perform calculations in the new coordinates. Formally, we want that the diagram

$$\begin{array}{ccc} U \subseteq \mathbb{R}^n & \xrightarrow{\quad f \quad} & V \subseteq \mathbb{R}^k \\ \phi \big\downarrow & & \big\downarrow \psi \\ \phi(U) \subseteq \mathbb{R}^n & \xrightarrow[\quad \widetilde{f} \quad]{} & \psi(V) \subseteq \mathbb{R}^k \end{array} \tag{C.1}$$

commutes, which implies

$$\widetilde{f} = \psi \circ f \circ \phi^{-1} \tag{C.2}$$

for the transformed function $\widetilde{f}$ in the new coordinates.

C.5 Coordinate transformations of derivatives

When it comes to derivatives, we have two options, assuming of course, that the function f is sufficiently differentiable. First, we can directly differentiate the expression of the function in the new coordinates, essentially forgetting that we have transformed the coordinates in the first place. This form of differentiation describes the gradient of the coordinate-dependent graph of a function. And since the expression/shape of a function changes when the coordinates are transformed, we need not be surprised to find that

$$\frac{\partial}{\partial x_i} f(x) \neq \frac{\partial}{\partial \widetilde{x}_i} \widetilde{f}(\widetilde{x}) \ , \tag{C.3}$$

in general.

Second, we can regard derivatives as abstract relationships that should not depend on our choice of coordinates. Take, for example, partial differential

equations, like Maxwell's equations, that describe the relationships between physical quantities. As a description of reality, it is only reasonable to demand that these relationships must be the same, no matter which coordinates are used.

To obtain the correct transformation behavior of general partial derivatives $\frac{\partial}{\partial x_i}$, we only need to apply the chain rule for partial derivatives (see, e.g., [KW13, Satz 9.2.13]). Here, it suffices to consider only coordinate transformations $\phi\colon U \subseteq \mathbb{R}^n \to V \subseteq \mathbb{R}^n$ of the domain, i.e., $\widetilde{f} = f \circ \phi^{-1}$, which is equivalent to $f = \widetilde{f} \circ \phi$. Thus, we calculate:

$$\frac{\partial}{\partial x_i} f(x) = \frac{\partial}{\partial x_i} \widetilde{f}(\phi(x)) = \sum_{j=1}^{n} \frac{\partial}{\partial y} \widetilde{f}(y)\Big|_{y=\phi(x)} \frac{\partial}{\partial x_i} \phi_j(x) \ .$$

Rearranging the terms and plugging in the notation $\widetilde{x} = \phi(x)$ for the transformed coordinates, we obtain

$$\frac{\partial f(x)}{\partial x_i} = \sum_{j=1}^{n} \frac{\partial \phi_j(x)}{\partial x_i} \frac{\partial \widetilde{f}(\widetilde{x})}{\partial \widetilde{x}_j} \ . \tag{C.4}$$

Using the identity $x = \phi^{-1}(\widetilde{x})$, the right-hand side can be expressed completely in terms of $\widetilde{x}$ by evaluating the partial derivatives $\frac{\partial \phi_j(x)}{\partial x_i}$ at $x = \phi^{-1}(\widetilde{x})$. In some cases, however, it is easier to use the opposite transformation

$$\frac{\partial \widetilde{f}(\widetilde{x})}{\partial \widetilde{x}_i} = \sum_{j=1}^{n} \frac{\partial \phi_j^{-1}(\widetilde{x})}{\partial \widetilde{x}_i} \frac{\partial f(x)}{\partial x_j}$$

and to solve the resulting system of equations (cf. [KW13, Satz 9.3.4 and Satz 9.3.9]).

C.6 Coordinate transformations of densities

Having discussed function transformations and derivative transformations, there remains a third operation that we need to discuss: integration. Since we only need one-dimensional integration in this dissertation and do not benefit from addressing exterior algebras, let us confine our considerations to the one-dimensional case. That is, we consider a sufficiently integrable function $f\colon \mathbb{R} \to \mathbb{R}$.

As with differentiation, integration can be understood in two ways: as a mere method to obtain the surface area under the graph of a function or as a generalization of summation for continuous variables. And as before, since

the shape of the graph depends on the choice of coordinates, we need not be surprised that the surface area under a graph generally depends on the coordinates.

Let $\phi\colon U \subseteq \mathbb{R} \to V \subseteq \mathbb{R}$ be a coordinate transformation. We already know how to express the function $f(x)$ in different coordinates as $\widetilde{f}(\widetilde{x})$. An interval $I \subseteq U$ simply becomes $\phi(I)$ in the new coordinates. However, although we have transformed both the function and the integration region, integration in the original coordinates

$$\int_I f(x)\ dx$$

still differs from integration in the new coordinates

$$\int_{\phi(I)} \widetilde{f}(\widetilde{x})\ d\widetilde{x}\ .$$

That is, at least as long as we treat the differentials dx and $d\widetilde{x}$ as mere notational aspects of (symbolic) integration.

To understand the necessary transformation behavior of the differentials, let us consider an orientation-preserving, i.e., strictly monotonically increasing coordinate transformation $\phi\colon U \subseteq \mathbb{R} \to V \subseteq \mathbb{R}$. In this way, we can ignore orientation issues for the moment. Furthermore, let us make the interval I explicit by considering $I = [a, b]$ for $a < b \in U$. Then the transformed interval $\phi(I)$ becomes $[\phi(a), \phi(b)]$.

Now we can use the integration by substitution rule from elementary calculus to obtain the required transformation behavior for the differentials. In its common form (cf. [KW13, Satz 5.4.2] or [Fis83, Chapter XIII, Section 7, Theorem 7.2]), integration by substitution is expressed as

$$\int_{g(\alpha)}^{g(\beta)} f(x)\ dx = \int_\alpha^\beta f(g(y))\frac{dg(y)}{dy}\ dy\ , \tag{C.5}$$

where $g\colon [\alpha, \beta] \to \mathbb{R}$ is continuously differentiable, and f is continuous on $g([\alpha, \beta])$. However, Riemann integrability on $g([\alpha, \beta])$ suffices for the substitution rule [Bag01]. Thus, we calculate

$$\begin{aligned}\int_I f(x)\ dx &= \int_a^b f(x)\ dx = \int_{\phi^{-1}(\phi(a))}^{\phi^{-1}(\phi(b))} f(x)\ dx \\ &= \int_{\phi(a)}^{\phi(b)} f(\phi^{-1}(\widetilde{x}))\frac{d\phi^{-1}(\widetilde{x})}{d\widetilde{x}}\ d\widetilde{x} = \int_{\phi(I)} \widetilde{f}(\widetilde{x})\ \left(\frac{d\phi^{-1}(\widetilde{x})}{d\widetilde{x}}\ d\widetilde{x}\right)\ .\end{aligned}$$

In the last step, we visually separated the terms that constitute the correct transformation behavior of the differential:

$$dx \quad \rightsquigarrow \quad \frac{d\phi^{-1}(\widetilde{x})}{d\widetilde{x}}\, d\widetilde{x} \ .$$

To remain consistent with our notation for coordinate transformations, we are inclined to define

$$dx = d\phi^{-1}(\widetilde{x}) \coloneqq \frac{d\phi^{-1}(\widetilde{x})}{d\widetilde{x}}\, d\widetilde{x} \ .$$

In fact, this definition is not only a notational convenience for consistency. It can be given a geometric and algebraic interpretation of its own. In differential geometry, the differentials dx and expressions of the form $f(x)dx$ become rigorously defined as differential 1-forms.

At this point, much could be said about differential forms and their properties. See, for example, [Gow08, III.16 (from Terrence Tao)] for an informal but brief introduction to differential forms and their properties, or [Jän05] for an undergraduate course on differentiable manifolds (and differential forms). However, in this dissertation, we are only interested in their existence as rigorously defined objects with a transformation behavior that ensures coordinate independent integration. In our notation, this transformation behavior reads

$$f(x)\ dx = f(\phi^{-1}(\widetilde{x}))\ d\phi^{-1}(\widetilde{x}) = \widetilde{f}(\widetilde{x}) \left(\frac{d}{d\widetilde{x}} \phi^{-1}(\widetilde{x}) \right)\ d\widetilde{x} \ . \tag{C.6}$$

In summary, we have seen that the transformation behavior of functions alone does not suffice to ensure that the value of an integral remains the same when coordinates are changed. For this coordinate independence of integration, differential forms are better suited as natural integrands, since they already transform according to the integration by substitution rule. So, we might be tempted to declare that proper densities are differential forms. But recall that we restricted our considerations to orientation-preserving coordinate changes. This simplification allowed us to delay the discussion about orientation-sensitive and orientation-invariant integration.

In [Gow08, III.16 (from Terrence Tao)], Tao introduces differential forms by explaining the different concepts underlying 1-dimensional integration, which are conflated by the notational identifications

$$\int_{[a,b]} f(x)\ dx = \int_a^b f(x)\ dx = -\int_b^a f(x)\ dx \ .$$

Here, we can use the same approach to motivate densities.

Let us first investigate the notational conventions more closely. The first identity connects integration over sets $[a, b]$ with integration over oriented paths (from a at the bottom of the integral sign to b at the top of the integral sign). To capture this orientation, we may denote oriented paths by $[a \rightsquigarrow b]$. The second identity expresses the orientation-sensitivity of the Riemann-integral. Reversing the orientation from $[a \rightsquigarrow b]$ to $[b \rightsquigarrow a]$ changes the sign of the integral.

Problems with these notational identifications become apparent when one considers orientation-reversing transformations. The orientation reversal of paths needs to be reflected in the transformation of differential forms to ensure that the integral remains the same. However, sets are not defined to have an orientation, and thus there is no way to indicate the orientation reversal. Using now the set as an integration region for a differential form leads to a conflict, as the differential form transformation reacts to the orientation reversal, while the set remains unaffected.

We can illustrate the problem with the simple coordinate transformation $\widetilde{x} = \phi(x) = -x$, which has the inverse $\phi^{-1}(\widetilde{x}) = -\widetilde{x}$. Note that $\phi([a \rightsquigarrow b]) = [-a \rightsquigarrow -b]$, while $\phi([a, b]) = [-b, -a]$, since $a < b$ yields $-b < -a$. A differential from $f(x)\ dx$ now becomes

$$-f(-\widetilde{x})\ d\widetilde{x}\ ,$$

according to (C.6). In agreement with the integration by substitution rule (C.5), we obtain

$$\int_a^b f(x)\ dx = \int_{-a}^{-b} -f(-\widetilde{x})\ d\widetilde{x} = \int_{-b}^{-a} f(-\widetilde{x})\ d\widetilde{x} = \int_{-b}^{-a} \widetilde{f}(\widetilde{x})\ d\widetilde{x}\ .$$

Carelessly using the set notation would lead to problems, since

$$\int_a^b f(x)\ dx = \int_{[a,b]} f(x)\ dx \neq \int_{[-b,-a]} -f(-\widetilde{x})\ d\widetilde{x} = \int_{-b}^{-a} -\widetilde{f}(\widetilde{x})\ d\widetilde{x}\ .$$

If we were only interested in the integration of functions, we could easily define separate transformation behaviors for the integration over sets and the integration over oriented paths. In fact, this is the reason for the absolute value in the multidimensional integration by substitution rule (cf. [KW13, Satz 10.2.9] and [AD19, Equation (C76)]).

However, we are not only interested in the transformation behavior for integration but in an object that exists on its own, describes a density, and that can be integrated over sets. In pursuit of an object that properly describes

a density, we encountered differential forms. They are objects that exist on their own, can be integrated, and transform such that the result of integration does not depend on the choice of coordinates. But, as it turns out, differential forms are naturally integrated over oriented paths in one dimension (orientable manifolds in general [Jän05, chapter 5] [BT82, §7]). So we should construct a second object, alongside differential forms, that can be naturally integrated over sets, i.e., a **density**.

For our purposes, it suffices to define densities alongside differential forms as terms in the shape of $f(x)\ |dx|$. This notation also suggests the transformation behavior of a density:

$$f(x)\ |dx| = f(\phi^{-1}(\widetilde{x}))\ |d\phi^{-1}(\widetilde{x})| = \widetilde{f}(\widetilde{x}) \left|\frac{d}{d\widetilde{x}}\phi^{-1}(\widetilde{x})\right|\ |d\widetilde{x}|\ . \tag{C.7}$$

What we introduced informally, can also be done rigorously by considering twisted/odd differential forms [BT82, §7], [Rha84, §5]; but as before, we would not benefit from the additional formalism. Hence, we are content with the existence of properly defined objects that transform according to (C.7).

Note that we have not yet defined the notation for differential forms and densities. So far, we have only considered the transformation behavior of the expressions that constitute differential forms and densities. It is quite common (cf. [BT82; Rha84; Bre93; Jän05]) to denote differential forms (and densities) by Greek letters without arguments, e.g., ω. When arguments are used, e.g., $\omega(X_1, \ldots, X_n)$, the arguments correspond to vector fields. The dependence of the point p is often denoted by ω_p.

Here, we deviate from this convention and choose a coordinate dependent notation to make the chosen coordinates (e.g., units) explicit. That is, we write

$$\omega(x) = f(x)\ |dx|\ .$$

This is quite uncommon, as differential forms and densities do not depend on the choice of coordinates because of their transformation behavior[2]. For our coordinate-dependent notation, we have to use a new symbol for the differential form when we change units, as was the case for functions, since

$$\omega(x) = f(x)\ |dx| \neq f(\widetilde{x})\ |d\widetilde{x}| = \omega(\widetilde{x})\ .$$

As with functions, we use $\widetilde{\omega}(\widetilde{x})$ to denote the expression in new coordinates $\widetilde{x} = \phi(x)$. Then, because of the transformation behavior (C.7), we obtain

$$\omega(x) = f(x)\ |dx| = f(\phi^{-1}(\widetilde{x})) \left|\frac{d}{d\widetilde{x}}\phi^{-1}(\widetilde{x})\right|\ |d\widetilde{x}| = \widetilde{\omega}(\widetilde{x})\ . \tag{C.8}$$

[2] In fact, this independence was the motivation to define the transformation behavior in the way we did.

When we express a density in new coordinates, we also have to express the integration region in the new coordinates (recall integration by substitution):

$$\int_M \omega(x) = \int_M f(x)\ |dx| = \int_{\phi(M)} f(\phi^{-1}(\widetilde{x}))\left|\frac{d}{d\widetilde{x}}\phi^{-1}(\widetilde{x})\right|\ |d\widetilde{x}| = \int_{\widetilde{M}} \widetilde{\omega}(\widetilde{x})\ . \tag{C.9}$$

C.7 Properties of logarithmic plots

Let us conclude this chapter by discussing the properties of plots on logarithmic scales. These properties will be rather trivial, especially with the name "logarithmic scale" in mind. Nevertheless, we use logarithmic scales frequently in this dissertation, so it is worthwhile to collect these properties in one place.

Here, we consider a function

$$f\colon \mathbb{R}_{>0} \longrightarrow \mathbb{R}\ , \qquad x \longmapsto f(x)\ .$$

A logarithmic scale is obtained by considering a coordinate transformation $\phi\colon \mathbb{R}_{>0} \to \mathbb{R}$, where $\mathcal{X} = \phi(x) = \log_c(x)$ and thus $x = \phi^{-1}(\mathcal{X}) = c^{\mathcal{X}}$. The resulting representation of f on the logarithmic scale then reads

$$\widetilde{f}(\mathcal{X}) = (f \circ \phi^{-1})(\mathcal{X}) = f(c^{\mathcal{X}})\ ,$$

according to (C.2).

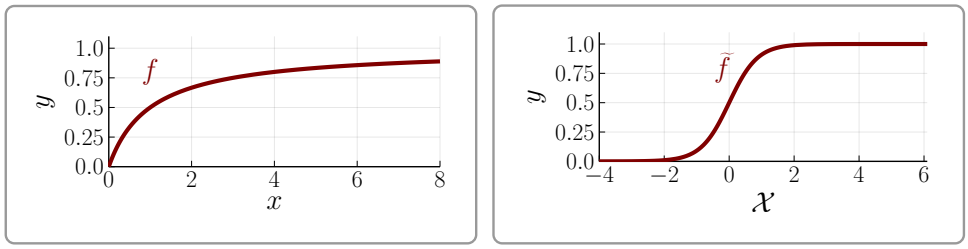

(a) linear scale **(b)** logarithmic scale

Figure C.1: Graph of the same function in a plot with linear scale (**a**) and a plot with logarithmic scale (**b**).

To visualize the properties of logarithmic plots, we may consider the following function (with base $c = 10$):

$$f(x) = \frac{1}{1+\frac{1}{x}} \qquad \Rightarrow \qquad \widetilde{f}(\mathcal{X}) = \frac{1}{1+\frac{1}{10^{\mathcal{X}}}}\ .$$

Figure C.1 shows the resulting plots.

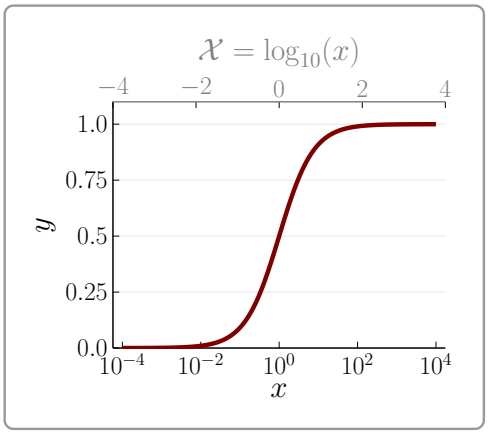

Figure C.2: Example of axis labels for plots with logarithmic scales.

Note that the axis ticks for the independent variable in Figure C.1b are linearly spaced. The logarithmic nature of the plot arises from our choice to use logarithmic coordinate values $\mathcal{X} = \log_c(x)$. However, using new coordinates does not seem to be the standard approach. Instead, logarithmic plots usually use the original coordinates with $x = c^{\mathcal{X}}$ as axis tick values. See Figure C.2 for the relationship between the different labeling approaches.

An important property of logarithmic scales is the conversion of multiplication to addition. For plots, this means that scalings of the independent/horizontal axis on a linear scale become translations on a logarithmic scale and vice versa. We can see this formally by considering the transformation

$$\Psi \colon \mathbb{R}_{>0} \longmapsto \mathbb{R}_{>0} \ , \qquad x \longmapsto \alpha x \ ,$$

where $\alpha > 0$. Scaling the function argument of f can then be achieved by composition:

$$f \circ \Psi \colon \mathbb{R}_{>0} \longrightarrow \mathbb{R} \ ,$$
$$x \longmapsto f(\Psi(x)) = f(\alpha x) \ .$$

To obtain the effect of the representation of Ψ in logarithmic coordinates, we consider the following diagram

$$\begin{array}{ccccc} \mathbb{R}_{>0} & \xrightarrow{\Psi} & \mathbb{R}_{>0} & \xrightarrow{f} & \mathbb{R} \\ {\scriptstyle\phi}\downarrow & & {\scriptstyle\phi}\downarrow & \nearrow_{\widetilde{f}} & \\ \mathbb{R} & \xrightarrow[\widetilde{\Psi}]{} & \mathbb{R} & & \end{array}$$

to obtain $\widetilde{\Psi} = \phi \circ \Psi \circ \phi^{-1}$. Evaluating this expression, we see that the scaling Ψ has become a translation:

$$\widetilde{\Psi}(\mathcal{X}) = (\phi \circ \Psi \circ \phi^{-1})(\mathcal{X}) = \log_c(\alpha c^{\mathcal{X}}) = \mathcal{X} + \log_c(\alpha) \ .$$

Remark C.7.1 (Unit conversions).
We observe that Ψ is the coordinate transformation for unit changes. Thus, unit conversions become translations on logarithmic scales.

For our example function, we may consider $\Psi(x) = 100x$, which leads to

$$(f \circ \Psi)(x) = \frac{1}{1 + \frac{1}{100x}} \qquad \text{and} \qquad (\widetilde{f} \circ \widetilde{\Psi})(\mathcal{X}) = \frac{1}{1 + \frac{1}{10^{\mathcal{X}+2}}} \ .$$

The corresponding plots are shown in Figure C.3.

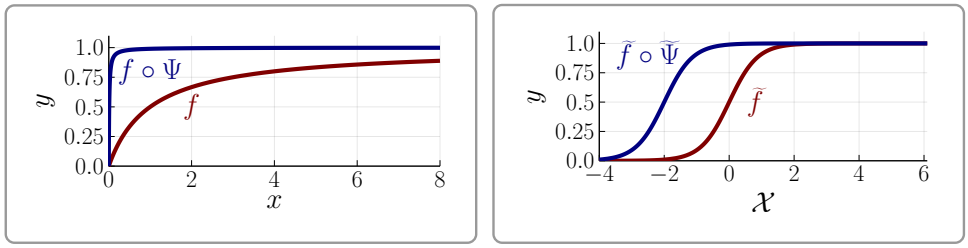

(a) linear scale **(b)** logarithmic scale

Figure C.3: Axis scalings on a linear scale (**a**) become translations on a logarithmic scale (**b**).

This page intentionally left blank.

Bibliography

[AD19] Alexander Altland and Jan von Delft. *Mathematics for Physicists. Introductory Concepts and Methods*. Cambridge University Press, 2019. DOI: 10.1017/9781108557917.

[AE94] Mohammad Asadzadeh and Kenneth Eriksson. "On Adaptive Finite Element Methods for Fredholm Integral Equations of the Second Kind". In: *SIAM Journal on Numerical Analysis* 31, 3, (1994), 831–855. DOI: 10.1137/0731045.

[Axe+24] Trine V. Axelsen et al. "Antibodies toward Na^+,HCO_3^-–cotransporter NBCn1/SLC4A7 block net acid extrusion and cause pH-dependent growth inhibition and apoptosis in breast cancer". In: *British Journal of Cancer* 130, 7, (2024), 1206–1220. DOI: 10.1038/s41416-024-02591-0.

[Bag01] Richard J. Bagby. "The Substitution Theorem for Riemann Integrals". In: *Real Analysis Exchange* 27, 1, (2001), 309–314.

[Bee17] Nelson H.F. Beebe. *The Mathematical-Function Computation Handbook. Programming Using the MathCW Portable Software Library*. Springer, 2017. DOI: 10.1007/978-3-319-64110-2.

[Bor+10] Jennifer Bordeaux et al. "Antibody validation". In: *BioTechniques* 48, 3, (2010), 197–209. DOI: 10.2144/000113382.

[Bre93] Glen E. Bredon. *Topology and Geometry*. Graduate Texts in Mathematics 139. Springer, 1993. DOI: 10.1007/978-1-4757-6848-0.

[BS19] Elco Bakker and Peter S. Swain. "Estimating numbers of intracellular molecules through analysing fluctuations in photobleaching". In: *Scientific Reports* 9, 1, (2019), 15238. DOI: 10.1038/s41598-019-50921-7.

[BT82] Raoul Bott and Loring W. Tu. *Differential Forms in Algebraic Topology*. Graduate texts in mathematics 82. Springer, 1982.

[Cam+15] Neil A. Campbell et al. *Campbell Biologie*. 10th ed. Pearson Deutschland, 2015.

[CB09] Patrick Chames and Daniel Baty. “Bispecific antibodies for cancer therapy: The light at the end of the tunnel?” In: *mAbs* 1, 6, (2009), 539–547. DOI: 10.4161/mabs.1.6.10015.

[Çin11] Erhan Çinlar. *Probability and Stochastics*. Graduate Texts in Mathematics 261. Springer, 2011. DOI: 10.1007/978-0-387-87859-1.

[CW12] Valerie C. Coffman and Jian-Qiu Wu. “Counting protein molecules using quantitative fluorescence microscopy”. In: *Trends in Biochemical Sciences* 37, 11, (2012), 499–506. DOI: 10.1016/j.tibs.2012.08.002.

[De +10] Leandro Luongo De Matos, Damila Cristina Trufelli, Maria Graciela Luongo De Matos, and Maria Aparecida Da Silva Pinhal. “Immunohistochemistry as an Important Tool in Biomarkers Detection and Clinical Practice”. In: *Biomarker Insights* 5, (2010), BMI.S2185. DOI: 10.4137/bmi.s2185.

[Dem06] Wolfgang Demtröder. *Experimentalphysik 2. Elektrizität und Optik*. 4th ed. Springer, 2006.

[Dem08] Wolfgang Demtröder. *Experimentalphysik 1. Mechanik und Wärme*. 5th ed. Springer, 2008. DOI: 10.1007/978-3-540-79295-6.

[Dud+22] Bertalan Dudás, Malcolm Lane, Nikitha Mupparaju, Hye Min Kim, and Istvan Merchenthaler. “A Forgotten Principle in Immunocytochemistry: Optimal Dilution”. In: *Journal of Histochemistry & Cytochemistry* 70, 11-12, (2022), 759–765. DOI: 10.1369/00221554221146213.

[Edf+18] Fredrik Edfors et al. “Enhanced validation of antibodies for research applications”. In: *Nature Communications* 9, 1, (2018), 4130. DOI: 10.1038/s41467-018-06642-y.

[Edw+98] Paul R. Edwards, Colin H. Maule, Robin J. Leatherbarrow, and Donald J. Winzor. “Second-Order Kinetic Analysis of IAsys Biosensor Data: Its Use and Applicability”. In: *Analytical Biochemistry* 263, 1, (1998), 1–12. DOI: 10.1006/abio.1998.2814.

[ET21] Simon Erlendsson and Kaare Teilum. “Binding Revisited—Avidity in Cellular Function and Signaling”. In: *Frontiers in Molecular Biosciences* 7, (2021). DOI: 10.3389/fmolb.2020.615565.

[Fis83] Emanuel Fischer. *Intermediate Real Analysis*. Undergraduate Texts in Mathematics. Springer, 1983. DOI: 10.1007/978-1-4613-9481-5.

[For+18] Patrik Forssén et al. “Reliable Strategy for Analysis of Complex Biosensor Data”. In: *Analytical Chemistry* 90, 8, (2018), 5366–5374. DOI: 10.1021/acs.analchem.8b00504.

[For+22] Isabella Fornacon-Wood et al. “Understanding the Differences Between Bayesian and Frequentist Statistics”. In: *International Journal of Radiation Oncology, Biology, Physics* 112, 5, (2022), 1076–1082. DOI: 10.1016/j.ijrobp.2021.12.011.

[Geo08] Hans-Otto Georgii. *Stochastics. Introduction to probability and statistics*. Walter de Gruyter, 2008.

[Gib11] J. C. Gibbings. *Dimensional Analysis*. Springer, 2011.

[Gor+08] Inna I. Gorshkova, Juraj Svitel, Faezeh Razjouyan, and Peter Schuck. “Bayesian Analysis of Heterogeneity in the Distribution of Binding Properties of Immobilized Surface Sites”. In: *Langmuir* 24, 20, (2008), 11577–11586. DOI: 10.1021/la801186w.

[Gow08] Timothy Gowers. *The Princeton Companion to Mathematics*. Princeton University Press, 2008.

[GR09] Izrail’ S. Gradštejn and Josif M. Ryžik. *Table of integrals, series and products*. 7th ed. Elsevier, 2009.

[Gua+24] Xiangnan Guan et al. “Anti-TIGIT antibody improves PD-L1 blockade through myeloid and T_{reg} cells”. In: *Nature* 627, 8004, (2024), 646–655. DOI: 10.1038/s41586-024-07121-9.

[Har+14] Brian D. Harms, Jeffrey D. Kearns, Sergio Iadevaia, and Alexey A. Lugovskoy. “Understanding the role of cross-arm binding efficiency in the activity of monoclonal and multispecific therapeutic antibodies”. In: *Methods* 65, 1, (2014), 95–104. DOI: 10.1016/j.ymeth.2013.07.017.

[Hir+04] Morris W. Hirsch, Stephen Smale, Robert L. Devaney, and Morris W. Hirsch. *Differential equations, dynamical systems, and an introduction to chaos*. 2nd ed. Vol. 60. Pure and applied mathematics. Elsevier, 2004.

[Jän05] Klaus Jänich. *Vektoranalysis*. 5th ed. Springer, 2005.

[Jay99] E. Jaynes. "Straight Line Fitting – A Bayesian Solution". In: *unpublished* (1999). URL: https://bayes.wustl.edu/etj/articles/leapz.pdf.

[Joh12] Mary Johnson. *Antibody Shelf Life/How to Store Antibodies*. Synatom Research, 2012. DOI: 10.13070/mm.en.2.120.

[Joh23] Syafiq Johar. *The Big Book of Real Analysis. From Numbers to Measures*. Springer, 2023. DOI: 10.1007/978-3-031-30832-1.

[Kah+24] Richard A Kahn et al. "Science Forum: Antibody characterization is critical to enhance reproducibility in biomedical research". In: *eLife* 13, (2024), e100211. DOI: 10.7554/elife.100211.

[Kar16] Robert Karlsson. "Biosensor binding data and its applicability to the determination of active concentration". In: *Biophysical Reviews* 8, 4, (2016), 347–358. DOI: 10.1007/s12551-016-0219-5.

[KB13] Nikolay Koshev and Larisa Beilina. "An adaptive finite element method for Fredholm integral equations of the first kind and its verification on experimental data". In: *Open Mathematics* 11, 8, (2013), 1489–1509. DOI: 10.2478/s11533-013-0247-3.

[KW13] Hans Kerner and Wolf von Wahl. *Mathematik für Physiker*. 3rd ed. Springer, 2013. DOI: 10.1007/978-3-642-37654-2.

[Lan18] Irving Langmuir. "THE ADSORPTION OF GASES ON PLANE SURFACES OF GLASS, MICA AND PLATINUM." In: *Journal of the American Chemical Society* 40, 9, (1918), 1361–1403. DOI: 10.1021/ja02242a004.

[Lat15] Robert A. Latour. “The langmuir isotherm: A commonly applied but misleading approach for the analysis of protein adsorption behavior”. In: *Journal of Biomedical Materials Research Part A* 103, 3, (2015), 949–958. DOI: 10.1002/jbm.a.35235.

[Lau93] Douglas Lauffenburger. *Receptors. models for binding, trafficking, and signaling*. Oxford University Press, 1993.

[Lip+05] Neil S. Lipman, Lynn R. Jackson, Laura J. Trudel, and Frances Weis-Garcia. “Monoclonal Versus Polyclonal Antibodies: Distinguishing Characteristics, Applications, and Information Resources”. In: *ILAR Journal* 46, 3, (2005), 258–268. DOI: 10.1093/ilar.46.3.258.

[LS08] Yu Liu and Liang Shen. “From Langmuir Kinetics to First- and Second-Order Rate Equations for Adsorption”. In: *Langmuir* 24, 20, (2008), 11625–11630. DOI: 10.1021/la801839b.

[Ma+21] Yingbo Ma, Vaibhav Dixit, Michael J Innes, Xingjian Guo, and Chris Rackauckas. “A Comparison of Automatic Differentiation and Continuous Sensitivity Analysis for Derivatives of Differential Equation Solutions”. In: *2021 IEEE High Performance Extreme Computing Conference (HPEC)*. 2021, 1–9. DOI: 10.1109/HPEC49654.2021.9622796.

[Mac03] David J. C. MacKay. *Information Theory, Inference and Learning Algorithms*. 6th ed. Cambridge University Press, 2003. URL: http://www.inference.org.uk/mackay/itila/book.html.

[Mal+20] Irina Malakhova, Alexey Golikov, Yuliya Azarova, and Svetlana Bratskaya. “Extended Rate Constants Distribution (RCD) Model for Sorption in Heterogeneous Systems: 2. Importance of Diffusion Limitations for Sorption Kinetics on Cryogels in Batch”. In: *Gels* 6, 2, (2020), 15. DOI: 10.3390/gels6020015.

[Mar10] Adam W. Marczewski. “Analysis of Kinetic Langmuir Model. Part I: Integrated Kinetic Langmuir Equation (IKL): A New Complete Analytical Solution of the Lang-

muir Rate Equation". In: *Langmuir* 26, 19, (2010), 15229–15238. DOI: 10.1021/la1010049.

[Mes15] Dieter Meschede. *Gerthsen Physik*. 25th ed. Springer, 2015. DOI: 10.1007/978-3-662-45977-5.

[Mon14] Partha Pratim Mondal. *Fundamentals of Fluorescence Microscopy. Exploring Life with Light*. Springer, 2014.

[MÓO20] Hui Ma, Ciarán Ó'Fágáin, and Richard O'Kennedy. "Antibody stability: A key to performance - Analysis, influences and improvement". In: *Biochimie* 177, (2020), 213–225. DOI: 10.1016/j.biochi.2020.08.019.

[MR18] Patrick Kofod Mogensen and Asbjørn Nilsen Riseth. "Optim: A mathematical optimization package for Julia". In: *Journal of Open Source Software* 3, 24, (2018), 615. DOI: 10.21105/joss.00615.

[Mye89] Joseph D. Myers. "Development and application of immunocytochemical staining techniques: A review". In: *Diagnostic Cytopathology* 5, 3, (1989), 318–330. DOI: 10.1002/dc.2840050317.

[NR11] Chitra R. Nayak and Andrew D. Rutenberg. "Quantification of Fluorophore Copy Number from Intrinsic Fluctuations during Fluorescence Photobleaching". In: *Biophysical Journal* 101, 9, (2011), 2284–2293. DOI: 10.1016/j.bpj.2011.09.032.

[Par+25] Gyutae Park, Sieun S. Kim, Jiwon Shim, and Seung-Jae V. Lee. "Brief guide to immunostaining". In: *Molecules and Cells* 48, 1, (2025), 100157. DOI: 10.1016/j.mocell.2024.100157.

[Phi+12] Rob Phillips, Jane Kondev, Julie Theriot, and Hernan G. Garcia. *Physical Biology of the Cell*. 2nd ed. Taylor & Francis, 2012.

[Pil+20] Lakshmi Pillai-Kastoori et al. "Antibody validation for Western blot: By the user, for the user". In: *Journal of Biological Chemistry* 295, 4, (2020), 926–939. DOI: 10.1016/s0021-9258(17)49905-4.

[Piñ+22] Ricardo Piña et al. “Ten Approaches That Improve Immunostaining: A Review of the Latest Advances for the Optimization of Immunofluorescence”. In: *International Journal of Molecular Sciences* 23, 3, (2022), 1426. DOI: 10.3390/ijms23031426.

[Pro82] Stephen W. Provencher. “A constrained regularization method for inverting data represented by linear algebraic or integral equations”. In: *Computer Physics Communications* 27, 3, (1982), 213–227. DOI: 10.1016/0010-4655(82)90173-4.

[Rab05] Semyon G. Rabinovich. *Measurement Errors and Uncertainties. Theory and Practice*. 3rd ed. Springer, 2005. DOI: 10.1007/0-387-29143-1.

[Raw-Data] *Data Repository for the raw data*. DOI: 10.5281/zenodo.17689412. URL: https://github.com/Translational-Pain-Research/Accessibility_Analysis_Data.

[RDW16] John J. Rhoden, Gregory L. Dyas, and Victor J. Wroblewski. “A Modeling and Experimental Investigation of the Effects of Antigen Density, Binding Affinity, and Antigen Expression Ratio on Bispecific Antibody Binding to Cell Surface Targets”. In: *Journal of Biological Chemistry* 291, 21, (2016), 11337–11347. DOI: 10.1074/jbc.m116.714287.

[Rha84] Georges de Rham. *Differentiable Manifolds*. Grundlehren der mathematischen Wissenschaften 266. Springer, 1984. DOI: 10.1007/978-3-642-61752-2.

[RN17] Christopher Rackauckas and Qing Nie. “DifferentialEquations.jl – A Performant and Feature-Rich Ecosystem for Solving Differential Equations in Julia”. In: *Journal of Open Research Software* 5, 1, (2017), 15. DOI: 10.5334/jors.151.

[RN19] Christopher Rackauckas and Qing Nie. “Confederated modular differential equation APIs for accelerated algorithm development and benchmarking”. In: *Advances in Engineering Software* 132, (2019), 1–6. DOI: 10.1016/j.advengsoft.2019.03.009.

[Run+18] Karie Runcie, Daniel R. Budman, Veena John, and Nagashree Seetharamu. “Bi-specific and tri-specific antibodies- the next big thing in solid tumor therapeutics”. In: *Molecular Medicine* 24, 1, (2018), 50. DOI: 10.1186/s10020-018-0051-4.

[Sal17] Stefano Salvestrini. “Analysis of the Langmuir rate equation in its differential and integrated form for adsorption processes and a comparison with the pseudo first and pseudo second order models”. In: *Reaction Kinetics, Mechanisms and Catalysis* 123, 2, (2017), 455–472. DOI: 10.1007/s11144-017-1295-7.

[San+14] Michael J. Sanderson, Ian Smith, Ian Parker, and Martin D. Bootman. “Fluorescence Microscopy”. In: *Cold Spring Harbor Protocols* 2014, 10, (2014), pdb.top071795. DOI: 10.1101/pdb.top071795.

[Seg+23] Aude I. Segaliny et al. “A high throughput bispecific antibody discovery pipeline”. In: *Communications Biology* 6, 1, (2023), 380. DOI: 10.1038/s42003-023-04746-w.

[Smi13] AA Smith. “Finding the best antibody dilution by repeated immunostaining of the same tissue section”. In: *Biotechnic & Histochemistry* 89, 3, (2013), 215–219. DOI: 10.3109/10520295.2013.834074.

[Sun+08] Y. S. Sun et al. “Effect of Fluorescently Labeling Protein Probes on Kinetics of Protein−Ligand Reactions”. In: *Langmuir* 24, 23, (2008), 13399–13405. DOI: 10.1021/la802097z.

[Svi+03] Juraj Svitel, Andrea Balbo, Roy A. Mariuzza, Noreen R. Gonzales, and Peter Schuck. “Combined Affinity and Rate Constant Distributions of Ligand Populations from Experimental Surface Binding Kinetics and Equilibria”. In: *Biophysical Journal* 84, 6, (2003), 4062–4077. DOI: 10.1016/s0006-3495(03)75132-7. URL: https://www.sciencedirect.com/science/article/pii/S0006349503751327.

[Svi+07] Juraj Svitel, Hacène Boukari, Donald Van Ryk, Richard C. Willson, and Peter Schuck. “Probing the Functional Heterogeneity of Surface Binding Sites by Analysis of Ex-

perimental Binding Traces and the Effect of Mass Transport Limitation". In: *Biophysical Journal* 92, 5, (2007), 1742–1758. DOI: 10.1529/biophysj.106.094615. URL: https://www.sciencedirect.com/science/article/pii/S0006349507709827.

[Uhl+16] Mathias Uhlen et al. "A proposal for validation of antibodies". In: *Nature Methods* 13, 10, (2016), 823–827. DOI: 10.1038/nmeth.3995.

[Wal98] Wolfgang Walter. *Ordinary differential equations*. Graduate texts in mathematics 182. Springer, 1998.

[Wel16] Michael G. Weller. "Quality Issues of Research Antibodies". In: *Analytical Chemistry Insights* 11, (2016), ACI.S31614. DOI: 10.4137/aci.s31614.

[Yin+15] Linliang Yin et al. "How does fluorescent labeling affect the binding kinetics of proteins with intact cells?" In: *Biosensors and Bioelectronics* 66, (2015), 412–416. DOI: 10.1016/j.bios.2014.11.036.

[Zha+13] Huaying Zhao, Inna I. Gorshkova, Gregory L. Fu, and Peter Schuck. "A comparison of binding surfaces for SPR biosensing using an antibody–antigen system and affinity distribution analysis". In: *Methods* 59, 3, (2013), 328–335. DOI: 10.1016/j.ymeth.2012.12.007.

[Zha+18] Y. Zhang, P. Forssén, T. Fornstedt, M. Gulliksson, and X. Dai. "An adaptive regularization algorithm for recovering the rate constant distribution from biosensor data". In: *Inverse Problems in Science and Engineering* 26, 10, (2018), 1464–1489. DOI: 10.1080/17415977.2017.1411912.

[Zha+19] Ye Zhang, Zhigang Yao, Patrik Forssén, and Torgny Fornstedt. "Estimating the rate constant from biosensor data via an adaptive variational Bayesian approach". In: *The Annals of Applied Statistics* 13, 4, (2019), 2011–2042. DOI: 10.1214/19-aoas1263.

This page intentionally left blank.

Index

The selective binding of antibodies to antigens has been used for decades in biological research and has become a useful tool for medical diagnostics and therapy. Perhaps one of the earliest applications are staining experiments that indicate the presence of antigens in cells or tissue. Despite the development of highly specialized applications, this simple staining still belongs to the standard repertoire of immunostaining.

In this dissertation, we model the macroscopically observable binding behavior of antibodies in staining experiments. The guiding principles are two aspects that apply to most staining experiments: the finite antibody incubation time, and washing steps that remove unbound antibodies prior to the evaluation of the staining result. Thus, the staining result can only comprise antibodies that have withstood washing, leading us to describe the binding of measurable antibodies as an accumulation process with finite stopping time.

We construct the equations for the accumulation model from Langmuir kinetics and corresponding adaptations to multiple binding-site types so that we can consider heterogeneous cellular structures. After describing the immediate consequences of the accumulation process, we prove that the accumulation model satisfies all the properties that are expected from the experimental setting of staining experiments. Next, we shift the focus to the estimation of the model parameters and develop the accessibility analysis, which is a characterization method for experimental systems. Using experimental data, we validate the underlying principles of the accumulation model and test the accessibility analysis that is implemented and published in the form of Julia packages. Finally, we take the opportunity to propose and illustrate two applications of the accessibility analysis: the selection of initial antibody concentrations for staining experiments and a multi-staining multiplexing method that separates staining signals based on antibody binding properties.

Faculty of Mathematics
and Natural Sciences **2026**